Lecture Notes in Physics 928

Roberto Bruno
Vincenzo Carbone

Turbulence in the Solar Wind

Springer

Lecture Notes in Physics

Volume 928

The Lecture Notes in Physics

The series Lecture Notes in Physics (LNP), founded in 1969, reports new developments in physics research and teaching-quickly and informally, but with a high quality and the explicit aim to summarize and communicate current knowledge in an accessible way. Books published in this series are conceived as bridging material between advanced graduate textbooks and the forefront of research and to serve three purposes:

- to be a compact and modern up-to-date source of reference on a well-defined topic
- to serve as an accessible introduction to the field to postgraduate students and nonspecialist researchers from related areas
- to be a source of advanced teaching material for specialized seminars, courses and schools

Both monographs and multi-author volumes will be considered for publication. Edited volumes should, however, consist of a very limited number of contributions only. Proceedings will not be considered for LNP.

Volumes published in LNP are disseminated both in print and in electronic formats, the electronic archive being available at springerlink.com. The series content is indexed, abstracted and referenced by many abstracting and information services, bibliographic networks, subscription agencies, library networks, and consortia.

Proposals should be sent to a member of the Editorial Board, or directly to the managing editor at Springer:

Christian Caron
Springer Heidelberg
Physics Editorial Department I
Tiergartenstrasse 17
69121 Heidelberg/Germany
christian.caron@springer.com

More information about this series at http://www.springer.com/series/5304

Roberto Bruno • Vincenzo Carbone

Turbulence in the Solar Wind

Springer

Roberto Bruno
Fisica dei Plasmi Spaziali
INAF - Istituto di Astrofisica e Planetologia Spaziali
Roma, Italy

Vincenzo Carbone
Università della Calabria
Dipartimento di Fisica
Rende (CS), Italy

ISSN 0075-8450 ISSN 1616-6361 (electronic)
Lecture Notes in Physics
ISBN 978-3-319-43439-1 ISBN 978-3-319-43440-7 (eBook)
DOI 10.1007/978-3-319-43440-7

Library of Congress Control Number: 2016954366

Printed on acid-free paper

This Springer imprint is published by Springer Nature
The registered company is Springer International Publishing AG Switzerland

For Adelina and Maria Carmela, for being so patient with us during the drafting of this book

Preface

Writing this tutorial review would have not been possible without a constructive and continuous interaction with our national and foreign colleagues. The many discussions we had with them and the many comments and advices we received guided us through the write-up of this work. In particular, we like to thank Bruno Bavassano and Pierluigi Veltri who initiated us into the study of space plasma turbulence many years ago. We also like to acknowledge the use of plasma and magnetic field data from Helios spacecraft to produce from scratch some of the figures shown in the present book. In particular, we would like to thank Helmut Rosenbauer and Rainer Schwenn, PIs of the plasma experiment; Fritz Neubauer, PI of the first magnetic experiment onboard Helios; and Franco Mariani and Norman Ness, PIs of the second magnetic experiment on board Helios. We thank Annick Pouquet, Helen Politano, and Vanni Antoni for the possibility to compare solar wind data with both high-resolution numerical simulations and laboratory plasmas. We owe special thanks and appreciation to Eckart Marsch and Sami Solanki who invited us to write the original Living Review version of this work and for the useful refereeing procedure. Finally, our wholehearted thanks go to Gary Zank for inviting us to transform it into a monographical volume for *Lecture Notes in Physics* series.

Roma, Italy — Roberto Bruno
Rende (CS), Italy — Vincenzo Carbone

Contents

Chapter 1
Introduction

The whole heliosphere is permeated by the solar wind, a supersonic and super-Alfvénic plasma flow of solar origin which continuously expands into the heliosphere. This medium offers the best opportunity to study directly collisionless plasma phenomena, mainly at low frequencies where large-amplitude fluctuations have been observed. During its expansion, the solar wind develops a strong turbulent character, which evolves towards a state that resembles the well known hydrodynamic turbulence described by Kolmogorov (1941, 1991). Because of the presence of a strong magnetic field carried by the wind, low-frequency fluctuations in the solar wind are usually described within a magnetohydrodynamic (MHD, hereafter) benchmark (Kraichnan 1965; Biskamp 1993; Tu and Marsch 1995; Biskamp 2003; Petrosyan et al. 2010). However, due to some peculiar characteristics, the solar wind turbulence contains some features hardly classified within a general theoretical framework.

Turbulence in the solar heliosphere plays a relevant role in several aspects of plasma behavior in space, such as solar wind generation, high-energy particles acceleration, plasma heating, and cosmic rays propagation. In the 1970s and 80s, impressive advances have been made in the knowledge of turbulent phenomena in the solar wind. However, at that time, spacecraft observations were limited by a small latitudinal excursion around the solar equator and, in practice, only a thin slice above and below the equatorial plane was accessible, i.e., a sort of 2D heliosphere.

In the 1990s, with the launch of the Ulysses spacecraft, investigations have been extended to the high-latitude regions of the heliosphere, allowing us to characterize and study how turbulence evolves in the polar regions. An overview of Ulysses results about polar turbulence can also be found in Horbury and Tsurutani (2001). With this new laboratory, relevant advances have been made. One of the main goals of the present work will be that of reviewing observations and theoretical efforts made to understand the near-equatorial and polar turbulence in order to provide the reader with a rather complete view of the low-frequency turbulence phenomenon in the 3D heliosphere.

R. Bruno, V. Carbone, *Turbulence in the Solar Wind*, Lecture Notes in Physics 928, DOI 10.1007/978-3-319-43440-7_1

New interesting insights in the theory of turbulence derive from the point of view which considers a turbulent flow as a complex system, a sort of benchmark for the theory of dynamical systems. The theory of chaos received the fundamental impulse just through the theory of turbulence developed by Ruelle and Takens (1971) who, criticizing the old theory of Landau and Lifshitz (1971), were able to put the numerical investigation by Lorenz (1963) in a mathematical framework. Gollub and Swinney (1975) set up accurate experiments on rotating fluids confirming the point of view of Ruelle and Takens (1971) who showed that a *strange attractor* in the phase space of the system is the best model for the birth of turbulence. This gave a strong impulse to the investigation of the phenomenology of turbulence from the point of view of dynamical systems (Bohr et al. 1998). For example, the criticism by Landau leading to the investigation of intermittency in fully developed turbulence was worked out through some phenomenological models for the energy cascade (cf. Frisch 1995). Recently, turbulence in the solar wind has been used as a big wind tunnel to investigate scaling laws of turbulent fluctuations, multifractals models, etc. The review by Tu and Marsch (1995) contains a brief introduction to this important argument, which was being developed at that time relatively to the solar wind (Burlaga 1993; Carbone 1993; Biskamp 1993, 2003; Burlaga 1995). The reader can convince himself that, because of the wide range of scales excited, space plasma can be seen as a very big laboratory where fully developed turbulence can be investigated not only per se, rather as far as basic theoretical aspects are concerned.

Turbulence is perhaps the most beautiful unsolved problem of classical physics, the approaches used so far in understanding, describing, and modeling turbulence are very interesting even from a historic point of view, as it clearly appears when reading, for example, the book by Frisch (1995). History of turbulence in interplanetary space is, perhaps, even more interesting since its knowledge proceeds together with the human conquest of space. Thus, whenever appropriate, we will also introduce some historical references to show the way particular problems related to turbulence have been faced in time, both theoretically and technologically. Finally, since turbulence is a phenomenon visible everywhere in nature, it will be interesting to compare some experimental and theoretical aspects among different turbulent media in order to assess specific features which might be universal, not limited only to turbulence in space plasmas. In particular, we will compare results obtained in interplanetary space with results obtained from ordinary fluid flows on Earth, and from experiments on magnetic turbulence in laboratory plasmas designed for thermonuclear fusion.

1.1 The Solar Wind

"Since the gross dynamical properties of the outward streaming gas are hydrodynamic in character, we refer to the streaming as the solar wind." This sentence, contained in Parker (1958b) seminal paper, represents the first time the name "solar wind" appeared in literature, about 60 years ago.

The idea of the presence of an ionized gas continuously streaming radially from the sun was firstly hypothesized by Biermann (1951, 1957) based on observations of the displacements of the comet tails from the radial direction and on the ionization of cometary molecules. A similar suggestion seemed to come out from the occurrence of auroral phenomena and the continuous fluctuations observed in the geomagnetic lines of force. The same author estimated that this ionized flow would have a bulk speed ranging from 500 to 1500 km/s.

Parker (1958a) showed that the birth of the wind was a direct consequence of the high coronal temperature and the fact that it was not possible for the solar corona, given the estimated particle number density and plasma temperature, to be in hydrostatic equilibrium out to large distances with vanishing pressure. He found that a steady expansion of the solar corona with bulk speed of the order of the observed one would require reasonable coronal temperatures.

As the wind expands into the interplanetary space, due to its high electrical conductivity, it carries the photospheric magnetic field lines with it and creates a magnetized bubble of hot plasma around the Sun, namely the heliosphere.

For an observer confined in the ecliptic plane, the interplanetary medium appears highly structured into recurrent high velocity streams coming from coronal holes regions dominated by open magnetic field lines, and slow plasma originating from regions dominated by closed magnetic field lines. This phenomenon is much more evident especially during periods of time around minimum of solar activity cycle, when the meridional boundaries of polar coronal holes extend to much lower heliographic latitude reaching the equatorial regions.

This particular configuration combined with the solar rotation is at the basis of the strong dynamical interactions between slow and fast wind that develops during the wind expansion. This dynamics ends up to mix together plasma and magnetic field features which are characteristic separately of fast and slow wind at the source regions. As a matter of fact, in-situ observations in the inner heliosphere unraveled the different nature of these two types of wind not only limited to the large scale average values of their plasma and magnetic field parameters but also referred to the nature of the associated fluctuations.

It is clear that a description of the wind MHD turbulence will result more profitable if performed within the frame of reference of the solar wind macro structure, i.e. separately for fast and slow wind, without averaging the two.

Just to strengthen the validity of this approach, that we will follow throughout this review, we like to mention the following concept: “Asking for the average solar wind might appear as silly as asking for the taste af an average drink. What is the average between wine and beer? Obviously a mere mixing and averaging means mixing does not lead to a meaningful result. Better taste and judge separately and then compare, if you wish.” (Schwenn 1983)

However, before getting deeper into the study of turbulence, it is useful to have an idea of the values of the most common physical parameters characterizing fast and slow wind.

Table 1.1 Typical values of several solar wind parameters as measured by Helios 2 at 1 AU

Wind parameter	Slow wind	Fast wind
Number density	$\sim 15\,\mathrm{cm}^{-3}$	$\sim 4\,\mathrm{cm}^{-3}$
Bulk velocity	$\sim 350\,\mathrm{km\,s}^{-1}$	$\sim 600\,\mathrm{km\,s}^{-1}$
Proton temperature	$\sim 5 \times 10^4$ K	$\sim 2 \times 10^5$ K
Electron temperature	$\sim 2 \times 10^5$ K	$\sim 1 \times 10^5$ K
α-Particles temperature	$\sim 2 \times 10^5$ K	$\sim 8 \times 10^5$ K
Magnetic field	~ 6 nT	~ 6 nT

Table 1.2 Typical values of different speeds obtained at 1 AU

Speed	Slow wind	Fast wind
Alfvén	$\sim$30 km s^{-1}	$\sim$60 km s^{-1}
Ion sound	$\sim$60 km s^{-1}	$\sim$60 km s^{-1}
Proton thermal	$\sim$35 km s^{-1}	$\sim$70 km s^{-1}
Electron thermal	$\sim$3000 km s^{-1}	$\sim$2000 km s^{-1}

These values have been obtained from the parameters reported in Table 1.1

Table 1.3 Typical values of different frequencies at 1 AU

Frequency	Slow wind	Fast wind
Proton cyclotron	$\sim$0.1 Hz	$\sim$0.1 Hz
Electron cyclotron	$\sim 2 \times 10^2$ Hz	$\sim 2 \times 10^2$ Hz
Plasma	$\sim 2 \times 10^5$ Hz	$\sim 1 \times 10^5$ Hz
Proton-proton collision	$\sim 2 \times 10^{-6}$ Hz	$\sim 1 \times 10^{-7}$ Hz

These values have been obtained from the parameters reported in Table 1.1

Table 1.4 Typical values of different lengths at 1 AU plus the distance traveled by a proton before colliding with another proton

Length	Slow wind	Fast wind
Debye	$\sim$4 m	$\sim$15 m
Proton gyroradius	$\sim$130 km	$\sim$260 km
Electron gyroradius	$\sim$2 km	$\sim$1.3 km
Distance between 2 proton collisions	$\sim$1.2 AU	$\sim$40 AU

These values have been obtained from the parameters reported in Table 1.1

Since the wind is an expanding medium, we ought to choose one heliocentric distance to refer to and, usually, this distance is 1 AU. In the following, we will provide different tables referring to several solar wind parameters, velocities, characteristic times, and lengths.

Based on the Tables above, we can conclude that, the solar wind is a super-Alfvénic, supersonic and collisionless plasma, and MHD turbulence can be investigated for frequencies smaller than $\sim 10^{-1}$ Hz (Table 1.3).

1.2 Dynamics vs. Statistics

The word *turbulent* is used in the everyday experience to indicate something which is *not regular*. In Latin the word *turba* means something confusing or something which does not follow an ordered plan. A *turbulent boy*, in all Italian schools, is a young fellow who rebels against ordered schemes. Following the same line, the behavior of a flow which rebels against the deterministic rules of classical dynamics is called turbulent. Even the opposite, namely a *laminar* motion, derives from the Latin word *lámina*, which means stream or sheet, and gives the idea of a regular streaming motion. Anyhow, even without the aid of a laboratory experiment and a Latin dictionary, we experience turbulence every day. It is relatively easy to observe turbulence and, in some sense, we generally do not pay much attention to it (apart when, sitting in an airplane, a nice lady asks us to fasten our seat belts during the flight because we are approaching some turbulence!). Turbulence appears everywhere when the velocity of the flow is high enough,[1] for example, when a flow encounters an obstacle (cf., e.g., Fig. 1.1) in the atmospheric flow, or during the circulation of blood, etc. Even charged fluids (plasma) can become turbulent. For example, laboratory plasmas are often in a turbulent state, as well as natural plasmas like the outer regions of stars. Living near a star, we have a big chance to directly investigate the turbulent motion inside the flow which originates from the Sun, namely the solar wind. This will be the main topic of the present review.

Turbulence that we observe in fluid flows appears as a very complicated state of motion, and at a first sight it looks (apparently!) strongly irregular and chaotic, both in space and time. The only dynamical rule seems to be the impossibility to predict any future state of the motion. However, it is interesting to recognize the fact that, when we take a picture of a turbulent flow at a given time, we see the presence

Fig. 1.1 Turbulence as observed in a river. Here we can see different turbulent wakes due to different obstacles encountered by the water flow: simple stones and pillars of the old Roman Cestio bridge across the Tiber river

[1] This concept will be explained better in the next sections.

of a lot of different *turbulent structures* of all sizes which are actively present during the motion. The presence of these structures was well recognized long time ago, as testified by the amazing pictures of *vortices* observed and reproduced by the Italian genius Leonardo da Vinci, as reported in the textbook by Frisch (1995). The left-hand-side panel of Fig. 1.2 shows, as an example, some drawings by Leonardo which can be compared with the right-hand-side panel taken from a typical experiment on a turbulent jet.

Turbulent features can be recognized even in natural turbulent systems like, for example, the atmosphere of Jupiter (see Fig. 1.3). A different example of turbulence in plasmas is reported in Fig. 1.4 where we show the result of a typical high resolution numerical simulations of 2D MHD turbulence. In this case the turbulent field shown is the current density. These basic features of mixing between order and chaos make the investigation of properties of turbulence terribly complicated, although extraordinarily fascinating.

When we look at a flow at two different times, we can observe that the general aspect of the flow has not changed appreciably, say vortices are present all the time but the flow in each single point of the fluid looks different. We recognize that the gross features of the flow are reproducible but details are not predictable. We have to use a statistical approach to turbulence, just as it is done to describe stochastic processes, even if the problem is born within the *strange* dynamics of a deterministic system!

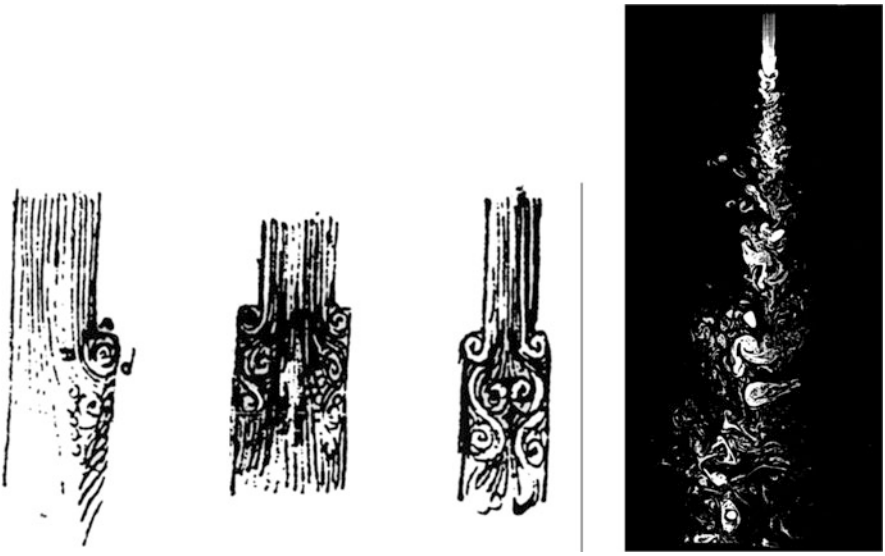

Fig. 1.2 *Left panel*: three examples of vortices taken from the pictures by Leonardo da Vinci (cf. Frisch 1995). *Right panel*: turbulence as observed in a turbulent water jet (Van Dyke 1982) reported in the book by Frisch (1995) (photograph by P. Dimotakis, R. Lye, and D. Papantoniu)

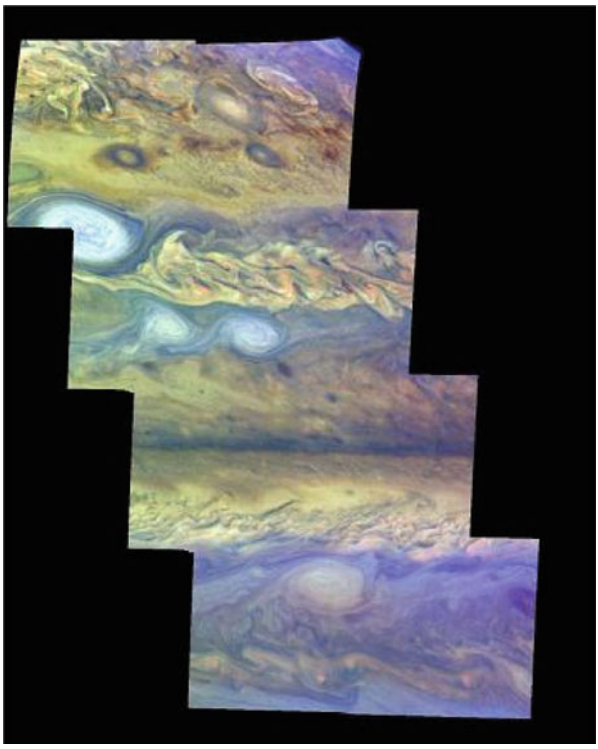

Fig. 1.3 Turbulence in the atmosphere of Jupiter as observed by Voyager

Turbulence increases the properties of transport in a flow. For example, the urban pollution, without atmospheric turbulence, would not be spread (or eliminated) in a relatively short time. Results from numerical simulations of the concentration of a passive scalar transported by a turbulent flow is shown in Fig. 1.5. On the other hand, in laboratory plasmas inside devices designed to achieve thermo-nuclear controlled fusion, anomalous transport driven by turbulent fluctuations is the main cause for the destruction of magnetic confinement. Actually, we are far from the achievement of controlled thermo-nuclear fusion. Turbulence, then, acquires the strange feature of something to be avoided in some cases, or to be invoked in some other cases.

Turbulence became an experimental science since Osborne Reynolds who, at the end of nineteenth century, observed and investigated experimentally the transition from laminar to turbulent flow. He noticed that the flow inside a pipe becomes turbulent every time a single parameter, a combination of the viscosity coefficient η, a characteristic velocity U, and length L, would increase. This parameter $Re = UL\rho/\eta$ (ρ is the mass density of the fluid) is now called the *Reynolds number*. At lower Re, say $Re \leq 2300$, the flow is regular (that is the motion is laminar), but when Re increases beyond a certain threshold of the order of $Re \simeq 4000$, the flow becomes turbulent. As Re increases, the transition from a laminar to a turbulent state

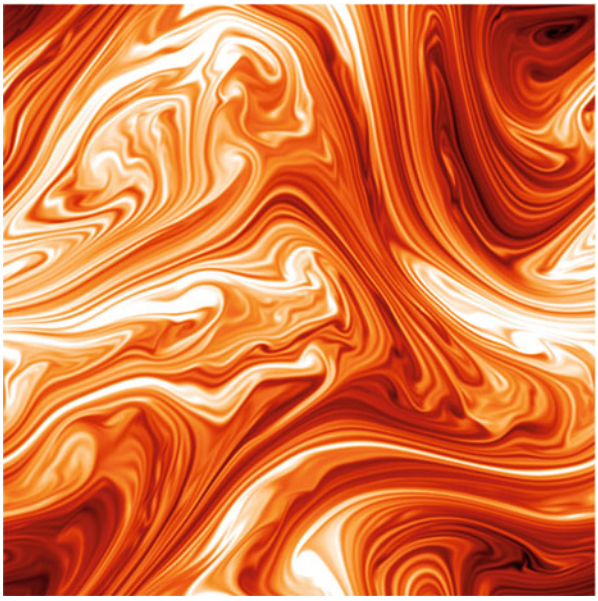

Fig. 1.4 High resolution numerical simulations of 2D MHD turbulence at resolution 2048×2048 (courtesy by H. Politano). Here, the authors show the current density $J(x, y)$, at a given time, on the plane (x, y)

occurs over a range of values of Re with different characteristics and depending on the details of the experiment. In the limit $Re \to \infty$ the turbulence is said to be in a fully developed turbulent state. The original pictures by Reynolds are shown in Fig. 1.6.

In Fig. 1.7 we report a typical sample of turbulence as observed in a fluid flow in the Earth's atmosphere. Time evolution of both the longitudinal velocity component and the temperature is shown. Measurements in the solar wind show the same typical behavior. A typical sample of turbulence as measured by Helios 2 spacecraft is shown in Fig. 1.8. A further sample of turbulence, namely the radial component of the magnetic field measured at the external wall of an experiment in a plasma device realized for thermonuclear fusion, is shown in Fig. 1.9.

As it is well documented in these figures, the main feature of fully developed turbulence is the chaotic character of the time behavior. Said differently, this means that the behavior of the flow is unpredictable. While the details of fully developed turbulent motions are extremely sensitive to triggering disturbances, average properties are not. If this was not the case, there would be little significance in the averaging process. Predictability in turbulence can be recast at a statistical level. In other words, when we look at two different samples of turbulence, even collected within the same medium, we can see that details look very different. What is actually common is a generic stochastic behavior. This means that the global statistical behavior does not change going from one sample to the other.

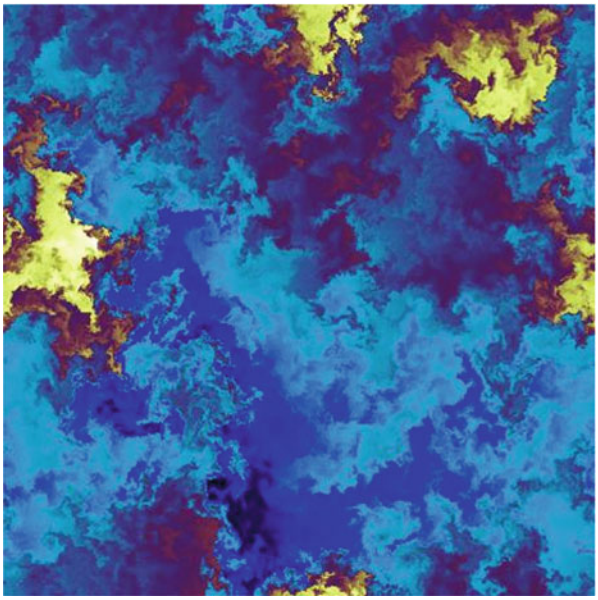

Fig. 1.5 Concentration field $c(x, y)$, at a given time, on the plane (x, y). The field has been obtained by a numerical simulation at resolution 2048×2048. The concentration is treated as a passive scalar, transported by a turbulent field. Low concentrations are reported in *blue* while high concentrations are reported in *yellow* (courtesy by A. Noullez)

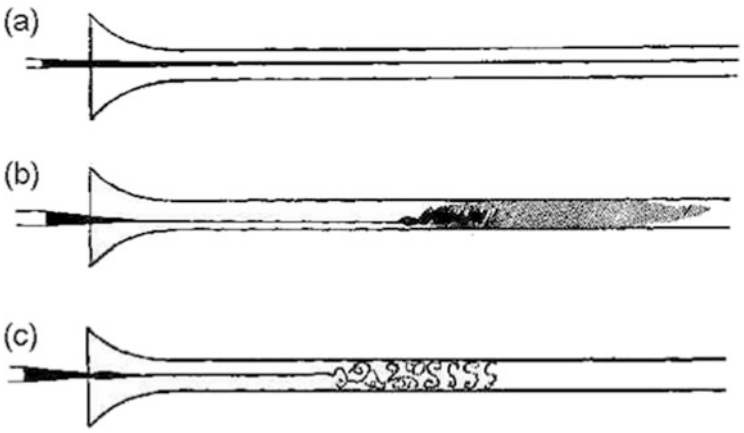

Fig. 1.6 The original pictures taken from Reynolds (1883) which show the transition to a turbulent state of a flow in a pipe as the Reynolds number increases [(**a**) and (**b**) panels]. Panel (**c**) shows eddies revealed through the light of an electric spark

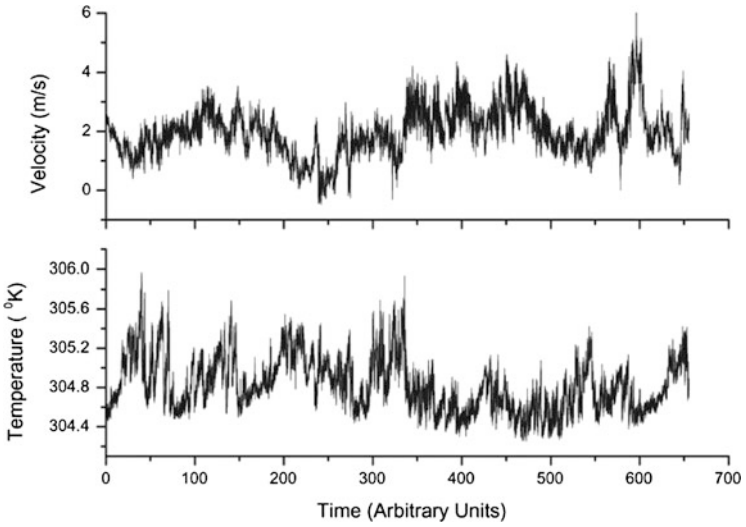

Fig. 1.7 Turbulence as measured in the atmospheric boundary layer. Time evolution of the longitudinal velocity and temperature are shown in the *upper and lower panels*, respectively. The turbulent samples have been collected above a grass-covered forest clearing at 5 m above the ground surface and at a sampling rate of 56 Hz (Katul et al. 1997)

The idea that fully developed turbulent flows are extremely sensitive to small perturbations but have statistical properties that are insensitive to perturbations is of central importance throughout this review. Fluctuations of a certain stochastic variable ψ are defined here as the difference from the average value $\delta\psi = \psi - \langle\psi\rangle$, where brackets mean some averaging process. Actually, the method of taking averages in a turbulent flow requires some care. We would like to recall that there are, at least, three different kinds of averaging procedures that may be used to obtain statistically-averaged properties of turbulence. The space averaging is limited to flows that are statistically homogeneous or, at least, approximately homogeneous over scales larger than those of fluctuations. The ensemble averages are the most versatile, where average is taken over an ensemble of turbulent flows prepared under nearly identical external conditions. Of course, these flows are not completely identical because of the large fluctuations present in turbulence. Each member of the ensemble is called a *realization*. The third kind of averaging procedure is the time average, which is useful only if the turbulence is statistically stationary over time scales much larger than the time scale of fluctuations. In practice, because of the convenience offered by locating a probe at a fixed point in space and integrating in time, experimental results are usually obtained as time averages. The ergodic theorem (Halmos 1956) assures that time averages coincide with ensemble averages under some standard conditions (see Sect. 3.2).

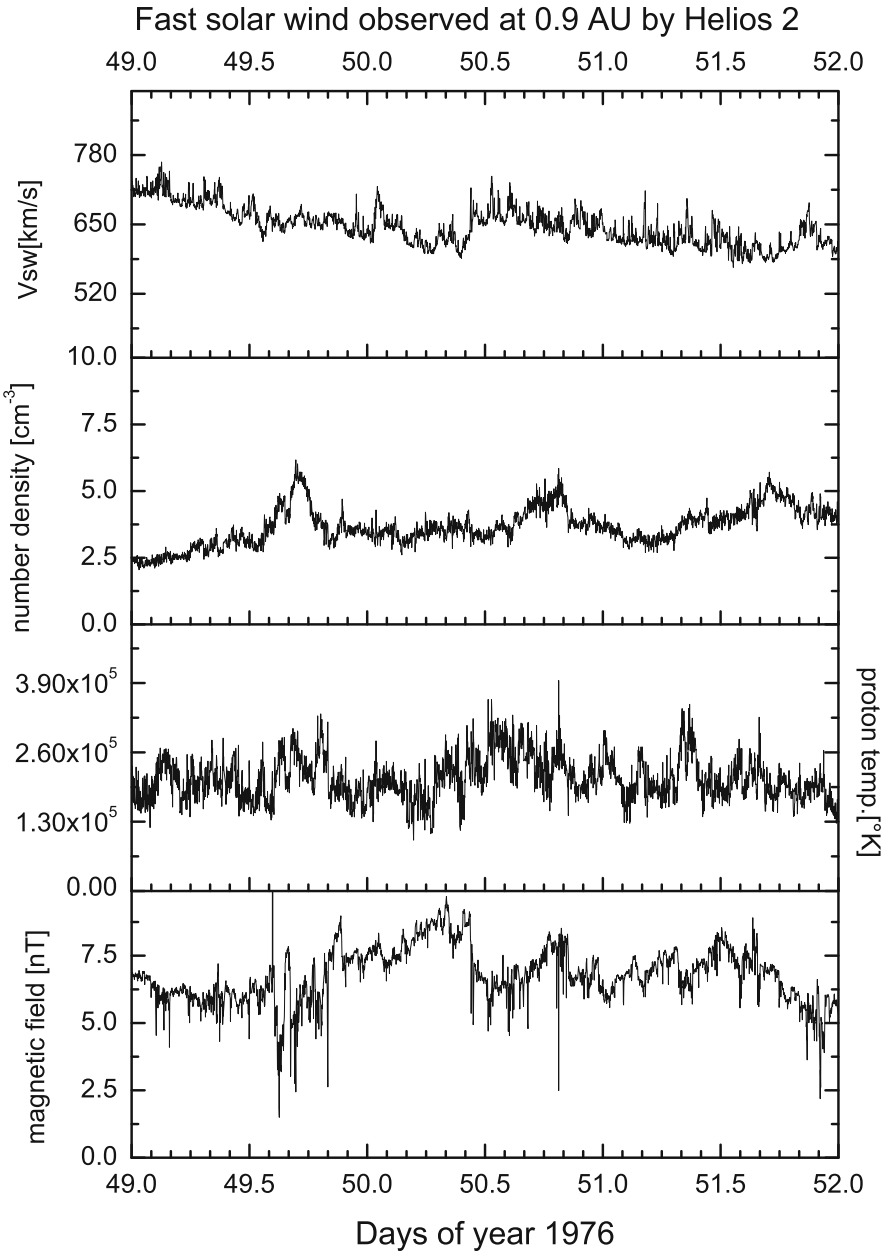

Fig. 1.8 A sample of fast solar wind at distance 0.9 AU measured by the Helios 2 spacecraft. *From top to bottom:* speed, number density, temperature, and magnetic field, as a function of time

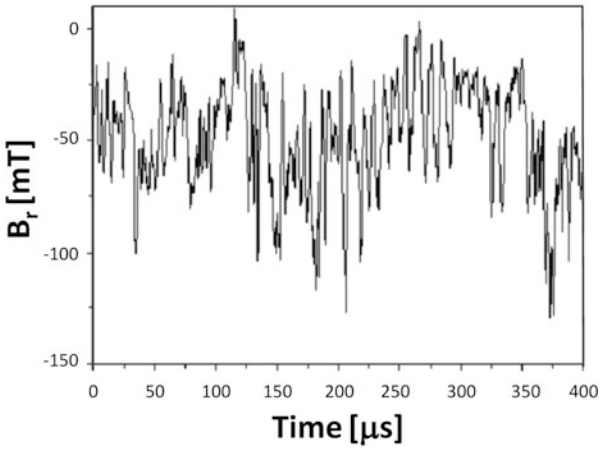

Fig. 1.9 Turbulence as measured at the external wall of a device designed for thermonuclear fusion, namely the RFX in Padua (Italy). The radial component of the magnetic field as a function of time is shown in the figure (courtesy by V. Antoni)

A different property of turbulence is that all dynamically interesting scales are excited, that is, energy is spread over all scales. This can be seen in Fig. 1.10 where we show the magnetic field intensity (see top panel) within a typical solar wind stream.

In the middle and bottom panels we show fluctuations at two different detailed scales. In particular, each panel contains an equal number of data points. From top to bottom, graphs have been produced using 1 h, 81 and 6 s averages, respectively. The different profiles appear statistically similar, in other words, we can say that interplanetary magnetic field fluctuations show similarity at all scales, i.e. they look self-similar.

Since fully developed turbulence involves a hierarchy of scales, a large number of interacting degrees of freedom are involved. Then, there should be an asymptotic statistical state of turbulence that is independent on the details of the flow. Hopefully, this asymptotic state depends, perhaps in a critical way, only on simple statistical properties like energy spectra, as much as in statistical mechanics equilibrium where the statistical state is determined by the energy spectrum (Huang 1987). Of course, we cannot expect that the statistical state would determine the details of individual realizations, because realizations need not to be given the same weight in different ensembles with the same low-order statistical properties.

It should be emphasized that there are no firm mathematical arguments for the existence of an asymptotic statistical state. As we have just seen, reproducible statistical results are obtained from observations, that is, it is suggested experimentally and from physical plausibility. Apart from physical plausibility, it is embarrassing that such an important feature of fully developed turbulence, as the existence of a statistical stability, should remain unsolved. However, such is the complex nature of turbulence.

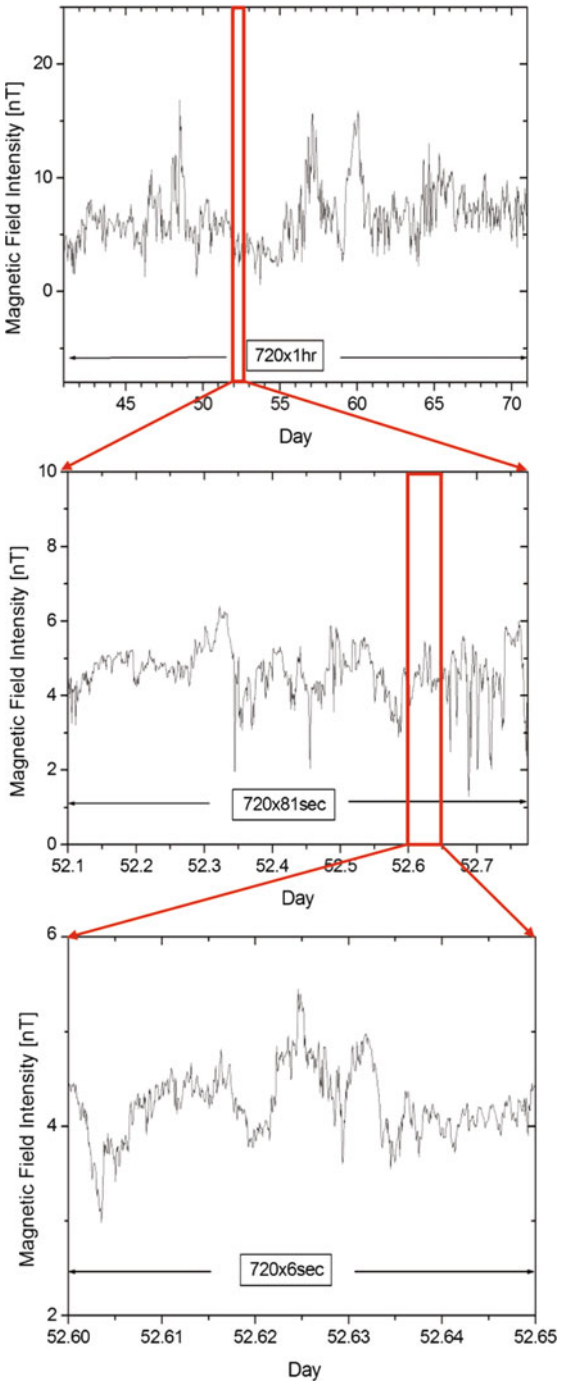

Fig. 1.10 Magnetic intensity fluctuations as observed by Helios 2 in the inner heliosphere at 0.9 AU, for different blow-ups. Each panel contains an equal number of data points. From *top to bottom*, graphs have been produced using 1 h, 81 and 6 s averages, respectively

References

L. Biermann, Kometenschweife und solare korpuskularstrahlung. Z. Astrophys. **29**, 274 (1951)

L. Biermann, Solar corpuscular radiation and the interplanetary gas. Observatory **77**, 109–110 (1957)

D. Biskamp, *Nonlinear Magnetohydrodynamics*. Cambridge Monographs on Plasma Physics, vol. 1 (Cambridge University Press, Cambridge, 1993)

D. Biskamp, *Magnetohydrodynamic Turbulence* (Cambridge University Press, Cambridge, 2003)

T. Bohr, M.H. Jensen, G. Paladin, A. Vulpiani, *Dynamical Systems Approach to Turbulence*. Cambridge Nonlinear Science Series, vol. 8 (Cambridge University Press, Cambridge, 1998)

L.F. Burlaga, Intermittent turbulence in large-scale velocity fluctuations at 1 AU near solar maximum. J. Geophys. Res. **98**(17), 17467–17474 (1993). doi:10.1029/93JA01630

L.F. Burlaga, Interplanetary Magnetohydrodynamics. *International Series on Astronomy and Astrophysics*, vol. 3 (Oxford University Press, New York, 1995)

V. Carbone, Cascade model for intermittency in fully developed magnetohydrodynamic turbulence. Phys. Rev. Lett. **71**, 1546–1548 (1993). doi:10.1103/PhysRevLett.71.1546

U. Frisch, *Turbulence: The Legacy of A.N. Kolmogorov* (Cambridge University Press, Cambridge, 1995)

J.P. Gollub, H.L. Swinney, Onset of turbulence in a rotating fluid. Phys. Rev. Lett. **35**, 927–930 (1975). doi:10.1103/PhysRevLett.35.927

P.R. Halmos, *Lectures on Ergodic Theory* (Chelsea, New York, 1956)

T.S. Horbury, B. Tsurutani, Ulysses measurements of waves, turbulence and discontinuities, in *The Heliosphere Near Solar Minimum: The Ulysses perspective*, ed. by A. Balogh, R.G. Marsden, E.J. Smith. Springer-Praxis Books in Astronomy and Space Sciences (Springer, Berlin, 2001), pp. 167–227

K. Huang, *Statistical Mechanics*, 2nd edn. (Wiley, New York, 1987)

G.G. Katul, C.I. Hsieh, J. Sigmon, Energy-inertial scale interaction for temperature and velocity in the unstable surface layer. Boundary-Layer Meteorol. **82**, 49–80 (1997). doi:10.1023/A:1000178707511

A.N. Kolmogorov, The local structure turbulence in incompressible viscous fluids for very large reynolds numbers. Dokl. Akad. Nauk. SSSR **30**, 301–305 (1941)

A.N. Kolmogorov, The local structure of turbulence in incompressible viscous fluid for very large reynolds numbers. Proc. R. Soc. London, Ser. A **434**, 9–13 (1991)

R.H. Kraichnan, Inertial range spectrum of hydromagnetic turbulence. Phys. Fluids **8**, 1385–1387 (1965)

L.D. Landau, E.M. Lifshitz, *Physique théorique*. Mécanique des fluides, vol. 6 (Editions MIR, Moscow, 1971)

E.N. Lorenz, Deterministic nonperiodic flow. J. Atmos. Sci. **20**, 130 (1963). doi:10.1175/1520-0469(1963)020<0130:DNF>2.0.CO;2

E.N. Parker, Dynamics of the interplanetary gas and magnetic fields. Astrophys. J **128**, 664 (1958a). doi:10.1086/146579

E.N. Parker, Interaction of the solar wind with the geomagnetic field. Phys. Fluids **1**, 171–187 (1958b). doi:10.1063/1.1724339

A. Petrosyan, A. Balogh, M.L. Goldstein, J. Léorat, E. Marsch, K. Petrovay, B. Roberts, R. von Steiger, J.C. Vial, Turbulence in the solar atmosphere and solar wind. Space Sci. Rev. **156**, 135–238 (2010). doi:10.1007/s11214-010-9694-3

O. Reynolds, An experimental investigation of the circumstances which determine whether the motion of water shall be direct or sinuous, and the law of resistance in parallel channels. Philos. Trans. R. Soc. London **174**, 935–982 (1883). doi:10.1098/rstl.1883.0029

D. Ruelle, F. Takens, On the nature of turbulence. Commun. Math. Phys. **20**, 167 (1971)

R. Schwenn, The ‘average’ solar wind in the inner heliosphere: structures and slow variations, in *Solar Wind Five*, ed. by M. Neugebauer. NASA Conference Publication, vol. 2280 (NASA, Washington, DC, 1983), pp. 489–507

C.-Y. Tu, E. Marsch, MHD structures, waves and turbulence in the solar wind: observations and theories. Space Sci. Rev. **73**(1/2), 1–210 (1995). doi:10.1007/BF00748891

M. Van Dyke, *An Album of Fluid Motion* (The Parabolic Press, Stanford, 1982)

Chapter 2
Equations and Phenomenology

In this section, we present the basic equations that are used to describe charged fluid flows, and the basic phenomenology of low-frequency turbulence. Readers interested in examining closely this subject can refer to the very wide literature on the subject of turbulence in fluid flows, as for example the recent books by, e.g., Pope (2000), McComb (1990), Frisch (1995) or many others, and the less known literature on MHD flows (Biskamp 1993; Boyd and Sanderson 2003; Biskamp 2003). In order to describe a plasma as a continuous medium it will be assumed collisional and, as a consequence, all quantities will be functions of space $\mathbf{r}$ and time t. Apart for the required quasi-neutrality, the basic assumption of MHD is that fields fluctuate on the same time and length scale as the plasma variables, say $\omega\tau_{\mathrm{H}} \simeq 1$ and $kL_{\mathrm{H}} \simeq 1$ (k and ω are, respectively, the wave number and the frequency of the fields, while τ_{H} and L_{H} are the hydrodynamic time and length scale, respectively). Since the plasma is treated as a single fluid, we have to take the slow rates of ions. A simple analysis shows also that the electrostatic force and the displacement current can be neglected in the non-relativistic approximation. Then, MHD equations can be derived as shown in the following sections.

2.1 The Navier–Stokes Equation and the Reynolds Number

Equations which describe the dynamics of real incompressible fluid flows have been introduced by Claude-Louis Navier in 1823 and improved by George G. Stokes. They are nothing but the momentum equation based on Newton's second law, which relates the acceleration of a fluid particle[1] to the resulting volume and

[1] A fluid particle is defined as an infinitesimal portion of fluid which moves with the local velocity. As usual in fluid dynamics, infinitesimal means small with respect to large scale, but large enough with respect to molecular scales.

R. Bruno, V. Carbone, *Turbulence in the Solar Wind*, Lecture Notes in Physics 928, DOI 10.1007/978-3-319-43440-7_2

body forces acting on it. These equations have been introduced by Leonhard Euler, however, the main contribution by Navier was to add a friction forcing term due to the interactions between fluid layers which move with different speed. This term results to be proportional to the viscosity coefficients η and ξ and to the variation of speed. By defining the velocity field $\mathbf{u}(\mathbf{r}, t)$ the kinetic pressure p and the density ρ, the equations describing a fluid flow are the continuity equation to describe the conservation of mass

$$\frac{\partial \rho}{\partial t} + (\mathbf{u} \cdot \nabla)\, \rho = -\rho \boldsymbol{\nabla} \cdot \mathbf{u}, \tag{2.1}$$

the equation for the conservation of momentum

$$\rho \left[\frac{\partial \mathbf{u}}{\partial t} + (\mathbf{u} \cdot \nabla)\, \mathbf{u} \right] = -\nabla p + \eta \nabla^2 \mathbf{u} + \left(\xi + \frac{\eta}{3} \right) \nabla \left(\boldsymbol{\nabla} \cdot \mathbf{u} \right), \tag{2.2}$$

and an equation for the conservation of energy

$$\rho T \left[\frac{\partial s}{\partial t} + (\mathbf{u} \cdot \nabla) s \right] = \boldsymbol{\nabla} \cdot (\chi \nabla T) + \frac{\eta}{2} \left(\frac{\partial u_i}{\partial x_k} + \frac{\partial u_k}{\partial x_i} - \frac{2}{3} \delta_{ik} \boldsymbol{\nabla} \cdot \mathbf{u} \right)^2 + \xi (\boldsymbol{\nabla} \cdot \mathbf{u})^2, \tag{2.3}$$

where s is the entropy per mass unit, T is the temperature, and χ is the coefficient of thermoconduction. An equation of state closes the system of fluid equations.

The above equations considerably simplify if we consider the incompressible fluid, where $\rho = \text{const.}$ so that we obtain the Navier–Stokes (NS) equation

$$\frac{\partial \mathbf{u}}{\partial t} + (\mathbf{u} \cdot \nabla)\, \mathbf{u} = -\left(\frac{\nabla p}{\rho} \right) + \nu \nabla^2 \mathbf{u}, \tag{2.4}$$

where the coefficient $\nu = \eta / \rho$ is the kinematic viscosity. The incompressibility of the flow translates in a condition on the velocity field, namely the field is divergence-free, i.e., $\boldsymbol{\nabla} \cdot \mathbf{u} = 0$. This condition eliminates all high-frequency sound waves and is called the incompressible limit. The non-linear term in equations represents the convective (or substantial) derivative. Of course, we can add on the right hand side of this equation all external forces, which eventually act on the fluid parcel.

We use the velocity scale U and the length scale L to define dimensionless independent variables, namely $\mathbf{r} = \mathbf{r}' L$ (from which $\nabla = \nabla' / L$) and $t = t'(L/U)$, and dependent variables $\mathbf{u} = \mathbf{u}' U$ and $p = p' U^2 \rho$. Then, using these variables in Eq. (2.4), we obtain

$$\frac{\partial \mathbf{u}'}{\partial t'} + \left(\mathbf{u}' \cdot \nabla' \right) \mathbf{u}' = -\nabla' p' + Re^{-1} \nabla'^2 \mathbf{u}'. \tag{2.5}$$

The Reynolds number $Re = UL/\nu$ is evidently the only parameter of the fluid flow. This defines a Reynolds number similarity for fluid flows, namely fluids with

the same value of the Reynolds number behaves in the same way. Looking at Eq. (2.5) it can be realized that the Reynolds number represents a measure of the relative strength between the non-linear convective term and the viscous term in Eq. (2.4). The higher *Re*, the more important the non-linear term is in the dynamics of the flow. Turbulence is a genuine result of the non-linear dynamics of fluid flows.

2.2 The Coupling Between a Charged Fluid and the Magnetic Field

Magnetic fields are ubiquitous in the Universe and are dynamically important. At high frequencies, kinetic effects are dominant, but at frequencies lower than the ion cyclotron frequency, the evolution of plasma can be modeled using the MHD approximation. Furthermore, dissipative phenomena can be neglected at large scales although their effects will be felt because of non-locality of non-linear interactions. In the presence of a magnetic field, the Lorentz force $\mathbf{j} \times \mathbf{B}$, where $\mathbf{j}$ is the electric current density, must be added to the fluid equations, namely

$$\rho\left[\frac{\partial \mathbf{u}}{\partial t} + (\mathbf{u}\cdot\nabla)\,\mathbf{u}\right] = -\nabla p + \eta\nabla^2\mathbf{u} + \left(\xi + \frac{\eta}{3}\right)\nabla\,(\nabla\cdot\mathbf{u}) - \frac{1}{4\pi}\mathbf{B}\times(\nabla\times\mathbf{B}), \tag{2.6}$$

and the Joule heat must be added to the equation for energy

$$\rho T\left[\frac{\partial s}{\partial t} + (\mathbf{u}\cdot\nabla)s\right] = \sigma_{ik}\frac{\partial u_i}{\partial x_k} + \chi\nabla^2 T + \frac{c^2}{16\pi^2\sigma}(\nabla\times\mathbf{B})^2, \tag{2.7}$$

where σ is the conductivity of the medium, and we introduced the viscous stress tensor

$$\sigma_{ik} = \eta\left(\frac{\partial u_i}{\partial x_k} + \frac{\partial u_k}{\partial x_i} - \frac{2}{3}\delta_{ik}\nabla\cdot\mathbf{u}\right) + \xi\delta_{ik}\nabla\cdot\mathbf{u}. \tag{2.8}$$

An equation for the magnetic field stems from the Maxwell equations in which the displacement current is neglected under the assumption that the velocity of the fluid under consideration is much smaller than the speed of light. Then, using

$$\nabla\times\mathbf{B} = \mu_0\mathbf{j}$$

and the Ohm's law for a conductor in motion with a speed $\mathbf{u}$ in a magnetic field

$$\mathbf{j} = \sigma\,(\mathbf{E} + \mathbf{u}\times\mathbf{B})\,,$$

we obtain the induction equation which describes the time evolution of the magnetic field

$$\frac{\partial \mathbf{B}}{\partial t} = \nabla \times (\mathbf{u} \times \mathbf{B}) + (1/\sigma\mu_0)\nabla^2 \mathbf{B}, \tag{2.9}$$

together with the constraint $\nabla \cdot \mathbf{B} = 0$ (no magnetic monopoles in the classical case).

In the incompressible case, where $\nabla \cdot \mathbf{u} = 0$, MHD equations can be reduced to

$$\frac{\partial \mathbf{u}}{\partial t} + (\mathbf{u} \cdot \nabla)\,\mathbf{u} = -\nabla P_{\text{tot}} + \nu \nabla^2 \mathbf{u} + (\mathbf{b} \cdot \nabla)\,\mathbf{b} \tag{2.10}$$

and

$$\frac{\partial \mathbf{b}}{\partial t} + (\mathbf{u} \cdot \nabla)\,\mathbf{b} = -\,(\mathbf{b} \cdot \nabla)\,\mathbf{u} + \eta \nabla^2 \mathbf{b}. \tag{2.11}$$

Here P_{tot} is the total kinetic $P_k = nkT$ plus magnetic pressure $P_{\text{m}} = B^2/8\pi$, divided by the constant mass density ρ. Moreover, we introduced the velocity variables $\mathbf{b} = \mathbf{B}/\sqrt{4\pi\rho}$ and the magnetic diffusivity η.

Similar to the usual Reynolds number, a magnetic Reynolds number R_{m} can be defined, namely

$$R_{\text{m}} = \frac{\mathbf{c}_{\text{A}} L_0}{\eta}\,,$$

where $\mathbf{c}_{\text{A}} = \mathbf{B_0}/\sqrt{4\pi\rho}$ is the Alfvén speed related to the large-scale L_0 magnetic field $\mathbf{B_0}$. This number in most circumstances in astrophysics is very large, but the ratio of the two Reynolds numbers or, in other words, the magnetic Prandtl number $P_{\text{m}} = \nu/\eta$ can differ widely. In absence of dissipative terms, for each volume V MHD equations conserve the total energy $E(t)$

$$E(t) = \int_V (v^2 + b^2)\, d^3\mathbf{r}\,, \tag{2.12}$$

the cross-helicity $H_{\text{c}}(t)$, which represents a measure of the degree of correlations between velocity and magnetic fields

$$H_{\text{c}}(t) = \int_V \mathbf{v} \cdot \mathbf{b}\, d^3\mathbf{r}\,, \tag{2.13}$$

and the magnetic helicity $H(t)$, which represents a measure of the degree of linkage among magnetic flux tubes

$$H(t) = \int_V \mathbf{a} \cdot \mathbf{b}\, d^3\mathbf{r}\,, \tag{2.14}$$

where $\mathbf{b} = \nabla \times \mathbf{a}$.

The change of variable due to Elsässer (1950), say $\mathbf{z}^{\pm} = \mathbf{u} \pm \mathbf{b}'$, where we explicitly use the background uniform magnetic field $\mathbf{b}' = \mathbf{b} + \mathbf{c}_{\mathrm{A}}$ (at variance with the bulk velocity, the largest scale magnetic field cannot be eliminated through a Galilean transformation), leads to the more symmetrical form of the MHD equations in the incompressible case

$$\frac{\partial \mathbf{z}^{\pm}}{\partial t} \mp (\mathbf{c}_{\mathrm{A}} \cdot \nabla)\, \mathbf{z}^{\pm} + \left(\mathbf{z}^{\mp} \cdot \nabla\right) \mathbf{z}^{\pm} = -\nabla P_{\mathrm{tot}} + \nu^{\pm} \nabla^2 \mathbf{z}^{\pm} + \nu^{\mp} \nabla^2 \mathbf{z}^{\mp} + \mathbf{F}^{\pm}, \qquad (2.15)$$

where $2\nu^{\pm} = \nu \pm \eta$ are the dissipative coefficients, and $\mathbf{F}^{\pm}$ are eventual external forcing terms. The relations $\nabla \cdot \mathbf{z}^{\pm} = 0$ complete the set of equations. On linearizing Eq. (2.15) and neglecting both the viscous and the external forcing terms, we have

$$\frac{\partial \mathbf{z}^{\pm}}{\partial t} \mp (\mathbf{c}_{\mathrm{A}} \cdot \nabla)\, \mathbf{z}^{\pm} \simeq 0,$$

which shows that $\mathbf{z}^{-}(\mathbf{x} - \mathbf{c}_{\mathrm{A}} t)$ describes Alfvénic fluctuations propagating in the direction of $\mathbf{B_0}$, and $\mathbf{z}^{+}(\mathbf{x} + \mathbf{c}_{\mathrm{A}} t)$ describes Alfvénic fluctuations propagating opposite to $\mathbf{B_0}$. Note that MHD equations (2.15) have the same structure as the Navier–Stokes equation, the main difference stems from the fact that non-linear coupling happens only between fluctuations propagating in opposite directions. As we will see, this has a deep influence on turbulence described by MHD equations.

It is worthwhile to remark that in the classical hydrodynamics, dissipative processes are defined through three coefficients, namely two viscosities and one thermoconduction coefficient. In the hydromagnetic case the number of coefficients increases considerably. Apart from few additional electrical coefficients, we have a large-scale (background) magnetic field $\mathbf{B_0}$. This makes the MHD equations intrinsically anisotropic. Furthermore, the stress tensor (2.8) is deeply modified by the presence of a magnetic field $\mathbf{B_0}$, in that kinetic viscous coefficients must depend on the magnitude and direction of the magnetic field (Braginskii 1965). This has a strong influence on the determination of the Reynolds number.

2.3 Scaling Features of the Equations

The scaled Euler equations are the same as Eqs. (2.4) and (2.5), but without the term proportional to R^{-1}. The scaled variables obtained from the Euler equations are, then, the same. Thus, scaled variables exhibit scaling similarity, and the Euler equations are said to be invariant with respect to scale transformations. Said differently, this means that NS equations (2.4) show scaling properties (Frisch 1995), that is, there exists a class of solutions which are invariant under scaling transformations. Introducing a length scale ℓ, it is straightforward to verify that the scaling transformations $\ell \rightarrow \lambda \ell'$ and $\mathbf{u} \rightarrow \lambda^h \mathbf{u}'$ (λ is a scaling factor and h is a scaling index) leave invariant the inviscid NS equation for any scaling

exponent h, providing $P \rightarrow \lambda^{2h} P'$. When the dissipative term is taken into account, a characteristic length scale exists, say the dissipative scale ℓ_{D}. From a phenomenological point of view, this is the length scale where dissipative effects start to be experienced by the flow. Of course, since ν is in general very low, we expect that ℓ_{D} is very small. Actually, there exists a simple relationship for the scaling of ℓ_{D} with the Reynolds number, namely $\ell_{\mathrm{D}} \sim LRe^{-3/4}$. The larger the Reynolds number, the smaller the dissipative length scale.

As it is easily verified, ideal MHD equations display similar scaling features. Say the following scaling transformations $\mathbf{u} \rightarrow \lambda^h \mathbf{u}'$ and $\mathbf{B} \rightarrow \lambda^\beta \mathbf{B}'$ (β here is a new scaling index different from h), leave the inviscid MHD equations unchanged, providing $P \rightarrow \lambda^{2\beta} P'$, $T \rightarrow \lambda^{2h} T'$, and $\rho \rightarrow \lambda^{2(\beta-h)} \rho'$. This means that velocity and magnetic variables have different scalings, say $h \neq \beta$, only when the scaling for the density is taken into account. In the incompressible case, we cannot distinguish between scaling laws for velocity and magnetic variables.

2.4 The Non-linear Energy Cascade

The basic properties of turbulence, as derived both from the Navier–Stokes equation and from phenomenological considerations, is the *legacy* of A. N. Kolmogorov (Frisch 1995).[2] Phenomenology is based on the old picture by Richardson who realized that turbulence is made by a collection of eddies at all scales. Energy, injected at a length scale L, is transferred by non-linear interactions to small scales where it is dissipated at a characteristic scale ℓ_{D}, the length scale where dissipation takes place. The main idea is that at very large Reynolds numbers, the injection scale L and the dissipative scale ℓ_{D} are completely separated. In a stationary situation, the energy injection rate must be balanced by the energy dissipation rate and must also be the same as the energy transfer rate ε measured at any scale ℓ within the inertial range $\ell_{\mathrm{D}} \ll \ell \ll L$. From a phenomenological point of view, the energy injection rate at the scale L is given by $\epsilon_L \sim U^2/\tau_L$, where τ_L is a characteristic time for the injection energy process, which results to be $\tau_L \sim L/U$. At the same scale L the energy dissipation rate is due to $\epsilon_D \sim U^2/\tau_D$, where τ_D is the characteristic dissipation time which, from Eq. (2.4), can be estimated to be of the order of $\tau_D \sim L^2/\nu$. As a result, the ratio between the energy injection rate and dissipation rate is

$$\frac{\epsilon_L}{\epsilon_D} \sim \frac{\tau_D}{\tau_L} \sim Re\,, \tag{2.16}$$

that is, the energy injection rate at the largest scale L is Re-times the energy dissipation rate. In other words, in the case of large Reynolds numbers, the fluid

[2] The translation of the original paper by Kolmogorov (1941) can be found in the book edited by Kolmogorov (1991).

system is unable to dissipate the whole energy injected at the scale L. The excess energy must be dissipated at small scales where the dissipation process is much more efficient. This is the physical reason for the energy cascade.

Fully developed turbulence involves a hierarchical process, in which many scales of motion are involved. To look at this phenomenon it is often useful to investigate the behavior of the Fourier coefficients of the fields. Assuming periodic boundary conditions the αth component of velocity field can be Fourier decomposed as

$$u_\alpha(\mathbf{r}, t) = \sum_{\mathbf{k}} u_\alpha(\mathbf{k}, t) \exp(i\mathbf{k} \cdot \mathbf{r}),$$

where $\mathbf{k} = 2\pi\mathbf{n}/L$ and $\mathbf{n}$ is a vector of integers. When used in the Navier–Stokes equation, it is a simple matter to show that the non-linear term becomes the convolution sum

$$\frac{\partial u_\alpha(\mathbf{k}, t)}{\partial t} = M_{\alpha\beta\gamma}(\mathbf{k}) \sum_{\mathbf{q}} u_\gamma(\mathbf{k} - \mathbf{q}, t) u_\beta(\mathbf{q}, t), \tag{2.17}$$

where $M_{\alpha\beta\gamma}(\mathbf{k}) = -ik_\beta(\delta_{\alpha\gamma} - k_\alpha k_\beta/k^2)$ (for the moment we disregard the linear dissipative term).

MHD equations can be written in the same way, say by introducing the Fourier decomposition for Elsässer variables

$$z_\alpha^\pm(\mathbf{r}, t) = \sum_{\mathbf{k}} z_\alpha^\pm(\mathbf{k}, t) \exp(i\mathbf{k} \cdot \mathbf{r}),$$

and using this expression in the MHD equations we obtain an equation which describes the time evolution of each Fourier mode. However, the divergence-less condition means that not all Fourier modes are independent, rather $\mathbf{k} \cdot \mathbf{z}^\pm(\mathbf{k}, t) = 0$ means that we can project the Fourier coefficients on two directions which are mutually orthogonal and orthogonal to the direction of $\mathbf{k}$, that is,

$$\mathbf{z}^\pm(\mathbf{k}, t) = \sum_{a=1}^{2} z_a^\pm(\mathbf{k}, t) \mathbf{e}^{(a)}(\mathbf{k}), \tag{2.18}$$

with the constraint that $\mathbf{k} \cdot \mathbf{e}^{(a)}(\mathbf{k}) = 0$. In presence of a background magnetic field we can use the well defined direction $\mathbf{B_0}$, so that

$$\mathbf{e}^{(1)}(\mathbf{k}) = \frac{i\mathbf{k} \times \mathbf{B_0}}{|\mathbf{k} \times \mathbf{B_0}|}; \qquad \mathbf{e}^{(2)}(\mathbf{k}) = \frac{i\mathbf{k}}{|\mathbf{k}|} \times \mathbf{e}^{(1)}(\mathbf{k}).$$

Note that in the linear approximation where the Elsässer variables represent the usual MHD modes, $z_1^\pm(\mathbf{k}, t)$ represent the amplitude of the Alfvén mode while $z_2^\pm(\mathbf{k}, t)$ represent the amplitude of the incompressible limit of the magnetosonic

mode. From MHD equations (2.15) we obtain the following set of equations:

$$\left[\frac{\partial}{\partial t} \mp i\,(\mathbf{k}\cdot\mathbf{c}_{\mathrm{A}})\right] z_a^{\pm}(\mathbf{k},t) = \left(\frac{L}{2\pi}\right)^3 \sum_{\mathbf{p}+\mathbf{q}=\mathbf{k}}^{\delta} \sum_{b,c=1}^{2} A_{abc}(-\mathbf{k},\mathbf{p},\mathbf{q}) z_b^{\pm}(\mathbf{p},t) z_c^{\mp}(\mathbf{q},t). \tag{2.19}$$

The coupling coefficients, which satisfy the symmetry condition $A_{abc}(\mathbf{k},\mathbf{p},\mathbf{q}) = -A_{bac}(\mathbf{p},\mathbf{k},\mathbf{q})$, are defined as

$$A_{abc}(-\mathbf{k},\mathbf{p},\mathbf{q}) = \left[(i\mathbf{k})^{\star}\cdot\mathbf{e}^{(c)}(\mathbf{q})\right]\left[\mathbf{e}^{(a)*}(\mathbf{k})\cdot\mathbf{e}^{(b)}(\mathbf{p})\right],$$

and the sum in Eq. (2.19) is defined as

$$\sum_{\mathbf{p}+\mathbf{q}=\mathbf{k}}^{\delta} \equiv \left(\frac{2\pi}{L}\right)^3 \sum_{\mathbf{p}}\sum_{\mathbf{q}} \delta_{\mathbf{k},\mathbf{p}+\mathbf{q}},$$

where $\delta_{\mathbf{k},\mathbf{p}+\mathbf{q}}$ is the Kronecher's symbol. Quadratic non-linearities of the original equations correspond to a convolution term involving wave vectors $\mathbf{k}$, $\mathbf{p}$ and $\mathbf{q}$ related by the triangular relation $\mathbf{p} = \mathbf{k} - \mathbf{q}$. Fourier coefficients locally couple to generate an energy transfer from any pair of modes $\mathbf{p}$ and $\mathbf{q}$ to a mode $\mathbf{k} = \mathbf{p} + \mathbf{q}$.

The pseudo-energies $E^{\pm}(t)$ are defined as

$$E^{\pm}(t) = \frac{1}{2}\frac{1}{L^3}\int_{L^3} |\mathbf{z}^{\pm}(\mathbf{r},t)|^2 d^3\mathbf{r} = \frac{1}{2}\sum_{\mathbf{k}}\sum_{a=1}^{2} |z_a^{\pm}(\mathbf{k},t)|^2$$

and, after some algebra, it can be shown that the non-linear term of Eq. (2.19) conserves separately $E^{\pm}(t)$. This means that both the total energy $E(t) = E^{+} + E^{-}$ and the cross-helicity $E_{\mathrm{c}}(t) = E^{+} - E^{-}$, say the correlation between velocity and magnetic field, are conserved in absence of dissipation and external forcing terms.

In the idealized homogeneous and isotropic situation we can define the pseudo-energy tensor, which using the incompressibility condition can be written as

$$U_{ab}^{\pm}(\mathbf{k},t) \equiv \left(\frac{L}{2\pi}\right)^3 \left\langle z_a^{\pm}(\mathbf{k},t) z_b^{\pm}(\mathbf{k},t)\right\rangle = \left(\delta_{ab} - \frac{k_a k_b}{k^2}\right) q^{\pm}(k),$$

brackets being ensemble averages, where $q^{\pm}(k)$ is an arbitrary odd function of the wave vector k and represents the pseudo-energies spectral density. When integrated over all wave vectors under the assumption of isotropy

$$Tr\left[\int d^3\mathbf{k}\; U_{ab}^{\pm}(\mathbf{k},t)\right] = 2\int_0^{\infty} E^{\pm}(k,t)dk,$$

where we introduce the spectral pseudo-energy $E^{\pm}(k,t) = 4\pi k^2 q^{\pm}(k,t)$. This last quantity can be measured, and it is shown that it satisfies the equations

$$\frac{\partial E^{\pm}(k,t)}{\partial t} = T^{\pm}(k,t) - 2\nu k^2 E^{\pm}(k,t) + F^{\pm}(k,t). \tag{2.20}$$

We use $\nu = \eta$ in order not to worry about coupling between $+$ and $-$ modes in the dissipative range. Since the non-linear term conserves total pseudo-energies we have

$$\int_0^{\infty} dk\, T^{\pm}(k,t) = 0,$$

so that, when integrated over all wave vectors, we obtain the energy balance equation for the total pseudo-energies

$$\frac{dE^{\pm}(t)}{dt} = \int_0^{\infty} dk\, F^{\pm}(k,t) - 2\nu \int_0^{\infty} dk\, k^2 E^{\pm}(k,t). \tag{2.21}$$

This last equation simply means that the time variations of pseudo-energies are due to the difference between the injected power and the dissipated power, so that in a stationary state

$$\int_0^{\infty} dk\, F^{\pm}(k,t) = 2\nu \int_0^{\infty} dk\, k^2 E^{\pm}(k,t) = \epsilon^{\pm}.$$

Looking at Eq. (2.20), we see that the role played by the non-linear term is that of a redistribution of energy among the various wave vectors. This is the physical meaning of the non-linear energy cascade of turbulence.

2.5 The Inhomogeneous Case

Equations (2.20) refer to the standard homogeneous and incompressible MHD. Of course, the solar wind is inhomogeneous and compressible and the energy transfer equations can be as complicated as we want by modeling all possible physical effects like, for example, the wind expansion or the inhomogeneous large-scale magnetic field. Of course, simulations of all turbulent scales requires a computational effort which is beyond the actual possibilities. A way to overcome this limitation is to introduce some turbulence modeling of the various physical effects. For example, a set of equations for the cross-correlation functions of both Elsässer fluctuations have been developed independently by Marsch and Tu (1989), Zhou and Matthaeus (1990), Oughton and Matthaeus (1992), and Tu and Marsch (1990), following Marsch and Mangeney (1987) (see review by Tu and Marsch

1996), and are based on some rather strong assumptions: (1) a two-scale separation, and (2) small-scale fluctuations are represented as a kind of stochastic process (Tu and Marsch 1996). These equations look quite complicated, and just a comparison based on order-of-magnitude estimates can be made between them and solar wind observations (Tu and Marsch 1996).

A different approach, introduced by Grappin et al. (1993), is based on the so-called "expanding-box model" (Grappin and Velli 1996; Liewer et al. 2001; Hellinger et al. 2005). The model uses transformation of variables to the moving solar wind frame that expands together with the size of the parcel of plasma as it propagates outward from the Sun. Despite the model requires several simplifying assumptions, like for example lateral expansion only for the wave-packets and constant solar wind speed, as well as a second-order approximation for coordinate transformation (Liewer et al. 2001) to remain tractable, it provides qualitatively good description of the solar wind expansions, thus connecting the disparate scales of the plasma in the various parts of the heliosphere.

2.6 Dynamical System Approach to Turbulence

In the limit of fully developed turbulence, when dissipation goes to zero, an infinite range of scales are excited, that is, energy lies over all available wave vectors. Dissipation takes place at a typical dissipation length scale which depends on the Reynolds number Re through $\ell_D \sim LRe^{-3/4}$ (for a Kolmogorov spectrum $E(k) \sim k^{-5/3}$). In 3D numerical simulations the minimum number of grid points necessary to obtain information on the fields at these scales is given by $N \sim (L/\ell_D)^3 \sim Re^{9/4}$. This rough estimate shows that a considerable amount of memory is required when we want to perform numerical simulations with high Re. At present, typical values of Reynolds numbers reached in 2D and 3D numerical simulations are of the order of 10^4 and 10^3, respectively. At these values the inertial range spans approximately one decade or a little more.

Given the situation described above, the question of the best description of dynamics which results from original equations, using only a small amount of degree of freedom, becomes a very important issue. This can be achieved by introducing turbulence models which are investigated using tools of dynamical system theory (Bohr et al. 1998). Dynamical systems, then, are solutions of minimal sets of ordinary differential equations that can mimic the gross features of energy cascade in turbulence. These studies are motivated by the famous Lorenz's model (Lorenz 1963) which, containing only three degrees of freedom, simulates the complex chaotic behavior of turbulent atmospheric flows, becoming a paradigm for the study of chaotic systems.

The Lorenz's model has been used as a paradigm as far as the transition to turbulence is concerned. Actually, since the solar wind is in a state of fully developed turbulence, the topic of the transition to turbulence is not so close to the main goal of this review. However, since their importance in the theory of dynamical systems,

we spend few sentences abut this central topic. Up to the Lorenz's chaotic model, studies on the birth of turbulence dealt with linear and, very rarely, with weak non-linear evolution of external disturbances. The first physical model of laminar-turbulent transition is due to Landau and it is reported in the fourth volume of the course on Theoretical Physics (Landau and Lifshitz 1971). According to this model, as the Reynolds number is increased, the transition is due to a infinite series of Hopf bifurcations at fixed values of the Reynolds number. Each subsequent bifurcation adds a new incommensurate frequency to the flow whose dynamics become rapidly quasi-periodic. Due to the infinite number of degree of freedom involved, the quasi-periodic dynamics resembles that of a turbulent flow.

The Landau transition scenario is, however, untenable because incommensurate frequencies cannot exist without coupling between them. Ruelle and Takens (1971) proposed a new mathematical model, according to which after few, usually three, Hopf bifurcations the flow becomes suddenly chaotic. In the phase space this state is characterized by a very intricate attracting subset, a *strange attractor*. The flow corresponding to this state is highly irregular and strongly dependent on initial conditions. This characteristic feature is now known as the *butterfly effect* and represents the true definition of deterministic chaos. These authors indicated as an example for the occurrence of a strange attractor the old strange time behavior of the Lorenz's model. The model is a paradigm for the occurrence of turbulence in a deterministic system, it reads

$$\frac{dx}{dt} = P_{\mathrm{r}}(y - x)\,, \qquad \frac{dy}{dt} = Rx - y - xz\,, \qquad \frac{dz}{dt} = xy - bz\,, \tag{2.22}$$

where $x(t)$, $y(t)$, and $z(t)$ represent the first three modes of a Fourier expansion of fluid convective equations in the Boussinesq approximation, P_{r} is the Prandtl number, b is a geometrical parameter, and R is the ratio between the Rayleigh number and the critical Rayleigh number for convective motion. The time evolution of the variables $x(t)$, $y(t)$, and $z(t)$ is reported in Fig. 2.1. A reproduction of the Lorenz *butterfly* attractor, namely the projection of the variables on the plane (x, z) is shown in Fig. 2.2. A few years later, Gollub and Swinney (1975) performed very sophisticated experiments,[3] concluding that the transition to turbulence in a flow between co-rotating cylinders is described by the Ruelle and Takens (1971) model rather than by the Landau scenario.

After this discovery, the strange attractor model gained a lot of popularity, thus stimulating a large number of further studies on the time evolution of non-linear dynamical systems. An enormous number of papers on chaos rapidly appeared in literature, quite in all fields of physics, and transition to chaos became a new topic. Of course, further studies on chaos rapidly lost touch with turbulence studies

[3]These authors were the first ones to use physical technologies and methodologies to investigate turbulent flows from an experimental point of view. Before them, experimental studies on turbulence were motivated mainly by engineering aspects.

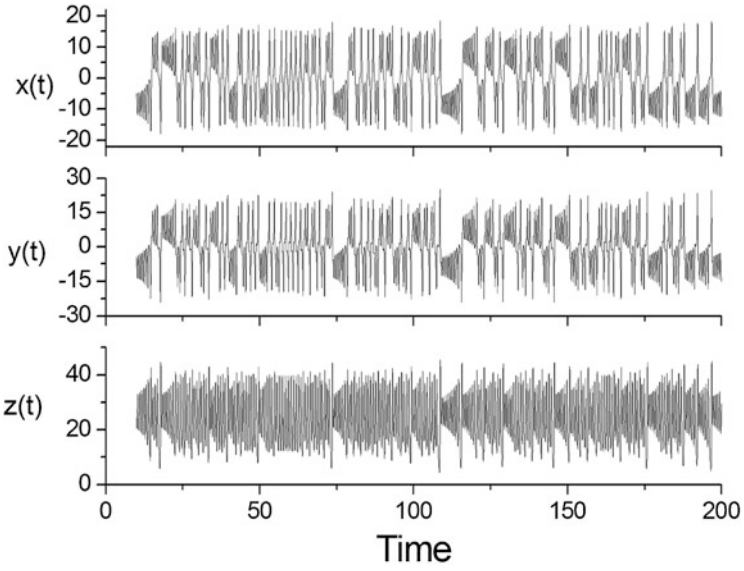

Fig. 2.1 Time evolution of the variables $x(t)$, $y(t)$, and $z(t)$ in the Lorenz's model [see Eq. (2.22)]. This figure has been obtained by using the parameters $P_r = 10$, $b = 8/3$, and $R = 28$

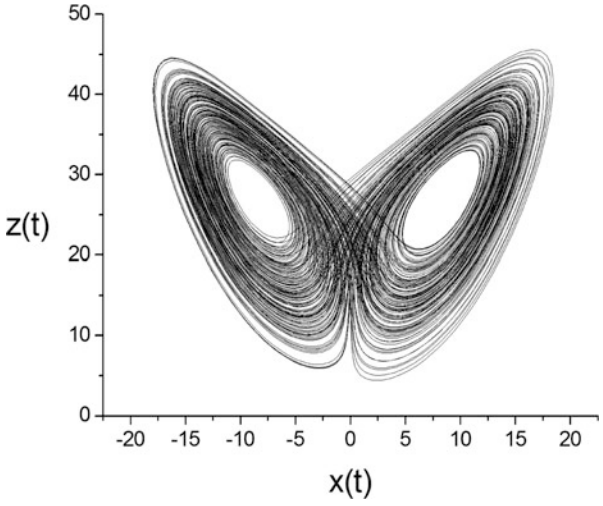

Fig. 2.2 The Lorenz *butterfly* attractor, namely the time behavior of the variables $z(t)$ vs. $x(t)$ as obtained from the Lorenz's model [see Eq. (2.22)]. This figure has been obtained by using the parameters $P_r = 10$, $b = 8/3$, and $R = 28$

and turbulence, as reported by Feynman et al. (1977), still remains ... *the last great unsolved problem of the classical physics*. Furthermore, we like to cite recent theoretical efforts made by Chian et al. (1998, 2003) related to the onset of Alfvénic turbulence. These authors, numerically solved the derivative non-linear Schrödinger equation (Mjølhus 1976; Ghosh and Papadopoulos 1987) which governs the spatio-temporal dynamics of non-linear Alfvén waves, and found that Alfvénic intermittent turbulence is characterized by strange attractors. Note that, the physics involved in the derivative non-linear Schrödinger equation, and in particular the spatio-temporal dynamics of non-linear Alfvén waves, cannot be described by the usual incompressible MHD equations. Rather dispersive effects are required. At variance with the usual MHD, this can be satisfied by requiring that the effect of ion inertia be taken into account. This results in a generalized Ohm's law by including a $(\underline{j}\times\underline{B})$-term, which represents the compressible Hall correction to MHD, say the so-called compressible Hall-MHD model.

In this context turbulence can evolve via two distinct routes: Pomeau–Manneville intermittency (Pomeau and Manneville 1980) and crisis-induced intermittency (Ott and Sommerer 1994). Both types of chaotic transitions follow episodic switching between different temporal behaviors. In one case (Pomeau–Manneville) the behavior of the magnetic fluctuations evolve from nearly periodic to chaotic while, in the other case the behavior intermittently assumes weakly chaotic or strongly chaotic features.

2.7 Shell Models for Turbulence Cascade

Since numerical simulations, in some cases, cannot be used, simple dynamical systems can be introduced to investigate, for example, statistical properties of turbulent flows which can be compared with observations. These models, which try to mimic the gross features of the time evolution of spectral Navier–Stokes or MHD equations, are often called "shell models" or "discrete cascade models". Starting from the old papers by Siggia (1977) different shell models have been introduced in literature for 3D fluid turbulence (Biferale 2003). MHD shell models have been introduced to describe the MHD turbulent cascade (Plunian et al. 2012), starting from the paper by Gloaguen et al. (1985).

The most used shell model is usually quoted in literature as the GOY model, and has been introduced some time ago by Gledzer (1973) and by Ohkitani and Yamada (1989). Apart from the first MHD shell model (Gloaguen et al. 1985), further models, like those by Frick and Sokoloff (1998) and Giuliani and Carbone (1998) have been introduced and investigated in detail. In particular, the latter ones represent the counterpart of the hydrodynamic GOY model, that is they coincide with the usual GOY model when the magnetic variables are set to zero.

In the following, we will refer to the MHD shell model as the FSGC model. The shell model can be built up through four different steps:

(a) Introduce discrete wave vectors:
As a first step we divide the wave vector space in a discrete number of shells whose radii grow according to a power $k_n = k_0\lambda^n$, where $\lambda > 1$ is the inter-shell ratio, k_0 is the fundamental wave vector related to the largest available length scale L, and $n = 1, 2, \ldots, N$.

(b) Assign to each shell discrete scalar variables:
Each shell is assigned two or more complex scalar variables $u_n(t)$ and $b_n(t)$, or Elsässer variables $Z_n^{\pm}(t) = u_n \pm b_n(t)$. These variables describe the chaotic dynamics of modes in the shell of wave vectors between k_n and k_{n+1}. It is worth noting that the discrete variable, mimicking the average behavior of Fourier modes within each shell, represents characteristic fluctuations across eddies at the scale $\ell_n \sim k_n^{-1}$. That is, the fields have the same scalings as field differences, for example $Z_n^{\pm} \sim |Z^{\pm}(x + \ell_n) - Z^{\pm}(x)| \sim \ell_n^h$ in fully developed turbulence. In this way, the possibility to describe spatial behavior within the model is ruled out. We can only get, from a dynamical shell model, time series for shell variables at a given k_n, and we loose the fact that turbulence is a typical temporal and spatial complex phenomenon.

(c) Introduce a dynamical model which describes non-linear evolution:
Looking at Eq. (2.19) a model must have quadratic non-linearities among opposite variables $Z_n^{\pm}(t)$ and $Z_n^{\mp}(t)$, and must couple different shells with free coupling coefficients.

(d) Fix as much as possible the coupling coefficients:
This last step is not standard. A numerical investigation of the model might require the scanning of the properties of the system when all coefficients are varied. Coupling coefficients can be fixed by imposing the conservation laws of the original equations, namely the total pseudo-energies

$$E^{\pm}(t) = \frac{1}{2}\sum_n \left|Z_n^{\pm}\right|^2 ,$$

that means the conservation of both the total energy and the cross-helicity:

$$E(t) = \frac{1}{2}\sum_n |u_n|^2 + |b_n|^2 \; ; \qquad H_c(t) = \sum_n 2\Re e\left(u_n b_n^*\right) ,$$

where $\Re e$ indicates the real part of the product $u_n b_n^*$. As we said before, shell models cannot describe spatial geometry of non-linear interactions in turbulence, so that we loose the possibility of distinguishing between two-dimensional and three-dimensional turbulent behavior. The distinction is, however, of primary importance, for example as far as the dynamo effect is

concerned in MHD. However, there is a third invariant which we can impose, namely

$$H(t) = \sum_n (-1)^n \frac{|b_n|^2}{k_n^\alpha}, \tag{2.23}$$

which can be dimensionally identified as the magnetic helicity when $\alpha = 1$, so that the shell model so obtained is able to mimic a kind of 3D MHD turbulence (Giuliani and Carbone 1998).

After some algebra, taking into account both the dissipative and forcing terms, FSGC model can be written as

$$\frac{dZ_n^\pm}{dt} = ik_n \Phi_n^{\pm *} + \frac{\nu \pm \mu}{2} k_n^2 Z_n^+ + \frac{\nu \mp \mu}{2} k_n^2 Z_n^- + F_n^\pm, \tag{2.24}$$

where

$$\begin{aligned} \Phi_n^\pm = & \left(\frac{2-a-c}{2}\right) Z_{n+2}^\pm Z_{n+1}^\mp + \left(\frac{a+c}{2}\right) Z_{n+1}^\pm Z_{n+2}^\mp + \\ & + \left(\frac{c-a}{2\lambda}\right) Z_{n-1}^\pm Z_{n+1}^\mp - \left(\frac{a+c}{2\lambda}\right) Z_{n-1}^\mp Z_{n+1}^\pm + \\ & - \left(\frac{c-a}{2\lambda^2}\right) Z_{n-2}^\mp Z_{n-1}^\pm - \left(\frac{2-a-c}{2\lambda^2}\right) Z_{n-1}^\mp Z_{n-2}^\pm, \end{aligned} \tag{2.25}$$

where[4] $\lambda = 2$, $a = 1/2$, and $c = 1/3$. In the following, we will consider only the case where the dissipative coefficients are the same, i.e., $\nu = \mu$.

2.8 The Phenomenology of Fully Developed Turbulence: Fluid-Like Case

Here we present the phenomenology of fully developed turbulence, as far as the scaling properties are concerned. In this way we are able to recover a universal form for the spectral pseudo-energy in the stationary case. In real space a common tool to investigate statistical properties of turbulence is represented by field increments $\Delta z_\ell^\pm(\mathbf{r}) = \left[\mathbf{z}^\pm(\mathbf{r}+\ell) - \mathbf{z}^\pm(\mathbf{r})\right] \cdot \mathbf{e}$, being $\mathbf{e}$ the longitudinal direction. These

[4] We can use a different definition for the third invariant $H(t)$, for example a quantity positive defined, without the term $(-1)^n$ and with $\alpha = 2$. This can be identified as the surrogate of the square of the vector potential, thus investigating a kind of 2D MHD. In this case, we obtain a shell model with $\lambda = 2$, $a = 5/4$, and $c = -1/3$. However, this model does not reproduce the inverse cascade of the square of magnetic potential observed in the true 2D MHD equations.

stochastic quantities represent fluctuations[5] across eddies at the scale ℓ. The scaling invariance of MHD equations (cf. Sect. 2.3), from a phenomenological point of view, implies that we expect solutions where $\Delta z_\ell^\pm \sim \ell^h$. All the statistical properties of the field depend only on the scale ℓ, on the mean pseudo-energy dissipation rates $\varepsilon^\pm$, and on the viscosity ν. Also, $\varepsilon^\pm$ is supposed to be the common value of the injection, transfer and dissipation rates. Moreover, the dependence on the viscosity only arises at small scales, near the bottom of the inertial range. Under these assumptions the typical pseudo-energy dissipation rate per unit mass scales as $\varepsilon^\pm \sim \left(\Delta z_\ell^\pm\right)^2 / t_\ell^\pm$. The time $t_\ell^\pm$ associated with the scale ℓ is the typical time needed for the energy to be transferred on a smaller scale, say the eddy turnover time $t_\ell^\pm \sim \ell / \Delta z_\ell^\mp$, so that

$$\varepsilon^\pm \sim \left(\Delta z_\ell^\pm\right)^2 \Delta z^\mp / \ell.$$

When we conjecture that both $\Delta z^\pm$ fluctuations have the same scaling laws, namely $\Delta z^\pm \sim \ell^h$, we recover the Kolmogorov scaling for the field increments

$$\Delta z_\ell^\pm \sim (\varepsilon^\pm)^{1/3} \ell^{1/3}. \tag{2.26}$$

Usually, we refer to this scaling as the K41 model (Kolmogorov 1941, 1991; Frisch 1995). Note that, since from dimensional considerations the scaling of the energy transfer rate should be $\varepsilon^\pm \sim \ell^{1-3h}$, $h = 1/3$ is the choice to guarantee the absence of scaling for $\varepsilon^\pm$.

In the real space turbulence properties can be described using either the probability distribution functions (PDFs hereafter) of increments, or the *longitudinal structure functions*, which represents nothing but the higher order moments of the field. Disregarding the magnetic field, in a purely fully developed fluid turbulence, this is defined as $S_\ell^{(p)} = \langle \Delta u_\ell^p \rangle$. These quantities, in the inertial range, behave as a power law $S_\ell^{(p)} \sim \ell^{\xi_p}$, so that it is interesting to compute the set of scaling exponent ξ_p. Using, from a phenomenological point of view, the scaling for field increments [see Eq. (2.26)], it is straightforward to compute the scaling laws $S_\ell^{(p)} \sim \ell^{p/3}$. Then $\xi_p = p/3$ results to be a linear function of the order p.

When we assume the scaling law $\Delta z_\ell^\pm \sim \ell^h$, we can compute the high-order moments of the structure functions for increments of the Elsässer variables, namely $\left\langle (\Delta z_\ell^\pm)^p \right\rangle \sim \ell^{\xi_p}$, thus obtaining a linear scaling $\xi_p = p/3$, similar to usual fluid flows. For Gaussianly distributed fields, a particular role is played by the second-order moment, because all moments can be computed from $S_\ell^{(2)}$. It is straightforward to translate the dimensional analysis results to Fourier spectra. The spectral property

[5] We have already defined fluctuations of a field as the difference between the field itself and its average value. This quantity has been defined as $\delta\psi$. Here, the differences $\Delta\psi_\ell$ of the field separated by a distance ℓ represents characteristic fluctuations *at the scale* ℓ, say characteristic fluctuations of the field across specific structures (eddies) that are present at that scale. The reader can realize the difference between both definitions.

of the field can be recovered from $S_\ell^{(2)}$, say in the homogeneous and isotropic case

$$S_\ell^{(2)} = 4 \int_0^\infty E(k) \left(1 - \frac{\sin k\ell}{k\ell}\right) dk,$$

where $k \sim 1/\ell$ is the wave vector, so that in the inertial range where Eq. (2.42) is verified

$$E(k) \sim \varepsilon^{2/3} k^{-5/3}. \tag{2.27}$$

The *Kolmogorov spectrum* [see Eq. (2.27)] is largely observed in all experimental investigations of turbulence, and is considered as the main result of the K41 phenomenology of turbulence (Frisch 1995). However, spectral analysis does not provide a complete description of the statistical properties of the field, unless this has Gaussian properties. The same considerations can be made for the spectral pseudo-energies $E^\pm(k)$, which are related to the second order structure functions $\left\langle \left[\Delta z_\ell^\pm\right]^2 \right\rangle$.

2.9 The Phenomenology of Fully Developed Turbulence: Magnetically-Dominated Case

The phenomenology of the magnetically-dominated case has been investigated by Iroshnikov (1963) and Kraichnan (1965), then developed by Dobrowolny et al. (1980) to tentatively explain the occurrence of the observed Alfvénic turbulence, and finally by Carbone (1993) and Biskamp (1993) to get scaling laws for structure functions. It is based on the Alfvén effect, that is, the decorrelation of interacting eddies, which can be explained phenomenologically as follows. Since non-linear interactions happen only between opposite propagating fluctuations, they are slowed down (with respect to the fluid-like case) by the sweeping of the fluctuations across each other. This means that $\varepsilon^\pm \sim \left(\Delta z_\ell^\pm\right)^2 / T_\ell^\pm$ but the characteristic time $T_\ell^\pm$ required to efficiently transfer energy from an eddy to another eddy at smaller scales cannot be the eddy-turnover time, rather it is increased by a factor $t_\ell^\pm / t_\mathrm{A}$ ($t_\mathrm{A} \sim \ell / \mathbf{c}_\mathrm{A} < t_\ell^\pm$ is the Alfvén time), so that $T_\ell^\pm \sim (t_\ell^\pm)^2 / t_\mathrm{A}$. Then, immediately

$$\varepsilon^\pm \sim \frac{[\Delta z_\ell^\pm]^2 [\Delta z_\ell^\mp]^2}{\ell \mathbf{c}_\mathrm{A}}.$$

This means that both $\pm$ modes are transferred at the same rate to small scales, namely $\epsilon^+ \sim \epsilon^- \sim \epsilon$, and this is the conclusion drawn by Dobrowolny et al. (1980). In reality, this is not fully correct, namely the Alfvén effect yields to the fact that energy transfer rates have the same scaling laws for $\pm$ modes but, we cannot say anything about the amplitudes of ε^+ and ε^- (Carbone 1993). Using the usual scaling law for fluctuations, it can be shown that the scaling behavior holds $\varepsilon \to \lambda^{1-4h} \varepsilon'$.

Then, when the energy transfer rate is constant, we found a scaling law different from that of Kolmogorov and, in particular,

$$\Delta z_\ell^{\pm} \sim (\varepsilon \mathbf{c}_\mathrm{A})^{1/4} \ell^{1/4}. \tag{2.28}$$

Using this phenomenology the high-order moments of fluctuations are given by $S_\ell^{(p)} \sim \ell^{p/4}$. Even in this case, $\xi_p = p/4$ results to be a linear function of the order p. The pseudo-energy spectrum can be easily found to be

$$E^{\pm}(k) \sim (\varepsilon \mathbf{c}_\mathrm{A})^{1/2} k^{-3/2}. \tag{2.29}$$

This is the Iroshnikov–Kraichnan spectrum. However, in a situation in which there is a balance between the linear Alfvén time scale or wave period, and the nonlinear time scale needed to transfer energy to smaller scales, the energy cascade is indicated as *critically balanced* (Goldreich and Sridhar 1995). In these conditions, it can be shown that the power spectrum $P(k)$ would scale as $f^{-5/3}$ when the angle θ_B between the mean field direction and the flow direction is 90° while, the same scaling would follow f^{-2} in case $\theta_B = 0°$ and the spectrum would also have a smaller energy content than in the other case.

2.10 Some Exact Relationships

So far, we have been discussing about the *inertial range* of turbulence. What this means from a heuristic point of view is somewhat clear, but when we try to identify the inertial range from the spectral properties of turbulence, in general the best we can do is to identify the inertial range with the intermediate range of scales where a Kolmogorov's spectrum is observed. The often used identity *inertial range* $\simeq$ *intermediate range*, is somewhat arbitrary. In this regard, a very important result on turbulence, due to Kolmogorov (1941, 1991), is the so-called "4/5-law" which, being obtained from the Navier–Stokes equation, is "*... one of the most important results in fully developed turbulence because it is both exact and nontrivial*" (cf. Frisch 1995). As a matter of fact, Kolmogorov analytically derived the following exact relation for the third order structure function of velocity fluctuations:

$$\left\langle (\Delta v_\parallel(\mathbf{r}, \ell))^3 \right\rangle = -\frac{4}{5}\epsilon \ell \,, \tag{2.30}$$

where $\mathbf{r}$ is the sampling direction, ℓ is the corresponding scale, and ϵ is the mean energy dissipation per unit mass, assumed to be finite and nonvanishing.

This important relation can be obtained in a more general framework from MHD equations. A Yaglom's relation for MHD can be obtained using the analogy of MHD equations with a transport equation, so that we can obtain a relation similar to the Yaglom's equation for the transport of a passive quantity (Monin and Yaglom 1975).

Using the above analogy, the Yaglom's relation has been extended some time ago to MHD turbulence by Chandrasekhar (1967), and recently it has been revised by Politano et al. (1998) and Politano and Pouquet (1998) in the framework of solar wind turbulence. In the following section we report an alternative and more general derivation of the Yaglom's law using structure functions (Sorriso-Valvo et al. 2007; Carbone et al. 2009a).

2.11 Yaglom's Law for MHD Turbulence

To obtain a general law we start from the incompressible MHD equations. If we write twice the MHD equations for two different and independent points x_i and $x'_i = x_i + \ell_i$, by substraction we obtain an equation for the vector differences $\Delta z_i^{\pm} = (z_i^{\pm})' - z_i^{\pm}$. Using the hypothesis of independence of points x'_i and x_i with respect to derivatives, namely $\partial_i (z_j^{\pm})' = \partial'_i z_j^{\pm} = 0$ (where ∂'_i represents derivative with respect to x'_i), we get

$$\partial_t \Delta z_i^{\pm} + \Delta z_\alpha^{\mp} \partial'_\alpha \Delta z_i^{\pm} + z_\alpha^{\mp} (\partial'_\alpha + \partial_\alpha) \Delta z_i^{\pm} = -(\partial'_i + \partial_i) \Delta P + \\ + (\partial_\alpha^{2\prime} + \partial_\alpha^2) \left[\nu^{\pm} \Delta z_i^{+} + \nu^{\mp} \Delta z_i^{-} \right] \tag{2.31}$$

($\Delta P = P'_{\rm tot} - P_{\rm tot}$). We look for an equation for the second-order correlation tensor $\langle \Delta z_i^{\pm} \Delta z_j^{\pm} \rangle$ related to pseudo-energies. Actually the more general thing should be to look for a mixed tensor, namely $\langle \Delta z_i^{\pm} \Delta z_j^{\mp} \rangle$, taking into account not only both pseudo-energies but also the time evolution of the mixed correlations $\langle z_i^{+} z_j^{-} \rangle$ and $\langle z_i^{-} z_j^{+} \rangle$. However, using the DIA closure by Kraichnan, it is possible to show that these elements are in general poorly correlated (Veltri 1980). Since we are interested in the energy cascade, we limit ourselves to the most interesting equation that describes correlations about Alfvénic fluctuations of the same sign. To obtain the equations for pseudo-energies we multiply Eq. (2.31) by $\Delta z_j^{\pm}$, then by averaging we get

$$\partial_t \langle \Delta z_i^{\pm} \Delta z_j^{\pm} \rangle + \frac{\partial}{\partial \ell_\alpha} \langle \Delta Z_\alpha^{\mp} (\Delta z_i^{\pm} \Delta z_j^{\pm}) \rangle = -\Lambda_{ij} - \Pi_{ij} + 2\nu \frac{\partial^2}{\partial \ell_\alpha^2} \langle \Delta z_i^{\pm} \Delta z_j^{\pm} \rangle \\ - \frac{4}{3} \frac{\partial}{\partial \ell_\alpha} (\epsilon_{ij}^{\pm} \ell_\alpha), \tag{2.32}$$

where we used the hypothesis of local homogeneity and incompressibility. In Eq. (2.32) we defined the average dissipation tensor

$$\epsilon_{ij}^{\pm} = \nu \langle (\partial_\alpha Z_i^{\pm}) (\partial_\alpha Z_j^{\pm}) \rangle. \tag{2.33}$$

The first and second term on the r.h.s. of the Eq. (2.32) represent respectively a tensor related to large-scales inhomogeneities

$$\Lambda_{ij} = \langle z_\alpha^\mp (\partial'_\alpha + \partial_\alpha)(\Delta z_i^\pm \Delta z_j^\pm)\rangle \tag{2.34}$$

and the tensor related to the pressure term

$$\Pi_{ij} = \langle \Delta z_j^\pm (\partial'_i + \partial_i)\Delta P + \Delta z_i^\pm (\partial'_j + \partial_j)\Delta P\rangle. \tag{2.35}$$

Furthermore, In order not to worry about couplings between Elsässer variables in the dissipative terms, we make the usual simplifying assumption that kinematic viscosity is equal to magnetic diffusivity, that is $\nu^\pm = \nu^\mp = \nu$. Equation (2.32) is an exact equation for anisotropic MHD equations that links the second-order complete tensor to the third-order mixed tensor via the average dissipation rate tensor. Using the hypothesis of global homogeneity the term $\Lambda_{ij} = 0$, while assuming local isotropy $\Pi_{ij} = 0$. The equation for the trace of the tensor can be written as

$$\partial_t \langle |\Delta z_i^\pm|^2\rangle + \frac{\partial}{\partial \ell_\alpha}\langle \Delta Z_\alpha^\mp |\Delta z_i^\pm|^2\rangle = 2\nu \frac{\partial^2}{\partial \ell_\alpha}\langle |\Delta z_i^\pm|^2\rangle - \frac{4}{3}\frac{\partial}{\partial \ell_\alpha}(\epsilon_{ii}^\pm \ell_\alpha), \tag{2.36}$$

where the various quantities depends on the vector ℓ_α. Moreover, by considering only the trace we ruled out the possibility to investigate anisotropies related to different orientations of vectors within the second-order moment. It is worthwhile to remark here that *only* the diagonal elements of the dissipation rate tensor, namely $\epsilon_{ii}^\pm$ are positive defined while, in general, the off-diagonal elements $\epsilon_{ij}^\pm$ are not positive. For a stationary state the Eq. (2.36) can be written as the divergenceless condition of a quantity involving the third-order correlations and the dissipation rates

$$\frac{\partial}{\partial \ell_\alpha}\left[\langle \Delta z_\alpha^\mp |\Delta z_i^\pm|^2\rangle - 2\nu \frac{\partial}{\partial \ell_\alpha}\langle |\Delta z_i^\pm|^2\rangle - \frac{4}{3}(\epsilon_{ii}^\pm \ell_\alpha)\right] = 0, \tag{2.37}$$

from which we can obtain the Yaglom's relation by projecting Eq. (2.37) along the longitudinal $\ell_\alpha = \ell \mathbf{e}_r$ direction. This operation involves the assumption that the flow is locally isotropic, that is fields depends locally only on the separation ℓ, so that

$$\left(\frac{2}{\ell} + \frac{\partial}{\partial \ell}\right)\left[\langle \Delta z_\ell^\mp |\Delta z_i^\pm|^2\rangle - 2\nu \frac{\partial}{\partial \ell}\langle |\Delta z_i^\pm|^2\rangle + \frac{4}{3}\epsilon_{ii}^\pm \ell\right] = 0. \tag{2.38}$$

The only solution that is compatible with the absence of singularity in the limit $\ell \to 0$ is

$$\langle \Delta z_\ell^\mp |\Delta z_i^\pm|^2\rangle = 2\nu \frac{\partial}{\partial \ell}\langle |\Delta z_i^\pm|^2\rangle - \frac{4}{3}\epsilon_{ii}^\pm \ell, \tag{2.39}$$

which reduces to the Yaglom's law for MHD turbulence as obtained by Politano and Pouquet (1998) in the inertial range when $\nu \to 0$

$$Y_\ell^\pm \equiv \langle \Delta z_\ell^\mp |\Delta z_i^\pm|^2 \rangle = -\frac{4}{3}\epsilon_{ii}^\pm \ell. \tag{2.40}$$

Finally, in the fluid-like case where $z_i^+ = z_i^- = v_i$ we obtain the usual Yaglom's law for fluid flows

$$\langle \Delta v_\ell |\Delta v_i|^2 \rangle = -\frac{4}{3}(\epsilon \ell), \tag{2.41}$$

which in the isotropic case, where $\langle \Delta v_\ell^3 \rangle = 3\langle \Delta v_\ell \Delta v_y^2 \rangle = 3\langle \Delta v_\ell \Delta v_z^2 \rangle$ (Monin and Yaglom 1975), immediately reduces to the Kolmogorov's law

$$\langle \Delta v_\ell^3 \rangle = -\frac{4}{5}\epsilon \ell \tag{2.42}$$

(the separation ℓ has been taken along the streamwise x-direction).

The relations we obtained can be used, or better, in a certain sense they *might* be used, as a formal definition of inertial range. Since they are exact relationships derived from Navier–Stokes and MHD equations under usual hypotheses, they represent a kind of "zeroth-order" conditions on experimental and theoretical analysis of the inertial range properties of turbulence. It is worthwhile to remark the two main properties of the Yaglom's laws. The first one is the fact that, as it clearly appears from the Kolmogorov's relation (Kolmogorov 1941), the third-order moment of the velocity fluctuations is different from zero. This means that some non-Gaussian features must be at work, or, which is the same, some hidden phase correlations. Turbulence is something more complicated than random fluctuations with a certain slope for the spectral density. The second feature is the minus sign which appears in the various relations. This is essential when the sign of the energy cascade must be inferred from the Yaglom relations, the negative asymmetry being a signature of a direct cascade towards smaller scales. Note that, Eq. (2.40) has been obtained in the limit of zero viscosity *assuming* that the pseudo-energy dissipation rates $\epsilon_{ii}^\pm$ remain finite in this limit. In usual fluid flows the analogous hypothesis, namely ϵ remains finite in the limit $\nu \to 0$, is an experimental evidence, confirmed by experiments in different conditions (Frisch 1995). In MHD turbulent flows this remains a conjecture, confirmed only by high resolution numerical simulations (Mininni and Pouquet 2009).

From Eq. (2.37), by defining $\Delta Z_i^\pm = \Delta v_i \pm \Delta b_i$ we immediately obtain the two equations

$$\frac{\partial}{\partial \ell_\alpha}\left[\langle \Delta v_\alpha \Delta E \rangle - 2\langle \Delta b_\alpha \Delta C \rangle - 2\nu \frac{\partial}{\partial \ell_\alpha}\langle \Delta E \rangle - \frac{4}{3}(\epsilon_E \ell_\alpha)\right] = 0 \tag{2.43}$$

$$\frac{\partial}{\partial \ell_\alpha}\left[-\langle \Delta b_\alpha \Delta E \rangle + 2\langle \Delta v_\alpha \Delta C \rangle - 4\nu \frac{\partial}{\partial \ell_\alpha}\langle \Delta C \rangle - \frac{4}{3}(\epsilon_C \ell_\alpha)\right] = 0, \tag{2.44}$$

where we defined the energy fluctuations $\Delta E = |\Delta v_i|^2 + |\Delta b_i|^2$ and the correlation fluctuations $\Delta C = \Delta v_i \Delta b_i$. In the same way the quantities $\epsilon_E = \left(\epsilon_{ii}^+ + \epsilon_{ii}^-\right)/2$ and $\epsilon_C = \left(\epsilon_{ii}^+ - \epsilon_{ii}^-\right)/2$ represent the energy and correlation dissipation rate, respectively. By projecting once more on the longitudinal direction, and assuming vanishing viscosity, we obtain the Yaglom's law written in terms of velocity and magnetic fluctuations

$$\langle \Delta v_\ell \Delta E \rangle - 2\langle \Delta b_\ell \Delta C \rangle = -\frac{4}{3}\epsilon_E \ell \tag{2.45}$$

$$-\langle \Delta b_\ell \Delta E \rangle + 2\langle \Delta v_\ell \Delta C \rangle = -\frac{4}{3}\epsilon_C \ell. \tag{2.46}$$

2.11.1 Density-Mediated Elsässer Variables and Yaglom's Law

Relation (2.40), which is of general validity within MHD turbulence, requires local characteristics of the turbulent fluid flow which can be not always satisfied in the solar wind flow, namely, large-scale homogeneity, isotropy, and incompressibility. Density fluctuations in solar wind have a low amplitude, so that nearly incompressible MHD framework is usually considered (Montgomery et al. 1987; Matthaeus and Brown 1988; Zank and Matthaeus 1993; Matthaeus et al. 1991; Bavassano and Bruno 1995). However, compressible fluctuations are observed, typically convected structures characterized by anticorrelation between kinetic pressure and magnetic pressure (Tu and Marsch 1994). Properties and interaction of the basic MHD modes in the compressive case have also been considered (Goldreich and Sridhar 1995; Cho and Lazarian 2002).

A first attempt to include density fluctuations in the framework of fluid turbulence was due to Lighthill (1955). He pointed out that, in a compressible energy cascade, the *mean energy transfer rate per unit volume* $\epsilon_V \sim \rho v^3/\ell$ should be constant in a statistical sense (v being the characteristic velocity fluctuations at the scale ℓ), thus obtaining the scaling relation $v \sim (\ell/\rho)^{1/3}$. Fluctuations of a density-weighted velocity field $\mathbf{u} \equiv \rho^{1/3}\mathbf{v}$ should thus follow the usual Kolmogorov scaling $u^3 \sim \ell$. The same phenomenological arguments can be introduced in MHD turbulence (Carbone et al. 2009b) by considering the pseudoenergy dissipation rates per unit volume $\epsilon_V^\pm = \rho\epsilon_{ii}^\pm$ and introducing density-weighted Elsässer fields, defined as $\mathbf{w}^\pm \equiv \rho^{1/3}\mathbf{z}^\pm$. A relation equivalent to the Yaglom-type relation (2.40)

$$W_\ell^\pm \equiv \langle \rho \rangle^{-1} \langle \Delta w_\ell^\mp |\Delta w_i^\pm|^2 \rangle = C\epsilon_{ii}^\pm \ell \tag{2.47}$$

(C is some constant assumed to be of the order of unit) should then hold for the density-weighted increments $\Delta \mathbf{w}^\pm$. Relation $W_\ell^\pm$ reduces to $Y_\ell^\pm$ in the case of constant density, allowing for comparison between the Yaglom's law for incompressible MHD flows and their compressible counterpart. Despite its simple

phenomenological derivation, the introduction of the density fluctuations in the Yaglom-type scaling (2.47) should describe the turbulent cascade for compressible fluid (or magnetofluid) turbulence. Even if the modified Yaglom's law (2.47) is not an exact relation as (2.40), being obtained from phenomenological considerations, the law for the velocity field in a compressible fluid flow has been observed in numerical simulations, the value of the constant C results negative and of the order of unity (Padoan et al. 2007; Kowal and Lazarian 2007).

2.11.2 Yaglom's Law in the Shell Model for MHD Turbulence

As far as the shell model is concerned, the existence of a cascade towards small scales is expressed by an exact relation, which is equivalent to Eq. (2.41). Using Eq. (2.24), the scale-by-scale pseudo-energy budget is given by

$$\frac{d}{dt}\sum_n |Z_n^{\pm}|^2 = k_n Im\left[T_n^{\pm}\right] - \sum_n 2\nu k_n^2 |Z_n^{\pm}|^2 + \sum_n 2\Re e\left[Z_n^{\pm} F_n^{\pm *}\right].$$

The second and third terms on the right hand side represent, respectively, the rate of pseudo-energy dissipation and the rate of pseudo-energy injection. The first term represents the flux of pseudo-energy along the wave vectors, responsible for the redistribution of pseudo-energies on the wave vectors, and is given by

$$\begin{aligned} T_n^{\pm} = (a+c) Z_n^{\pm} Z_{n+1}^{\pm} Z_{n+2}^{\mp} + \left(\frac{2-a-c}{\lambda}\right) Z_{n-1}^{\pm} Z_{n+1}^{\pm} Z_n^{\mp} + \\ + (2-a-c) Z_n^{\pm} Z_{n+2}^{\pm} Z_{n+1}^{\mp} + \left(\frac{c-a}{\lambda}\right) Z_) Z_n^{\pm} Z_{n+1}^{\pm} Z_{n-1}^{\mp}. \end{aligned} \tag{2.48}$$

Using the same assumptions as before, namely: (1) the forcing terms act only on the largest scales, (2) the system can reach a statistically stationary state, and (3) in the limit of fully developed turbulence, $\nu \to 0$, the mean pseudo-energy dissipation rates tend to finite positive limits $\epsilon^{\pm}$, it can be found that

$$\langle T_n^{\pm} \rangle = -\epsilon^{\pm} k_n^{-1}. \tag{2.49}$$

This is an exact relation which is valid in the inertial range of turbulence. Even in this case it can be used as an operative definition of the inertial range in the shell model, that is, the inertial range of the energy cascade in the shell model is defined as the range of scales k_n, where the law from Eq. (2.49) is verified.

References

B. Bavassano, R. Bruno, Density fluctuations and turbulent mach number in the inner solar wind. J. Geophys. Res. **100**, 9475–9480 (1995)

L. Biferale, Shell models of energy cascade in turbulence. Annu. Rev. Fluid Mech. **35**, 441–468 (2003). doi:10.1146/annurev.fluid.35.101101.161122

D. Biskamp, *Nonlinear Magnetohydrodynamics*. Cambridge Monographs on Plasma Physics, vol. 1 (Cambridge University Press, Cambridge, 1993)

D. Biskamp, *Magnetohydrodynamic Turbulence* (Cambridge University Press, Cambridge, 2003)

T. Bohr, M.H. Jensen, G. Paladin, A. Vulpiani, *Dynamical Systems Approach to Turbulence*. Cambridge Nonlinear Science Series, vol. 8 (Cambridge University Press, Cambridge, 1998)

T.J.M. Boyd, J.J. Sanderson, *The Physics of Plasmas* (Cambridge University Press, Cambridge, 2003)

S.I. Braginskii, Transport processes in plasma, in *Review of Plasma Physics*, ed. by M.A. Leontovich. Review of Plasma Physics, vol. 1 (Consultants Bureau, New York, 1965), pp. 201–311

V. Carbone, Cascade model for intermittency in fully developed magnetohydrodynamic turbulence. Phys. Rev. Lett. **71**, 1546–1548 (1993). doi:10.1103/PhysRevLett.71.1546

V. Carbone, L. Sorriso-Valvo, R. Marino, On the turbulent energy cascade in anisotropic magnetohydrodynamic turbulence. Europhys. Lett. **88**, 25001 (2009a). doi:10.1209/0295-5075/88/25001

V. Carbone, R. Marino, L. Sorriso-Valvo, A. Noullez, R. Bruno, Scaling laws of turbulence and heating of fast solar wind: the role of density fluctuations. Phys. Rev. Lett. **103**(6) (2009b). doi:10.1103/PhysRevLett.103.061102

S. Chandrasekhar, *An Introduction to the Study of Stellar Structure* (Dover, New York, 1967)

A.C.L. Chian, F.A. Borotto, W.D. Gonzalez, Alfvén intermittent turbulence driven by temporal chaos. Astrophys. J. **505**, 993–998 (1998). doi:10.1086/306214

A.C.L. Chian, E.L. Rempel, E.E.N. Macau, R.R. Rosa, F. Christiansen, Alfvén turbulence driven by high-dimensional interior crisis in the solar wind, in *Solar Wind Ten*, ed. by M. Velli, R. Bruno, F. Malara. AIP Conference Proceedings, vol. 679 (American Institute of Physics, Melville, 2003), pp. 558–561

J. Cho, A. Lazarian, Numerical simulations of compressible MHD turbulence. Bull. Am. Astron. Soc. **34**, 1124 (2002)

M. Dobrowolny, A. Mangeney, P. Veltri, Properties of magnetohydrodynamic turbulence in the solar wind. Astron. Astrophys. **83**, 26–32 (1980)

W.M. Elsässer, The hydromagnetic equations. Phys. Rev. **79**, 183 (1950). doi:10.1103/PhysRev.79.183

R.P. Feynman, R.B. Leighton, M. Sands, *The Feynman Lectures On Physics, Volume II: Mainly Electromagnetism and Matter* (Addison Wesley, Reading 1964)

P. Frick, D.D. Sokoloff, Cascade and dynamo action in a shell model of magnetohydrodynamic turbulence. Phys. Rev. E **57**, 4155–4164 (1998). doi:10.1103/PhysRevE.57.4155

U. Frisch, *Turbulence: The Legacy of A.N. Kolmogorov* (Cambridge University Press, Cambridge, 1995)

S. Ghosh, K. Papadopoulos, The onset of alfvénic turbulence. Phys. Fluids **30**, 1371–1387 (1987). doi:10.1063/1.866252

P. Giuliani, V. Carbone, A note on shell models for MHD turbulence. Europhys. Lett. **43**, 527–532 (1998). doi:10.1209/epl/i1998-00386-y

E.B. Gledzer, System of hydrodynamic type admitting two quadratic integrals of motion. Sov. Phys. Dokl. **18**, 216 (1973)

C. Gloaguen, J. Léorat, A. Pouquet, R. Grappin, A scalar model for MHD turbulence. Physica D **17**, 154–182 (1985). doi:10.1016/0167-2789(85)90002-8

P. Goldreich, S. Sridhar, Toward a theory of interstellar turbulence. 2: Strong alfvenic turbulence. Astrophys. J. **438**, 763–775 (1995). doi:10.1086/175121

J.P. Gollub, H.L. Swinney, Onset of turbulence in a rotating fluid. Phys. Rev. Lett. **35**, 927–930 (1975). doi:10.1103/PhysRevLett.35.927

R. Grappin, M. Velli, Waves and streams in the expanding solar wind. J. Geophys. Res. **101**, 425–444 (1996). doi:10.1029/95JA02147

R. Grappin, M. Velli, A. Mangeney, Nonlinear wave evolution in the expanding solar wind. Phys. Rev. Lett. **70**, 2190–2193 (1993). doi:10.1103/PhysRevLett.70.2190

P. Hellinger, M. Velli, P. Trávníček, S.P. Gary, B.E. Goldstein, P.C. Liewer, Alfvén wave heating of heavy ions in the expanding solar wind: hybrid simulations. J. Geophys. Res. **110**(9), 12109 (2005). doi:10.1029/2005JA011244

P.S. Iroshnikov, Turbulence of a conducting fluid in a strong magnetic field. Sov. Astron. **7**, 566 (1963)

A.N. Kolmogorov, The local structure turbulence in incompressible viscous fluids for very large reynolds numbers. Dokl. Akad. Nauk. SSSR **30**, 301–305 (1941)

A.N. Kolmogorov, The local structure of turbulence in incompressible viscous fluid for very large reynolds numbers. Proc. R. Soc. Lond. A **434**, 9–13 1991. doi:10.1098/rspa.1991.0075. Published 8 July 1991; J.C.R. Hunt, O.M. Phillips, D. Williams (eds.) Kolmogorov's ideas 50 years on Turbulence and stochastic processes (English version)

G. Kowal, A. Lazarian, Scaling relations of compressible MHD turbulence. Astrophys. J. Lett. **666**, 69–72 (2007). doi:10.1086/521788

R.H. Kraichnan, Inertial range spectrum of hydromagnetic turbulence. Phys. Fluids **8**, 1385–1387 (1965)

L.D. Landau, E.M. Lifshitz, *Physique théorique.* Mécanique des fluides, vol. 6 (Editions MIR, Moscow, 1971)

P.C. Liewer, M. Velli, B.E. Goldstein, Alfvén wave propagation and ion cyclotron interactions in the expanding solar wind: one-dimensional hybrid simulations. J. Geophys. Res. **106**, 29261–29282 (2001). doi:10.1029/2001JA000086

M.J. Lighthill, The effect of compressibility on turbulence, in *Gas Dynamics of Cosmic Clouds*. IAU Symposium, vol. 2 (North-Holland, Amsterdam, 1955), pp. 121–130

E.N. Lorenz, Deterministic nonperiodic flow. J. Atmos. Sci. **20**, 130 (1963). doi:10.1175/1520-0469(1963)020<0130:DNF>2.0.CO;2

E. Marsch, A. Mangeney, Ideal MHD equations in terms of compressive elsässer variables. J. Geophys. Res. **92**(11), 7363–7367 (1987). doi:10.1029/JA092iA07p07363

E. Marsch, C.-Y. Tu, Dynamics of correlation functions with elsässer variables for inhomogeneous MHD turbulence. J. Plasma Phys. **41**, 479–491 (1989). doi:10.1017/S0022377800014033

W.H. Matthaeus, M.R. Brown, Nearly incompressible magnetohydrodynamics at low mach number. Phys. Fluids **31**, 3634–3644 (1988). doi:10.1063/1.866880

W.H. Matthaeus, L.W. Klein, S. Ghosh, M.R. Brown, Nearly incompressible magnetohydrodynamics, pseudosound, and solar wind fluctuations. J. Geophys. Res. **96**(15), 5421–5435 (1991). doi:10.1029/90JA02609

W.D. McComb, *The Physics of Fluid Turbulence*. Oxford Engineering Science Series, vol. 25 (Oxford University Press, Oxford, 1990)

P.D. Mininni, A. Pouquet, Finite dissipation and intermittency in magnetohydrodynamics. Phys. Rev. E **80**(2) (2009). doi:10.1103/PhysRevE.80.025401

E. Mjølhus, On the modulational instability of hydromagnetic waves parallel to the magnetic field. J. Plasma Phys. **16**, 321–334 (1976). doi:10.1017/S0022377800020249

A.S. Monin, A.M. Yaglom, *Statistical Fluid Mechanics – Mechanics of Turbulence*, vol. 2 (MIT Press, Cambridge, 1975)

D. Montgomery, M.R. Brown, W.H. Matthaeus, Density fluctuation spectra in magnetohydrodynamic turbulence. J. Geophys. Res. **92**(11), 282–284 (1987). doi:10.1029/JA092iA01p00282

K. Ohkitani, M. Yamada, Temporal intermittency in the energy cascade process and local Lyapunov analysis in fully-developed model turbulence. Prog. Theor. Phys. **89**, 329–341 (1989). doi:10.1143/PTP.81.329

E. Ott, J.C. Sommerer, Blowout bifurcations: the occurrence of riddled basins and on-off intermittency. Phys. Lett. A **188**, 39–47 (1994). doi:10.1016/0375-9601(94)90114-7

S. Oughton, W.H. Matthaeus, Evolution of solar wind fluctuations and the influence of turbulent 'mixing', in *Solar Wind Seven*, ed. by E. Marsch, R. Schwenn. COSPAR Colloquia Series, vol. 3 (Pergamon Press, Oxford, 1992), pp. 523–526

P. Padoan, Å. Nordlund, A.G. Kritsuk, M.L. Norman, P.S. Li, Two regimes of turbulent fragmentation and the stellar initial mass function from primordial to present-day star formation. Astrophys. J. **661**, 972–981 (2007). doi:10.1086/516623

F. Plunian, R. Stepanov, P. Frick, Shell models of magnetohydrodynamic turbulence. Phys. Rep. **523**, 1–60 (2012)

H. Politano, A. Pouquet, von Kármán–Howarth equation for magnetohydrodynamics and its consequences on third-order longitudinal structure and correlation functions. Phys. Rev. E **57**, 21–25 (1998). doi:10.1103/PhysRevE.57.R21

H. Politano, A. Pouquet, V. Carbone, Determination of anomalous exponents of structure functions in two-dimensional magnetohydrodynamic turbulence. Europhys. Lett. **43**, 516–521 (1998). doi:10.1209/epl/i1998-00391-2

Y. Pomeau, P. Manneville, Intermittent transition to turbulence in dissipative dynamical systems. Commun. Math. Phys. **74**, 189–197 (1980). doi:10.1007/BF01197757

S.B. Pope, *Turbulent Flows* (Cambridge University Press, Cambridge, 2000)

D. Ruelle, F. Takens, On the nature of turbulence. Commun. Math. Phys. **20**, 167 (1971)

E.D. Siggia, Origin of intermittency in fully developed turbulence. Phys. Rev. A **15**, 1730–1750 (1977). doi:10.1103/PhysRevA.15.1730

L. Sorriso-Valvo, R. Marino, V. Carbone, A. Noullez, F. Lepreti, P. Veltri, R. Bruno, B. Bavassano, E. Pietropaolo, Observation of inertial energy cascade in interplanetary space plasma. Phys. Rev. Lett. **99**(11) (2007). doi:10.1103/PhysRevLett.99.115001

C.-Y. Tu, E. Marsch, Transfer equations for spectral densities of inhomogeneous MHD turbulence. J. Plasma Phys. **44**, 103–122 (1990). doi:10.1017/S002237780001504X

C.-Y. Tu, E. Marsch, On the nature of compressive fluctuations in the solar wind. J. Geophys. Res. **99**(18), 21481 (1994)

C.-Y. Tu, E. Marsch, Energy spectrum transfer equations of solar wind turbulence, in *Solar Wind Eight*, ed. by D. Winterhalter, J.T. Gosling, S.R. Habbal, W.S. Kurth, M. Neugebauer. AIP Conference Proceedings, vol. 382 (American Institute of Physics, Woodbury, 1996), pp. 233–238

P. Veltri, An observational picture of solar-wind MHD turbulence. Nuovo Cimento C **3**, 45–55 (1980). doi:10.1007/BF02509190

G.P. Zank, W.H. Matthaeus, Nearly incompressible fluids. ii – magnetohydrodynamics, turbulence, and waves. Phys. Fluids **5**, 257–273 (1993)

Y. Zhou, W.H. Matthaeus, Transport and turbulence modeling of solar wind fluctuations. J. Geophys. Res. **95**(14), 10291–10311 (1990). doi:10.1029/JA095iA07p10291

Chapter 3
Early Observations of MHD Turbulence

Here we briefly present the history, since the first Mariner missions during the 1960s, of the main steps towards the completion of an observational picture of turbulence in interplanetary space. This retrospective look at all the advances made in this field shows that space flights allowed us to discover a very large laboratory in space. As a matter of fact, in a wind tunnel we deal with characteristic dimensions of the order of $L \leq 10\,\mathrm{m}$ and probes of the size of about $d \simeq 1\,\mathrm{cm}$. In space, $L \simeq 10^8\,\mathrm{m}$, while "probes" (say spacecrafts) are about $d \simeq 5\,\mathrm{m}$. Thus, space provides a much larger laboratory but most of the available data derive from single point measurements. The ESA-Cluster project at the beginning of the past decade and, recently, the NASA-MMS project are the only space missions that allow multiple measurements, i.e. 3D measurements. In this context, after a short definition of the main reference systems in which data is provided, it is useful to recall the basic statistical concepts and numerical tools used to describe MHD turbulence in space.

3.1 Interplanetary Data Reference Systems

Magnetic field and plasma data are provided, usually, in two main reference systems: RTN and SE. The RTN system (see top part of Fig. 3.1) has the R axis along the radial direction, positive from the Sun to the s/c, the T component perpendicular to the plane formed by the rotation axis of the Sun Ω and the radial direction, i.e., $T = \Omega \times R$, and the N component resulting from the vector product $N = R \times T$.

The Solar Ecliptic reference system SE, is shown (see bottom part of Fig. 3.1) in the configuration used for Helios magnetic field data, i.e., s/c centered, with the X-axis positive towards the Sun, and the Y-axis lying in the ecliptic plane and oriented opposite to the orbital motion. The third component Z is defined as $Z = X \times Y$.

R. Bruno, V. Carbone, *Turbulence in the Solar Wind*, Lecture Notes in Physics 928, DOI 10.1007/978-3-319-43440-7_3

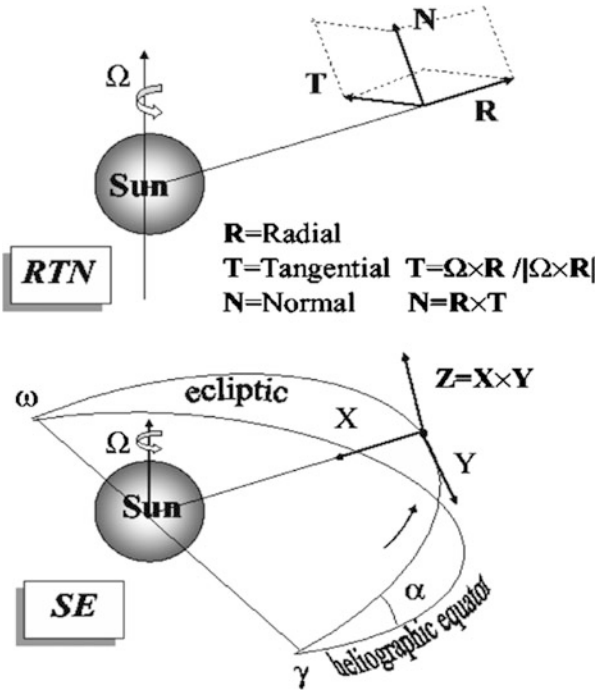

Fig. 3.1 The *top* reference system is the RTN while the one at the *bottom* is the Solar Ecliptic reference system. This last one is shown in the configuration used for Helios magnetic field data, with the *X*-axis positive towards the Sun

However, solar wind velocity is given in the Sun-centered SE system, which is obtained from the previous one after a rotation of 180° around the *Z*-axis.

Particular studies, especially those focussing on spectral anisotropy, are more meaningful if the data to be analyzed is rotated with respect to the reference system in which it is originally provided.

Let us suppose to have magnetic field data sampled in the RTN reference system. If the large-scale mean magnetic field is oriented in the $[x, y, z]$ direction, we will look for a new reference system within the RTN reference system with the x-axis oriented along the mean field and the other two axes lying on a plane perpendicular to this direction.

Thus, we firstly determine the direction of the unit vector parallel to the mean field, normalizing its components

$$
\begin{aligned}
e_{x1} &= B_x/|\mathbf{B}|, \\
e_{x2} &= B_y/|\mathbf{B}|, \\
e_{x3} &= B_z/|\mathbf{B}|,
\end{aligned}
$$

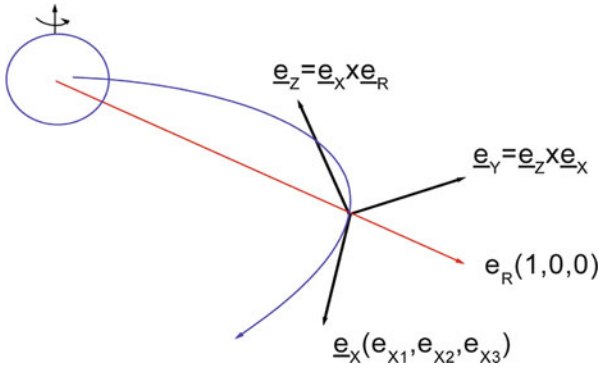

Fig. 3.2 Mean field reference system

so that $\hat{e}'_x(e_{x1}, e_{x2}, e_{x3})$ is the orientation of the first axis, parallel to the ambient field. As second direction it is convenient to choose the radial direction in RTN, which is roughly the direction of the solar wind flow, $\hat{e}_R(1, 0, 0)$. At this point, we compute a new direction perpendicular to the plane $\hat{e}_R - \hat{e}_x$

$$\hat{e}'_z(e_{z1}, e_{z2}, e_{z3}) = \hat{e}'_x \times \hat{e}_R.$$

Consequently, the third direction will be

$$\hat{e}'_y(e_{y1}, e_{y2}, e_{y3}) = \hat{e}'_z \times \hat{e}'_x.$$

Now, we can rotate our data into the new reference system (Fig. 3.2). Data indicated as $B(x, y, z)$ in the old reference system, will become $B^{'}(x^{'}, y^{'}, z^{'})$ in the new reference system. The transformation is obtained applying the rotation matrix A

$$A = \begin{pmatrix} e_{x1} & e_{x2} & e_{x3} \\ e_{y1} & e_{y2} & e_{y3} \\ e_{z1} & e_{z2} & e_{z3} \end{pmatrix}$$

to the vector B, i.e., $B^{'} = AB$.

3.2 Basic Concepts and Numerical Tools to Analyze MHD Turbulence

No matter where we are in the solar wind, short scale data always look rather random.

This aspect introduces the problem of determining the time stationarity of the dataset. The concept of stationarity is related to ensembled averaged properties of

a random process. The random process is the collection of the N samples $x(t)$, it is called ensemble and indicated as $\{x(t)\}$.

Properties of a random process $\{x(t)\}$ can be described by averaging over the collection of all the N possible sample functions $x(t)$ generated by the process. So, chosen a begin time t_1, we can define the mean value μ_x and the autocorrelation function R_x, i.e., the first and the joint moment:

$$\mu_x(t_1) = \lim_{N \longrightarrow \infty} \sum_{k=1}^{N} x_k(t_1), \tag{3.1}$$

$$R_x(t_1, t_1 + \tau) = \lim_{N \longrightarrow \infty} \sum_{k=1}^{N} x_k(t_1) x_k(t_1 + \tau). \tag{3.2}$$

In case $\mu_x(t_1)$ and $R_x(t_1, t_1 + \tau)$ do not vary as time t_1 varies, the sample function $x(t)$ is said to be weakly stationary, i.e.,

$$\mu_x(t_1) = \mu_x, \tag{3.3}$$

$$R_x(t_1, t_1 + \tau) = R_x(\tau). \tag{3.4}$$

Strong stationarity would require all the moments and joint moments to be time independent. However, if $x(t)$ is normally distributed, the concept of weak stationarity naturally extends to strong stationarity.

Generally, it is possible to describe the properties of $\{x(t)\}$ simply computing time-averages over just one $x(t)$. If the random process is stationary and $\mu_x(k)$ and $R_x(\tau, k)$ do not vary when computed over different sample functions, the process is said ergodic. This is a great advantage for data analysts, especially for those who deals with data from s/c, since it means that properties of stationary random phenomena can be properly measured from a single time history. In other words, we can write:

$$\mu_x(k) = \mu_x, \tag{3.5}$$

$$R_x(\tau, k) = R_x(\tau). \tag{3.6}$$

Thus, the concept of stationarity, which is related to ensembled averaged properties, can now be transferred to single time history records whenever properties computed over a short time interval do not vary from one interval to the next more than the variation expected for normal dispersion.

Fortunately, Matthaeus and Goldstein (1982b) established that interplanetary magnetic field often behaves as a stationary and ergodic function of time, if coherent and organized structures are not included in the dataset. Actually, they proved the weak stationarity of the data, i.e., the stationarity of the average and two-point correlation function. In particular, they found that the average and the autocorrelation function computed within a subinterval would converge to the values

estimated from the whole interval after a few correlation times t_c. More recent analysis (Perri and Balogh 2010) extended the above studies to different parameter ranges by using Ulysses data, showing that the stationarity assumption in the inertial range of turbulence on timescales of 10 min to 1 day is reasonably satisfied in fast and uniform solar wind flows, but that in mixed, interacting fast, and slow solar wind streams the assumption is frequently only marginally valid. If our time series approximates a Markov process (a process whose relation to the past does not extend beyond the immediately preceding observation), its autocorrelation function can be shown (Doob 1953) to approximate a simple exponential:

$$R(t) = R(0)e^{-\frac{t}{t_c}} \tag{3.7}$$

from which we obtain the definition given by Batchelor (1970):

$$t_c = \int_0^\infty \frac{R(t)}{R(0)}\, dt. \tag{3.8}$$

Just to have an idea of the correlation time of magnetic field fluctuations, we show in Fig. 3.3 magnetic field correlation time computed at 1 AU using Voyager 2's data. In this case, using the above definition, $t_c \simeq 3.2 \times 10^3$ s.

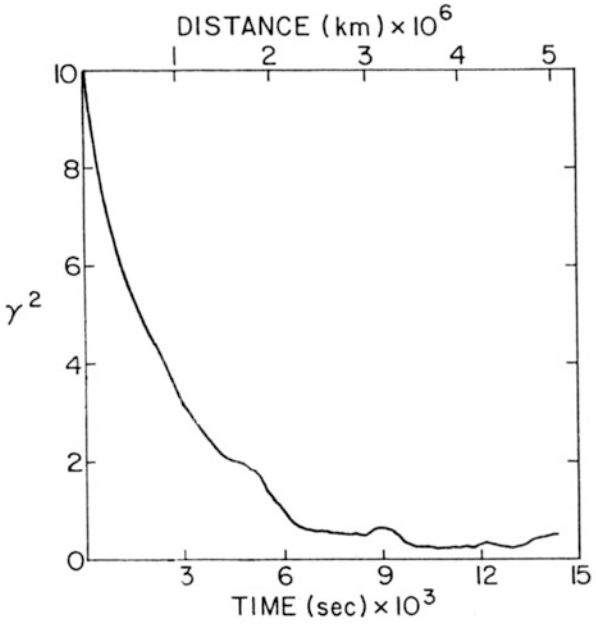

Fig. 3.3 Magnetic field auto-correlation function at 1 AU. Image reproduced by permission from Matthaeus and Goldstein (1982a), copyright by AGU

3.2.1 Correlation Length and Reynolds Number in the Solar Wind

Properties of solar wind fluctuations have been widely studied in the past, relying on the "frozen-in approximation" Taylor (1938). The hypothesis at the basis of Taylor's approximation is that, since large integral scales in turbulence contain most of the energy, the advection due to the smallest turbulent scales fluctuations can be disregarded and, consequently, the advection of a turbulent field past an observer in a fixed location is considered solely due to the larger scales. In experimental physics, this hypothesis allows time series measured at a single point in space to be interpreted as spatial variations in the mean flow being swept past the observer. However, the canonical way to establish the presence of spatial structures relies in the computation of two-point single time measurements. Only recently, the simultaneous presence of several spacecraft sampling solar wind parameters allowed to correlate simultaneous in-situ observations in two different observing locations in space. Matthaeus et al. (2005) and Weygand et al. (2007) firstly evaluated the two-point correlation function using simultaneous measurements of interplanetary magnetic field from the Wind, ACE, and Cluster spacecraft. Their technique allowed to compute for the first time fundamental turbulence parameters previously determined from single spacecraft measurements. In particular, these authors evaluated the correlation scale λ_C and the Taylor microscale λ_T which allow to determine empirically the effective magnetic Reynolds number.

As a matter of fact, there are three standard turbulence length scales which can be identified in a typical turbulence power spectrum as shown in Fig. 3.4: the correlation length λ_C, the Taylor scale λ_T and the Kolmogorov scale λ_K. The Correlation or integral length scale represents the largest separation distance over which eddies are still correlated, i.e., the largest turbulent eddy size. The Taylor scale is the scale size at which viscous dissipation begins to affect the eddies, it is several times larger than Kolmogorov scale and marks the transition from the inertial range to the dissipation range. The Kolmogorov scale is the one that characterizes the smallest dissipation-scale eddies.

The Taylor scale λ_T and the correlation length λ_C, as indicated in Fig. 3.5, can be obtained from the two-point correlation function being the former the radius of curvature of the Correlation function at the origin and the latter the scale at which turbulent fluctuation are no longer correlated. Thus, λ_T can be obtained from Taylor expansion of the two point correlation function for $\mathbf{r} \to 0$ (Tennekes and Lumely 1972):

$$R(\mathbf{r}) \approx 1 - \frac{r^2}{2\lambda_T^2} + \ldots \tag{3.9}$$

where $\mathbf{r}$ is the spacecraft separation and $R(\mathbf{r}) = \langle \mathbf{b}(\mathbf{x}) \cdot \mathbf{b}(\mathbf{x} + \mathbf{r}) \rangle$ is the auto-correlation function computed along the $\mathbf{x}$ direction for the fluctuating field $\mathbf{b}(x)$. On the other hand, the correlation length λ_C can be obtained integrating the normalized

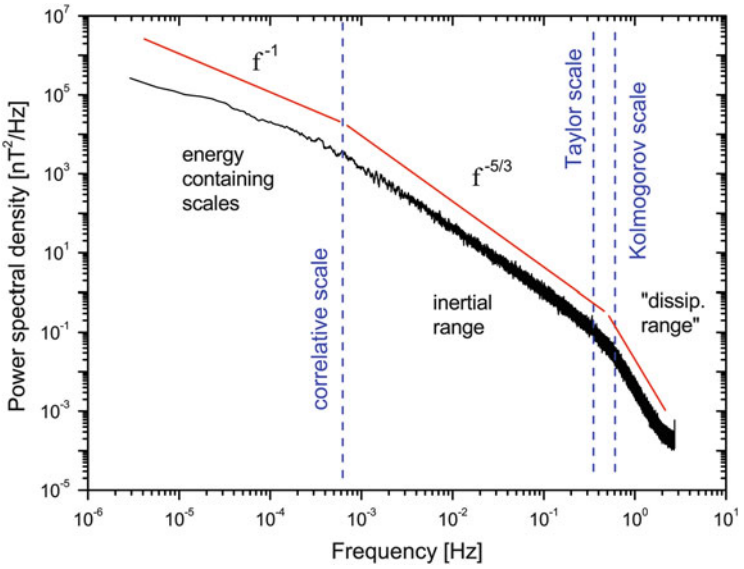

Fig. 3.4 Typical fast stream magnetic field power density spectrum as observed by WIND s/c at 1 AU. *Vertical dashed lines* indicate the correlative, Taylor and Kolmogorov scales. Data available at daweb.gsfc.nasa.gov, P.I. of WIND magnetic field experiment R. P. Lepping (Lepping et al. 1995)

correlation function along a chosen direction of integration ξ:

$$\lambda_C = \int_0^\infty \frac{R(\xi)}{R(0)}\, d\xi. \tag{3.10}$$

At this point, following Batchelor (1970) it is possible to obtain the effective magnetic Reynolds number:

$$R_{\mathrm{m}}^{\mathrm{eff}} = \left(\frac{\lambda_C}{\lambda_T}\right)^2. \tag{3.11}$$

Figure 3.6 shows estimates of the correlation function from ACE-Wind for separation distances 20–350 R_E and two sets of Cluster data for separations 0.02–0.04 R_E and 0.4–1.2 R_E, respectively.

Following the definitions of λ_C and λ_T given above, Matthaeus et al. (2005) were able to fit the first data set of Cluster, i.e., the one with shorter separations, with a parabolic fit while they used an exponential fit for ACE-Wind and the second Cluster data set. These fits provided estimates for λ_C and λ_T from which these authors obtained the first empirical determination of R_m^{eff} which resulted to be of the order of 2.3×10^5, as illustrated in Fig. 3.7.

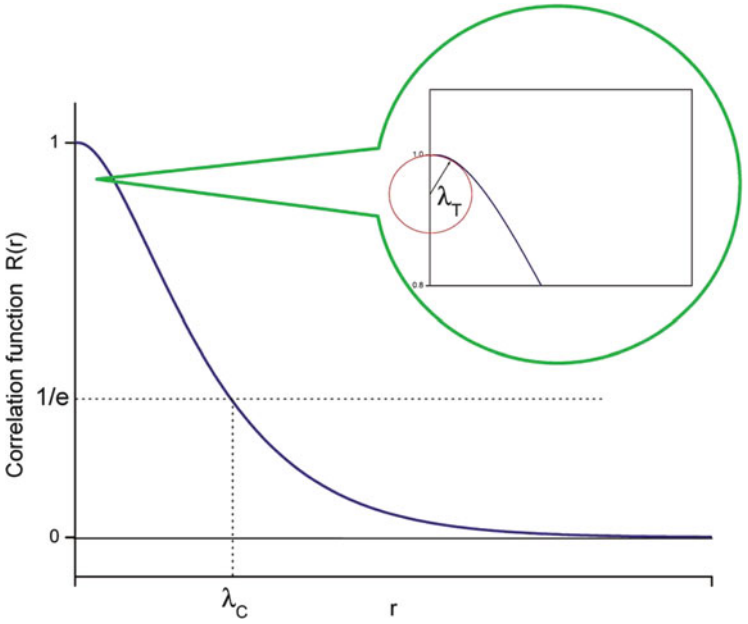

Fig. 3.5 Typical two-point correlation function. The Taylor scale λ_T and the correlation length λ_C are the radius of curvature of the Correlation function at the origin (see inset graph) and the scale at which turbulent fluctuation are no longer correlated, respectively

3.2.2 Statistical Description of MHD Turbulence

When an MHD fluid is turbulent, it is impossible to know the detailed behavior of velocity field $v(x,t)$ and magnetic field $b(x,t)$, and the only description available is the statistical one. Very useful is the knowledge of the invariants of the ideal equations of motion for which the dissipative terms $\mu\nabla^2\mathbf{b}$ and $\nu\nabla^2\mathbf{v}$ are equal to zero because the magnetic resistivity μ and the viscosity ν are both equal to zero. Following Frisch et al. (1975) there are three quadratic invariants of the ideal system which can be used to describe MHD turbulence: total energy E, cross-helicity H_c, and magnetic helicity H_m. The above quantities are defined as follows:

$$E = \frac{1}{2}\langle v^2 + b^2\rangle, \tag{3.12}$$

$$H_c = \langle \mathbf{v}\cdot\mathbf{b}\rangle, \tag{3.13}$$

$$H_m = \langle \mathbf{A}\cdot\mathbf{B}\rangle, \tag{3.14}$$

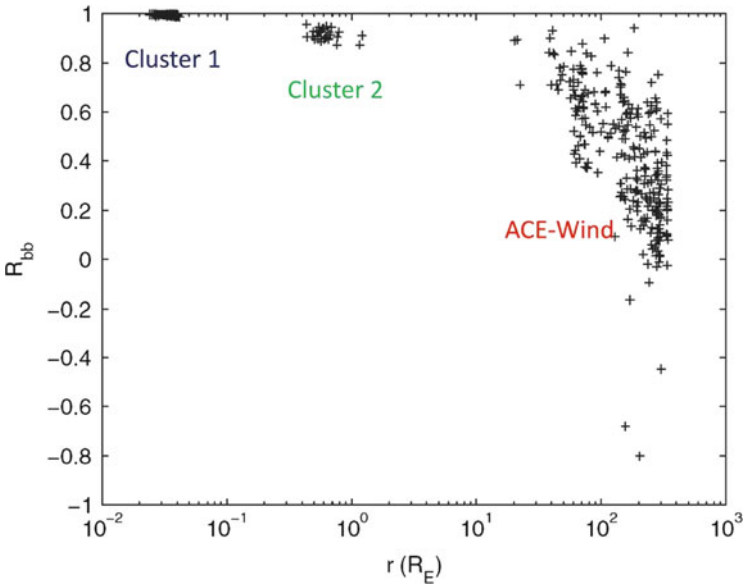

Fig. 3.6 Estimates of the correlation function from ACE-Wind for separation distances 20–350 R_E and two sets of Cluster data for separations 0.02–0.04 R_E and 0.4–1.2 R_E, respectively. Image adapted from Matthaeus et al. (2005)

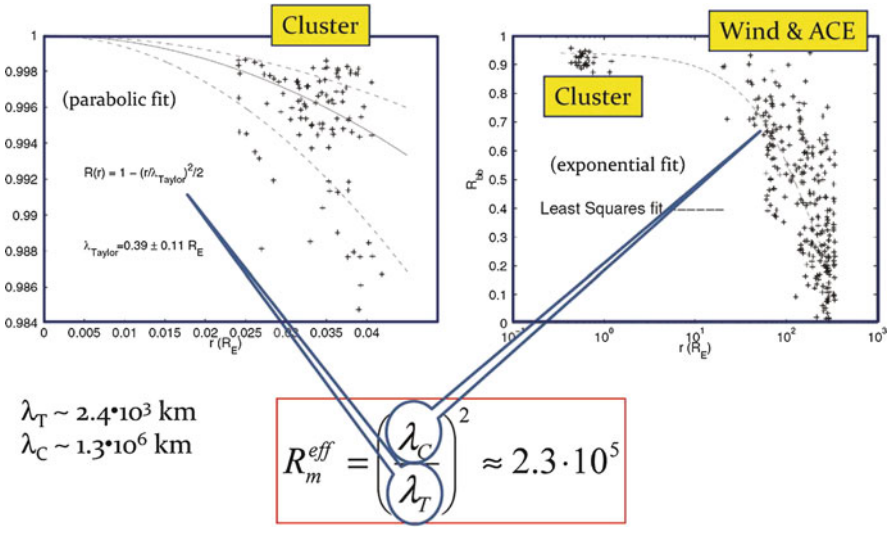

Fig. 3.7 *Left panel:* parabolic fit at small scales in order to estimate λ_T. *Right panel:* exponential fit at intermediate and large scales in order to estimate λ_C. The square of the ratio of these two length scales gives an estimate of the effective magnetic Reynolds number. Image adapted from Matthaeus et al. (2005)

where $\mathbf{v}$ and $\mathbf{b}$ are the fluctuations of velocity and magnetic field, this last one expressed in Alfvén units ($b \longrightarrow \frac{b}{\sqrt{4\pi\rho}}$), and $\mathbf{A}$ is the vector potential so that $\mathbf{B} = \nabla \times \mathbf{A}$. The integrals of these quantities over the entire plasma containing regions are the invariants of the ideal MHD equations:

$$E = \frac{1}{2}\int (v^2 + b^2) d^3x, \tag{3.15}$$

$$H_\mathrm{c} = \frac{1}{2}\int (\mathbf{v} \cdot \mathbf{b}) d^3x, \tag{3.16}$$

$$H_\mathrm{m} = \int (\mathbf{A} \cdot \mathbf{B}) d^3x, \tag{3.17}$$

In particular, in order to describe the degree of correlation between v and b, it is convenient to use the normalized cross-helicity σ_c:

$$\sigma_\mathrm{c} = \frac{2H_\mathrm{c}}{E}, \tag{3.18}$$

since this quantity simply varies between $+1$ and -1.

3.2.3 *Spectra of the Invariants in Homogeneous Turbulence*

Statistical information about the state of a turbulent fluid is contained in the n-point correlation function of the fluctuating fields. In homogeneous turbulence these correlations are invariant under arbitrary translation or rotation of the experimental apparatus. We can define the magnetic field auto-correlation matrix

$$R^b_{ij}(r) = \langle b_i(x) b_j(x + r) \rangle, \tag{3.19}$$

the velocity auto-correlation matrix

$$R^v_{ij}(r) = \langle v_i(x) v_j(x + r) \rangle, \tag{3.20}$$

and the cross-correlation matrix

$$R^{vb}_{ij}(r) = \frac{1}{2}\langle v_i(x) b_j(x + r) + b_i(x) v_j(x + r) \rangle. \tag{3.21}$$

At this point, we can construct the spectral matrix in terms of Fourier transform of R_{ij}

$$S_{ij}^{b}(\mathbf{k}) = \frac{1}{2\pi}\int R_{ij}^{b}(\mathbf{r})e^{-i\mathbf{k}\cdot\mathbf{r}}d^3r, \tag{3.22}$$

$$S_{ij}^{v}(\mathbf{k}) = \frac{1}{2\pi}\int R_{ij}^{v}(\mathbf{r})e^{-i\mathbf{k}\cdot\mathbf{r}}d^3r, \tag{3.23}$$

$$S_{ij}^{vb}(\mathbf{k}) = \frac{1}{2\pi}\int R_{ij}^{vb}(\mathbf{r})e^{-i\mathbf{k}\cdot\mathbf{r}}d^3r. \tag{3.24}$$

However, in space experiments, especially in the solar wind, data from only a single spacecraft are available. This provides values of R_{ij}^{b}, R_{ij}^{v}, and R_{ij}^{vb}, for separations along a single direction $\mathbf{r}$. In this situation, only reduced (i.e., one-dimensional) spectra can be measured. If $\mathbf{r}_1$ is the direction of co-linear separations, we may only determine $R_{ij}(r_1, 0, 0)$ and, as a consequence, the Fourier transform on R_{ij} yields the reduced spectral matrix

$$S_{ij}^{r}(\mathbf{k_1}) = \frac{1}{2\pi}\int R_{ij}(r_1,0,0)e^{-i\mathbf{k_1}\cdot\mathbf{r_1}}\,dr_1 = \int S_{ij}(k_1,k_2,k_3)\,dk_2\,dk_3. \tag{3.25}$$

Then, we define H_m^r, H_c^r, and $E^r = E_b^r + E_v^r$ as the reduced spectra of the invariants, depending only on the wave number k_1. Complete information about S_{ij} might be lost when computing its reduced version since we integrate over the two transverse k. However, for isotropic symmetry no information is lost performing the transverse wave number integrals (Batchelor 1970). That is, the same spectral information is obtained along any given direction.

Coming back to the ideal invariants, now we have to deal with the problem of how to extract information about H_{m} from $R_{ij}(r)$. We know that the Fourier transform of a real, homogeneous matrix $R_{ij}(r)$ is an Hermitian form S_{ij}, i.e., $S = \tilde{S}^* \longrightarrow s_{ij} = s_{ji}^*$, and that any square matrix A can be decomposed into a symmetric and an antisymmetric part, A^s and A^a:

$$A = A^s + A^a, \tag{3.26}$$

where

$$A^s = \frac{1}{2}(A + \tilde{A}), \tag{3.27}$$

$$A^a = \frac{1}{2}(A - \tilde{A}). \tag{3.28}$$

Since the Hermitian form implies that

$$S = \tilde{S}^* \longrightarrow s_{ij} = s_{ji}^*, \tag{3.29}$$

it follows that

$$S^s = \frac{1}{2}(S + \tilde{S}) = \frac{1}{2}(S_{ij} + S_{ji}) = \text{real}, \tag{3.30}$$

and

$$S^a = \frac{1}{2}(S - \tilde{S}) = \frac{1}{2}(S_{ij} - S_{ji}) = \text{imaginary}. \tag{3.31}$$

It has been shown Batchelor (1970); Matthaeus and Goldstein (1982a); Montgomery (1983) that, while the trace of the symmetric part of the spectral matrix accounts for the magnetic energy, the imaginary part of the spectral matrix accounts for the magnetic helicity. In particular, Matthaeus and Goldstein (1982a) showed that

$$H_{\text{m}}^r(k_1) = 2\text{Im}\, S_{23}^r(k_1)/k_1, \tag{3.32}$$

where H_{m} has been integrated over the two transverse components

$$\int \text{Im}\, S_{23}(\mathbf{k})\, dk_2\, dk_3 = \frac{k_1}{2} \int H_{\text{m}}(\mathbf{k})\, dk_2\, dk_3. \tag{3.33}$$

In practice, if co-linear measurements are made along the X direction, the reduced magnetic helicity spectrum is given by:

$$H_{\text{m}}^r(k_1) = 2\text{Im}\, S_{23}^r(k_1)/k_1 = 2\text{Im}\, (YZ^*)/k_1, \tag{3.34}$$

where Y and Z are the Fourier transforms of B_y and B_z components, respectively.

H_{m} can be interpreted as a measure of the correlation between the two transverse components, being one of them shifted by 90° in phase at frequency f. This parameter gives also an estimate of how magnetic field lines are knotted with each other. H_{m} can assume positive and negative values depending on the sense of rotation of the correlation between the two transverse components.

However, another parameter, which is a combination of H_{m} and E_b, is usually used in place of H_{m} alone. This parameter is the normalized magnetic helicity

$$\sigma_{\text{m}}(k) = kH_{\text{m}}(k)/E_b(k), \tag{3.35}$$

where E_b is the magnetic spectral power density and σ_{m} varies between $+1$ and -1.

Since the cross-correlation function is not necessarily an even function, the cross-spectral density function is generally a complex number:

$$W_{xy}(f) = C_{xy}(f) + jQ_{xy}(f),$$

where the real part $C_{xy}(f)$ is the coincident spectral density function, and the imaginary part $Q_{xy}(f)$ is the quadrature spectral density function Bendat and Piersol (1971). While $C_{xy}(f)$ can be thought of as the average value of the product $x(t)y(t)$ within a narrow frequency band $(f, f + \delta f)$, $Q_{xy}(f)$ is similarly defined but one of the components is shifted in time sufficiently to produce a phase shift of 90° at frequency f.

In polar notation

$$W_{xy}(f) = |W_{xy}(f)|e^{-j\theta_{xy}(f)}.$$

In particular,

$$|W_{xy}(f)| = \sqrt{C_{xy}^2(f) + Q_{xy}^2(f)},$$

and the phase between C and Q is given by

$$\theta_{xy}(f) = \arctan \frac{Q_{xy}(f)}{C_{xy}(f)}.$$

Moreover,

$$|W_{xy}(f)|^2 \leq W_x(f)W_y(f),$$

so that the following relation holds

$$\gamma_{xy}^2(f) = \frac{|W_{xy}(f)|^2}{W_x(f)W_y(f)} \leq 1.$$

This function $\gamma_{xy}^2(f)$, called *coherence*, estimates the correlation between $x(t)$ and $y(t)$ for a given frequency f. Just to give an example, for an Alfvén wave at frequency f whose $\mathbf{k}$ vector is outwardly oriented as the interplanetary magnetic field, we expect to find $\theta_{vb}(f) = 180°$ and $\gamma_{vb}^2(f) = 1$, where the indexes v and b refer to the magnetic field and velocity field fluctuations.

3.3 Turbulence in the Ecliptic

When dealing with laboratory turbulence it is important to know all the aspects of the experimental device where turbulent processes take place in order to estimate related possible effects driven or influenced by the environment. In the solar wind, the situation is, in some aspects, similar although the plasma does not experience any confinement due to the "experimental device", which would be represented by free interplanetary space. However, it is a matter of fact that the turbulent

state of the wind fluctuations and the subsequent radial evolution during the wind expansion greatly differ from fast to slow wind, and it is now well accepted that the macrostructure convected by the wind itself plays some role (see reviews by Tu and Marsch 1995b; Goldstein et al. 1995).

Fast solar wind originates from the polar regions of the Sun, within the open magnetic field line regions identified by coronal holes. Beautiful observations by SOHO spacecraft (see Fig. 3.8) have localized the birthplace of the solar wind within the intergranular lane, generally where three or more granules get together. Clear outflow velocities of up to 10 km s^{-1} have been recorded by SOHO/SUMER instrument (Hassler et al. 1999).

Slow wind, on the contrary, originates from the equatorial zone of the Sun. The slow wind plasma leaks from coronal features called "helmets", which can be easily seen protruding into the Sun's atmosphere during a solar eclipse (see Fig. 3.9). Moreover, plasma emissions due to violent and abrupt phenomena also contribute to the solar wind in these regions of the Sun. An alternative view is that both high- and low- speed winds come from coronal holes (defined as open field regions) and that the wind speed at 1 AU is determined by the rate of flux-tube expansion near the Sun as firstly suggested by Levine et al. (1977) (see also: Wang and Sheeley Jr 1990; Bravo and Stewart 1997; Arge and Pizzo 2000; Poduval and Zhao 2004; Whang et al. 2005) and/or by the location and strength of the coronal heating Leer and Holzer (1980); Hammer (1982); Hollweg (1986); Withbroe (1988); Wang (1993, 1994); Sandbaek et al. (1994); Hansteen and Leer (1995); Cranmer et al. (2007).

However, this situation greatly changes during different phases of the solar activity cycle. Polar coronal holes, which during the maximum of activity are

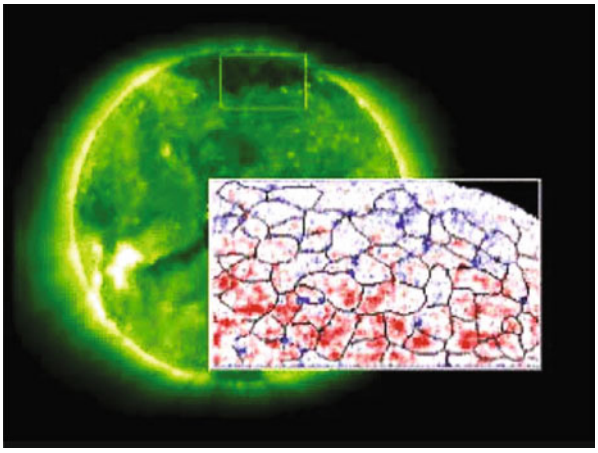

Fig. 3.8 Composite picture built on SOHO/EIT and SOHO/SUMER observations of the solar-wind source regions and magnetic structure of the chromospheric network. Outflow velocities, at the network cell boundaries and lane junctions below the polar coronal hole, reach up to 10 km s^{-1} are represented by the blue colored areas (original figures from Hassler et al. 1999)

Fig. 3.9 Helmet streamer during a solar eclipse. Slow wind leaks into the interplanetary space along the flanks of this coronal structure. Original image can be found at http://solarscience.msfc.nasa.gov/SolarWind.shtml

limited to small and not well defined regions around the poles, considerably widen up during solar minimum, reaching the equatorial regions (Forsyth et al. 1997; Forsyth and Breen 2002; Balogh et al. 1999). This new configuration produces an alternation of fast and slow wind streams in the ecliptic plane, the plane where most of the spacecraft operate and record data. During the expansion, a dynamical interaction between fast and slow wind develops, generating the so called "stream interface", a thin region ahead of the fast stream characterized by strong compressive phenomena.

Figure 3.10 shows a typical situation in the ecliptic where fast streams and slow wind were observed by Helios 2 s/c during its primary mission to the Sun. At that time, the spacecraft moved from 1 AU (around day 17) to its closest approach to the Sun at 0.29 AU (around day 108). During this radial excursion, Helios 2 had a chance to observe the same co-rotating stream, that is plasma coming from the same solar source, at different heliocentric distances. This fortuitous circumstance, gave us the unique opportunity to study the radial evolution of turbulence under the reasonable hypothesis of time-stationarity of the source regions. Obviously, similar hypotheses decay during higher activity phase of the solar cycle since, as shown in Fig. 3.11, the nice and regular alternation of fast co-rotating streams and slow wind is replaced by a much more irregular and spiky profile also characterized by a lower average speed.

Figure 3.12 focuses on a region centered on day 75, recognizable in Fig. 3.10, when the s/c was at approximately 0.7 AU from the Sun. Slow wind on the left-hand side of the plot, fast wind on the right hand side, and the stream interface in between, can be clearly seen. This is a sort of canonical situation often encountered in the ecliptic, within the inner heliosphere, during solar activity minimum. Typical solar

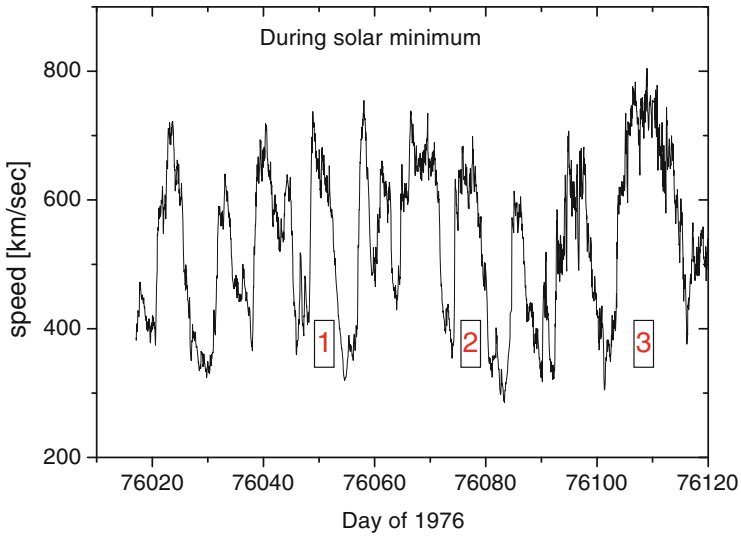

Fig. 3.10 High velocity streams and slow wind as seen in the ecliptic during solar minimum as function of time [*yyddd*]. Streams identified by labels are the same co-rotating stream observed by Helios 2, during its primary mission to the Sun in 1976, at different heliocentric distances. These streams, named "The Bavassano streams" after Tu and Marsch (1995b), have been of fundamental importance in understanding the radial evolution of MHD turbulence in the solar wind

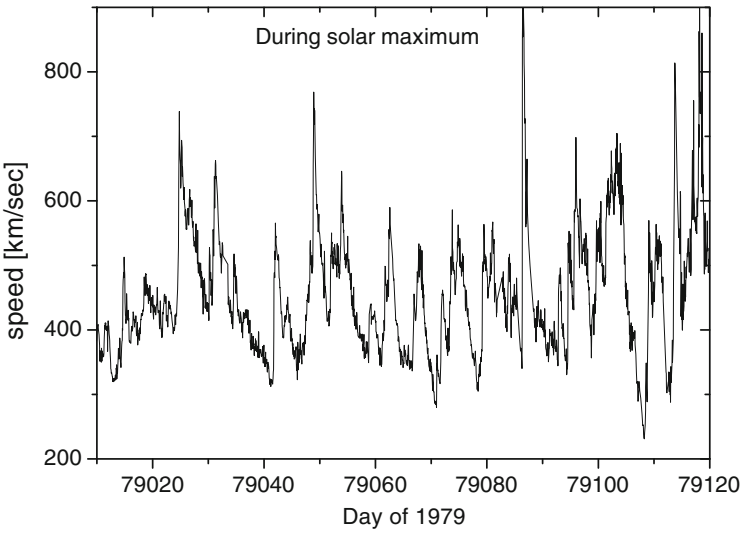

Fig. 3.11 High velocity streams and slow wind as seen in the ecliptic during solar maximum. Data refer to Helios 2 observations in 1979

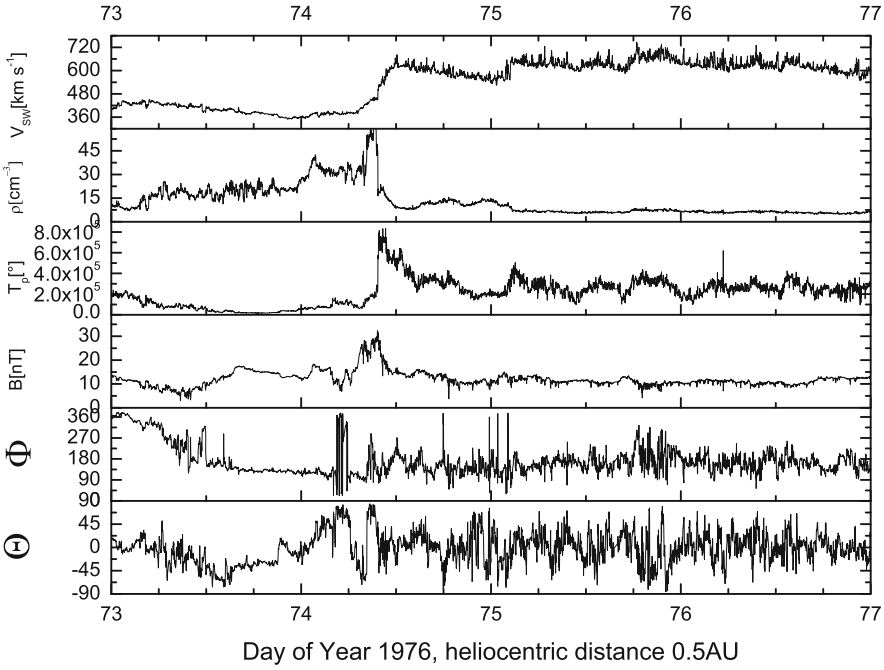

Fig. 3.12 High velocity streams and slow wind as seen in the ecliptic during solar minimum

wind parameters, like proton number density ρ_p, proton temperature T_p, magnetic field intensity $|B|$, azimuthal angle Φ, and elevation angle Θ are shown in the panels below the wind speed profile. A quick look at the data reveals that fast wind is less dense but hotter than slow wind. Moreover, both proton number density and magnetic field intensity are more steady and, in addition, the bottom two panels show that magnetic field vector fluctuates in direction much more than in slow wind. This last aspect unravels the presence of strong Alfvénic fluctuations which act mainly on magnetic field and velocity vector direction, and are typically found within fast wind (Belcher and Davis Jr 1971; Belcher and Solodyna 1975). The region just ahead of the fast wind, namely the stream interface, where dynamical interaction between fast and slow wind develops, is characterized by compressive effects which enhance proton density, temperature and field intensity. Within slow wind, a further compressive region precedes the stream interface but it is not due to dynamical effects but identifies the heliospheric current sheet, the surface dividing the two opposite polarities of the interplanetary magnetic field. As a matter of fact, the change of polarity can be noted within the first half of day 73 when the azimuthal angle Φ rotates by about 180°. Detailed studies Bavassano et al. (1997) based on interplanetary scintillations (IPS) and in-situ measurements have been able to find a clear correspondence between the profile of path-integrated density obtained from IPS measurements and in-situ measurements by Helios 2 when the s/c was around 0.3 AU from the Sun.

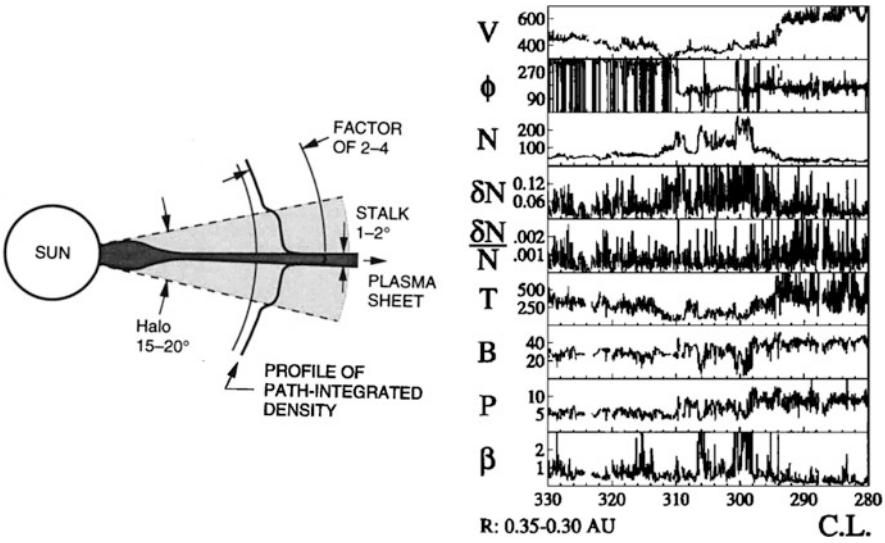

Fig. 3.13 *Left panel:* a simple sketch showing the configuration of a helmet streamer and the density profile across this structure. *Right panel:* Helios 2 observations of magnetic field and plasma parameters across the heliospheric current sheet. *From top to bottom:* wind speed, magnetic field azimuthal angle, proton number density, density fluctuations and normalized density fluctuations, proton temperature, magnetic field magnitude, total pressure, and plasma beta, respectively. Image reproduced by permission from Bavassano et al. (1997), copyright by AGU

Figure 3.13 shows measurements of several plasma and magnetic field parameters. The third panel from the top is the proton number density and it shows an enhancement within the slow wind just preceding the fast stream, as can be seen at the top panel. In this case the increase in density is not due to the dynamical interaction between slow and fast wind but it represents the profile of the heliospheric current sheet as sketched on the left panel of Fig. 3.13. As a matter of fact, at these short distances from the Sun, dynamical interactions are still rather weak and this kind of compressive effects can be neglected with respect to the larger density values proper of the current sheet.

3.3.1 Spectral Properties

First evidences of the presence of turbulent fluctuations were showed by Coleman (1968), who, using Mariner 2 magnetic and plasma observations, investigated the statistics of interplanetary fluctuations during the period August 27 – October 31, 1962, when the spacecraft orbited from 1.0 to 0.87 AU. At variance with Coleman (1968), Barnes and Hollweg (1974) analyzed the properties of the observed low-frequency fluctuations in terms of simple waves, disregarding the presence of an

energy spectrum. Here we review the gross features of turbulence as observed in space by Mariner and Helios spacecraft. By analyzing spectral densities, Coleman (1968) concluded that the solar wind flow is often turbulent, energy being distributed over an extraordinarily wide frequency range, from one cycle per solar rotation to 0.1 Hz. The frequency spectrum, in a range of intermediate frequencies $[2 \times 10^{-5}$–$2.3 \times 10^{-3}]$, was found to behave roughly as $f^{-1.2}$, the difference with the expected Kraichnan $f^{-1.5}$ spectral slope was tentatively attributed to the presence of high-frequency transverse fluctuations resulting from plasma garden-hose instability (Scarf et al. 1967). Waves generated by this instability contribute to the spectrum only in the range of frequencies near the proton cyclotron frequency and would weaken the frequency dependence relatively to the Kraichnan scaling. The magnetic spectrum obtained by Coleman (1968) is shown in Fig. 3.14.

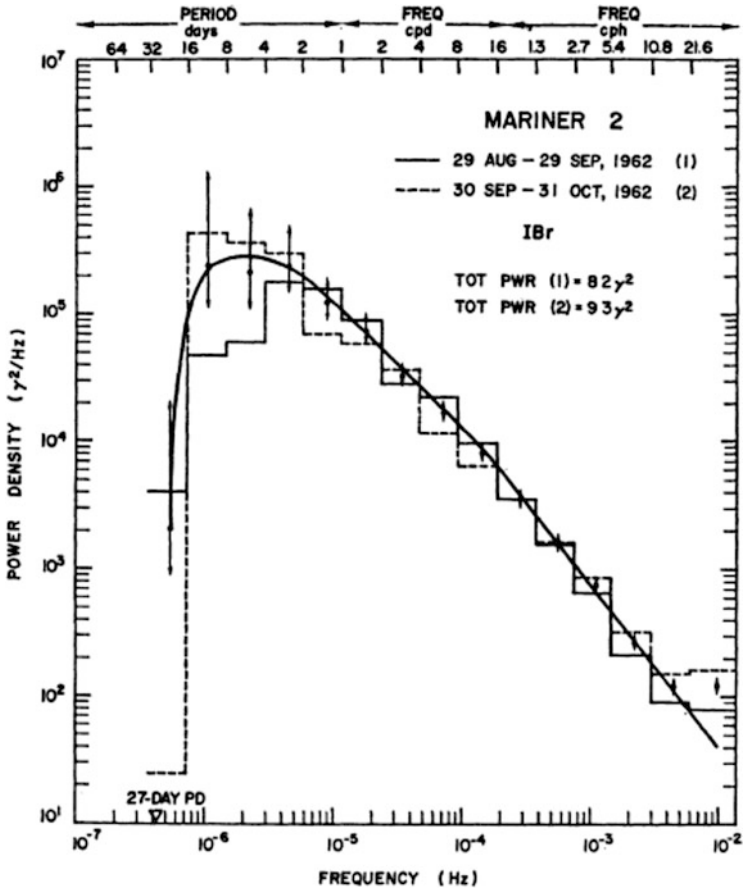

Fig. 3.14 The magnetic energy spectrum as obtained by Coleman (1968)

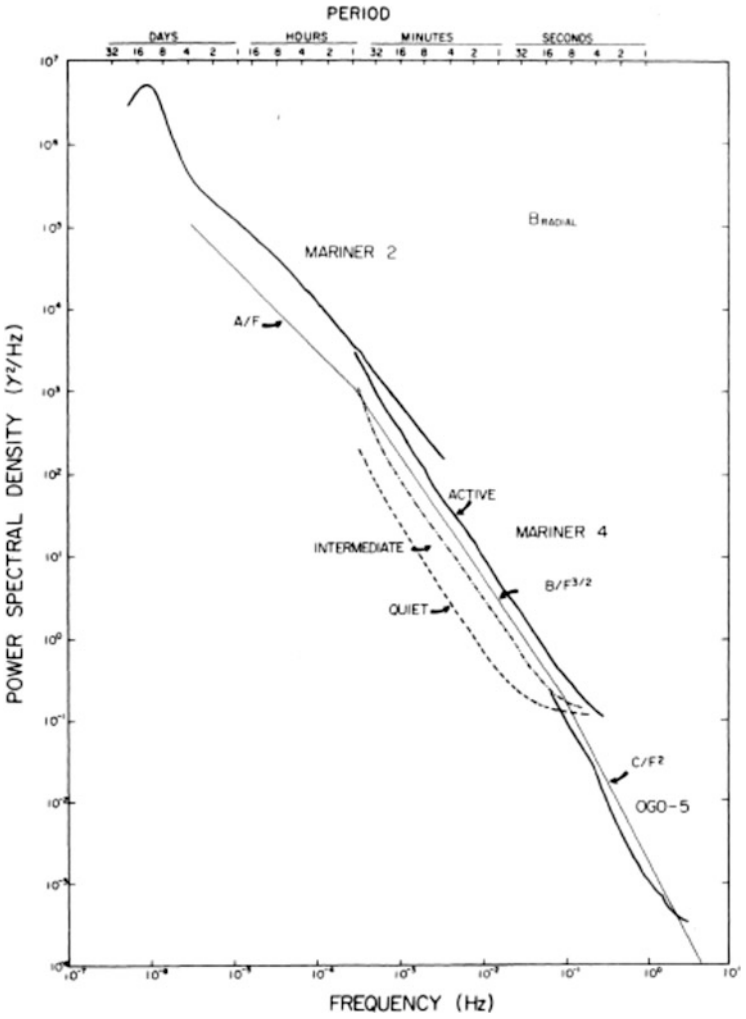

Fig. 3.15 A composite figure of the magnetic spectrum obtained by Russell (1972)

Spectral properties of the interplanetary medium have been summarized by Russell (1972), who published a composite spectrum of the radial component of magnetic fluctuations as observed by Mariner 2, Mariner 4, and OGO 5 (see Fig. 3.15). The frequency spectrum so obtained was divided into three main ranges: (1) up to about 10^{-4} Hz the spectral slope is about $1/f$; (2) at intermediate frequencies $10^{-4} \leq f \leq 10^{-1}$ Hz a spectrum which roughly behaves as $f^{-3/2}$ has been found; (3) the high-frequency part of the spectrum, up to 1 Hz, behaves as $1/f^2$.

The intermediate range[1] of frequencies shows the same spectral properties as that introduced by Kraichnan (1965) in the framework of MHD turbulence. It is worth reporting that scatter plots of the values of the spectral index of the intermediate region do not allow us to distinguish between a Kolmogorov spectrum $f^{-5/3}$ and a Kraichnan spectrum $f^{-3/2}$ (Veltri 1980).

Only lately, Podesta et al. (2007) addressed again the problem of the spectral exponents of kinetic and magnetic energy spectra in the solar wind. Their results, instead of clarifying once forever the ambiguity between $f^{-5/3}$ and $f^{-3/2}$ scaling, placed new questions about this unsolved problem.

As a matter of fact, Podesta et al. (2007) chose different time intervals between 1995 and 2003 lasting 2 or 3 solar rotations during which WIND spacecraft recorded solar wind velocity and magnetic field conditions. Figure 3.16 shows the results obtained for the time interval that lasted about 3 solar rotations between November 2000 and February 2001, and is representative also of the other analyzed time intervals. Quite unexpectedly, these authors found that the power law exponents of velocity and magnetic field fluctuations often have values near $3/2$ and $5/3$, respectively. In addition, the kinetic energy spectrum is characterized by a power law exponent slightly greater than or equal to $3/2$ due to the effects of density fluctuations.

It is worth mentioning that this difference was first observed by Salem (2000) years before, but, at that time, the accuracy of the data was questioned (Salem et al. 2009). Thus, to corroborate previous results, Salem et al. (2009) investigated anomalous scaling and intermittency effects of both magnetic field and solar wind velocity fluctuations in the inertial range using WIND data. These authors used a wavelet technique for a systematic elimination of intermittency effects on spectra and structure functions in order to recover the actual scaling properties in the inertial range. They found that magnetic field and velocity fluctuations exhibit a well-defined, although different, monofractal behavior, following a Kolmogorov $-5/3$ scaling and a Iroshnikov–Kraichnan $-3/2$ scaling, respectively. These results are clearly opposite to the expected scaling for kinetic and magnetic fluctuations which should follow Kolmogorov and Kraichnan scaling, respectively (see Sect. 2.8). However, as remarked by Roberts (2007), Voyager observations of the velocity spectrum have demonstrated a likely asymptotic state in which the spectrum steepens towards a spectral index of $-5/3$, finally matching the magnetic spectrum and the theoretical expectation of Kolmogorov turbulence. Moreover, the same authors examined Ulysses spectra to determine if the Voyager result, based on a very few sufficiently complete intervals, were correct. Preliminary results confirmed the $-5/3$ slope for velocity fluctuations at ~ 5 AU from the Sun in the ecliptic.

[1]To be precise, it is worth remarking again that there are no convincing arguments to identify as *inertial range* the intermediate range of frequencies where the observed spectral properties are typical of fully developed turbulence. From a theoretical point of view here the association "intermediate range" $\simeq$ "inertial range" is somewhat arbitrary. Really an operative definition of inertial range of turbulence is the range of scales ℓ where relation (2.42) (for fluid flows) or (2.41) (for MHD flows) is verified.

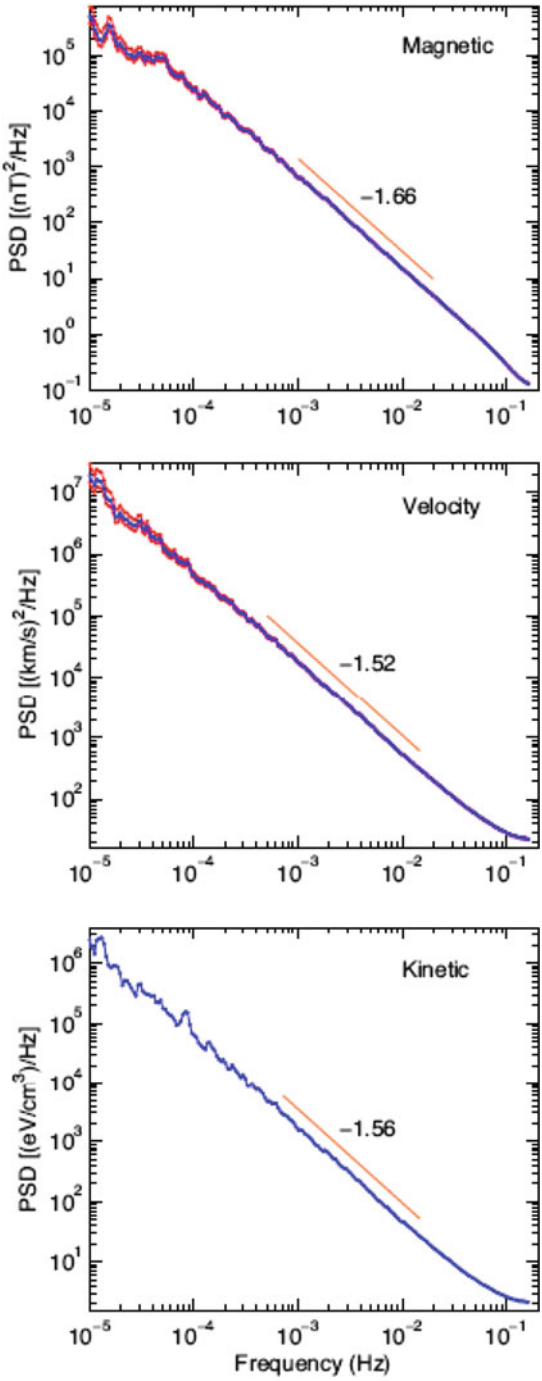

Fig. 3.16 Magnetic energy spectra, velocity spectra and kinetic energy spectra obtained by Podesta et al. (2007). Image reproduced by permission, copyright by AAS

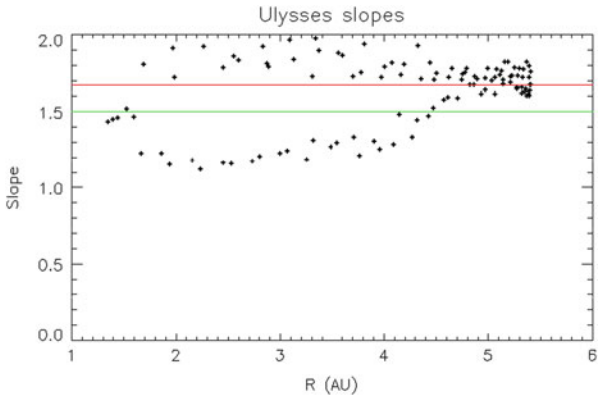

Fig. 3.17 Velocity spectral index vs. heliocentric distance (Roberts 2007)

Figure 3.17, taken from Roberts (2007), shows the evolution of the spectral index during the radial excursion of Ulysses. These authors examined many intervals in order to develop a more general picture of the spectral evolution in various conditions, and how magnetic and velocity spectra differ in these cases. The general trend shown in Fig. 3.17 is towards $-5/3$ as the distance increases. Lower values are due to the highly Alfvénic fast polar wind while higher values, around 2, are mainly due to the jumps at the stream fronts as previously shown by Roberts (2007). Thus, the discrepancy between magnetic and velocity spectral slope is only temporary and belongs to the evolutionary phase of the spectra towards a well developed Kolmogorov like turbulence spectrum.

Horbury et al. (2008) performed a study on the anisotropy of the energy spectrum of magnetohydrodynamic (MHD) turbulence with respect to the magnetic field orientation to test the validity of the critical balance theory (Goldreich and Sridhar 1995) in space plasma environment. This theory predicts that the power spectrum $P(k)$ would scale as $f^{-5/3}$ when the angle θ_B between the mean field direction and the flow direction is 90°. On the other hand, in case $\theta_B = 0°$ the scaling would follow f^{-2}. Moreover, the latter spectrum would also have a smaller energy content.

Horbury et al. (2008) used 30 days of Ulysses magnetic field observations (1995, days 100–130) with a resolution of 1 s. At that time, Ulysses was immersed in the steady high speed solar wind coming from the Sun's Northern polar coronal hole at 1.4 AU from the Sun. These authors studied the anisotropies of the turbulence by measuring how the spacecraft frame spectrum of magnetic fluctuations varies with θ_B. They adopted a method based on wavelet analysis which was sensitive to the frequent changes of the local magnetic field direction.

The lower panel of Fig. 3.18 clearly shows that for angles larger than about 45° the spectral index smoothly fluctuates around $-5/3$ while, for smaller angles, it tends to a value of -2, as predicted by the *critical balance* type of cascade. However, although the same authors recognize that a spectral index of -2 has not been routinely observed in the fast solar wind and that the range of θ_B over which

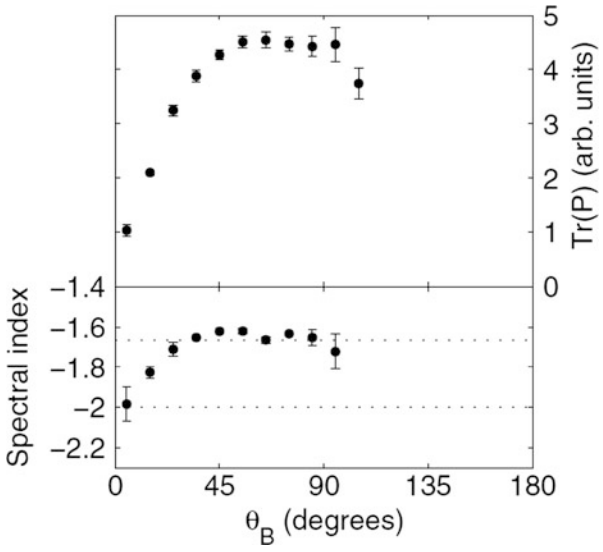

Fig. 3.18 *Top panel:* Trace of power in the magnetic field as a function of the angle between the local magnetic field and the sampling direction at a spacecraft frequency of 61 mHz. The larger scatter for $\theta_B > 90$ is the result of fewer data points at these angles. *Bottom panel:* spectral index of the trace, fitted over spacecraft frequencies from 15.98 mHz. Image reproduced by permission from Horbury et al. (2008), copyright by APS

the spectral index deviates from $-5/3$ is wider than expected, they consider these findings to be a robust evidence of the validity of critical balance theory in space plasma environment.

3.3.2 Magnetic Helicity Spectrum

Another important aspect of magnetic fluctuations is the magnetic helicity H_m. This quantity, as defined in Sect. 3.2.2, measures the "knottedness" of magnetic field lines (Moffatt 1978).

Moreover, H_m is a pseudo scalar and changes sign for coordinate inversion. The plus or minus sign, for circularly polarized magnetic fluctuations in a slab geometry, indicates right or left-hand polarization. Statistical information about the magnetic helicity is derived from the Fourier transform of the magnetic field auto-correlation matrix $R_{ij}(\mathbf{r}) = \langle B_i(\mathbf{x}) \cdot B_j(\mathbf{x}+\mathbf{r}) \rangle$ as shown by Matthaeus and Goldstein (1982a). While the trace of the symmetric part of the spectral matrix accounts for the magnetic energy, the imaginary part of the spectral matrix accounts for the magnetic helicity (Batchelor 1970; Montgomery 1982; Matthaeus and Goldstein 1982a). However, what is really available from in-situ measurements in space experiments are data from a single spacecraft, and we can obtain values of R only for collinear

sequences of **r** along the **x** direction which corresponds to the radial direction from the Sun. In these conditions the Fourier transform of R allows us to obtain only a reduced spectral tensor along the radial direction so that $H_{\mathrm{m}}(k)$ will depend only on the wave-number k in this direction. Although the reduced spectral tensor does not carry the complete spectral information of the fluctuations, for slab and isotropic symmetries it contains all the information of the full tensor. The expression used by Matthaeus and Goldstein (1982a) to compute the reduced H_{m} is given in Sect. 3.2.3. In the following, we will drop the suffix r for sake of simplicity.

The general features of the reduced magnetic helicity spectrum in the solar wind were described for the first time by Matthaeus and Goldstein (1982a) in the outer heliosphere, and by Bruno and Dobrowolny (1986) in the inner heliosphere. A useful dimensionless way to represent both the degree of and the sense of polarization is the normalized magnetic helicity σ_{m} (see Sect. 3.2.3). This quantity can randomly vary between $+1$ and -1, as shown in Fig. 3.19 from the work by Matthaeus and Goldstein (1982a) and relative to Voyager's data taken at 1 AU. However, net values of ± 1 are reached only for pure circularly polarized waves.

Based on these results, Goldstein et al. (1991) were able to reproduce the distribution of the percentage of occurrence of values of $\sigma_{\mathrm{m}}(f)$ adopting a model where the magnitude of the magnetic field was allowed to vary in a random way and the tip of the vector moved near a sphere. By this way they showed that the interplanetary magnetic field helicity measurements were inconsistent with the previous idea that fluctuations were randomly circularly polarized at all scales and were also magnitude preserving.

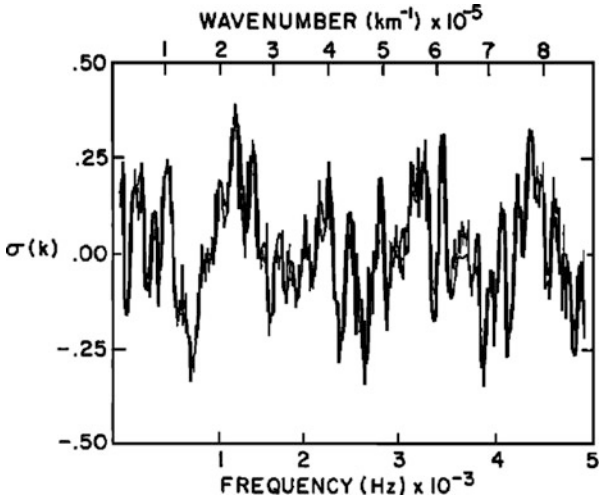

Fig. 3.19 σ_{m} vs. frequency and wave number relative to an interplanetary data sample recorded by Voyager 1 at approximately 1 AU. Image reproduced by permission from Matthaeus and Goldstein (1982a), copyright by AGU

However, evidence for circular polarized MHD waves in the high frequency range was provided by Polygiannakis et al. (1994), who studied interplanetary magnetic field fluctuations from various datasets at various distances ranging from 1 to 20 AU. They also concluded that the difference between left- and right-hand polarizations is significant and continuously varying.

As already noticed by Smith et al. (1983, 1984), knowing the sign of σ_m and the sign of the normalized cross-helicity σ_c it is possible to infer the sense of polarization of the fluctuations. As a matter of fact, a positive cross-helicity indicates an Alfvén mode propagating outward, while a negative cross-helicity indicates a mode propagating inward. On the other hand, we know that a positive magnetic-helicity indicates a right-hand polarized mode, while a negative magnetic-helicity indicates a left-hand polarized mode. Thus, since the sense of polarization depends on the propagating direction with respect to the observer, $\sigma_m(f)\sigma_c(f) < 0$ will indicate *right circular polarization* while $\sigma_m(f)\sigma_c(f) > 0$ will indicate *left circular polarization*. Thus, each time magnetic helicity and cross-helicity are available from measurements in a super-Alfvénic flow, it is possible to infer the rest frame polarization of the fluctuations from a single point measurements, assuming the validity of the slab geometry.

The high variability of σ_m, observable in Voyager's data (see Fig. 3.19), was equally observed in Helios 2 data in the inner heliosphere (Bruno and Dobrowolny 1986). The authors of this last work computed the difference $(MH > 0) - |MH < 0|$ of magnetic helicity for different frequency bands and noticed that most of the resulting magnetic helicity was contained in the lowest frequency band. This result supported the theoretical prediction of an inverse cascade of magnetic helicity from the smallest to the largest scales during turbulence development (Pouquet et al. 1976).

Numerical simulations of the incompressible MHD equations by Mininni et al. (2003a), discussed in Sect. 3.3.8, clearly confirm the tendency of magnetic helicity to follow an inverse cascade. The generation of magnetic field in turbulent plasmas and the successive inverse cascade has strong implications in the emergence of large scale magnetic fields in stars, interplanetary medium and planets (Brandenburg 2001).

This phenomenon was firstly demonstrated in numerical simulations based on the eddy damped quasi normal Markovian (EDQNM) closure model of three-dimensional MHD turbulence by Pouquet et al. (1976). Successively, other investigators confirmed such a tendency for the magnetic helicity to develop an inverse cascade (Meneguzzi et al. 1981; Cattaneo and Hughes 1996; Brandenburg 2001).

Mininni et al. (2003a) performed the first direct numerical simulations of turbulent Hall dynamo. They showed that the Hall current can have strong effects on turbulent dynamo action, enhancing or even suppressing the generation of the large-scale magnetic energy. These authors injected a weak magnetic field at small scales in a system kept in a stationary regime of hydrodynamic turbulence and followed the exponential growth of magnetic energy due to the dynamo action. This evolution can be seen in Fig. 3.20 in the same format described for Fig. 3.31, shown in Sect. 3.3.8. Now, the forcing is applied at wave number $k_{force} = 10$ in order to give enough

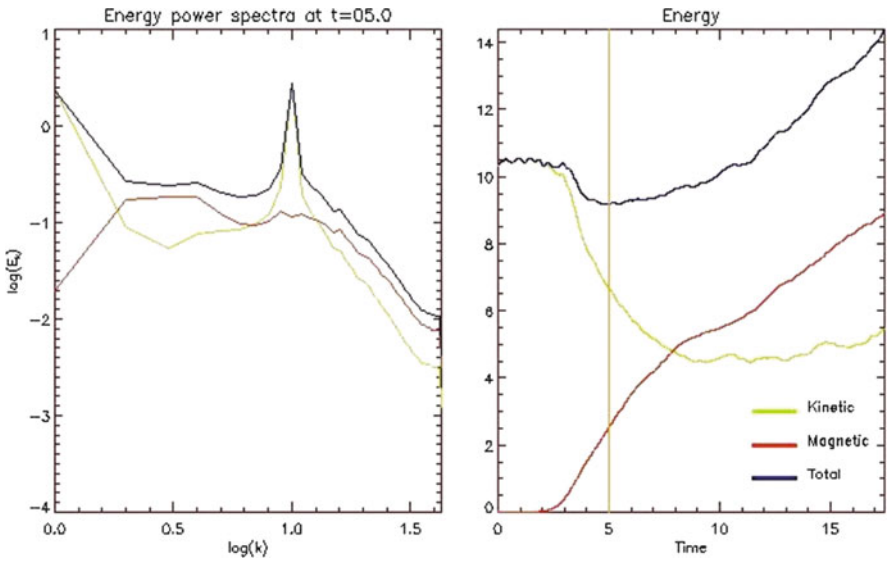

Fig. 3.20 A numerical simulation of the incompressible MHD equations in three dimensions, assuming periodic boundary conditions (see details in Mininni et al. 2003a). The *left panel* shows the power spectra for kinetic energy (*green*), magnetic energy (*red*), and total energy (*blue*) vs. time. *The right panel* shows the spatially integrated kinetic, magnetic, and total energies vs. time. The *vertical (orange) line* indicates the current time. These results correspond to a 128^3 simulation with an external force applied at wave number $k_{\text{force}} = 10$ (Figure kindly provided by D. Gómez)

room for the inverse cascade to develop. The fluid is initially in a strongly turbulent regime as a result of the action of the external force at wave number $k_{\text{force}} = 10$. An initial magnetic fluctuation is introduced at $t = 0$ at $k_{\text{seed}} = 35$. The magnetic energy starts growing exponentially fast and, when the saturation is reached, the magnetic energy is larger than the kinetic energy. Notably, it is much larger at the largest scales of the system (i.e., $k = 1$). At these large scales, the system is very close to a magnetostatic equilibrium characterized by a force-free configuration.

3.3.3 Evidence for Non-linear Interactions

As we said previously, Helios 2 s/c gave us the unique opportunity to study the radial evolution of turbulent fluctuations in the solar wind within the inner heliosphere. Most of the theoretical studies which aim to understand the physical mechanism at the base of this evolution originate from these observations (Bavassano et al. 1982a; Denskat and Neubauer 1983).

In Fig. 3.21 we consider again similar observations taken by Helios 2 during its primary mission to the Sun together with observations taken by Ulysses in the ecliptic at 1.4 and 4.8 AU in order to extend the total radial excursion.

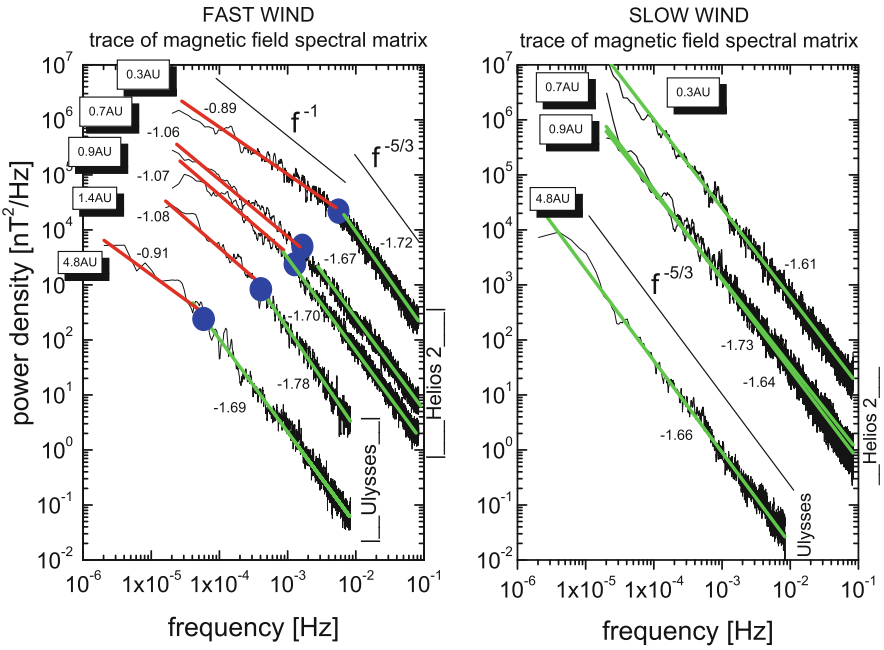

Fig. 3.21 *Left panel:* power density spectra of magnetic field fluctuations observed by Helios 2 between 0.3 and 1 AU within the trailing edge of the same corotating stream shown in Fig. 3.10, during the first mission to the Sun in 1976 and by Ulysses between 1.4 and 4.8 AU during the ecliptic phase. Ulysses observations at 4.8 AU refer to the end of 1991 while observations taken at 1.4 AU refer to the end of August of 2007. While the spectral index of slow wind does not show any radial dependence, the spectral break, clearly present in fast wind and marked by a *blue dot*, moves to lower and lower frequency as the heliocentric distance increases. Image adapted from Bruno et al. (2009)

Helios 2 power density spectra were obtained from the trace of the spectral matrix of magnetic field fluctuations, and belong to the same co-rotating stream observed on day 49, at a heliocentric distance of 0.9 AU, on day 75 at 0.7 AU and, finally, on day 104 at 0.3 AU. Ulysses spectra, constructed in the same way as those of Helios 2, were taken at 1.4 and 4.8 AU during the ecliptic phase of the orbit. Observations at 4.8 AU refer to the end of 1991 (fast wind period started on day 320, slow wind period started on day 338) while observations taken at 1.4 AU refer to fast wind observed at the end of August of 2007, starting on day 241:12.

While the spectral index of slow wind does not show any radial dependence, being characterized by a single Kolmogorov type spectral index, fast wind is characterized by two distinct spectral slopes: about -1 within low frequencies and about a Kolmogorov like spectrum at higher frequencies. These two regimes are clearly separated by a knee in the spectrum often referred to as "frequency break". As the wind expands, the frequency break moves to lower and lower frequencies so that larger and larger scales become part of the Kolmogorov-like turbulence

spectrum, i.e., of what we will indicate as "inertial range" (see discussion at the end of the previous section). Thus, the power spectrum of solar wind fluctuations is not solely function of frequency f, i.e., $P(f)$, but it also depends on heliocentric distance r, i.e., $P(f) \rightarrow P(f, r)$.

Figure 3.22 shows the frequency location of the spectral breaks observed in the left-hand-side panel of Fig. 3.21 as a function of heliocentric distance. The radial distribution of these 5 points suggests that the frequency break moves at lower and lower frequencies during the wind expansion following a power-law of the order of $R^{-1.5}$. Previous results, obtained for long data sets spanning hundreds of days and inevitably mixing fast and slow wind, were obtained by Matthaeus and Goldstein (1986) who found the breakpoint around 10 h at 1 AU, and Klein et al. (1992) who found that the breakpoint was near 16 h at 4 AU. Obviously, the frequency location of the breakpoint provided by these early determinations is strongly affected by the fact that mixing fast and slow wind would shift the frequency break to lower frequencies with respect to solely fast wind. In any case, this frequency break is strictly related to the correlation length (Klein 1987) and the shift to lower frequency, during the wind expansion, is consistent with the growth of the correlation length observed in the inner (Bruno and Dobrowolny 1986) and outer heliosphere (Matthaeus and Goldstein 1982b). Analogous behavior for the low frequency shift of the spectral break, similar to the one observed in the ecliptic, has been reported by Horbury et al. (1996) studying the rate of turbulent evolution over the Sun's poles. These authors used Ulysses magnetic field observations between 1.5 and 4.5 AU selecting mostly undisturbed, high speed polar flows. They found a radial gradient of the order of $R^{-1.1}$, clearly slower than the one reported in Fig. 3.22 or that can be inferred from results by Bavassano et al. (1982a) confirming that the

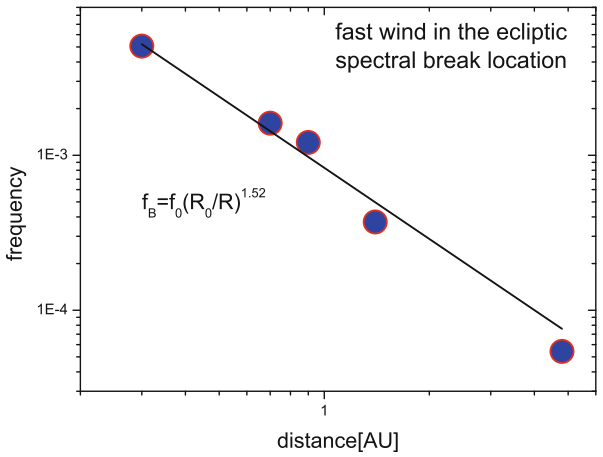

Fig. 3.22 Radial dependence of the frequency break observed in the ecliptic within fast wind as shown in the previous Fig. 3.21. The radial dependence seems to be governed by a power-law of the order of $R^{-1.5}$

turbulence evolution in the polar wind is slower than the one in the ecliptic, as qualitatively predicted by Bruno (1992), because of the lack of large scale stream shears. However, these results will be discussed more extensively in Sect. 4.3.1.

However, the phenomenology described above only apparently resembles hydrodynamic turbulence where the large eddies, below the frequency break, govern the whole process of energy cascade along the spectrum (Tu and Marsch 1995a). As a matter of fact, when the relaxation time increases, the largest eddies provide the energy to be transferred along the spectrum and dissipated, with a decay rate approximately equal to the transfer rate and, finally, to the dissipation rate at the smallest wavelengths where viscosity dominates. Thus, we expect that the energy containing scales would loose energy during this process but would not become part of the turbulent cascade, say of the inertial range. Scales on both sides of the frequency break would remain separated. Accurate analysis performed in the solar wind (Bavassano et al. 1982a; Marsch and Tu 1990b; Roberts 1992) have shown that the low frequency range of the solar wind magnetic field spectrum radially evolves following the WKB model, or geometrical optics, which predicts a radial evolution of the power associated with the fluctuations $\sim r^{-3}$. Moreover, a steepening of the spectrum towards a Kolmogorov like spectral index can be observed. On the contrary, the same in-situ observations established that the radial decay for the higher frequencies was faster than $\sim r^{-3}$ and the overall spectral slope remained unchanged. This means that the energy contained in the largest eddies does not decay as it would happen in hydrodynamic turbulence and, as a consequence, the largest eddies cannot be considered equivalent to the energy containing eddies identified in hydrodynamic turbulence. So, this low frequency range is not separated from the inertial range but becomes part of it as the turbulence ages. These observations cast some doubts on the applicability of hydrodynamic turbulence paradigm to interplanetary MHD turbulence. A theoretical help came from adopting a local energy transfer function (Tu et al. 1984; Tu 1987a,b, 1988), which would take into account the non-linear effects between eddies of slightly differing wave numbers, together with a WKB description which would mainly work for the large scale fluctuations. This model was able to reproduce the displacement of the frequency break with distance by combining the linear WKB law and a model of nonlinear coupling besides most of the features observed in the magnetic power spectra $P(f, r)$ observed by Bavassano et al. (1982a). In particular, the concept of the "frequency break", just mentioned, was pointed out for the first time by Tu et al. (1984) who, developing the analytic solution for the radially evolving power spectrum $P(f, r)$ of fluctuations, obtained a critical frequency "f_c" such that for frequencies $f \ll f_c, P(f, r) \propto f^{-1}$ and for $f \gg f_c, P(f, r) \propto f^{-1.5}$.

3.3.4 Power Anisotropy and Minimum Variance Technique

Interplanetary magnetic field (IMF) and velocity fluctuations are rather anisotropic as for the first time observed by Belcher and Davis Jr (1971), Belcher and Solodyna

(1975), Chang and Nishida (1973), Burlaga and Turner (1976), Solodyna and Belcher (1976), Parker (1980), Bavassano et al. (1982b), Tu et al. (1989), and Marsch and Tu (1990a). This feature can be better observed if fluctuations are rotated into the minimum variance reference system.

This is a reference system with one of its axes aligned with a direction along which the field has the smallest fluctuations (Sonnerup and Cahill 1967). This method provides information on the spatial distribution of the fluctuations of a given vector.

Given a generic field $B(x, y, z)$, the variance of its components is

$$\langle B_x^2\rangle - \langle B_x\rangle^2; \langle B_y^2\rangle - \langle B_y\rangle^2; \langle B_z^2\rangle - \langle B_z\rangle^2.$$

Similarly, the variance of B along the direction S would be given by

$$V_S = \langle B_S^2\rangle - \langle B_S\rangle^2.$$

Let us assume, for sake of simplicity, that all the three components of B fluctuate around zero, then

$$\langle B_x\rangle = \langle B_y\rangle = \langle B_z\rangle = 0 \Longrightarrow \langle B_S\rangle = \mathbf{x}\langle B_x\rangle + \mathbf{y}\langle B_y\rangle + \mathbf{z}\langle B_z\rangle = 0.$$

Then, the variance V_S can be written as

$$V_S = \langle B_S^2\rangle = x^2\langle B_x^2\rangle + y^2\langle B_y^2\rangle + z^2\langle B_z^2\rangle + 2\mathbf{xy}\langle B_xB_y\rangle + 2\mathbf{xz}\langle B_xB_z\rangle + 2\mathbf{yz}\langle B_yB_z\rangle,$$

which can be written (omitting the sign of average $\langle\rangle$) as

$$V_S = \mathbf{x}(\mathbf{x}B_x^2 + \mathbf{y}B_xB_y + \mathbf{z}B_xB_z) + \mathbf{y}(\mathbf{y}B_y^2 + \mathbf{x}B_xB_y + \mathbf{z}B_yB_z) + \mathbf{z}(\mathbf{z}B_z^2 + \mathbf{x}B_xB_z + \mathbf{y}B_yB_z).$$

This expression can be interpreted as a scalar product between a vector $\mathbf{S}(x, y, z)$ and another vector whose components are the terms in parentheses. Moreover, these last ones can be expressed as a product between a matrix M built with the terms B_x^2, B_y^2, B_z^2, B_xB_y, B_xB_z, B_yB_z, and a vector $\mathbf{S}(x, y, z)$. Thus,

$$V_S = (S, MS),$$

where

$$S \equiv \begin{pmatrix} x \\ y \\ z \end{pmatrix}$$

and

$$M \equiv \begin{pmatrix} {B_x}^2 & B_x B_y & B_x B_z \\ B_x B_y & {B_y}^2 & B_y B_z \\ B_x B_z & B_y B_z & {B_z}^2 \end{pmatrix}.$$

At this point, M is a symmetric matrix and is the matrix of the quadratic form V_S which, in turn, is defined positive since it represents a variance. It is possible to determine a new reference system $[x, y, z]$ such that the quadratic form V_S does not contain mix terms, i.e.,

$$V_S = x'^2 {B'_x}^2 + y'^2 {B'_y}^2 + z'^2 {B'_z}^2.$$

Thus, the problem reduces to compute the eigenvalues λ_i and eigenvectors $\tilde{V}_i$ of the matrix M. The eigenvectors represent the axes of the new reference system, the eigenvalues indicate the variance along these axes as shown in Fig. 3.23.

At this point, since we know the components of unit vectors of the new reference system referred to the old reference system, we can easily rotate any vector, defined in the old reference system, into the new one.

The statistical properties of eigenvalues approximately satisfy the following statements:

- One of the eigenvalues of the variance matrix is always much smaller than the others, say $\lambda_1 \ll (\lambda_2, \lambda_3)$, and the corresponding eigenvector $\tilde{V}_1$ is the minimum-variance direction. This indicates that, at least locally, the magnetic fluctuations are confined in a plane perpendicular to the minimum-variance direction.

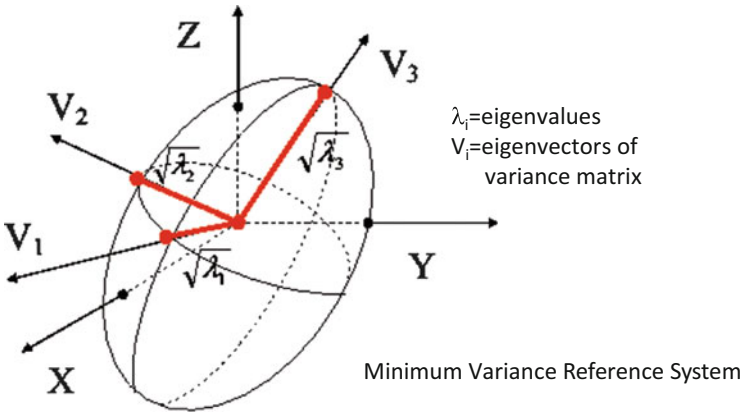

Fig. 3.23 Original reference system $[x, y, z]$ and minimum variance reference system whose axes are V_1, V_2, and V_3 and represent the *eigenvectors* of M. Moreover, λ_1, λ_2, and λ_3 are the *eigenvalues* of M

- In the plane perpendicular to $\tilde{V}_1$, fluctuations appear to be anisotropically distributed, say $\lambda_3 > \lambda_2$. Typical values for eigenvalues are $\lambda_3 : \lambda_2 : \lambda_1 = 10 : 3.5 : 1.2$ (Chang and Nishida 1973; Bavassano et al. 1982b).
- The direction $\tilde{V}_1$ is nearly parallel to the average magnetic field $\mathbf{B_0}$, that is, the distribution of the angles between $\tilde{V}_1$ and $\mathbf{B_0}$ is narrow with width of about 10° and centered around zero.

As shown in Fig. 3.24, in this new reference system it is readily seen that the maximum and intermediate components have much more power compared with the minimum variance component. Generally, this kind of anisotropy characterizes Alfvénic intervals and, as such, it is more commonly found within high velocity streams (Marsch and Tu 1990a).

A systematic analysis for both magnetic and velocity fluctuations was performed by Klein et al. (1991, 1993) between 0.3 and 10 AU. These studies showed that magnetic field and velocity minimum variance directions are close to each other within fast wind and mainly clustered around the local magnetic field direction. The effects of expansion are such as to separate field and velocity minimum variance directions. While magnetic field fluctuations keep their minimum variance direction loosely aligned with the mean field direction, velocity fluctuations tend to have their minimum variance direction oriented along the radial direction. The depleted

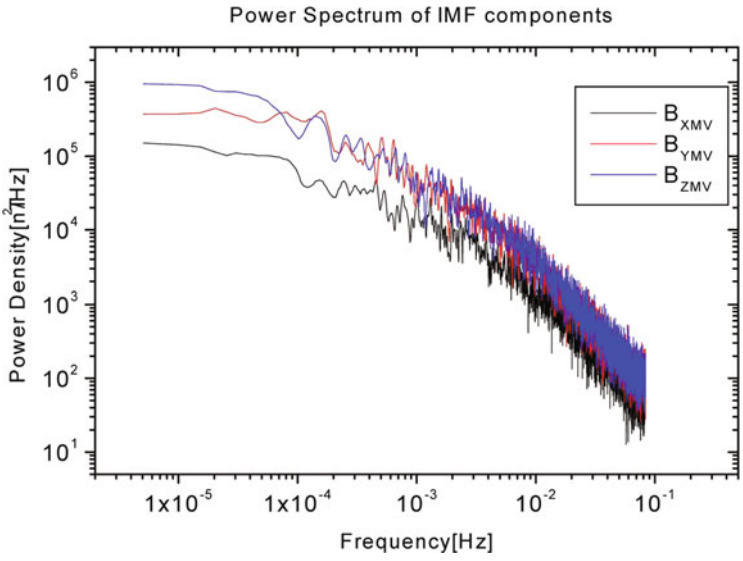

Fig. 3.24 Power density spectra of the three components of IMF after rotation into the minimum variance reference system. The *black curve* corresponds to the minimum variance component, the *blue curve* to the maximum variance, and the *red* one to the intermediate component. This case refers to fast wind observed at 0.3 AU and the minimum variance direction forms an angle of $\sim 8°$ with respect to the ambient magnetic field direction. Thus, most of the power is associated with the two components quasi-transverse to the ambient field

alignment to the background magnetic field would suggest a smaller anisotropy of the fluctuations. As a matter of fact, Klein et al. (1991) found that the degree of anisotropy, which can be defined as the ratio between the power perpendicular to and that along the minimum variance direction, decreases with heliocentric distance in the outer heliosphere.

At odds with these conclusions were the results by Bavassano et al. (1982b) who showed that the ratio λ_1/λ_3, calculated in the inner heliosphere within a co-rotating high velocity stream, clearly decreased with distance, indicating that the degree of magnetic anisotropy increased with distance. Moreover, this radial evolution was more remarkable for fluctuations of the order of a few hours than for those around a few minutes. Results by Klein et al. (1991) in the outer heliosphere and by Bavassano et al. (1982b) in the inner heliosphere remained rather controversial until recent studies (see Sect. 7.4), performed by Bruno et al. (1999), found a reason for this discrepancy.

A different approach to anisotropic fluctuations in solar wind turbulence have been made by Bigazzi et al. (2006) and Sorriso-Valvo et al. (2006, 2010). In these studies the full tensor of the mixed second-order structure functions has been used to quantitatively measure the degree of anisotropy and its effect on small-scale turbulence through a fit of the various elements of the tensor on a typical function (Sorriso-Valvo et al. 2006). Moreover three different regions of the near-Earth space have been studied, namely the solar wind, the Earth's foreshock and magnetosheath showing that, while in the undisturbed solar wind the observed strong anisotropy is mainly due to the large-scale magnetic field, near the magnetosphere other sources of anisotropy influence the magnetic field fluctuations (Sorriso-Valvo et al. 2010).

3.3.5 Simulations of Anisotropic MHD

In the presence of a DC background magnetic field $\mathbf{B_0}$ which, differently from the bulk velocity field, cannot be eliminated by a Galilean transformation, MHD incompressible turbulence becomes anisotropic (Shebalin et al. 1983; Montgomery 1982; Zank and Matthaeus 1992; Carbone and Veltri 1990; Oughton 1993). The main effect produced by the presence of the background field is to generate an anisotropic distribution of wave vectors as a consequence of the dependence of the characteristic time for the non-linear coupling on the angle between the wave vector and the background field. This effect can be easily understood if one considers the MHD equation. Due to the presence of a term $(\mathbf{B_0} \cdot \nabla)\mathbf{z}^{\pm}$, which describes the convection of perturbations in the average magnetic field, the non-linear interactions between Alfvénic fluctuations are weakened, since convection decorrelates the interacting eddies on a time of the order $(\mathbf{k} \cdot \mathbf{B_0})^{-1}$. Clearly fluctuations with wave vectors almost perpendicular to $\mathbf{B_0}$ are interested by such an effect much less than fluctuations with $\mathbf{k} \parallel \mathbf{B_0}$. As a consequence, the former are transferred along the spectrum much faster than the latter (Shebalin et al. 1983; Grappin 1986; Carbone and Veltri 1990).

To quantify anisotropy in the distribution of wave vectors $\mathbf{k}$ for a given dynamical variable $Q(\mathbf{k}, t)$ (namely the energy, cross-helicity, etc.), it is useful to introduce the parameter

$$\Omega_Q = \tan^{-1} \sqrt{\frac{\langle k_\perp^2 \rangle_Q}{2\langle k_\parallel^2 \rangle_Q}} \tag{3.36}$$

(Shebalin et al. 1983; Carbone and Veltri 1990), where the average of a given quantity $g(\mathbf{k})$ is defined as

$$\langle g(\mathbf{k}) \rangle_Q = \frac{\int d^3\mathbf{k}\, g(\mathbf{k}) Q(\mathbf{k}, t)}{\int d^3\mathbf{k}\, Q(\mathbf{k}, t)}.$$

For a spectrum with wave vectors perpendicular to $\mathbf{B_0}$ we have a spectral anisotropy $\Omega = 90°$, while for an isotropic spectrum $\Omega = 45°$. Numerical simulations in 2D configuration by Shebalin et al. (1983) confirmed the occurrence of anisotropy, and found that anisotropy increases with the Reynolds number. Unfortunately, in these old simulations, the Reynolds numbers used are too small to achieve a well defined spectral anisotropy. Carbone and Veltri (1990) started from the spectral equations obtained through the Direct Interaction Approximation closure by Veltri et al. (1982), and derived a shell model analogous for the anisotropic MHD turbulence. Of course the anisotropy is over-simplified in the model, in particular the Alfvén time is assumed isotropic. However, the model was useful to investigate spectral anisotropy at very high Reynolds numbers. The phenomenological anisotropic spectrum obtained from the model, for both pseudo-energies obtained through polarizations $a = 1, 2$ defined through Eq. (2.18), can be written as

$$E_a^{\pm}(\mathbf{k}, t) \sim C_a^{\pm} \left[\ell_\parallel^2 k_\parallel^2 + \ell_\perp^2 k_\perp^2 \right]^{-\mu^{\pm}}. \tag{3.37}$$

The spectral anisotropy is different within the injection, inertial, and dissipative ranges of turbulence (Carbone and Veltri 1990). Wave vectors perpendicular to $\mathbf{B_0}$ are present in the spectrum, but when the process of energy transfer generates a strong anisotropy (at small times), a competing process takes place which redistributes the energy over all wave vectors. The dynamical balance between these tendencies fixes the value of the spectral anisotropy $\Omega \simeq 55°$ in the inertial range. On the contrary, since the redistribution of energy cannot take place, in the dissipation domain the spectrum remains strongly anisotropic, with $\Omega \simeq 80°$. When the Reynolds number increases, the contribution of the inertial range extends, and the increases of the total anisotropy tends to saturate at about $\Omega \simeq 60°$ at Reynolds number of 10^5. This value corresponds to a rather low value for the ratio between parallel and perpendicular correlation lengths $\ell_\parallel/\ell_\perp \simeq 2$, too small with respect to the observed value $\ell_\parallel/\ell_\perp \geq 10$. This suggests that the non-linear dynamical

evolution of an initially isotropic spectrum of turbulence is perhaps not sufficient to explain the observed anisotropy. These results have been confirmed numerically (Oughton et al. 1994).

3.3.6 *Spectral Anisotropy in the Solar Wind*

The correlation time, as defined in Sect. 3.2, estimates how much an element of our time series $x(t)$ at time t_1 depends on the value assumed by $x(t)$ at time t_0, being $t_1 = t_0 + \delta t$. This concept can be transferred from the time domain to the space domain if we adopt the Taylor hypothesis and, consequently, we can talk about spatial scales.

Correlation lengths in the solar wind generally increase with heliocentric distance (Matthaeus and Goldstein 1982a; Bruno and Dobrowolny 1986), suggesting that large scale correlations are built up during the wind expansion. This kind of evolution is common to both fast and slow wind as shown in Fig. 3.25, where we can observe the behavior of the B_z correlation function for fast and slow wind at 0.3 and 0.9 AU.

Moreover, the fast wind correlation functions decrease much faster than those related to slow wind. This behavior reflects also the fact that the stochastic character

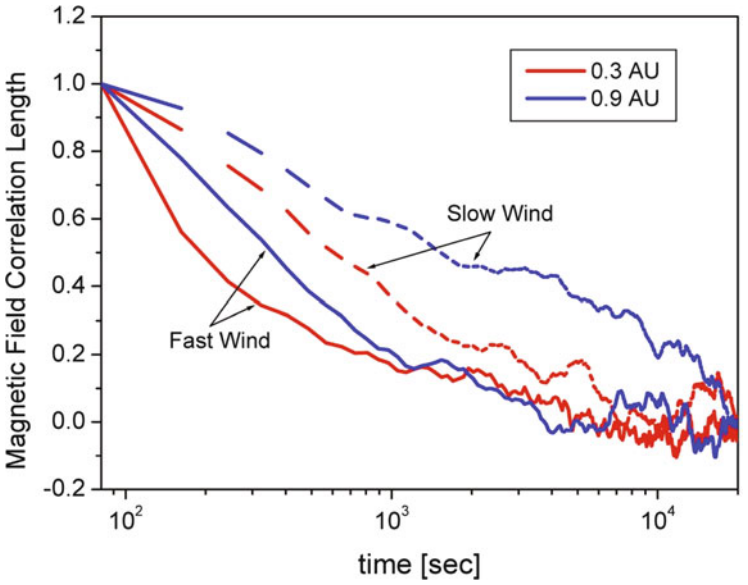

Fig. 3.25 Correlation function just for the Z component of interplanetary magnetic field as observed by Helios 2 during its primary mission to the Sun. The *blue* color refers to data recorded at 0.9 AU while the *red* color refers to 0.3 AU. *Solid lines* refer to fast wind, *dashed lines* refer to slow wind

of Alfvénic fluctuations in the fast wind is very efficient in decorrelating the fluctuations of each of the magnetic field components.

More detailed studies performed by Matthaeus et al. (1990) provided for the first time the two-dimensional correlation function of solar wind fluctuations at 1 AU. The original dataset comprised approximately 16 months of almost continuous magnetic field 5-min averages. These results, based on ISEE 3 magnetic field data, are shown in Fig. 3.26, also called the "The Maltese Cross".

This figure has been obtained under the hypothesis of cylindrical symmetry. Real determination of the correlation function could be obtained only in the positive quadrant, and the whole plot was then made by mirroring these results on the remaining three quadrants. The iso-contour lines show contours mainly elongated along the ambient field direction or perpendicular to it. Alfvénic fluctuations with $\mathbf{k} \parallel \mathbf{B_0}$ contribute to contours elongated parallel to $r_\perp$. Fluctuations in the two-dimensional turbulence limit (Montgomery 1982) contribute to contours elongated parallel to $r_\parallel$. This two-dimensional turbulence is characterized for having both the wave vector $\mathbf{k}$ and the perturbing field $\delta\mathbf{b}$ perpendicular to the ambient field $\mathbf{B_0}$. Given the fact that the analysis did not select fast and slow wind, separately, it is likely that most of the slab correlations came from the fast wind while the 2D correlations came from the slow wind. As a matter of fact, Dasso et al. (2005), using 5 years of spacecraft observations at roughly 1 AU, showed that fast

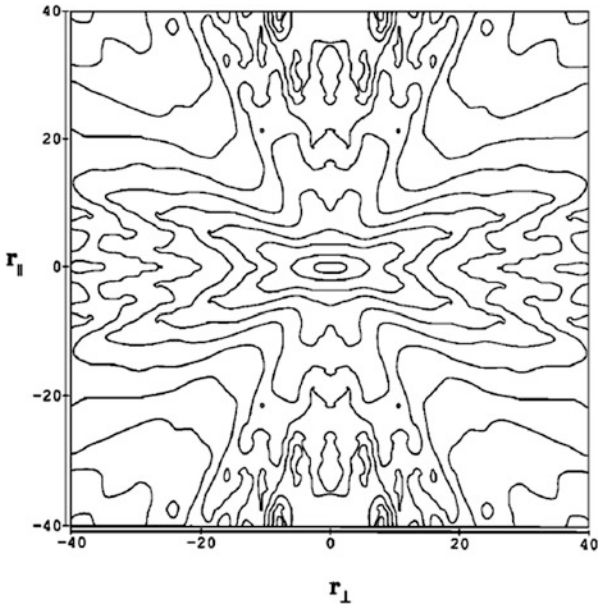

Fig. 3.26 Contour plot of the 2D correlation function of interplanetary magnetic field fluctuations as a function of parallel and perpendicular distance with respect to the mean magnetic field. The separation in $r_\parallel$ and $r_\perp$ is in units of 10^{10} cm. Image reproduced by permission from Matthaeus et al. (1990), copyright by AGU

streams are dominated by fluctuations with wavevectors quasi-parallel to the local magnetic field, while slow streams are dominated by quasi-perpendicular fluctuation wavevectors. Anisotropic turbulence has been observed in laboratory plasmas and reverse pinch devices (Zweben et al. 1979).

Bieber et al. (1996) formulated an observational test to distinguish the slab (Alfvénic) from the 2D component within interplanetary turbulence. These authors assumed a mixture of transverse fluctuations, some of which have wave vectors perpendicular $\mathbf{k} \perp \mathbf{B_0}$ and polarization of fluctuations $\delta\mathbf{B}(\mathbf{k}_\perp)$ perpendicular to both vectors (2D geometry with $k_\parallel \simeq 0$), and some parallel to the mean magnetic field $\mathbf{k} \parallel \mathbf{B_0}$, the polarization of fluctuations $\delta\mathbf{B}(k_\parallel)$ being perpendicular to the direction of $\mathbf{B_0}$ (slab geometry with $\mathbf{k}_\perp \simeq 0$). The magnetic field is then rotated into the same mean field coordinate system used by Belcher and Davis Jr (1971) and Belcher and Solodyna (1975), where the y-coordinate is perpendicular to both $\mathbf{B_0}$ and the radial direction, while the x-coordinate is perpendicular to $\mathbf{B_0}$ but with a component also in the radial direction.

The mean field reference system (see Fig. 3.2) reduces the problem of cross-talking between the components due to the fact that the interplanetary magnetic field is not oriented like the axes of the reference system in which we perform the measurement and, as a consequence, any component will experience a contribution from the other ones.

Using this new reference system, and defining the power spectrum matrix as

$$P_{ij}(\mathbf{k}) = \frac{1}{(2\pi)^3}\int d^3\mathbf{r}\langle \mathbf{B}_i(\mathbf{x})B_j(\mathbf{x}+\mathbf{r})\rangle e^{-i\mathbf{k}\cdot\mathbf{r}},$$

it can be found that, assuming axisymmetry, a two-component model can be written in the frequency domain

$$fP_{yy}(f) = rC_s\left(\frac{2\pi f}{U_w\cos\psi}\right)^{1-q} + (1-r)C_s\frac{2q}{(1+q)}\left(\frac{2\pi f}{U_w\sin\psi}\right)^{1-q}, \tag{3.38}$$

$$fP_{xx}(f) = rC_s\left(\frac{2\pi f}{U_w\cos\psi}\right)^{1-q} + (1-r)C_s\frac{2}{(1+q)}\left(\frac{2\pi f}{U_w\sin\psi}\right)^{1-q}, \tag{3.39}$$

where the anisotropic energy spectrum is the sum of both components:

$$fT(f) = 2rC_s\left(\frac{2\pi f}{U_w\cos\psi}\right)^{1-q} + 2(1-r)C_s\left(\frac{2\pi f}{U_w\sin\psi}\right)^{1-q}. \tag{3.40}$$

Here f is the frequency, C_s is a constant defining the overall spectrum amplitude in wave vector space, U_w is the bulk solar wind speed and ψ is the angle between $\mathbf{B_0}$ and the wind direction. Finally, r is the fraction of slab components and $(1-r)$ is the fraction of 2D components.

The ratio test adopted by these authors was based on the ratio between the reduced perpendicular spectrum (fluctuations $\perp$ to the mean field and solar wind flow direction) and the reduced quasi-parallel spectrum (fluctuations $\perp$ to the mean field and in the plane defined by the mean field and the flow direction). This ratio, expected to be 1 for slab turbulence, resulted to be ~ 1.4 for fluctuations within the inertial range, consistent with 74 % of 2D turbulence and 26 % of slab. A further test, the anisotropy test, evaluated how the spectrum should vary with the angle between the mean magnetic field and the flow direction of the wind. The measured slab spectrum should decrease with the field angle while the 2D spectrum should increase, depending on how these spectra project on the flow direction. The results from this test were consistent with 95 % of 2D turbulence and 5 % of slab. In other words, the slab turbulence due to Alfvénic fluctuations would be a minor component of interplanetary MHD turbulence. A third test derived from Mach number scaling associated with the nearly incompressible theory Zank and Matthaeus (1992), assigned the same fraction ~ 80 % to the 2D component. However, the data base for this analysis was derived from Helios magnetic measurements, and all data were recorded near times of solar energetic particle events. Moreover, the quasi totality of the data belonged to slow solar wind Wanner and Wibberenz (1993) and, as such, this analysis cannot be representative of the whole phenomenon of turbulence in solar wind. As a matter of fact, using Ulysses observations, Smith (2003) found that in the polar wind the percentage of slab and 2D components is about the same, say the high latitude slab component results unusually higher as compared with ecliptic observations.

Successive theoretical works by Ghosh et al. (1998b,a) in which they used compressible models in large variety of cases were able to obtain, in some cases, parallel and perpendicular correlations similar to those obtained in the solar wind. However, they concluded that the "Maltese" cross does not come naturally from the turbulent evolution of the fluctuations but it strongly depends on the initial conditions adopted when the simulation starts. It seems that the existence of these correlations in the initial data represents an unavoidable constraint. Moreover, they also stressed the importance of time-averaging since the interaction between slab waves and transverse pressure-balanced magnetic structures causes the slab turbulence to evolve towards a state in which a two-component correlation function emerges during the process of time averaging.

The presence of two populations, i.e., a slab-like and a quasi-2D like, was also inferred by Dasso et al. (2003). These authors computed the reduced spectra of the normalized cross-helicity and the Alfvén ratio from ACE dataset. These parameters, calculated for different intervals of the angle θ between the flow direction and the orientation of the mean field $\mathbf{B_0}$, showed a remarkable dependence on θ.

The geometry used in these analyses assumes that the energy spectrum in the rest frame of the plasma is axisymmetric and invariant for rotations about the direction of $\mathbf{B_0}$. Even if these assumption are good when we want to translate results coming from 2D numerical simulations to 3D geometry, these assumptions are quite in contrast with the observational fact that the eigenvalues of the variance matrix are different, namely $\lambda_3 \neq \lambda_2$.

Going back from the correlation tensor to the power spectrum is a complicated technical problem. However, Carbone et al. (1995) derived a description of the observed anisotropy in terms of a model for the three-dimensional energy spectra of magnetic fluctuations. The divergence-less of the magnetic field allows to decompose the Fourier amplitudes of magnetic fluctuations in two independent polarizations: The first one $I^{[1]}(\mathbf{k})$ corresponds, in the weak turbulence theory, to the Alfvénic mode, while the second polarization $I^{[2]}(\mathbf{k})$ corresponds to the magnetosonic mode. By using *only* the hypothesis that the medium is statistically homogeneous and some algebra, authors found that the energy spectra of both polarizations can be related to the two-points correlation tensor and to the variance matrix. Through numerical simulations of the shell model (see later in the review) it has been shown that the anisotropic energy spectrum can be described in the inertial range by a phenomenological expression

$$I^{[s]}(\mathbf{k}) = C_s \left[\left(\ell_x^{[s]} k_x\right)^2 + \left(\ell_y^{[s]} k_y\right)^2 + \left(\ell_z^{[s]} k_z\right)^2 \right]^{-1-\mu_s/2}, \tag{3.41}$$

where k_i are the Cartesian components of the wave vector $\mathbf{k}$, and C_s, $\ell_i^{[s]}$, and μ_s ($s = 1, 2$ indicates both polarizations; $i = x, y, z$) are free parameters. In particular, C_s gives information on the energy content of both polarizations, $\ell_i^{[s]}$ represent the spectral extensions along the direction of a given system of coordinates, and μ_s are two spectral indices.

A fit to the eigenvalues of the variance matrix allowed Carbone et al. (1995) to fix the free parameters of the spectrum for both polarizations. They used data from Bavassano et al. (1982b) who reported the values of λ_i at five wave vectors calculated at three heliocentric distances, selecting periods of high correlation (Alfvénic periods) using magnetic field measured by the Helios 2 spacecraft. They found that the spectral indices of both polarizations, in the range $1.1 \leq \mu_1 \leq 1.3$ and $1.46 \leq \mu_2 \leq 1.8$ increase systematically with increasing distance from the Sun, the polarization [2] spectra are always steeper than the corresponding polarization [1] spectra, while polarization [1] is always more energetic than polarization [2]. As far as the characteristic lengths are concerned, it can be found that $\ell_x^{[1]} > \ell_y^{[1]} \gg \ell_z[1]$, indicating that wave vectors $\mathbf{k} \parallel \mathbf{B_0}$ largely dominate. Concerning polarization [2], it can be found that $\ell_x[2] \gg \ell_y^{[2]} \simeq \ell_z^{[2]}$, indicating that the spectrum $I^{[2]}(\mathbf{k})$ is strongly flat on the plane defined by the directions of $\mathbf{B_0}$ and the radial direction. Within this plane, the energy distribution does not present any relevant anisotropy.

Let us compare these results with those by Matthaeus et al. (1990), the comparison being significant as far as the plane yz is taken into account. The decomposition of Carbone et al. (1995) in two independent polarizations is similar to that of Matthaeus et al. (1990), a contour plot of the trace of the correlation tensor Fourier transform $T(\mathbf{k}) = I^{[1]}(\mathbf{k}) + I^{[2]}(\mathbf{k})$ on the plane $(k_y; k_z)$ shows two populations of fluctuations, with wave vectors nearly parallel and nearly perpendicular to $\mathbf{B_0}$, respectively. The first population is formed by all the polarization [1] fluctuations and by the fluctuations with $\mathbf{k} \parallel \mathbf{B_0}$ belonging to polarization [2]. The latter

fluctuations are physically indistinguishable from the former, in that when $\mathbf{k}$ is nearly parallel to $\mathbf{B_0}$, both polarization vectors are quasi-perpendicular to $\mathbf{B_0}$. On the contrary, the second population is almost entirely formed by fluctuations belonging to polarization [2]. While it is clear that fluctuations with $\mathbf{k}$ nearly parallel to $\mathbf{B_0}$ are mainly polarized in the plane perpendicular to $\mathbf{B_0}$ (a consequence of $\nabla \cdot \mathbf{B} = 0$), fluctuations with $\mathbf{k}$ nearly perpendicular to $\mathbf{B_0}$ are polarized nearly parallel to $\mathbf{B_0}$.

Although both models yield to the occurrence of two populations, Matthaeus et al. (1990) give an interpretation of their results which is in contrast with that of Carbone et al. (1995). Namely Matthaeus et al. (1990) suggest that a nearly 2D incompressible turbulence characterized by wave vectors and magnetic fluctuations, both perpendicular to $\mathbf{B_0}$, is present in the solar wind. However, this interpretation does not arise from data analysis, rather from the 2D numerical simulations by Shebalin et al. (1983) and from analytical studies (Montgomery 1982). Let us note, however, that in the former approach, which is strictly 2D, when $\mathbf{k} \perp \mathbf{B_0}$ magnetic fluctuations are necessarily parallel to $\mathbf{B_0}$. In the latter one, along with incompressibility, it is assumed that the energy in the fluctuations is much less than in the DC magnetic field; both hypotheses do not apply to the solar wind case. On the contrary, results by Carbone et al. (1995) can be directly related to the observational data. In any case, it is worth reporting that a model like that discussed here, that is a superposition of fluctuations with both slab and 2D components, has been used to describe turbulence also in the Jovian magnetosphere (Saur et al. 2002, 2003). In addition, several theoretical and observational works indicate that there is a competition between the radial axis and the mean field axis in shaping the polarization and spectral anisotropies in the solar wind.

In this respect, Grappin and Velli (1996) used numerical simulations of MHD equations which included expansion effects (Expanding Box Model) to study the formation of anisotropy in the wind and the interaction of Alfvén waves within a transverse magnetic structures. These authors found that a large-scale isotropic Alfvénic eddy stretched by expansion naturally mixes with smaller scale transverse Alfvén waves with a different anisotropy.

Saur and Bieber (1999), on the other hand, employed three different tests on about three decades of solar wind observations at 1 AU in order to better understand the anisotropic nature of solar wind fluctuations. Their data analysis strongly supported the composite model of a turbulence made of slab and 2-D fluctuations.

Narita et al. (2011), using the four Cluster spacecraft, determined the three-dimensional wave-vector spectra of fluctuating magnetic fields in the solar wind within the inertial range. These authors found that the spectra are anisotropic throughout the analyzed frequency range and the power is extended primarily in the directions perpendicular to the mean magnetic field, as might be expected of 2-D turbulence, however, the analyzed fluctuations cannot be considered axisymmetric.

Finally, Turner et al. (2011) suggested that the non-axisymmetry anisotropy of the frequency spectrum observed using in-situ observations may simply arise from a sampling effect related to the fact that the s/c samples three dimensional fluctuations as a one-dimensional series and that the energy density is not equally distributed among the different scales (i.e., spectral index > 1).

3.3.7 *Alfvénic Correlations as Incompressive Turbulence*

In a famous paper, Belcher and Davis Jr (1971) showed that a strong correlation exists between velocity and magnetic field fluctuations, in the form

$$\delta \mathbf{v} \simeq \pm \frac{\delta \mathbf{B}}{\sqrt{4\pi\rho}}, \tag{3.42}$$

where the sign of the correlation is given by the $sign[-\mathbf{k} \cdot \mathbf{B_0}]$, being $\mathbf{k}$ the wave vector and $\mathbf{B_0}$ the background magnetic field vector. These authors showed that in about 25 day of data from Mariner 5, out of the 160 day of the whole mission, fluctuations were described by Eq. (3.42), and the sign of the correlation was such to indicate always an outward sense of propagation with respect to the Sun. Authors also noted that these periods mainly occur within the trailing edges of high-speed streams. Moreover, in the regions where Eq. (3.42) is verified to a high degree, the magnetic field magnitude is almost constant ($B^2 \sim$ const.).

Today we know that Alfvénic correlations are ubiquitous in the solar wind and that these correlations are much stronger and are found at lower and lower frequencies, as we look at shorter and shorter heliocentric distances. In the right panel of Fig. 3.27 we show results from Belcher and Solodyna (1975) obtained on

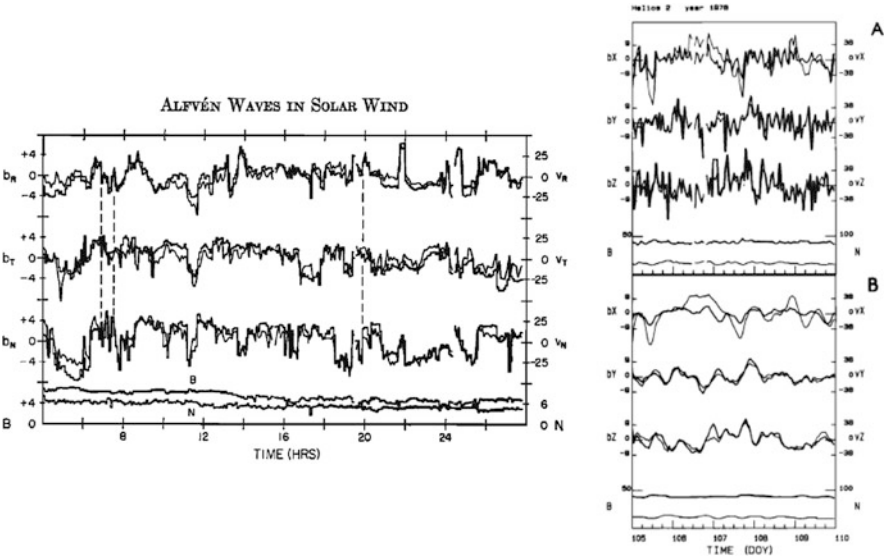

Fig. 3.27 Alfvénic correlation in fast solar wind. *Left panel:* small scale Alfvénic fluctuations for the first time found by Belcher and Davis Jr (1971). *Right panel:* large scale Alfvénic fluctuations found by Bruno et al. (1985); Panel A shows 1-h averages of magnetic field (*heavy lines*) and velocity (*light lines*) components, Panel B shows filtered data highlighting the presence of Alfvénic correlations lasting several hours. Image reproduced by permission, copyright by AGU

the basis of 5 min averages of velocity and magnetic field recorded by Mariner 5 in 1967, during its mission to Venus. On the left panel of Fig. 3.27 we show results from a similar analysis performed by Bruno et al. (1985) obtained on the basis of 1 h averages of velocity and magnetic field recorded by Helios 2 in 1976, when the s/c was at 0.29 AU from the Sun. These last authors found that, in their case, Alfvénic correlations extended to time periods as low as 15 h in the s/c frame at 0.29 AU, and to periods a factor of two smaller near the Earth's orbit. Now, if we think that this long period of the fluctuations at 0.29 AU was larger than the transit time from the Sun to the s/c, this results might be the first evidence for a possible solar origin for these fluctuations, probably caused by the shuffling of the foot-points of the solar surface magnetic field.

Alfvén modes are not the only low frequency plasma fluctuations allowed by the MHD equations but they certainly are the most frequent fluctuations observed in the solar wind. The reason why other possible propagating modes like the slow sonic mode and the fast magnetosonic mode cannot easily be found, besides the fact that the eigenvectors associated with these modes are not directly identifiable because they necessitate prior identification of wavevectors, contrary to the simple Alfvén eigenvectors, depends also on the fact that these compressive modes are strongly damped in the solar wind shortly after they are generated (see Sect. 5). On the contrary, Alfvénic fluctuations, which are difficult to be damped because of their incompressive nature, survive much longer and dominate solar wind turbulence. Nevertheless, there are regions where Alfvénic correlations are much stronger like the trailing edge of fast streams, and regions where these correlations are weak like intervals of slow wind (Belcher and Davis Jr 1971; Belcher and Solodyna 1975). However, the degree of Alfvénic correlations unavoidably fades away with increasing heliocentric distance, although it must be reported that there are cases when the absence of strong velocity shears and compressive phenomena favor a high Alfvénic correlation up to very large distances from the Sun (Roberts et al. 1987a; see Sect. 4.2.3).

Just to give a qualitative quick example about Alfvénic correlations in fast and slow wind, we show in Fig. 3.28 the speed profile for about 100 day of 1976 as observed by Helios 2, and the traces of velocity and magnetic field Z components (see Sect. 3.3.6 for the orientation of the reference system) V_Z and B_Z (this last one expressed in Alfvén units, see Sect. 3.2.2) for two different time intervals, which have been enlarged in the two inserted small panels. The high velocity interval shows a remarkable anti-correlation which, since the mean magnetic field $\mathbf{B_0}$ is oriented away from the Sun, suggests a clear presence of outward oriented Alfvénic fluctuations given that the sign of the correlation is the $sign[-\mathbf{k}\cdot\mathbf{B_0}]$. At odds with the previous interval, the slow wind shows that the two traces are rather uncorrelated. For sake of brevity, we omit to show the very similar behavior for the other two components, within both fast and slow wind.

The discovery of Alfvénic correlations in the solar wind stimulated fundamental remarks by Kraichnan (1974) who, following previous theoretical works by

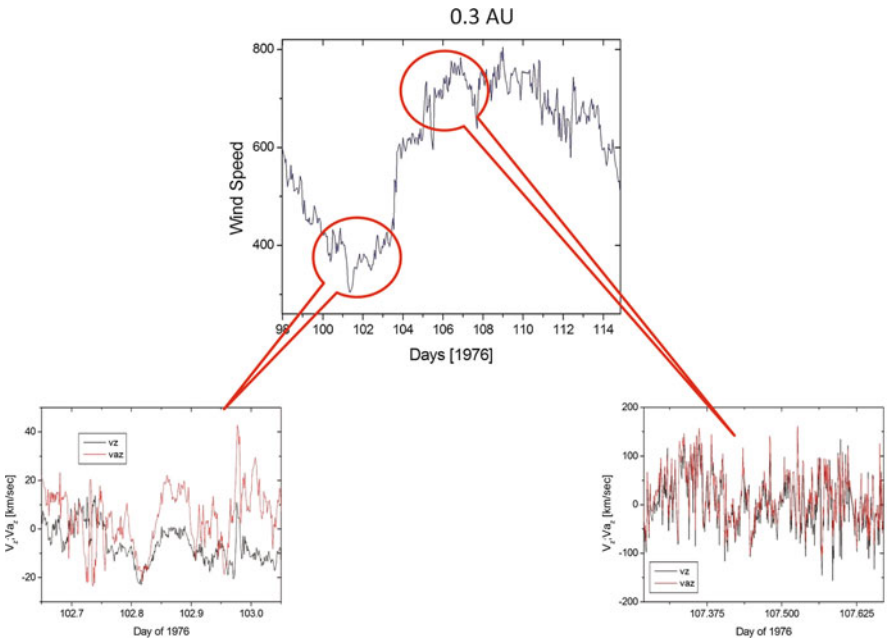

Fig. 3.28 Alfvénic correlation in fast and slow wind. Notice the different degree of correlation between these two types of wind

Kraichnan (1965) and Iroshnikov (1963), showed that the presence of a strong correlation between velocity and magnetic fluctuations renders non-linear transfer to small scales less efficient than for the Navier–Stokes equations, leading to a turbulent behavior which is different from that described by Kolmogorov (1941). In particular, when Eq. (3.42) is exactly satisfied, non-linear interactions in MHD turbulent flows cannot exist. This fact introduces a problem in understanding the evolution of MHD turbulence as observed in the interplanetary space. Both a strong correlation between velocity and magnetic fluctuations and a well defined turbulence spectrum (Figs. 3.21 and 3.28) are observed, and the existence of the correlations is in contrast with the existence of a spectrum which in turbulence is due to a non-linear energy cascade. Dobrowolny et al. (1980) started to solve the puzzle on the existence of *Alfvénic turbulence*, say the presence of predominately outward propagation and the fact that MHD turbulence with the presence of both Alfvénic modes present will evolve towards a state where one of the mode disappears. However, a lengthy debate based on whether the highly Alfvénic nature of fluctuations is what remains of the turbulence produced at the base of the corona or the solar wind itself is an evolving turbulent magnetofluid, has been stimulating the scientific community for quite a long time.

3.3.8 *Radial Evolution of Alfvénic Turbulence*

The degree of correlation not only depends on the type of wind we look at, i.e., fast or slow, but also on the radial distance from the Sun and on the time scale of the fluctuations.

Figure 3.29 shows the radial evolution of σ_c (see Sect. 3.2.2) as observed by Helios and Voyager s/c (Roberts et al. 1987b). It is clear enough that σ_c not only tends to values around 0 as the heliocentric distance increases, but larger and larger time scales are less and less Alfvénic. Values of $\sigma_c \sim 0$ suggest a comparable amount of "outward" and "inward" correlations.

The radial evolution affects also the Alfvén ratio r_A (see Sect. 4.1.1) as it was found by Bruno et al. (1985). However, early analyses (Belcher and Davis Jr 1971; Solodyna and Belcher 1976; Matthaeus and Goldstein 1982a) had already shown that this parameter is usually less than unit. Spectral studies by Marsch and Tu (1990a), reported in Fig. 3.30, showed that within slow wind it is the lowest frequency range the one that experiences the strongest decrease with distance, while the highest frequency range remains almost unaffected. Moreover, the same study showed that, within fast wind, the whole frequency range experiences a general depletion. The evolution is such that close to 1 AU the value of r_A in fast wind approaches that in slow wind.

Moreover, comparing these results with those by Matthaeus and Goldstein (1982a) obtained from Voyager at 2.8 AU, it seems that the evolution recorded within fast wind tends to a sort of limit value around 0.4–0.5.

Also Roberts et al. (1990), analyzing fluctuations between 9 h and 3 day found a similar radial trend. These authors showed that r_A dramatically decreases from values around unit at the Earth's orbit towards 0.4–0.5 at approximately 8 AU. For larger heliocentric distances, r_A seems to stabilize around this last value.

The reason why r_A tends to a value less than unit is still an open question although MHD computer simulations (Matthaeus 1986) showed that magnetic reconnection and high plasma viscosity can produce values of $r_A < 1$ within the inertial range. Moreover, the magnetic energy excess can be explained as a competing action between the equipartition trend due to linear propagation (or Alfvén effect, Kraichnan 1965), and a local dynamo effect due to non-linear terms (Grappin et al. 1991), see closure calculations by Grappin et al. (1983); DNS by Müller and Grappin (2005).

However, this argument forecasts an Alfvén ratio $r_A \neq 1$ but, it does not say whether it would be larger or smaller than "1", i.e., we could also have a final excess of kinetic energy.

Similar unbalance between magnetic and kinetic energy has recently been found in numerical simulations by Mininni et al. (2003a), already cited in Sect. 3.3.2. These authors studied the effect of a weak magnetic field at small scales in a system kept in a stationary regime of hydrodynamic turbulence. In these conditions, the dynamo action causes the initial magnetic energy to grow exponentially towards a state of quasi equipartition between kinetic and magnetic energy. This simulation

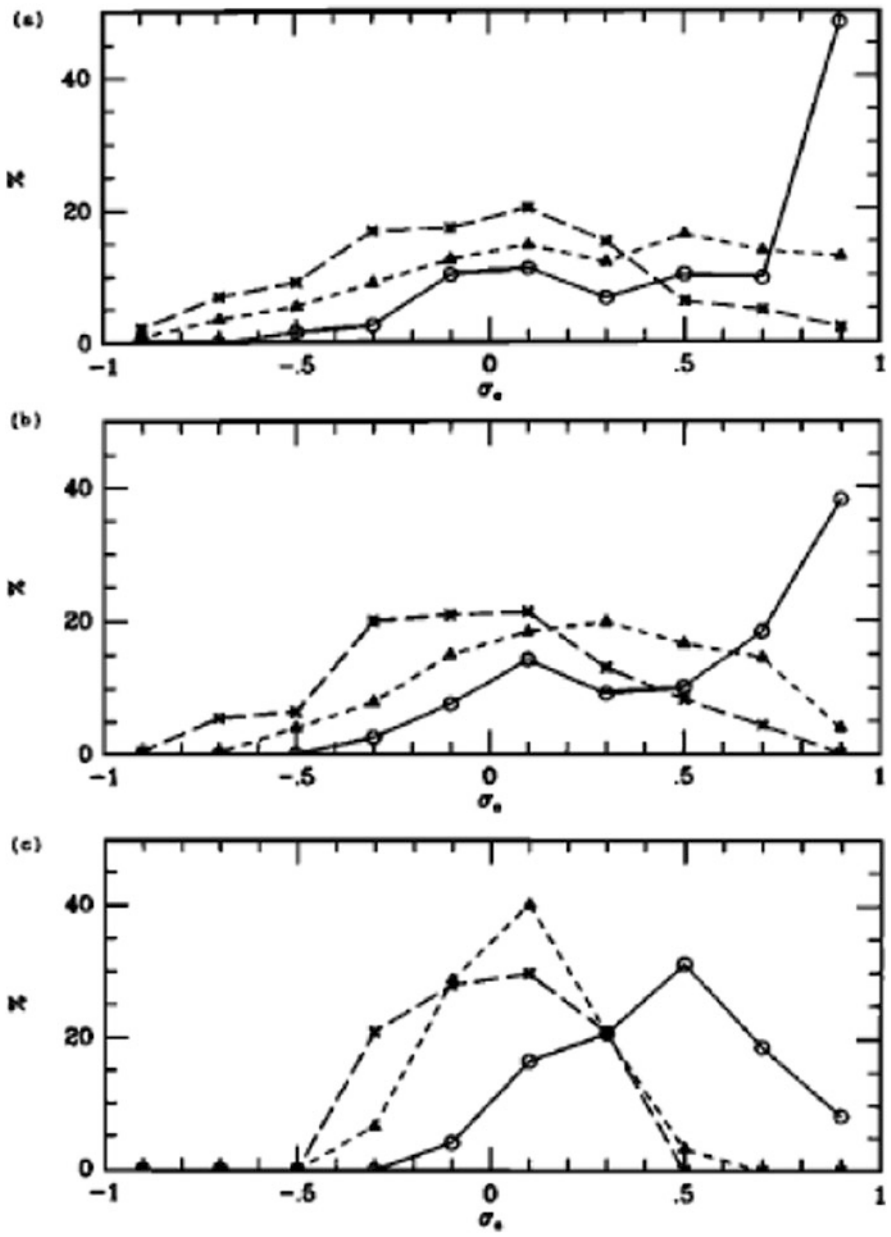

Fig. 3.29 Histograms of normalized cross-helicity σ_c showing its evolution between 0.3 (*circles*), 2 (*triangles*), and 20 (*squares*) AU for different time scales: 3 h (*top panel*), 9 h (*middle panel*), and 81 h (*bottom panel*). Image reproduced by permission from Roberts et al. (1987b), copyright by AGU

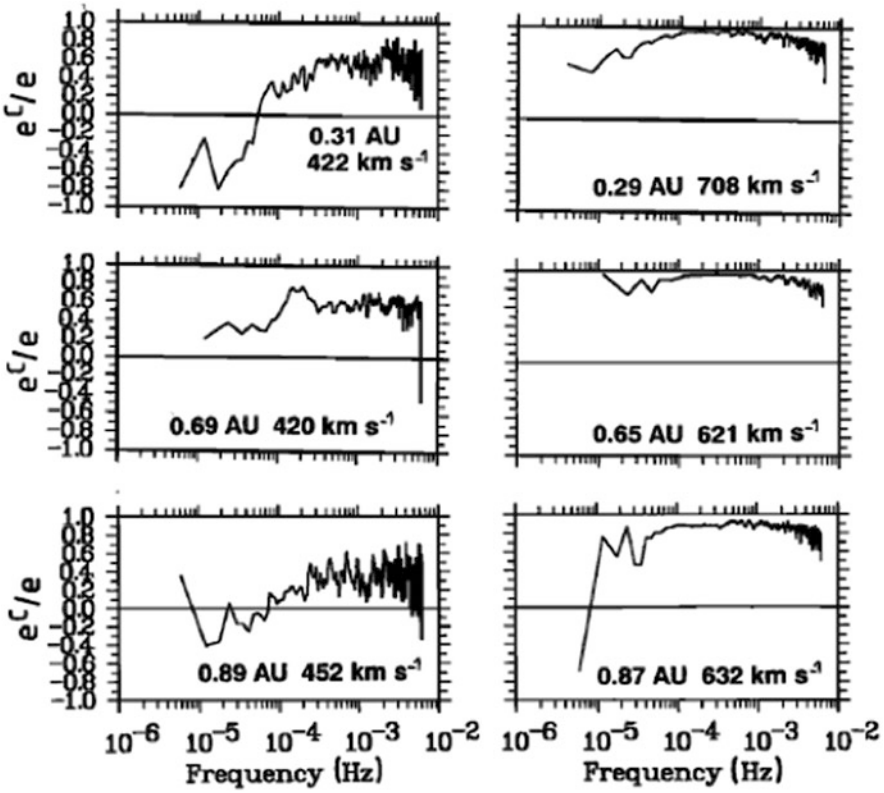

Fig. 3.30 Values of the Alfvén ratio r_A as a function of frequency and heliocentric distance, within slow (*left column*) and fast (*right column*) wind. Image reproduced by permission from Marsch and Tu (1990a), copyright by AGU

was aiming to provide more insights on a microscopic theory of the *alpha*-effect, which is responsible to convert part of the toroidal magnetic field on the Sun back to poloidal to sustain the cycle. However, when the simulation saturates, the unbalance between kinetic and magnetic energy reminds the conditions in which the Alfvén ratio is found in interplanetary space. At very early time the fluid is in a strongly turbulent regime as a result of the action of the external force at wave number $k_{\text{force}} = 3$. An initial magnetic fluctuation is introduced at $t = 0$ at $k_{\text{seed}} = 35$. The magnetic energy starts growing exponentially fast and, when the simulation reaches the saturation stage, the magnetic power spectrum exceeds the kinetic power spectrum at large wave numbers (i.e., $k > k_{\text{force}}$), as also observed in Alfvénic fluctuations of the solar wind (Bruno et al. 1985; Tu and Marsch 1990) as an asymptotic state (Roberts et al. 1987a,b; Bavassano et al. 2000) of turbulence.

However, when the two-fluid effect, such as the Hall current and the electron pressure (Mininni et al. 2003b), is included in the simulation, the dynamo can work more efficiently and the final stage of the simulation is towards equipartition between kinetic and magnetic energy (Fig. 3.31).

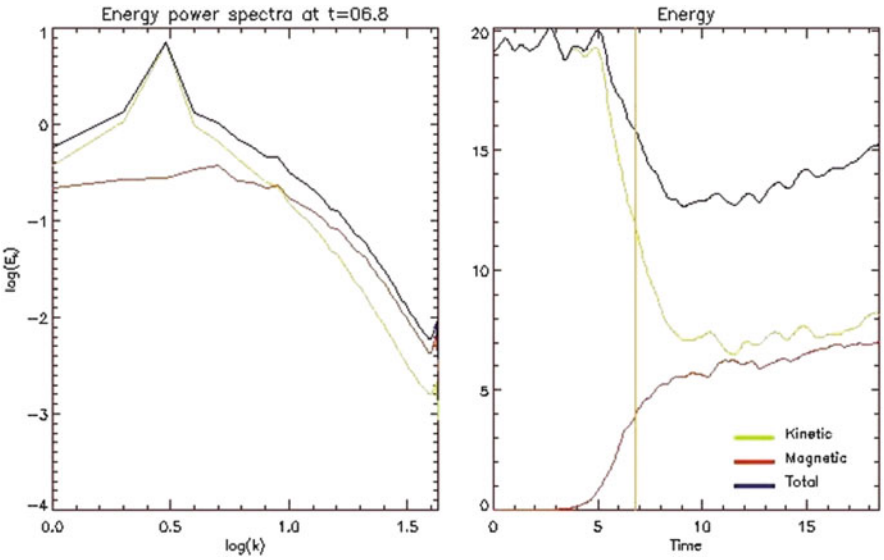

Fig. 3.31 A 128^3 numerical simulation, as in Fig. 3.20, but with an external force applied at wave number $k_{\text{force}} = 3$ (Figure kindly provided by D. Gómez)

On the other hand, Marsch and Tu (1993) analyzed several intervals of interplanetary observations to look for a linear relationship between the mean electromotive force $\boldsymbol{\varepsilon} = \langle \delta \mathbf{V} \delta \mathbf{B} \rangle$, generated by the turbulent motions, and the mean magnetic field B_0, as predicted by simple dynamo theory (Krause and Rädler 1980). Although sizable electromotive force was found in interplanetary fluctuations, these authors could not establish any simple linear relationship between B_0 and ε.

Lately, Bavassano and Bruno (2000) performed a three-fluid analysis of solar wind Alfvénic fluctuations in the inner heliosphere, in order to evaluate the effect of disregarding the multi-fluid nature of the wind on the factor relating velocity and magnetic field fluctuations. It is well known that converting magnetic field fluctuations into Alfvén units we divide by the factor $F_p = (4\pi M_p N_p)^{1/2}$. However, fluctuations in velocity tend to be smaller than fluctuations in Alfvén units. In Fig. 3.32 we show scatter plots between the z-component of the Alfvén velocity and the proton velocity fluctuations. The z-direction has been chosen as the same of $\mathbf{V_p} \times \mathbf{B}$, where $\mathbf{V_p}$ is the proton bulk flow velocity and $\mathbf{B}$ is the mean field direction. The reason for such a choice is due to the fact that this direction is the least affected by compressive phenomena deriving from the wind dynamics. These results show that although the correlation coefficient in both cases is around -0.95, the slope of the best fit straight line passes from 1 at 0.29 AU to a slope considerably different from 1 at 0.88 AU.

Belcher and Davis Jr (1971) suggested that this phenomenon had to be ascribed to the presence of α particles and to an anisotropy in the thermal pressure. Moreover, taking into account the multi-fluid nature of the solar wind, the dividing factor

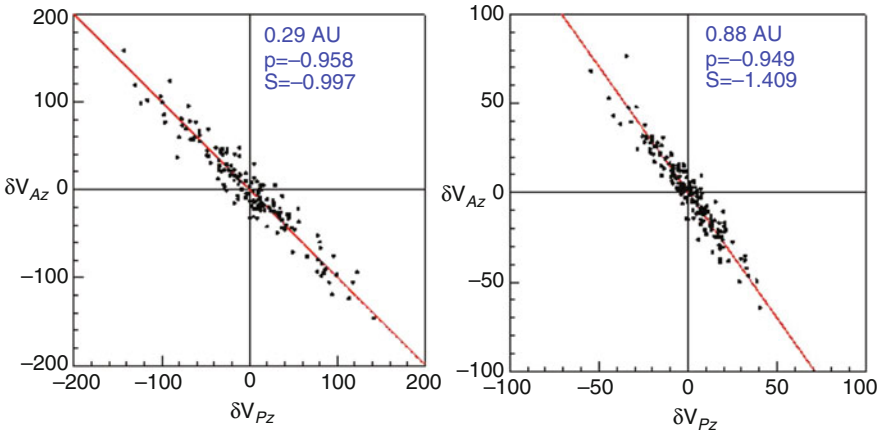

Fig. 3.32 Scatter plot between the z-component of the Alfvén velocity and the proton velocity fluctuations at about 2 mHz. Data refer to Helios 2 observations at 0.29 AU (*left panel*) and 0.88 AU (*right panel*). Image adapted from Bavassano and Bruno (2000)

should become $F = F_p F_i F_a$, where F_i would take into account the presence of other species besides protons, and F_a would take into account the presence of pressure anisotropy $P_\parallel \neq P_\perp$, where $\parallel$ and $\perp$ refer to the background field direction. In particular, following Bavassano and Bruno (2000), the complete expressions for F_i and F_a are

$$F_i = \left[1 + \sum_s (M_s N_s)/(M_p N_p)\right]^{1/2}$$

and

$$F_a = \left[1 - \frac{4\pi}{B_0^2} \sum_s (P_{\parallel s} - P_{\perp s} + M_s N_s \mathbf{U}_s^2)\right]^{-1/2},$$

where the letter "s" stands for the s-th species, being $\mathbf{U}_s = \mathbf{V}_s - \mathbf{V}$ its velocity in the center of mass frame of reference. $\mathbf{V}_s$ is the velocity of the species "s" in the s/c frame and $\mathbf{V} = (\sum_s M_s N_s \mathbf{V}_s)/(\sum_s M_s N_s)$ is the velocity of the center of mass.

Bavassano and Bruno (2000) analyzed several time intervals within the same co-rotating high velocity stream observed at 0.3 and 0.9 AU and performed the analysis using the new factor "F" to express magnetic field fluctuations in Alfvén units, taking into account the presence of α particles and electrons, besides the protons. However, the correction resulted to be insufficient to bring back to "1" the slope of the $\delta V_{\mathrm{P}z} - \delta V_{\mathrm{A}z}$ relationship shown in the right panel of Fig. 3.32. In conclusion, the radial variation of the Alfvén ratio r_{A} towards values less than 1 is not completely due to a missed inclusion of multi-fluid effects in the conversion from magnetic field

to Alfvén units. Thus, we are left with the possibility that the observed depletion of r_A is due to a natural evolution of turbulence towards a state in which magnetic energy becomes dominant (Grappin et al. 1991; Roberts et al. 1992; Roberts 1992), as observed in numerical simulations by Mininni et al. (2003a) or, it is due to the increased presence of magnetic structures like MFDT (Tu and Marsch 1993).

References

C.N. Arge, V.J. Pizzo, Improvement in the prediction of solar wind conditions using near-real time solar magnetic field updates. J. Geophys. Res. **105**, 10465–10480 (2000). doi:10.1029/1999JA900262

A. Balogh, R.J. Forsyth, E.A. Lucek, T.S. Horbury, E.J. Smith, Heliospheric magnetic field polarity inversions at high heliographic latitudes. Geophys. Res. Lett. **26**, 631–634 (1999). doi:10.1029/1999GL900061

A. Barnes, J.V. Hollweg, Large-amplitude hydromagnetic waves. J. Geophys. Res. **79**, 2302–2318 (1974). doi:10.1029/JA079i016p02302

G.K. Batchelor, *Theory of Homogeneous Turbulence* (Cambridge University Press, Cambridge/New York, 1970). Originally published 1953

B. Bavassano, R. Bruno, Velocity and magnetic field fluctuations in alfvénic regions of the inner solar wind: three-fluid observations. J. Geophys. Res. **105**(14), 5113–5118 (2000). doi:10.1029/1999JA000336

B. Bavassano, E. Pietropaolo, R. Bruno, Alfvénic turbulence in the polar wind: a statistical study on cross helicity and residual energy variations. J. Geophys. Res. **105**(14), 12697–12704 (2000). doi:10.1029/2000JA900004

B. Bavassano, R. Woo, R. Bruno, Heliospheric plasma sheet and coronal streamers. Geophys. Res. Lett. **24**, 1655–1658 (1997). doi:10.1029/97GL01630

B. Bavassano, M. Dobrowolny, F. Mariani, N.F. Ness, Radial evolution of power spectra of interplanetary alfvénic turbulence. J. Geophys. Res. **87**, 3617–3622 (1982a). doi:10.1029/JA087iA05p03617

B. Bavassano, M. Dobrowolny, G. Fanfoni, F. Mariani, N.F. Ness, Statistical properties of MHD fluctuations associated with high-speed streams from helios 2 observations. Solar Phys. **78**, 373–384 (1982b). doi:10.1007/BF00151617

J.W. Belcher, L. Davis Jr, Large amplitude alfvén waves in the interplanetary medium. J. Geophys. Res. **76**, 3534–3563 (1971). doi:10.1029/JA076i016p03534

J.W. Belcher, C.V. Solodyna, Alfvén waves and directional discontinuities in the interplanetary medium. J. Geophys. Res. **80**(9), 181–186 (1975). doi:10.1029/JA080i001p00181

J.S. Bendat, A.G. Piersol, *Random Data: Analysis and Measurement Procedures* (Wiley-Interscience, New York, 1971)

J.W. Bieber, W. Wanner, W.H. Matthaeus, Dominant two-dimensional solar wind turbulence with implications for cosmic ray transport. J. Geophys. Res. **101**(A2), 2511–2522 (1996). doi:10.1029/95JA02588

A. Bigazzi, L. Biferale, S.M.A. Gama, M. Velli, Small-scale anisotropy and intermittence in high- and low-latitude solar wind. Astrophys. J. **638**, 499–507 (2006). doi:10.1086/498665

A. Brandenburg, The inverse cascade and nonlinear alpha-effect in simulations of isotropic helical hydromagnetic turbulence. Astrophys. J. **550**, 824–840 (2001). doi:10.1086/319783

S. Bravo, G.A. Stewart, Flux tube expansion factors and solar wind velocity: results from a self-consistent MHD model. Adv. Space Res. **20**, 35 (1997). doi:10.1016/S0273-1177(97)00477-8

R. Bruno, Inner heliosphere observations of MHD turbulence in the solar wind – challenges to theory, in *Solar Wind Seven*, ed. by E. Marsch, R. Schwenn. COSPAR Colloquia Series, vol. 3 (Pergamon Press, Oxford/New York, 1992), pp. 423–428

R. Bruno, M. Dobrowolny, Spectral measurements of magnetic energy and magnetic helicity between 0.29 and 0.97 au. Ann. Geophys. **4**, 17–22 (1986)

R. Bruno, B. Bavassano, U. Villante, Evidence for long period alfvén waves in the inner solar system. J. Geophys. Res. **90**(9), 4373–4377 (1985). doi:10.1029/JA090iA05p04373

R. Bruno, B. Bavassano, E. Pietropaolo, V. Carbone, P. Veltri, Effects of intermittency on interplanetary velocity and magnetic field fluctuations anisotropy. Geophys. Res. Lett. **26**, 3185–3188 (1999). doi:10.1029/1999GL010668

R. Bruno, V. Carbone, Z. Vörös, R. D'Amicis, B. Bavassano, M.B. Cattaneo, A. Mura, A. Milillo, S. Orsini, P. Veltri, L. Sorriso-Valvo, T. Zhang, H. Biernat, H. Rucker, W. Baumjohann, D. Jankovičová, P. Kovács, Coordinated study on solar wind turbulence during the Venus-express, ace and ulysses alignment of August 2007. Earth Moon Planets **104**, 101–104 (2009). doi:10.1007/s11038-008-9272-9

L.F. Burlaga, J.M. Turner, Microscale 'alfvén waves' in the solar wind at 1 au. J. Geophys. Res. **81**(10), 73–77 (1976). doi:10.1029/JA081i001p00073

V. Carbone, P. Veltri, A shell model for anisotropic magnetohydrodynamic turbulence. Geophys. Astrophys. Fluid Dyn. **52**, 153–181 (1990). doi:10.1080/03091929008219845

V. Carbone, F. Malara, P. Veltri, A model for the three-dimensional magnetic field correlation spectra of low-frequency solar wind fluctuations during alfvénic periods. J. Geophys. Res. **100**(9), 1763–1778 (1995). doi:10.1029/94JA02500

F. Cattaneo, D.W. Hughes, Nonlinear saturation of the turbulent α effect. Phys. Rev. E **54**, 4532 (1996). doi:10.1103/PhysRevE.54.R4532

S.C. Chang, A. Nishida, Spatial structure of transverse oscillations in the interplanetary magnetic field. Astrophys. Space Sci. **23**, 301–301 (1973). doi:10.1007/BF00645159

P.J. Coleman, Turbulence, viscosity, and dissipation in the solar-wind plasma. Astrophys. J. **153**, 371 (1968). doi:10.1086/149674

S.R. Cranmer, A.A. van Ballegooijen, R.J. Edgar, Self-consistent coronal heating and solar wind acceleration from anisotropic magnetohydrodynamic turbulence. Astrophys. J. Suppl. Ser. **171**, 520–551 (2007). doi:10.1086/518001

S. Dasso, L.J. Milano, W.H. Matthaeus, C.W. Smith, Cross-helicity correlations in the solar wind, in *Solar Wind Ten*, ed. by M. Velli, R. Bruno, F. Malara. AIP Conference Proceedings, vol. 679 (American Institute of Physics, Melville, 2003), pp. 546–549

S. Dasso, L.J. Milano, W.H. Matthaeus, C.W. Smith, Anisotropy in fast and slow solar wind fluctuations. Astrophys. J. Lett. **635**, 181–184 (2005). doi:10.1086/499559

K.U. Denskat, F.M. Neubauer, Observations of hydromagnetic turbulence in the solar wind, in *Solar Wind Five*, ed. by M. Neugebauer. NASA Conference Publication, vol. 2280 (NASA, Washington, DC, 1983), pp. 81–91

M. Dobrowolny, A. Mangeney, P. Veltri, Properties of magnetohydrodynamic turbulence in the solar wind. Astron. Astrophys. **83**, 26–32 (1980)

J.L. Doob, *Stochastic Processes* (Wiley, New York, 1953)

B. Forsyth, A. Breen, Meeting report: the 3-d sun and heliosphere at solar maximum. Astron. Geophys. **43**, 3–32 (2002). doi:10.1046/j.1468-4004.2002.43332.x

F.J. Forsyth, A. Balogh, T.S. Horbury, E.J. Smith, The heliospheric magnetic field at solar minimum as observed by ulysses. Adv. Space Res. **19**, 839–842 (1997). doi:10.1016/S0273-1177(97)00288-3

U. Frisch, A. Pouquet, J. Leorat, A. Mazure, Possibility of an inverse cascade of magnetic helicity in magnetohydrodynamic turbulence. J. Fluid Mech. **68**, 769–778 (1975). doi:10.1017/S002211207500122X

S. Ghosh, W.H. Matthaeus, D.A. Roberts, M.L. Goldstein, The evolution of slab fluctuations in the presence of pressure-balanced magnetic structures and velocity shears. J. Geophys. Res. **103**(A10), 23691–23704 (1998a). doi:10.1029/98JA02195

S. Ghosh, W.H. Matthaeus, D.A. Roberts, M.L. Goldstein, Waves, structures, and the appearance of two-component turbulence in the solar wind. J. Geophys. Res. **103**(A10), 23705–23716 (1998b). doi:10.1029/98JA02194

P. Goldreich, S. Sridhar, Toward a theory of interstellar turbulence. 2: strong alfvenic turbulence. Astrophys. J. **438**, 763–775 (1995). doi:10.1086/175121

M.L. Goldstein, D.A. Roberts, C.A. Fitch, The structure of helical interplanetary magnetic fields. Geophys. Res. Lett. **18**, 1505–1508 (1991). doi:10.1029/91GL01608

M.L. Goldstein, D.A. Roberts, W.H. Matthaeus, Magnetohydrodynamic turbulence in the solar wind. Ann. Rev. Astron. Astrophys. **33**, 283–326 (1995). doi:10.1146/annurev.aa.33.090195.001435

R. Grappin, Onset and decay of two-dimensional magnetohydrodynamic turbulence with velocity magnetic field correlation. Phys. Fluids **29**, 2433–2443 (1986). doi:10.1063/1.865536

R. Grappin, M. Velli, Waves and streams in the expanding solar wind. J. Geophys. Res. **101**, 425–444 (1996). doi:10.1029/95JA02147

R. Grappin, J. Leorat, A. Pouquet, Dependence of MHD turbulence spectra on the velocity field-magnetic field correlation. Astron. Astrophys. **126**, 51–58 (1983)

R. Grappin, M. Velli, A. Mangeney, Alfvénic versus standard turbulence in the solar wind. Ann. Geophys. **9**, 416–426 (1991)

R. Hammer, Energy balance and stability. Adv. Space Res. **2**, 261–269 (1982). doi:10.1016/0273-1177(82)90276-9

V.H. Hansteen, E. Leer, Coronal heating, densities, and temperatures and solar wind acceleration. J. Geophys. Res. **100**, 21577–21594 (1995). doi:10.1029/95JA02300

D.M. Hassler, I.E. Dammasch, P. Lemaire, P. Brekke, W. Curdt, H.E. Mason, J.-C. Vial, K. Wilhelm, Solar wind outflow and the chromospheric magnetic network. Science **283**(5403), 810–813 (1999). doi:10.1126/science.283.5403.810

J.V. Hollweg, Transition region, corona, and solar wind in coronal holes. J. Geophys. Res. **91**, 4111–4125 (1986). doi:10.1029/JA091iA04p04111

T.S. Horbury, M.A. Forman, S. Oughton, Anisotropic scaling of magnetohydrodynamic turbulence. Phys. Rev. Lett. **807**(17) (2008). doi:10.1103/PhysRevLett.101.175005

T.S. Horbury, A. Balogh, R.J. Forsyth, E.J. Smith, The rate of turbulent evolution over the sun's poles. Astron. Astrophys. **316**, 333–341 (1996)

P.S. Iroshnikov, Turbulence of a conducting fluid in a strong magnetic field. Sov. Astron. **7**, 566 (1963)

L. Klein, R. Bruno, B. Bavassano, H. Rosenbauer, Anisotropy and minimum variance of magnetohydrodynamic fluctuations in the inner heliosphere. J. Geophys. Res. **98**(17), 17461–17466 (1993). doi:10.1029/93JA01522

L.W. Klein, Observations of turbulence and fluctuations in the solar wind. Ph.D Thesis, Catholic University of America, Washington, DC, 1987

L.W. Klein, D.A. Roberts, M.L. Goldstein, Anisotropy and minimum variance directions of solar wind fluctuations in the outer heliosphere. J. Geophys. Res. **96**(15), 3779–3788 (1991). doi:10.1029/90JA02240

L.W. Klein, W.H. Matthaeus, D.A. Roberts, M.L. Goldstein, Evolution of spatial and temporal correlations in the solar wind – Observations and interpretation, in *Solar Wind Seven*, ed. by E. Marsch, R. Schwenn. COSPAR Colloquia Series, vol. 3 (Pergamon Press, Oxford/New York, 1992), pp. 197–200

A.N. Kolmogorov, The local structure turbulence in incompressible viscous fluids for very large Reynolds numbers. Dokl. Akad. Nauk. SSSR **30**, 301–305 (1941)

R.H. Kraichnan, Inertial range spectrum of hydromagnetic turbulence. Phys. Fluids **8**, 1385–1387 (1965)

R.H. Kraichnan, On kolmogorov's inertial-range theories. J. Fluid Mech. **62**, 305–330 (1974). doi:10.1017/S002211207400070X

F. Krause, K.H. Rädler, *Mean field magnetohydrodynamics and dynamo theory* (Akademie, Berlin, 1980)

E. Leer, T.E. Holzer, Energy addition in the solar wind. J. Geophys. Res. **85**, 4681–4688 (1980). doi:10.1029/JA085iA09p04681

R.P. Lepping, M.H. Acũna, L.F. Burlaga, W.M. Farrell, J.A. Slavin, K.H. Schatten, F. Mariani, N.F. Ness, F.M. Neubauer, Y.C. Whang, J.B. Byrnes, R.S. Kennon, P.V. Panetta, J. Scheifele,

E.M. Worley, The wind magnetic field investigation. Space Sci. Rev. **71**, 207–229 (1995). doi:10.1007/BF00751330. http://adsabs.harvard.edu/abs/1995SSRv...71..207L; Provided by the SAO/NASA Astrophysics Data System

R.H. Levine, M.D. Altschuler, J.W. Harvey, Solar sources of the interplanetary magnetic field and solar wind. J. Geophys. Res. **82**, 1061–1065 (1977). doi:10.1029/JA082i007p01061

E. Marsch, C.-Y. Tu, On the radial evolution of MHD turbulence in the inner heliosphere. J. Geophys. Res. **95**(14), 8211–8229 (1990a). doi:10.1029/JA095iA06p08211

E. Marsch, C.-Y. Tu, Spectral and spatial evolution of compressible turbulence in the inner solar wind. J. Geophys. Res. **95**(14), 11945–11956 (1990b). doi:10.1029/JA095iA08p11945

E. Marsch, C.-Y. Tu, Modeling results on spatial transport and spectral transfer of solar wind alfvénic turbulence. J. Geophys. Res. **98**(17), 21045–21059 (1993). doi:10.1029/93JA02365

W.H. Matthaeus, The Alfvén effect reconsidered, in *Paper presented at 1986 Sherwood Controlled Fusion Theory Conference* (Courant Institute of Mathematical Sciences, New York, 1986)

W.H. Matthaeus, M.L. Goldstein, Measurement of the rugged invariants of magnetohydrodynamic turbulence in the solar wind. J. Geophys. Res. **87**(16), 6011–6028 (1982a). doi:10.1029/JA087iA08p06011

W.H. Matthaeus, M.L. Goldstein, Stationarity of magnetohydrodynamic fluctuations in the solar wind. J. Geophys. Res. **87**(16), 10347–10354 (1982b). doi:10.1029/JA087iA12p10347

W.H. Matthaeus, M.L. Goldstein, Low-frequency 1/f noise in the interplanetary magnetic field. Phys. Rev. Lett. **57**, 495–498 (1986). doi:10.1103/PhysRevLett.57.495

W.H. Matthaeus, M.L. Goldstein, D.A. Roberts, Evidence for the presence of quasi-two-dimensional nearly incompressible fluctuations in the solar wind. J. Geophys. Res. **95**, 20673–20683 (1990). doi:10.1029/JA095iA12p20673

W.H. Matthaeus, S. Dasso, J.M. Weygand, L.J. Milano, C.W. Smith, M.G. Kivelson, Spatial correlation of solar-wind turbulence from two-point measurements. Phys. Rev. Lett. **95**(23) (2005). doi:10.1103/PhysRevLett.95.231101

M. Meneguzzi, U. Frisch, A. Pouquet, Helical and nonhelical turbulent dynamos. Phys. Rev. Lett. **47**, 1060–1064 (1981). doi:10.1103/PhysRevLett.47.1060

P.D. Mininni, D.O. Gómez, S.M. Mahajan, Dynamo action in magnetohydrodynamics and hall-magnetohydrodynamics. Astrophys. J. **587**, 472–481 (2003a). doi:10.1086/368181

P.D. Mininni, D.O. Gómez, S.M. Mahajan, Role of the hall current in magnetohydrodynamic dynamos. Astrophys. J. **584**, 1120–1126 (2003b). doi:10.1086/345777

H.K. Moffatt, *Magnetic Field Generation in Electrically Conducting Fluids*. Cambridge Monographs on Mechanics and Applied Mathematics (Cambridge University Press, Cambridge/New York, 1978)

D. Montgomery, Major disruptions, inverse cascades, and the strauss equations. Phys. Scripta **2**, 83–88 (1982). doi:10.1088/0031-8949/1982/T2A/009

D. Montgomery, Theory of hydromagnetic turbulence, in *Solar Wind Five*, ed. by M. Neugebauer. NASA Conference Publication, vol. 2280 (NASA, Washington, DC, 1983), pp. 107–130

W.-C. Müller, R. Grappin, Spectral energy dynamics in magnetohydrodynamic turbulence. Phys. Rev. Lett. **95**, 114502 (2005). doi:10.1103/PhysRevLett.95.114502

Y. Narita, K.-H. Glassmeier, M.L. Goldstein, U. Motschmann, F. Sahraoui, Three-dimensional spatial structures of solar wind turbulence from 10,000-km to 100-km scales. Ann. Geophys. **29**, 1731–1738 (2011). doi:10.5194/angeo-29-1731-2011

S. Oughton, Transport of solar wind fluctuations: a turbulence approach. Ph.D Thesis, Delaware University, Wilmington, 1993

S. Oughton, E. Priest, W.H. Matthaeus, The influence of a mean magnetic field on three-dimensional MHD turbulence. J. Fluid Mech. **280**, 95–117 (1994). doi:10.1017/S0022112094002867

E.N. Parker, Book note: Cosmical magnetic fields: Their origin and their activity. Astron. Quart. **3**, 201–201 (1980)

S. Perri, A. Balogh, Stationarity in solar wind flows. Astrophys. J. **714**, 937–943 (2010). doi:10.1088/0004-637X/714/1/937

J.J. Podesta, D.A. Roberts, M.L. Goldstein, Spectral exponents of kinetic and magnetic energy spectra in solar wind turbulence. Astrophys. J. **664**, 543–548 (2007). doi:10.1086/519211

B. Poduval, X.P. Zhao, Discrepancies in the prediction of solar wind using potential field source surface model: An investigation of possible sources. J. Geophys. Res. **109**(A18), 8102 (2004). doi:10.1029/2004JA010384

J.M. Polygiannakis, X. Moussas, J.J. Quenby, E.J. Smith, Spectral polarization analysis of the interplanetary magnetic field fluctuations. Solar Phys. **149**, 381–389 (1994). doi:10.1007/BF00690623

A. Pouquet, U. Frish, J. Leorat, Strong MHD helical turbulence and the nonlinear dynamo effect. J. Fluid Mech. **77**, 321–354 (1976). doi:10.1017/S0022112076002140

D.A. Roberts, Observation and simulation of the radial evolution and stream structure of solar wind turbulence, in *Solar Wind Seven*, ed. by E. Marsch, R. Schwenn. COSPAR Colloquia Series, vol. 3 (Pergamon Press, Oxford; New York, 1992), pp. 533–538

D.A. Roberts, The evolution of the spectrum of velocity fluctuations in the solar wind. Eos Trans. AGU **88**(52), 31–06 (2007)

D.A. Roberts, M.L. Goldstein, L.W. Klein, The amplitudes of interplanetary fluctuations – stream structure, heliocentric distance, and frequency dependence. J. Geophys. Res. **95**(14), 4203–4216 (1990). doi:10.1029/JA095iA04p04203

D.A. Roberts, M.L. Goldstein, L.W. Klein, W.H. Matthaeus, The nature and evolution of magnetohydrodynamic fluctuations in the solar wind: Voyager observations. J. Geophys. Res. **92**(11), 11021–11040 (1987a)

D.A. Roberts, M.L. Goldstein, L.W. Klein, W.H. Matthaeus, Origin and evolution of fluctuations in the solar wind: Helios observations and helios–voyager comparisons. J. Geophys. Res. **92**(11), 12023–12035 (1987b). doi:10.1029/JA092iA11p12023

D.A. Roberts, M.L. Goldstein, W.H. Matthaeus, S. Ghosh, Velocity shear generation of solar wind turbulence. J. Geophys. Res. **97**(16), 17115– (1992). doi:10.1029/92JA01144

C.T. Russell, Comments on the measurement of power spectra of the interplanetary magnetic field, in *Solar Wind*, ed. by C.P. Sonett, P.J. Coleman, J.M. Wilcox (NASA, Washington, DC, 1972), pp. 365–374

C. Salem, A. Mangeney, S.D. Bale, P. Veltri, Solar wind magnetohydrodynamics turbulence: Anomalous scaling and role of intermittency. Astrophys. J. **702**, 537–553 (2009). doi:10.1088/0004-637X/702/1/537

C.J. Salem, Ondes, turbulence et phénomènes dissipatifs dans le vent solaire à partir des observations de la sonde WIND. Ph.D Thesis, Université Paris VII, Observatoire de Paris, Paris, 2000

O. Sandbaek, E. Leer, V.H. Hansteen, On the relation between coronal heating, flux tube divergence, and the solar wind proton flux and flow speed. Astrophys. J. **436**, 390–399 (1994). doi:10.1086/174913

J. Saur, J.W. Bieber, Geometry of low-frequency solar wind magnetic turbulence: evidence for radially aligned alfénic fluctuations. J. Geophys. Res. **104**, 9975–9988 (1999). doi:10.1029/1998JA900077

J. Saur, A. Pouquet, W.H. Matthaeus, Correction to "an acceleration mechanism for the generation of the main auroral oval on Jupiter". Geophys. Res. Lett. **30**, 19–22 (2003)

J. Saur, H. Politano, A. Pouquet, W.H. Matthaeus, Evidence for weak MHD turbulence in the middle magnetosphere of jupiter. Astron. Astrophys. **386**, 699–708 (2002). doi:10.1051/0004-6361:20020305

F.L. Scarf, J.H. Wolfe, R.W. Silva, A plasma instability associated with thermal anisotropies in the solar wind. J. Geophys. Res. **72**(11), 993–999 (1967). doi:10.1029/JZ072i003p00993

J.V. Shebalin, W.H. Matthaeus, D. Montgomery, Anisotropy in MHD turbulence due to a mean magnetic field. J. Plasma Phys. **29**, 525–547 (1983). doi:10.1017/S0022377800000933

C.W. Smith, The geometry of turbulent magnetic fluctuations at high heliographic latitudes, in *Solar Wind Ten*, ed. by M. Velli, R. Bruno, F. Malara. AIP Conference Proceedings, vol. 679 (American Institute of Physics, Melville, NY, 2003), pp. 413–416

C.W. Smith, M.L. Goldstein, W.H. Matthaeus, Turbulence analysis of the jovian upstream 'wave' phenomenon. J. Geophys. Res. **88**(17), 5581–5593 (1983). doi:10.1029/JA088iA07p05581

C.W. Smith, M.L. Goldstein, W.H. Matthaeus, A.F. Viñas, Erratum: Correction to 'turbulence analysis of the Jovian upstream 'wave' phenomenon'. J. Geophys. Res. **89**(18), 9159–9160 (1984). doi:10.1029/JA089iA10p09159

C.V. Solodyna, J.W. Belcher, On the minimum variance direction of magnetic field fluctuations in the azimuthal velocity structure of the solar wind. Geophys. Res. Lett. **3**, 565–568 (1976). doi:10.1029/GL003i009p00565

B.U.O. Sonnerup, L.J. Cahill, Magnetopause structure and attitude from explorer 12 observations. J. Geophys. Res. **72**(11), 171 (1967). doi:10.1029/JZ072i001p00171

L. Sorriso-Valvo, E. Yordanova, V. Carbone, On the scaling properties of anisotropy of interplanetary magnetic turbulent fluctuations. Europhys. Lett. **90** (2010). doi:10.1209/0295-5075/90/59001

L. Sorriso-Valvo, V. Carbone, R. Bruno, P. Veltri, Persistence of small-scale anisotropy of magnetic turbulence as observed in the solar wind. Europhys. Lett. **75**, 832–838 (2006). doi:10.1209/epl/i2006-10172-y

G.I. Taylor, The spectrum of turbulence. Proc. R. Soc. Lond. Ser. A **164**, 476–490 (1938)

H. Tennekes, J.L. Lumely, *A First Course In Turbulence*, vol. MCFL-49 (MIT, Cambridge, 1972)

C.-Y. Tu, A self-consistent two-time scale solar wind model, in *Solar Wind Six*, ed. by V.J. Pizzo, T. Holzer, D.G. Sime. NCAR Technical Notes, vol. 306 (National Center for Atmospheric Research, Boulder, 1987a), p. 112

C.-Y. Tu, A solar wind model with the power spectrum of alfvénic fluctuations. Solar Phys. **109**, 149–186 (1987b). doi:10.1007/BF00167405

C.-Y. Tu, The damping of interplanetary alfvénic fluctuations and the heating of the solar wind. J. Geophys. Res. **93**, 7–20 (1988). doi:10.1029/JA093iA01p00007

C.-Y. Tu, E. Marsch, Transfer equations for spectral densities of inhomogeneous MHD turbulence. J. Plasma Phys. **44**, 103–122 (1990). doi:10.1017/S002237780001504X

C.-Y. Tu, E. Marsch, A model of solar wind fluctuations with two components: alfvén waves and convective structures. J. Geophys. Res. **98**(17), 1257–1276 (1993). doi:10.1029/92JA01947

C.-Y. Tu, E. Marsch, Comment on 'evolution of energy-containing turbulent eddies in the solar wind' by W.H. Matthaeus, S. Oughton, D.H. Pontius, Jr., and Y. Zhou. J. Geophys. Res. **100**(9), 12323–12328 (1995a). doi:10.1029/95JA01103

C.-Y. Tu, E. Marsch, MHD structures, waves and turbulence in the solar wind: observations and theories. Space Sci. Rev. **73**(1/2), 1–210 (1995b). doi:10.1007/BF00748891

C.-Y. Tu, J.W. Freeman, R.E. Lopez, The proton temperature and the total hourly variance of the magnetic field components in different solar wind speed regions. Solar Phys. **119**, 197–206 (1989). doi:10.1007/BF00146220

C.-Y. Tu, Z.-Y. Pu, F.-S. Wei, The power spectrum of interplanetary alfvénic fluctuations derivation of the governing equation and its solution. J. Geophys. Res. **89**(18), 9695–9702 (1984). doi:10.1029/JA089iA11p09695

A.J. Turner, G. Gogoberidze, S.C. Chapman, B. Hnat, W.-C. Müller, Nonaxisymmetric anisotropy of solar wind turbulence. Phys. Rev. Lett. **107** (2011). doi:10.1103/PhysRevLett.107.095002

P. Veltri, An observational picture of solar-wind MHD turbulence. Nuovo Cimento C **3**, 45–55 (1980). doi:10.1007/BF02509190

P. Veltri, A. Mangeney, M. Dobrowolny, Cross-helicity effects in anisotropic MHD turbulence. Nuovo Cimento B **68**, 235–251 (1982). doi:10.1007/BF02890146

Y.-M. Wang, Flux-tube divergence, coronal heating, and the solar wind. Astrophys. J. Lett. **410**, 123–126 (1993). doi:10.1086/186895

Y.-M. Wang, Two types of slow solar wind. Astrophys. J. Lett. **437**, 67–70 (1994). doi:10.1086/187684

Y.-M. Wang, N.R. Sheeley Jr, Solar wind speed and coronal flux-tube expansion. Astrophys. J. **355**, 726–732 (1990). doi:10.1086/168805

W. Wanner, G. Wibberenz, A study of the propagation of solar energetic protons in the inner heliosphere. J. Geophys. Res. **98**(17), 3513–3528 (1993). doi:10.1029/92JA02546

J.M. Weygand, W.H. Matthaeus, S. Dasso, M.G. Kivelson, R.J. Walker, Taylor scale and effective magnetic reynolds number determination from plasma sheet and solar wind magnetic field fluctuations. J. Geophys. Res. **112** (2007). doi:10.1029/2007JA012486

Y.C. Whang, Y.-M. Wang, N.R. Sheeley Jr, L.F. Burlaga, Global structure of the out-of-ecliptic solar wind. J. Geophys. Res. **110**(A9), 3103 (2005). doi:10.1029/2004JA010875

G.L. Withbroe, The temperature structure, mass, and energy flow in the corona and inner solar wind. Astrophys. J. **325**, 442–467 (1988). doi:10.1086/166015

G.P. Zank, W.H. Matthaeus, Waves and turbulence in the solar wind. J. Geophys. Res. **97**(16), 17189–17194 (1992). doi:10.1029/92JA01734

S.J. Zweben, C.R. Menyuk, R.J. Taylor, Small-scale magnetic fluctuations inside the Macrotor tokamak. Phys. Rev. Lett. **42**, 1720 (1979)

Chapter 4
Turbulence Studied via Elsässer Variables

The Alfvénic character of solar wind fluctuations, especially within co-rotating high velocity streams, suggests to use the Elsässer variables (Sect. 4.1) to separate the "outward" from the "inward" contribution to turbulence. These variables, used in theoretical studies by Dobrowolny et al. (1980a,b), Veltri et al. (1982), Marsch and Mangeney (1987), and Zhou and Matthaeus (1989), were for the first time used in interplanetary data analysis by Grappin et al. (1990) and Tu et al. (1989).

4.1 Introducing the Elsässer Variables

The Alfvénic character of turbulence suggests to use the Elsässer variables to better describe the inward and outward contributions to turbulence. Following Elsässer (1950), Dobrowolny et al. (1980b), Goldstein et al. (1986), Grappin et al. (1989), Marsch and Tu (1989), Tu and Marsch (1990b), and Tu et al. (1989), Elsässer variables are defined as

$$\mathbf{z}^{\pm} = \mathbf{v} \pm \frac{\mathbf{b}}{\sqrt{4\pi\rho}}, \tag{4.1}$$

where $\mathbf{v}$ and $\mathbf{b}$ are the proton velocity and the magnetic field measured in the s/c reference frame, which can be looked at as an inertial reference frame. The sign in front of $\mathbf{b}$, in Eq. (4.1), is decided by $sign[-\mathbf{k} \cdot \mathbf{B}_0]$. In other words, for an outward directed mean field $\mathbf{B}_0$, a negative correlation would indicate an outward directed wave vector $\mathbf{k}$ and vice-versa. However, it is more convenient to define the Elsässers variables in such a way that z^+ always refers to waves going outward and z^- to waves going inward. In order to do so, the background magnetic field $\mathbf{B}_0$ is artificially rotated by 180° every time it points away from the Sun, in other words, magnetic sectors are rectified (Roberts et al. 1987a,b).

R. Bruno, V. Carbone, *Turbulence in the Solar Wind*, Lecture Notes in Physics 928, DOI 10.1007/978-3-319-43440-7_4

4.1.1 Definitions and Conservation Laws

If we express **b** in Alfvén units, that is we normalize it by $\sqrt{4\pi\rho}$ we can use the following handy formulas relative to definitions of fields and second order moments. Fields:

$$\mathbf{z}^{\pm} = \mathbf{v} \pm \mathbf{b}, \tag{4.2}$$

$$\mathbf{v} = \frac{1}{2}(\mathbf{z}^{+} + \mathbf{z}^{-}), \tag{4.3}$$

$$\mathbf{b} = \frac{1}{2}(\mathbf{z}^{+} - \mathbf{z}^{-}). \tag{4.4}$$

Second order moments:

$$z^{+} \text{ and } z^{-} \text{ energies} \longrightarrow e^{\pm} = \frac{1}{2}\langle (z^{\pm})^2 \rangle\,, \tag{4.5}$$

$$\text{kinetic energy} \longrightarrow e^{v} = \frac{1}{2}\langle v^2 \rangle\,, \tag{4.6}$$

$$\text{magnetic energy} \longrightarrow e^{b} = \frac{1}{2}\langle b^2 \rangle\,, \tag{4.7}$$

$$\text{total energy} \longrightarrow e = e^{v} + e^{b}\,, \tag{4.8}$$

$$\text{residual energy} \longrightarrow e^{r} = e^{v} - e^{b}\,, \tag{4.9}$$

$$\text{cross-helicity} \longrightarrow e^{c} = \frac{1}{2}\langle \mathbf{v} \cdot \mathbf{b} \rangle\,. \tag{4.10}$$

Normalized quantities:

$$\text{normalized cross-helicity} \longrightarrow \sigma_{\mathrm{c}} = \frac{e^{+} - e^{-}}{e^{+} + e^{-}} = \frac{2e^{c}}{e^{v} + e^{b}}\,, \tag{4.11}$$

$$\text{normalized residual-energy} \longrightarrow \sigma_{\mathrm{r}} = \frac{e^{v} - e^{b}}{e^{v} + e^{b}} = \frac{2e^{r}}{e^{+} + e^{-}}\,, \tag{4.12}$$

$$\text{Alfvén ratio} \longrightarrow r_{\mathrm{A}} = \frac{e^{v}}{e^{b}} = \frac{1 + \sigma_{\mathrm{r}}}{1 - \sigma_{\mathrm{r}}}\,, \tag{4.13}$$

$$\text{Elsässer ratio} \longrightarrow r_{\mathrm{E}} = \frac{e^{-}}{e^{+}} = \frac{1 - \sigma_{\mathrm{c}}}{1 + \sigma_{\mathrm{c}}}\,. \tag{4.14}$$

We expect an Alfvèn wave to satisfy the following relations (Table 4.1):

Table 4.1 Expected values for Alfvèn ratio r_A, normalized cross-helicity σ_c, and normalized residual energy σ_r for a pure Alfvèn wave outward or inward oriented

Parameter	Definition	Expected value
r_A	e^V/e^B	1
σ_c	$(e^+ - e^-)/(e^+ + e^-)$	± 1
σ_r	$(e^V - e^B)/(e^V + e^B)$	0

4.1.2 Spectral Analysis Using Elsässer Variables

A spectral analysis of interplanetary data can be performed using z^+ and z^- fields. Following Tu and Marsch (1995) the energy spectrum associated with these two variables can be defined in the following way:

$$e_j^{\pm}(f_k) = \frac{2\delta T}{n}\delta z_{j,k}^{\pm}(\delta z_{j,k}^{\pm})^*, \tag{4.15}$$

where $\delta z_{j,k}^{\pm}$ are the Fourier coefficients of the j-component among x, y, and z, n is the number of data points, δT is the sampling time, and $f_k = k/n\delta T$, with $k = 0, 1, 2, \ldots, n/2$ is the kth frequency. The total energy associated with the two Alfvèn modes will be the sum of the energy of the three components, i.e.,

$$e^{\pm}(f_k) = \sum_{j=x,y,z} e_j^{\pm}(f_k). \tag{4.16}$$

Obviously, using Eqs. (4.15) and (4.16), we can redefine in the frequency domain all the parameters introduced in the previous section.

4.2 Ecliptic Scenario

In the following, we will describe and discuss several differences between "outward" and "inward" modes, but the most important one is about their origin. As a matter of fact, the existence of the Alfvénic critical point implies that only "outward" propagating waves of solar origin will be able to escape from the Sun. "Inward" waves, being faster than the wind bulk speed, will precipitate back to the Sun if they are generated before this point. The most important implication due to this scenario is that "inward" modes observed beyond the Alfvénic point cannot have a solar origin but they must have been created locally by some physical process. Obviously, for the other Alfvénic component, both solar and local origins are still possible.

Early studies by Belcher and Davis Jr (1971), performed on magnetic field and velocity fluctuations recorded by Mariner 5 during its trip to Venus in 1967, already suggested that the majority of the Alfvénic fluctuations are characterized

by an "outward" sense of propagation, and that the best regions where to observe these fluctuations are the trailing edge of high velocity streams. Moreover, Helios spacecraft, repeatedly orbiting around the Sun between 0.3 and 1 AU, gave the first and unique opportunity to study the radial evolution of turbulence (Bavassano et al. 1982a; Denskat and Neubauer 1983). Successively, when Elsässer variables were introduced in the analysis (Grappin et al. 1989), it was finally possible not only to evaluate the "inward" and "outward" Alfvénic contribution to turbulence but also to study the behavior of these modes as a function of the wind speed and radial distance from the Sun.

Figure 4.1 This figure from Tu et al. (1990) clearly shows the behavior of $e^{\pm}$ (see Sect. 4.1) across a high speed stream observed at 0.3 AU. Within fast wind e^{+}

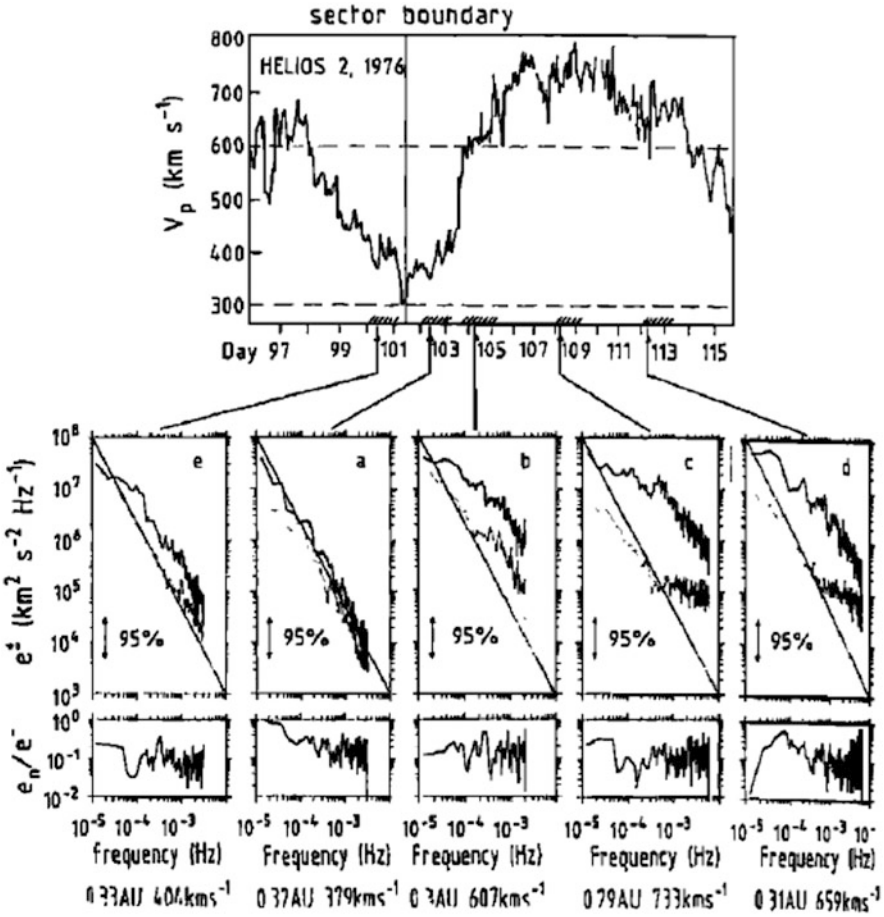

Fig. 4.1 Power density spectra $e^{\pm}$ computed from $\delta z^{\pm}$ fluctuations for different time intervals indicated by the *arrows*. Image reproduced by permission from Tu et al. (1990), copyright by AGU

is much higher than e^- and its spectral slope shows a break. Lower frequencies have a flatter slope while the slope of higher frequencies is closer to a Kolmogorov-like. e^- has a similar break but the slope of lower frequencies follows the Kolmogorov slope, while higher frequencies form a sort of plateau.

This configuration vanishes when we pass to the slow wind where both spectra have almost equivalent power density and follow the Kolmogorov slope. This behavior, for the first time reported by Grappin et al. (1990), is commonly found within co-rotating high velocity streams, although much more clearly expressed at shorter heliocentric distances, as shown below.

Spectral power associated with outward (right panel) and inward (left panel) Alfvénic fluctuations, based on Helios 2 observations in the inner heliosphere, are concisely reported in Fig. 4.2. The e^- spectrum, if we exclude the high frequency range of the spectrum relative to fast wind at 0.4 AU, shows an average power law profile with a slope of -1.64, consistent with Kolmogorov's scaling. The lack of radial evolution of e^- spectrum brought Tu and Marsch (1990b) to name it "the background spectrum" of solar wind turbulence.

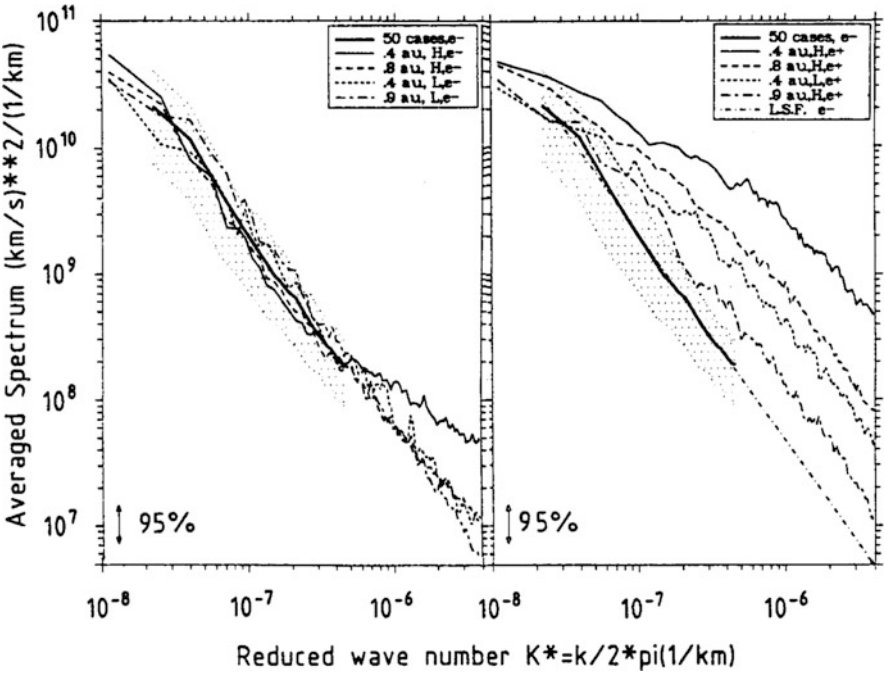

Fig. 4.2 Power density spectra e^- and e^+ computed from δz^- and δz^+ fluctuations. Spectra have been computed within fast (H) and slow (L) streams around 0.4 and 0.9 AU as indicated by *different line styles*. The *thick line* represents the average power spectrum obtained from all the about 50 e^- spectra, regardless of distances and wind speed. The *shaded area* is the 1σ width related to the average. Image reproduced by permission from Tu and Marsch (1990a), copyright by AGU

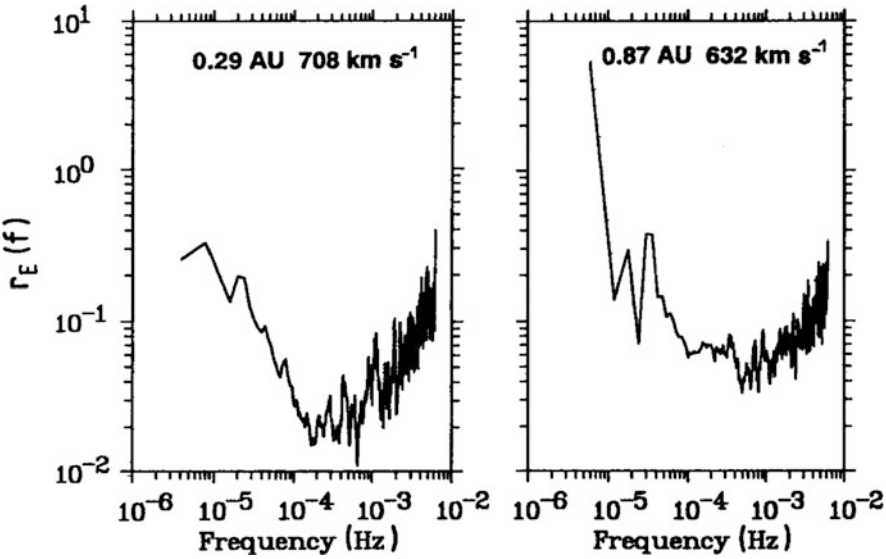

Fig. 4.3 Ratio of e^- over e^+ within fast wind at 0.3 and 0.9 AU in the *left and right panels*, respectively. Image reproduced by permission from Marsch and Tu (1990), copyright by AGU

Quite different is the behavior of e^+ spectrum. Close to the Sun and within fast wind, this spectrum appears to be flatter at low frequency and steeper at high frequency. The overall evolution is towards the "background spectrum" by the time the wind reaches 0.8 AU.

In particular, Fig. 4.2 tells us that the radial evolution of the normalized cross-helicity has to be ascribed mainly to the radial evolution of e^+ rather than to both Alfvénic fluctuations (Tu and Marsch 1990b). In addition, Fig. 4.3, relative to the Elsässer ratio r_E, shows that the hourly frequency range, up to $\sim 2 \times 10^{-3}$ Hz, is the most affected by this radial evolution.

As a matter of fact, this radial evolution can be inferred from Fig. 4.4 where values of e^- and e^+ together with solar wind speed, magnetic field intensity, and magnetic field and particle density compression are shown between 0.3 and 1 AU during the primary mission of Helios 2. It clearly appears that enhancements of e^- and depletion of e^+ are connected to compressive events, particularly within slow wind. Within fast wind the average level of e^- is rather constant during the radial excursion while the level of e^+ dramatically decreases with a consequent increase of the Elsässer ratio (see Sect. 4.1.1).

Further ecliptic observations (see Fig. 4.5) do not indicate any clear radial trend for the Elsässer ratio between 1 and 5 AU, and its value seems to fluctuate between 0.2 and 0.4.

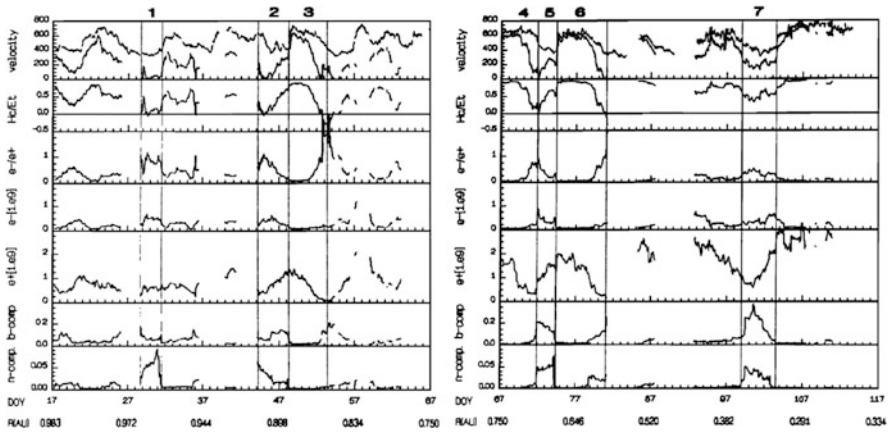

Fig. 4.4 *Upper panel:* solar wind speed and solar wind speed multiplied by σ_c. In the *lower panels* the authors reported: σ_c, r_E, e^-, e^+, magnetic compression, and number density compression, respectively. Image reproduced by permission from Bruno and Bavassano (1991), copyright by AGU

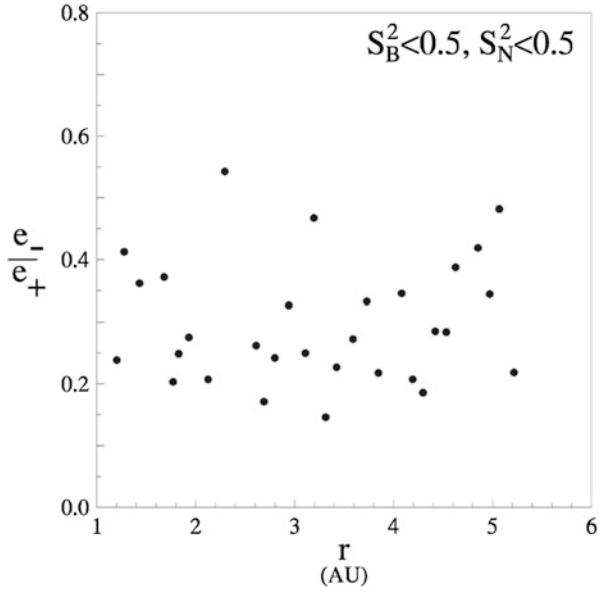

Fig. 4.5 Ratio of e^- over e^+ within fast wind between 1 and 5 AU as observed by Ulysses in the ecliptic. Image reproduced by permission from Bavassano et al. (2001), copyright by AGU

However, low values of the normalized cross-helicity can also be associated with a particular type of incompressive events, which Tu and Marsch (1991) called Magnetic Field Directional Turnings or MFDT. These events, found within slow wind, were characterized by very low values of σ_c close to zero and low values of the Alfvén ratio, around 0.2. Moreover, the spectral slope of e^+, e^- and the power associated with the magnetic field fluctuations was close to the Kolmogorov slope. These intervals were only scarcely compressive, and short period fluctuations, from a few minutes to about 40 min, were nearly pressure balanced. Thus, differently from what had previously been observed by Bruno et al. (1989), who found low values of cross-helicity often accompanied by compressive events, these MFDTs were mainly incompressive. In these structures most of the fluctuating energy resides in the magnetic field rather than velocity as shown in Fig. 4.6 taken from Tu and Marsch (1991). It follows that the amplitudes of the fluctuating Alfvénic fields $\delta z^{\pm}$ result to be comparable and, consequently, the derived parameter $\sigma_c \to 0$. Moreover, the presence of these structures would also be able to explain the fact that $r_A < 1$. Tu and Marsch (1991) suggested that these fluctuations might derive from a special kind of magnetic structures, which obey the MHD equations, for which $(\mathbf{B} \cdot \nabla)\mathbf{B} = 0$, field magnitude, proton density, and temperature are all constant. The same authors suggested the possibility of an interplanetary turbulence mainly made of outwardly propagating Alfvén waves and convected structures represented by MFDTs. In other words, this model assumed that the spectrum of e^- would be caused by MFDTs. The different radial evolution of the power associated with these two kind of components would determine the radial evolution observed in both σ_c and r_A. Although the results were not quantitatively satisfactory, they did show a qualitative agreement with the observations.

These convected structures are an important ingredient of the turbulent evolution of the fluctuations and can be identified as the 2D incompressible turbulence suggested by Matthaeus et al. (1990) and Tu and Marsch (1991).

As a matter of fact, a statistical analysis by Bruno et al. (2007) showed that magnetically dominated structures represent an important component of the interplanetary fluctuations within the MHD range of scales. As a matter of fact, these magnetic structures and Alfvénic fluctuations dominate at scales typical of MHD turbulence. For instance, this analysis suggested that more than 20 % of all analyzed intervals of 1 h scale are magnetically dominated and only weakly Alfvénic. Observations in the ecliptic performed by Helios and WIND s/c and out of the ecliptic, performed by Ulysses, showed that these advected, mostly incompressive structures are ubiquitous in the heliosphere and can be found in both fast and slow wind.

It proves interesting enough to look at the radial evolution of interplanetary fluctuations in terms of normalized cross-helicity σ_c and normalized residual energy σ_r (see Sect. 4.1).

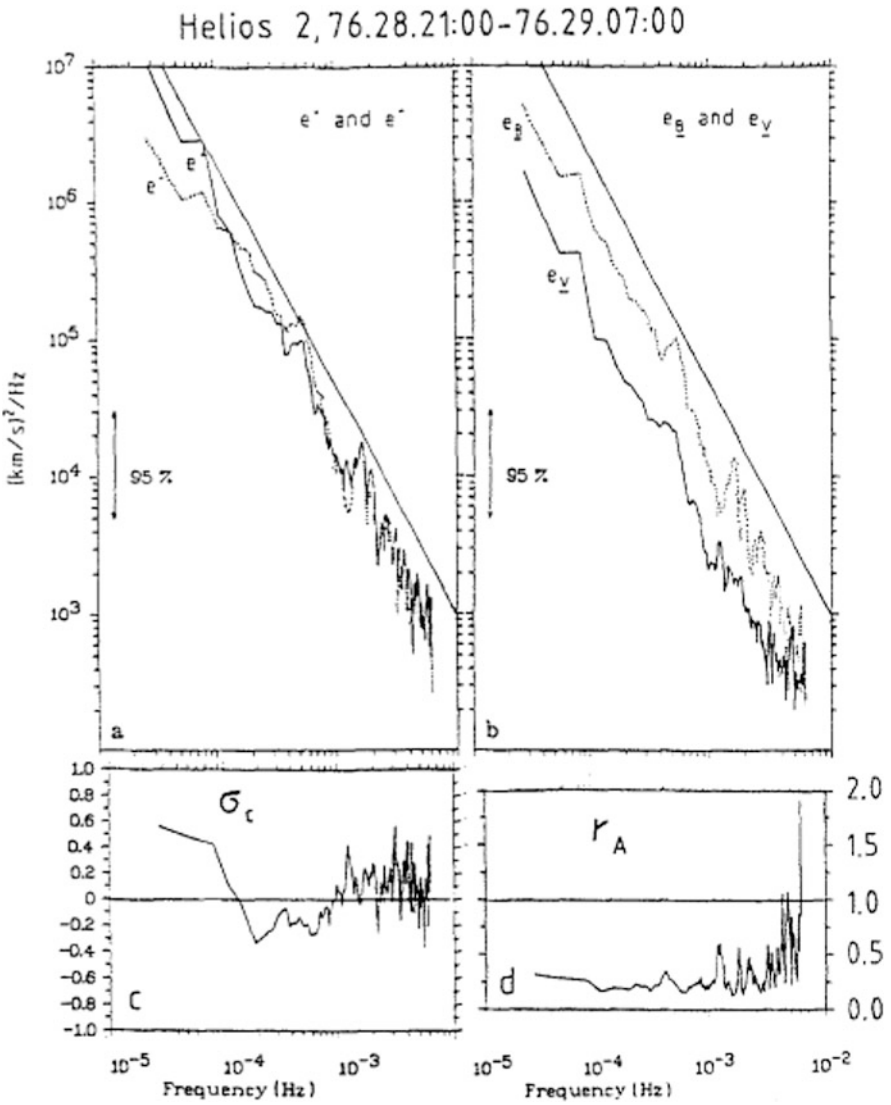

Fig. 4.6 *Left column:* e^+ and e^- spectra (*top*) and σ_c (*bottom*) during a slow wind interval at 0.9 AU. *Right column:* kinetic e_v and magnetic e_B energy spectra (*top*) computed from the trace of the relative spectral tensor, and spectrum of the Alfvén ratio r_A (*bottom*) Image reproduced by permission from Tu and Marsch (1995)

These results, shown in the left panels of Fig. 4.7, highlight the presence of a radial evolution of the fluctuations towards a double-peaked distribution during the expansion of the solar wind. The relative analysis has been performed on a co-rotating fast stream observed by Helios 2 at three different heliocentric distances

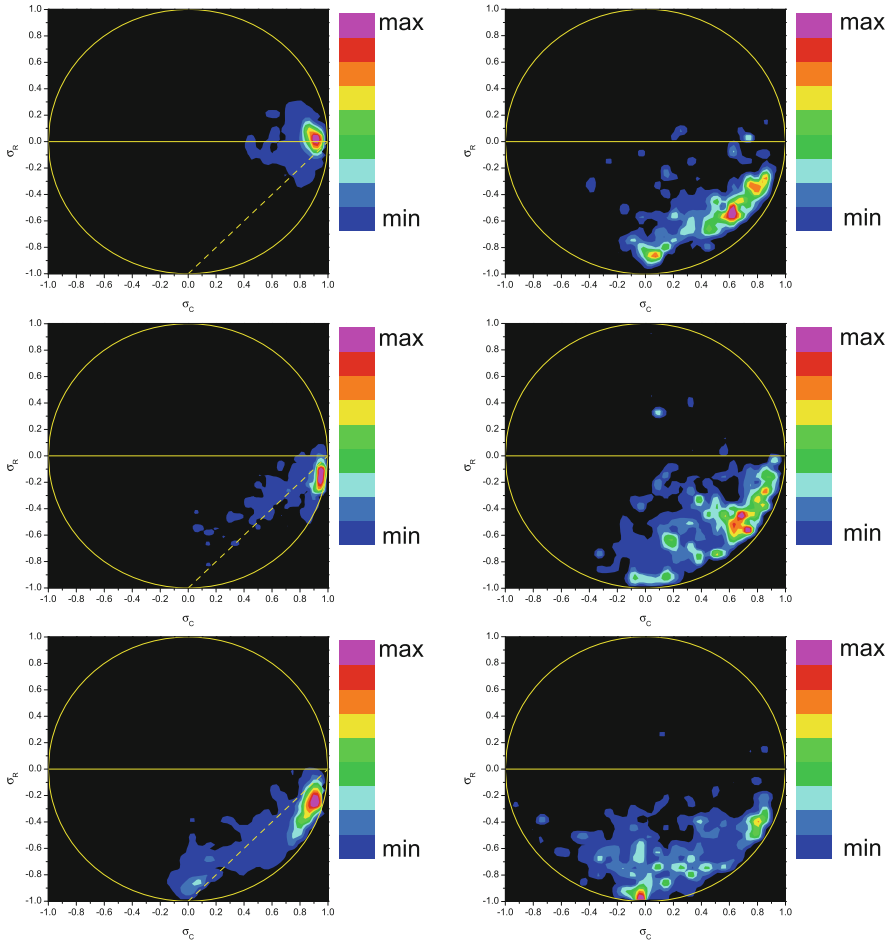

Fig. 4.7 *Left, from top to bottom:* frequency histograms of σ_r vs. σ_c (here σ_C and σ_R) for fast wind observed by Helios 2 at 0.29, 0.65 and 0.88 AU, respectively. The color code, for each panel, is normalized to the maximum of the distribution. The *yellow circle* represents the limiting value given by $\sigma_c^2 + \sigma_r^2 = 1$ while, the *yellow dashed line* represents the relation $\sigma_r = \sigma_c - 1$, see text for details. *Right, from top to bottom:* frequency histograms of σ_r vs. σ_c (here σ_C and σ_R) for slow wind observed by Helios 2 at 0.32, 0.69 and 0.90 AU, respectively. The color code, for each panel, is normalized to the maximum of the distribution. Image reproduced by permission from Bruno et al. (2007), copyright EGU

over consecutive solar rotations (see Fig. 3.10 and related text). Closer to the Sun, at 0.3 AU, the distribution is well centered around $\sigma_r = 0$ and $\sigma_c = 1$, suggesting that Alfvénic fluctuations, outwardly propagating, dominate the scenario. By the time the wind reaches 0.7 AU, the appearance of a tail towards negative values of σ_r and lower values of σ_c indicates a partial loss of the Alfvénic character in favor of fluctuations characterized by a stronger magnetic energy content. This

clear tendency ends up with the appearance of a secondary peak by the time the wind reaches 0.88 AU. This new family of fluctuations forms around $\sigma_r = -1$ and $\sigma_c = 0$. The values of σ_r and σ_c which characterize this new population are typical of MFDT structures described by Tu and Marsch (1991). Together with the appearance of these fluctuations, the main peak characterized by Alfvén like fluctuations looses much of its original character shown at 0.3 AU. The yellow straight line that can be seen in the left panels of Fig. 4.7 would be the linear relation between σ_r and σ_c in case fluctuations were made solely by Alfvén waves outwardly propagating and advected MFDTs (Tu and Marsch 1991) and it would replace the canonical, quadratic relation $\sigma_r^2 + \sigma_c^2 \leq 1$ represented by the yellow circle drawn in each panel. However, the yellow dashed line shown in the left panels of Fig. 4.7 does not seem to fit satisfactorily the observed distributions.

Quite different is the situation within slow wind, as shown in the right panels of Fig. 4.7. As a matter of fact, these histograms do not show any striking radial evolution like in the case of fast wind. High values of σ_c are statistically much less relevant than in fast wind and a well defined population characterized by $\sigma_r = -1$ and $\sigma_c = 0$, already present at 0.3 AU, becomes one of the dominant peaks of the histogram as the wind expands. This last feature is really at odds with what happens in fast wind and highlights the different nature of the fluctuations which, in this case, are magnetically dominated. The same authors obtained very similar results for fast and slow wind also from the same type of analysis performed on WIND and Ulysses data which, in addition, confirmed the incompressive character of the Alfvénic fluctuations and highlighted a low compressive character also for the populations characterized by $\sigma_r \sim -1$ and $\sigma_c \sim 0$.

About the origin of these structures, these authors suggest that they might be not only created locally during the non linear evolution of the fluctuations but they might also have a solar origin. The reason why they are not seen close to the Sun, within fast wind, might be due to the fact that these fluctuations, mainly non-compressive, change the direction of the magnetic field similarly to Alfvénic fluctuations but produce a much smaller effect since the associated δb is smaller than the one corresponding to Alfvénic fluctuations. As the wind expands, the Alfvénic component undergoes non-linear interactions which produce a transfer of energy to smaller and smaller scales while, these structures, being advected, have a much longer lifetime. As the expansion goes on, the relative weight of these fluctuations grows and they start to be detected.

4.2.1 On the Nature of Alfvénic Fluctuations

The Alfvénic nature of outward modes has been widely recognized through several frequency decades up to periods of the order of several hours in the s/c rest frame (Bruno et al. 1985). Conversely, the nature of those fluctuations identified by δz^-, called “inward Alfvén modes”, is still not completely clear. There are many clues

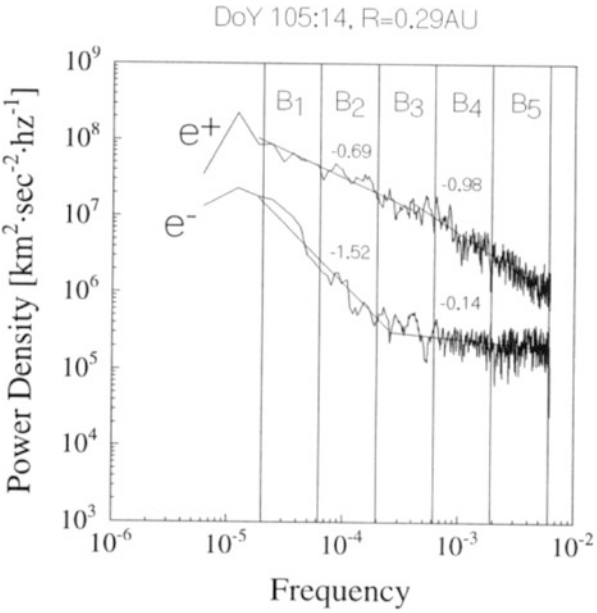

Fig. 4.8 Power density spectra for e^+ and e^- during a high velocity stream observed at 0.3 AU. Best fit lines for different frequency intervals and related spectral indices are also shown. *Vertical lines* fix the limits of five different frequency intervals analyzed by Bruno et al. (1996). Image reproduced by permission, copyright by AIP

which would suggest that these fluctuations, especially in the hourly frequencies range, have a non-Alfvénic nature. Several studies on this topic in the low frequency range have suggested that structures convected by the wind could well mimic non-existent inward propagating modes (see the review by Tu and Marsch 1995). However, other studies (Tu et al. 1989) have also found, in the high frequency range and within fast streams, a certain anisotropy in the components which resembles the same anisotropy found for outward modes. So, these observations would suggest a close link between inward modes at high frequency and outward modes, possibly the same nature.

Figure 4.8 shows power density spectra for e^+ and e^- during a high velocity stream observed at 0.3 AU [similar spectra can be also found in the paper by Grappin et al. (1990) and Tu et al. (1989)]. The observed spectral indices, reported on the plot, are typically found within high velocity streams encountered at short heliocentric distances. Bruno et al. (1996) analyzed the power relative to e^+ and e^- modes, within five frequency bands, ranging from roughly 12 h to 3 min, delimited by the vertical solid lines equally spaced in log-scale. The integrated power associated with e^+ and e^- within the selected frequency bands is shown in Fig. 4.9. Passing from slow to fast wind e^+ grows much more within the highest frequency bands. Moreover, there is a good correlation between the profiles of

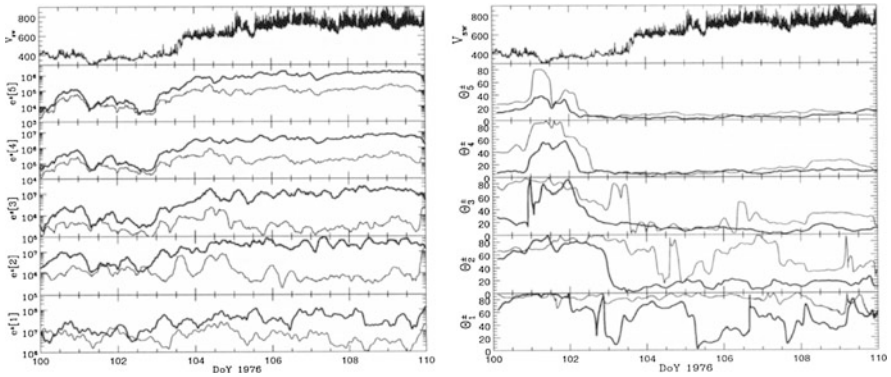

Fig. 4.9 *Left panel:* wind speed profile is shown in the *top panel*. Power density associated with e^+ (*thick line*) and e^- (*thin line*), within the five frequency bands chosen, is shown in the *lower panels*. *Right panel:* wind speed profile is shown in the *top panel*. Values of the angle $\theta^{\pm}$ between the minimum variance direction of δz^+ (*thick line*) and δz^- (*thin line*) and the direction of the ambient magnetic field are shown in the lower panels, relatively to each frequency band. Image reproduced by permission from Bruno et al. (1996), copyright by AIP

e^- and e^+ within the first two highest frequency bands, as already noticed by Grappin et al. (1990) who looked at the correlation between daily averages of e^- and e^+ in several frequency bands, even widely separated in frequency. The above results stimulated these authors to conclude that it was reminiscent of the non-local coupling in **k**-space between opposite modes found by Grappin et al. (1982) in homogeneous MHD. Expansion effects were also taken into account by Velli et al. (1990) who modeled inward modes as that fraction of outward modes back-scattered by the inhomogeneities of the medium due to expansion effects (Velli et al. 1989). However, following this model we would often expect the two populations to be somehow related to each other but, in situ observations do not favor this kind of forecast (Bavassano and Bruno 1992).

An alternative generation mechanism was proposed by Tu et al. (1989) based on the parametric decay of e^+ in high frequency range (Galeev and Oraevskii 1963). This mechanism is such that large amplitude Alfvén waves, unstable to perturbations of random field intensity and density fluctuations, would decay into two secondary Alfvén modes propagating in opposite directions and a sound-like wave propagating in the same direction of the pump wave. Most of the energy of the mother wave would go into the sound-like fluctuation and the backward propagating Alfvén mode. On the other hand, the production of e^- modes by parametric instability is not particularly fast if the plasma $\beta \sim 1$, like in the case of solar wind (Goldstein 1978; Derby 1978), since this condition slows down the growth rate of the instability. It is also true that numerical simulations by Malara et al. (2000, 2001b, 2002), and Primavera et al. (2003) have shown that parametric decay can still be thought as a possible mechanism of local production of turbulence within the polar wind (see Sect. 4.3). However, the strong correlation between e^+ and e^- profiles found

only within the highest frequency bands would support this mechanism and would suggest that e^- modes within these frequency bands would have an Alfvénic nature. Another feature shown in Fig. 4.9 that favors these conclusions is the fact that both δz^+ and δz^- keep the direction of their minimum variance axis aligned with the background magnetic field only within the fast wind, and exclusively within the highest frequency bands. This would not contradict the view suggested by Barnes (1981). Following this model, the majority of Alfvénic fluctuations propagating in one direction have the tip of the magnetic field vector randomly wandering on the surface of half a sphere of constant radius, and centered along the ambient field $\mathbf{B}_\circ$. In this situation the minimum variance would be oriented along $\mathbf{B}_\circ$, although this would not represent the propagation direction of each wave vector which could propagate even at large angles from this direction. This situation can be seen in the right hand panel of Fig. 7.7 of Sect. 7.3, which refers to a typical Alfvénic interval within fast wind. Moreover, δz^+ fluctuations show a persistent anisotropy throughout the fast stream since the minimum variance axis remains quite aligned to the background field direction. This situation downgrades only at the very low frequencies where θ^+, the angle between the minimum variance direction of δz^+ and the direction of the ambient magnetic field, starts wandering between 0° and 90°. On the contrary, in slow wind, since Alfvénic modes have a smaller amplitude, compressive structures due to the dynamic interaction between slow and fast wind or, of solar origin, push the minimum variance direction to larger angles with respect to $\mathbf{B}_\circ$, not depending on the frequency range.

In a way, we can say that within the stream, both θ^+ and θ^-, the angle between the minimum variance direction of δz^- and the direction of the ambient magnetic field, show a similar behavior as we look at lower and lower frequencies. The only difference is that θ^- reaches higher values at higher frequencies than θ^+. This was interpreted by Bruno et al. (1996) as due to transverse fluctuations of δz^- which carry much less power than those of δz^+ and, consequently, they are more easily influenced by perturbations represented by the background, convected structure of the wind (e.g., TD's and PBS's). As a consequence, at low frequency δz^- fluctuations may represent a signature of the compressive component of the turbulence while, at high frequency, they might reflect the presence of inward propagating Alfvén modes. Thus, while for periods of several hours δz^+ fluctuations can still be considered as the product of Alfvén modes propagating outward (Bruno et al. 1985), δz^- fluctuations are rather due to the underlying convected structure of the wind. In other words, high frequency turbulence can be looked at mainly as a mixture of inward and outward Alfvénic fluctuations plus, presumably, sound-like perturbations (Marsch and Tu 1993b). On the other hand, low frequency turbulence would be made of outward Alfvénic fluctuations and static convected structures representing the inhomogeneities of the background medium.

4.2.2 Numerical Simulations

Numerical simulations currently represent one of the main source of information about non-linear evolution of fluid flows. The actual super-computers are now powerful enough to simulate equations (NS or MHD) that describe turbulent flows with Reynolds numbers of the order of 10^4 in two-dimensional configurations, or 10^3 in three-dimensional one. Of course, we are far from achieving realistic values, but now we are able to investigate turbulence with an inertial range extended for more than one decade. Rather the main source of difficulties to get results from numerical simulations is the fact that they are made under some obvious constraints (say boundary conditions, equations to be simulated, etc.), mainly dictated by the limited physical description that we are able to use when numerical simulations are made, compared with the extreme richness of the phenomena involved: numerical simulations, even in standard conditions, are used *tout court* as models for the solar wind behavior. Perhaps the only exception, to our knowledge, is the attempt to describe the effects of the solar wind expansion on turbulence evolution like, for example, in the papers by Velli et al. (1989, 1990), and Hellinger and Trávníček (2008). Even with this far too pessimistic point of view, used here solely as a few words of caution, simulations in some cases were able to reproduce some phenomena observed in the solar wind.

Nevertheless, numerical simulations have been playing a key role, and will continue to do so in our seeking an understanding of turbulent flows. Numerical simulations allows us to get information that cannot be obtained in laboratory. For example, high resolution numerical simulations provide information at every point on a grid and, for some times, about basic vector quantities and their derivatives. The number of degree of freedom required to resolve the smaller scales is proportional to a power of the Reynolds number, say to $Re^{9/4}$, although the dynamically relevant number of modes may be much less. Then one of the main challenge remaining is how to handle and analyze the huge data files produced by large simulations (of the order of Terabytes). Actually a lot of papers appeared in literature on computer simulations related to MHD turbulence. The interested reader can look at the book by Biskamp (1993) and the reviews by Pouquet (1993, 1996).

4.2.3 Local Production of Alfvénic Turbulence in the Ecliptic

The discovery of the strong correlation between velocity and magnetic field fluctuations has represented the motivation for some MHD numerical simulations, aimed to confirm the conjecture by Dobrowolny et al. (1980b). The high level of correlation seems to be due to a kind of self-organization (dynamical alignment) of MHD turbulence, generated by the natural evolution of MHD towards the strongest attractive fixed point of equations (Ting et al. 1986; Carbone and Veltri 1987, 1992). Numerical simulations (Carbone and Veltri 1992; Ting et al. 1986) confirmed this

conjecture, say MHD turbulence spontaneously can tends towards a state were correlation increases, that is, the quantity $\sigma_c = 2H_c/E$, where H_c is the cross-helicity and E the total energy of the flow (see Sect. 3.2.2), tends to be maximal.

The picture of the evolution of *incompressible* MHD turbulence, which comes out is rather nice but solar wind turbulence displays a more complicated behavior. In particular, as we have reported above, observations seems to point out that solar wind evolves in the opposite way. The correlation is high near the Sun, at larger radial distances, from 1 to 10 AU the correlation is progressively lower, while the level in fluctuations of mass density and magnetic field intensity increases. What is more difficult to understand is why correlation is progressively destroyed in the solar wind, while the natural evolution of MHD is towards a state of maximal normalized cross-helicity. A possible solution can be found in the fact that solar wind is neither incompressible nor statistically homogeneous, and some efforts to tentatively take into account more sophisticated effects have been made.

A mechanism, responsible for the radial evolution of turbulence, was suggested by Roberts and Goldstein (1988), Goldstein et al. (1989), and Roberts et al. (1991, 1992) and was based on velocity shear generation. The suggestion to adopt such a mechanism came from a detailed analysis made by Roberts et al. (1987a,b) of Helios and Voyager interplanetary observations of the radial evolution of the normalized cross-helicity σ_c at different time scales. Moreover, Voyager's observations showed that plasma regions, which had not experienced dynamical interactions with neighboring plasma, kept the Alfvénic character of the fluctuations at distances as far as 8 AU (Roberts et al. 1987b). In particular, the vicinity of Helios trajectory to the interplanetary current sheet, characterized by low velocity flow, suggested Roberts et al. (1991) to include in his simulations a narrow low speed flow surrounded by two high speed flows. The idea was to mimic the slow, equatorial solar wind between north and south fast polar wind. Magnetic field profile and velocity shear were reconstructed using the six lowest $Z^{\pm}$ Fourier modes as shown in Fig. 4.10. An initial population of purely outward propagating Alfvénic fluctuations (z^+) was added at large k and was characterized by a spectral slope of k^{-1}. No inward modes were present in the same range. Results of Fig. 4.10 show that the time evolution of z^+ spectrum is quite rapid at the beginning, towards a steeper spectrum, and slows down successively. At the same time, z^- modes are created by the generation mechanism at higher and higher k but, along a Kolmogorov-type slope $k^{-5/3}$.

These results, although obtained from simulations performed using 2D incompressible spectral and pseudo-spectral codes, with fairly small Reynolds number of $Re \simeq 200$, were similar to the spectral evolution observed in the solar wind (Marsch and Tu 1990). Moreover, spatial averages across the simulation box revealed a strong cross-helicity depletion right across the slow wind, representing the heliospheric current sheet. However, magnetic field inversions and even relatively small velocity shears would largely affect an initially high Alfvénic flow (Roberts et al. 1992). However, Bavassano and Bruno (1992) studied an interaction region, repeatedly observed between 0.3 and 0.9 AU, characterized by a large velocity shear and previously thought to be a good candidate for shear generation (Bavassano and

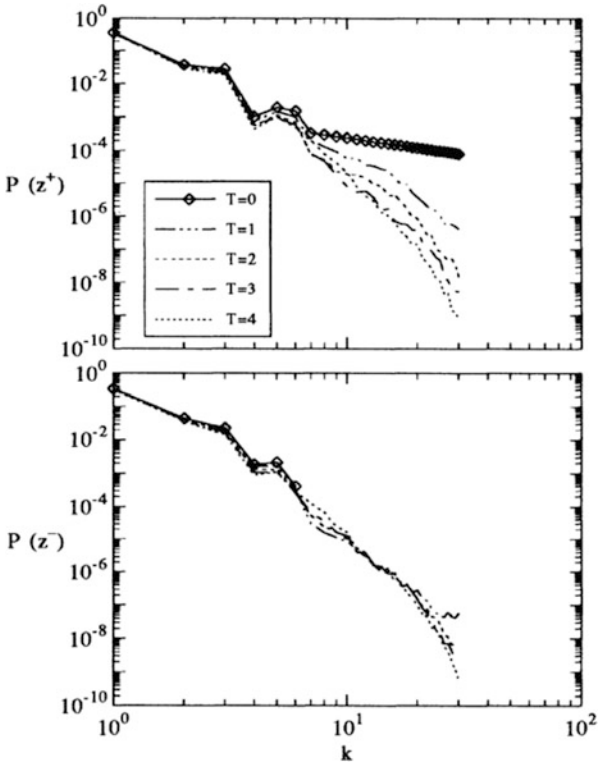

Fig. 4.10 Time evolution of the power density spectra of z^+ and z^- showing the turbulent evolution of the spectra due to velocity shear generation (from Roberts et al. 1991)

Bruno 1989). They concluded that, even in the hypothesis of a very fast growth of the instability, inward modes would not have had enough time to fill up the whole region as observed by Helios 2.

The above simulations by Roberts et al. (1991) were successively implemented with a compressive pseudo-spectral code (Ghosh and Matthaeus 1990) which provided evidence that, during this turbulence evolution, clear correlations between magnetic field magnitude and density fluctuations, and between z^- and density fluctuations should arise. However, such a clear correlation, by-product of the non-linear evolution, was not found in solar wind data (Marsch and Tu 1993a; Bruno et al. 1996). Moreover, their results did not show the flattening of e^- spectrum at higher frequency, as observed by Helios (Tu et al. 1989). As a consequence, velocity shear alone cannot explain the whole phenomenon, other mechanisms must also play a relevant role in the evolution of interplanetary turbulence.

Compressible numerical simulations have been performed by Veltri et al. (1992) and Malara et al. (1996, 2000) which invoked the interactions between small scale waves and large scale magnetic field gradients and the parametric instability,

as characteristic effects to reduce correlations. In a compressible, statistically inhomogeneous medium such as the heliosphere, there are many processes which tend to destroy the natural evolution toward a maximal correlation, typical of standard MHD. In such a medium an Alfvén wave is subject to parametric decay instability (Viñas and Goldstein 1991; Del Zanna et al. 2001; Del Zanna 2001), which means that the mother wave decays in two modes: (1) a compressive mode that dissipates energy because of the steepening effect, and (2) a backscattered Alfvénic mode with lower amplitude and frequency. Malara et al. (1996) showed that in a compressible medium, the correlation between the velocity and the magnetic field fluctuations is reduced because of the generation of the backward propagating Alfvénic fluctuations, and of a compressive component of turbulence, characterized by density fluctuations $\delta\rho \neq 0$ and magnetic intensity fluctuations $\delta|\mathbf{B}| \neq 0$.

From a technical point of view it is worthwhile to remark that, when a large scale field which varies on a narrow region is introduced (typically a tanh-like field), periodic boundary conditions should be used with some care. Roberts et al. (1991, 1992) used a double shear layer, while Malara et al. (1992) introduced an interesting numerical technique based on both the glue between two simulation boxes and a Chebyshev expansion, to maintain a single shear layer, say non periodic boundary conditions, and an increased resolution where the shear layer exists.

Grappin et al. (1992) observed that the solar wind expansion increases the lengths normal to the radial direction, thus producing an effect similar to a kind of inverse energy cascade. This effect perhaps should be able to compete with the turbulent cascade which transfers energy to small scales, thus stopping the non-linear interactions. In absence of non-linear interactions, the natural tendency towards an increase of σ_c is stopped. These inferences have been corroborated by further studies like those by Grappin and Velli (1996) and Goldstein and Roberts (1999). A numerical model treating the evolution of e^+ and e^-, including parametric decay of e^+, was presented by Marsch and Tu (1993b). The parametric decay source term was added in order to reproduce the decreasing cross-helicity observed during the wind expansion. As a matter of fact, the cascade process, when spectral equations for both e^+ and e^- are included and solved self-consistently, can only steepen the spectra at high frequency. Results from this model, shown in Fig. 4.11, partially reproduce the observed evolution of the normalized cross-helicity. While the radial evolution of e^+ is correctly reproduced, the behavior of e^- shows an over-production of inward modes between 0.6 and 0.8 AU probably due to an overestimation of the strength of the pump-wave. However, the model is applied to the situation observed by Helios at 0.3 AU where a rather flat e^- spectrum already exists.

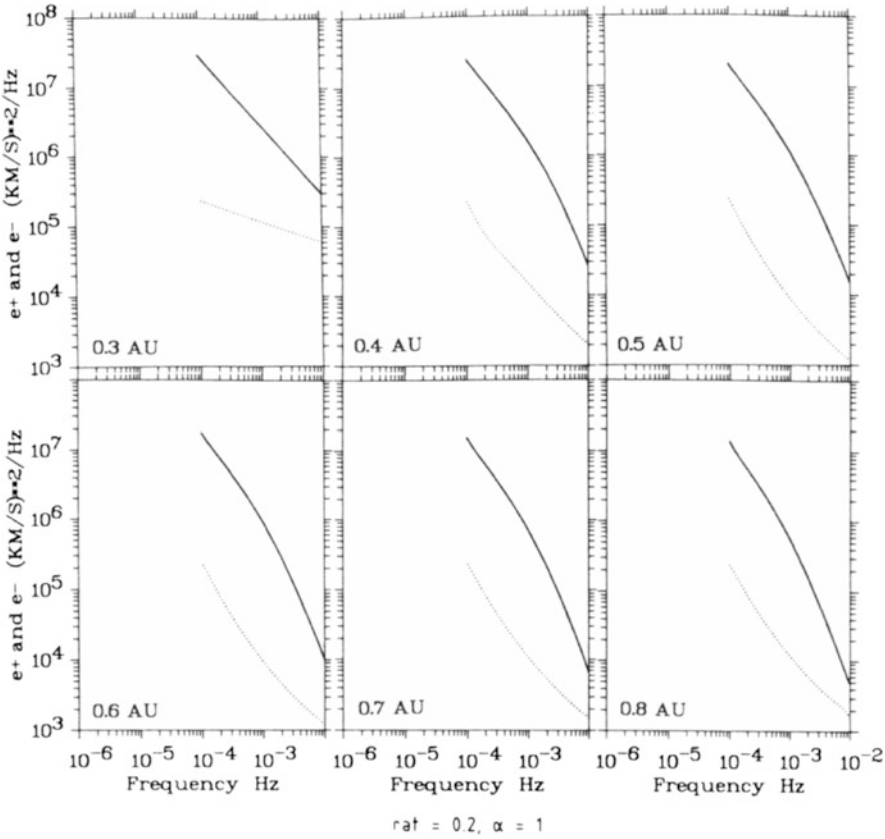

Fig. 4.11 Radial evolution of e^+ and e^- spectra obtained from the Marsch and Tu (1993b) model, in which a parametric decay source term was added to the Tu's model (Tu et al. 1984) that was, in turn, extended by including both spectrum equations for e^+ and e^- and solved them self-consistently. Image reproduced by permission from Marsch and Tu (1993b), copyright by AGU

4.3 Turbulence in the Polar Wind

In 1994 and 1995, Ulysses gave us the opportunity to look at the solar wind out-of-the-ecliptic, providing us with new exciting observations. For the first time heliospheric instruments were sampling pure, fast solar wind, free of any dynamical interaction with slow wind. There is one figure that within our scientific community has become as popular as "La Gioconda" by Leonardo da Vinci within the world of art. This figure produced at LANL (McComas et al. 1998) is shown in the upper left panel of Fig. 4.12, which has been taken from a successive paper by McComas et al. (2003), and summarizes the most important aspects of the large scale structure of the polar solar wind during the minimum of the solar activity phase, as indicated by the low value of the Wolf's number reported in the lower panel. It shows speed

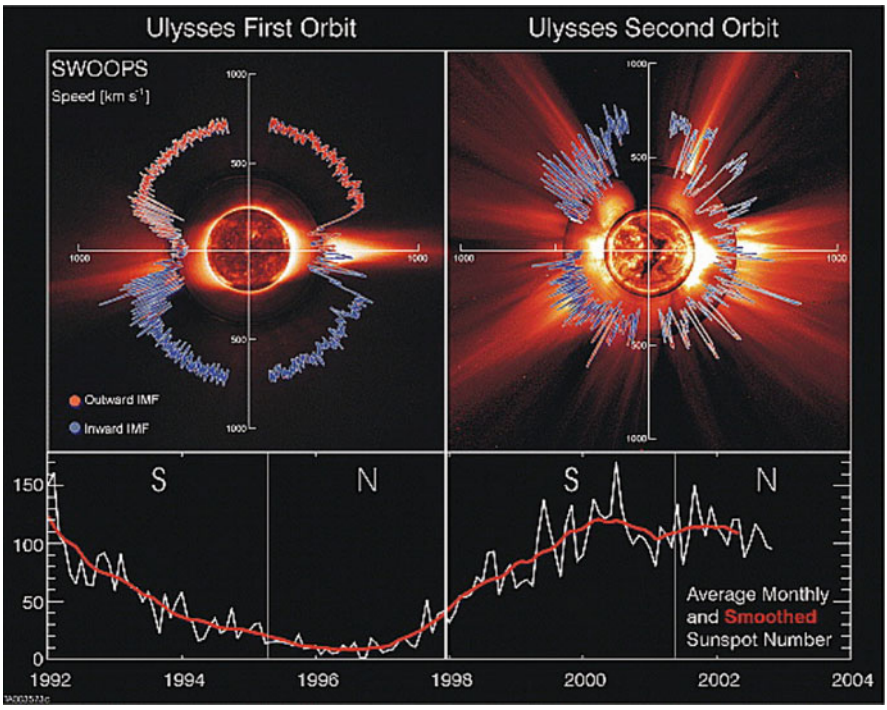

Fig. 4.12 Large scale solar wind profile as a function of latitude during minimum (*left panel*) and maximum (*right panel*) solar cycle phases. The sunspot number is also shown at the *bottom panels*. Image reproduced by permission from McComas et al. (2003), copyright by AGU

profile, proton number density profile and magnetic field polarity vs. heliographic latitude during the first complete Ulysses' polar orbit. Fast wind fills up north and south hemispheres of the Sun almost completely, except a narrow latitudinal belt around the equator, where the slow wind dominates. Flow velocity, which rapidly increases from the equator towards higher latitudes, quickly reaches a plateau and the wind escapes the polar regions with a rather uniform speed. Moreover, polar wind is characterized by a lower number density and shows rather uniform magnetic polarity of opposite sign, depending on the hemisphere. Thus, the main difference between ecliptic and polar wind is that this last one completely lacks of dynamical interactions with slower plasma and freely flows into the interplanetary space. The presence or not of this phenomenon, as we will see in the following pages, plays a major role in the development of MHD turbulence during the wind expansion. During solar maximum (look at the upper right panel of Fig. 4.12) the situation dramatically changes and the equatorial wind extends to higher latitudes, to the extent that there is no longer difference between polar and equatorial wind.

4.3.1 Evolving Turbulence in the Polar Wind

Ulysses observations gave us the possibility to test whether or not we could forecast the turbulent evolution in the polar regions on the basis of what we had learned in the ecliptic. We knew that, in the ecliptic, velocity shear, parametric decay, and interaction of Alfvénic modes with convected structures (see Sects. 4.2 and 4.2.3) all play some role in the turbulent evolution and, before Ulysses reached the polar regions of the Sun, three possibilities were given:

1. Alfvénic turbulence would have not relaxed towards standard turbulence because the large scale velocity shears would have been much less relevant (Grappin et al. 1991);
2. since the magnetic field would be smaller far from the ecliptic, at large heliocentric distances, even small shears would lead to an isotropization of the fluctuations and produce a turbulent cascade faster than the one observed at low latitudes, and the subsequent evolution would take less time (Roberts et al. 1990);
3. there would still be evolution due to interaction with convected plasma and field structures but it would be slower than in the ecliptic since the power associated with Alfvénic fluctuations would largely dominate over the inhomogeneities of the medium. Thus, Alfvénic correlations should last longer than in the ecliptic plane, with a consequent slower evolution of the normalized cross-helicity (Bruno 1992).

A fourth possibility was added by Tu and Marsch (1995), based on their model (Tu and Marsch 1993). Following this model they assumed that polar fluctuations were composed by outward Alfvénic fluctuations and MFDT. The spectra of these components would decrease with radial distance because of a WKB evolution and convective effects of the diverging flow. As the distance increases, the field becomes more transverse with respect to the radial direction, the s/c would sample more convective structures and, as a consequence, would observe a decrease of both σ_c and r_A.

Today we know that polar Alfvénic turbulence evolves in the same way it does in the ecliptic plane, but much more slowly. Moreover, the absence of strong velocity shears and enhanced compressive phenomena suggests that also some other mechanism based on parametric decay instability might play some role in the local production of turbulence (Bavassano et al. 2000b; Malara et al. 2001b, 2002; Primavera et al. 2003).

The first results of Ulysses magnetic field and plasma measurements in the polar regions, i.e., above $\pm 30^\circ$ latitude (left panel of Fig. 4.12), revealed the presence of Alfvénic correlations in a frequency range from less than 1 to more than 10 h (Balogh et al. 1995; Smith et al. 1995; Goldstein et al. 1995) in very good agreement with ecliptic observations (Bruno et al. 1985). However, it is worth noticing that Helios observations referred to very short heliocentric distances around 0.3 AU while the above Ulysses observations were taken up to 4 AU. As a matter of fact, these long period Alfvén waves observed in the ecliptic, in the inner solar

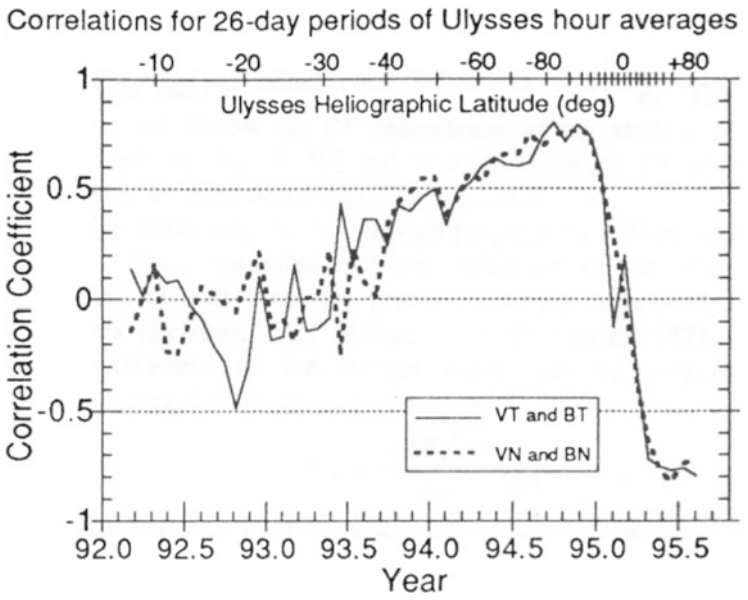

Fig. 4.13 Magnetic field and velocity hourly correlation vs. heliographic latitude. Image reproduced by permission from Smith et al. (1995), copyright by AGU

wind, become less prominent as the wind expands due to stream–stream dynamical interaction effects (Bruno et al. 1985) and strong velocity shears (Roberts et al. 1987a). At high latitude, the relative absence of enhanced dynamical interaction between flows at different speed and, as a consequence, the absence of strong velocity shears favors the survival of these extremely low frequency Alfvénic fluctuations for larger heliocentric excursions.

Figure 4.13 shows the hourly correlation coefficient for the transverse components of magnetic and velocity fields as Ulysses climbs to the south pole and during the fast latitude scanning that brought the s/c from the south to the north pole of the Sun in just half a year. While the equatorial phase of Ulysses journey is characterized by low values of the correlation coefficients, a gradual increase can be noticed starting at half of year 1993 when the s/c starts to increase its heliographic latitude from the ecliptic plane up to 80.2° south, at the end of 1994. Not only the degree of $\delta\mathbf{b} - \delta\mathbf{v}$ correlation resembled Helios observations but also the spectra of these fluctuations showed characteristics which were very similar to those observed in the ecliptic within fast wind like the spectral index of the components, that was found to be flat at low frequency and more Kolmogorov-like at higher frequencies (Smith et al. 1995). Balogh et al. (1995) and Forsyth et al. (1996) discussed magnetic fluctuations in terms of latitudinal and radial dependence of their variances. Similarly to what had been found within fast wind in the ecliptic (Mariani et al. 1978; Bavassano et al. 1982a; Tu et al. 1989; Roberts et al. 1992), variance of magnetic magnitude was much less than the variance

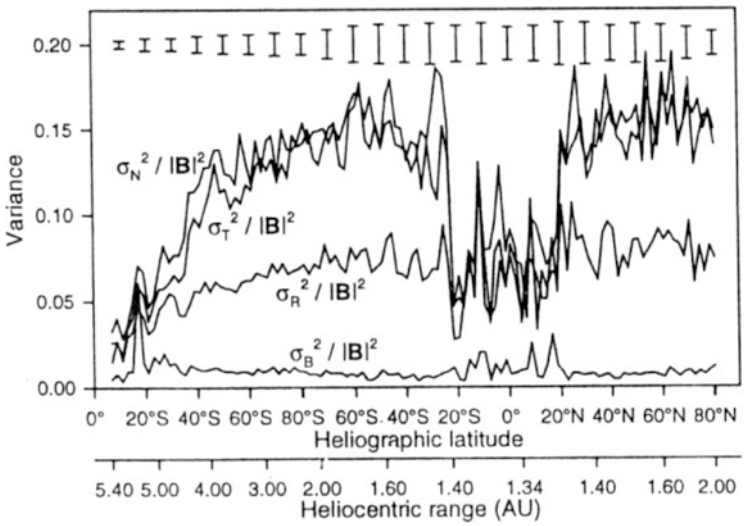

Fig. 4.14 Normalized magnetic field components and magnitude hourly variances plotted vs. heliographic latitude during a complete latitude survey by Ulysses. Image reproduced by permission from Forsyth et al. (1996), copyright by AGU

associated with the components. Moreover, transverse variances had consistently higher values than the one along the radial direction and were also much more sensitive to latitude excursion, as shown in Fig. 4.14. In addition, the level of the normalized hourly variances of the transverse components observed during the ecliptic phase, right after the compressive region ahead of co-rotating interacting regions, was maintained at the same level once the s/c entered the pure polar wind. Again, these observations showed that the fast wind observed in the ecliptic was coming from the equatorward extension of polar coronal holes.

Horbury et al. (1995b) and Forsyth et al. (1996) showed that the interplanetary magnetic field fluctuations observed by Ulysses continuously evolve within the fast polar wind, at least out to 4 AU. Since this evolution was observed within the polar wind, rather free of co-rotating and transient events like those characterizing low latitudes, they concluded that some other mechanism was at work and this evolution was an intrinsic property of turbulence.

Results in Fig. 4.15 show the evolution of the spectral slope computed across three different time scale intervals. The smallest time scales show a clear evolution that keeps on going past the highest latitude on day 256, strongly suggesting that this evolution is radial rather than latitudinal effect. Horbury et al. (1996b) worked on determining the rate of turbulent evolution for the polar wind.

They calculated the spectral index at different frequencies from the scaling of the second order structure function [see Sect. 6 and papers by Burlaga (1992a), Burlaga (1992b), Marsch and Tu (1993b), Ruzmaikin et al. (1995), and Horbury et al. (1996a)] since the spectral scaling α is related to the scaling of the structure

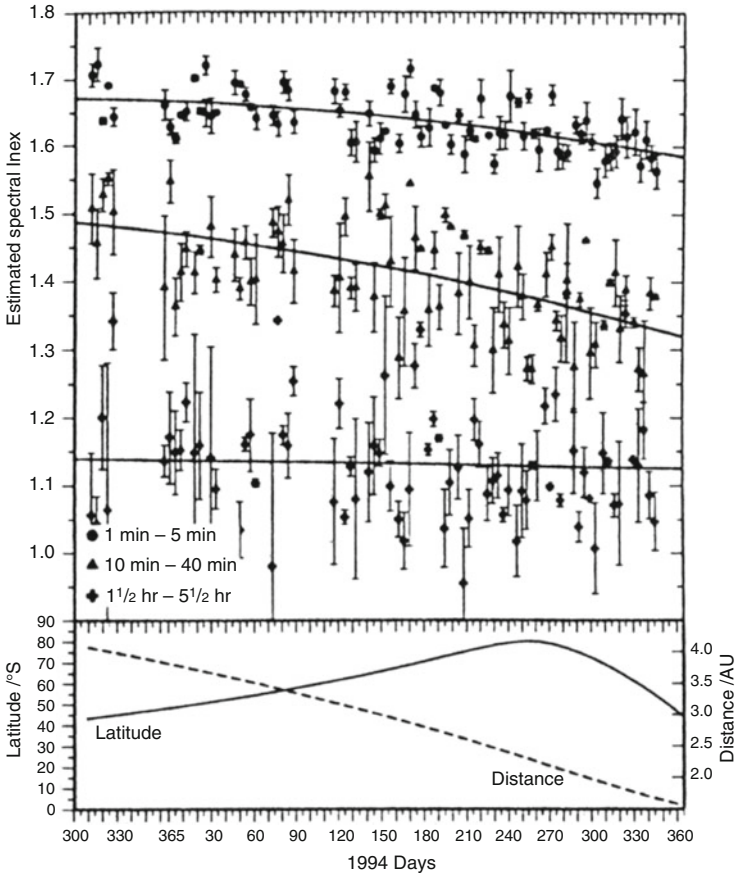

Fig. 4.15 Spectral indexes of magnetic fluctuations within three different time scale intervals as indicated in the plot. The *bottom panel* shows heliographic latitude and heliocentric distance of Ulysses. Image reproduced by permission from Horbury et al. (1995b), copyright by AGU

function s by the following relation: $\alpha = s + 1$ (Monin and Yaglom 1975). Horbury et al. (1996b), studying variations of the spectral index with frequency for polar turbulence, found that there are two frequency ranges where the spectral index is rather steady. The first range is around 10^{-2} Hz with a spectral index around $-5/3$, while the second range is at very low frequencies with a spectral index around -1. This last range is the one where Goldstein et al. (1995) found the best example of Alfvénic fluctuations. Similarly, ecliptic studies found that the best Alfvénic correlations belonged to the hourly, low frequency regime (Bruno et al. 1985).

Horbury et al. (1995c) presented an analysis of the high latitude magnetic field using a fractal method. Within the solar wind context, this method has been described for the first time by Burlaga and Klein (1986) and Ruzmaikin et al. (1993), and is based on the estimate of the scaling of the length function $L(\tau)$ with the

scale τ. This function is closely related to the first order structure function and, if statistical self-similar, has scaling properties $L(\tau) \sim \tau^{\ell}$, where ℓ is the scaling exponent. It follows that $L(\tau)$ is an estimate of the amplitude of the fluctuations at scale τ, and the relation that binds $L(\tau)$ to the variance of the fluctuations $(\delta B)^2 \sim \tau^{s(2)}$ is:

$$L(\tau) \sim N(\tau)[(\delta B)^2]^{1/2} \propto \tau^{s(2)/2-1},$$

where $N(\tau)$ represents the number of points at scale τ and scales like τ^{-1}. Since the power density spectrum $W(f)$ is related to $(\delta B)^2$ through the relation $fW(f) \sim (\delta B)^2$, if $W(f) \sim f^{-\alpha}$, then $s(2) = \alpha - 1$, and, as a consequence $\alpha = 2\ell + 3$ (Marsch and Tu 1996). Thus, it results very easy to estimate the spectral index at a given scale or frequency, without using spectral methods but simply computing the length function.

Results in Fig. 4.16 show the existence of two different regimes, one with a spectral index around the Kolmogorov scaling extending from $10^{1.5}$ to 10^3 s and, separated by a clear break-point at scales of 10^3 s, a flatter and flatter spectral exponent for larger and larger scales. These observations were quite similar to what had been observed by Helios 2 in the ecliptic, although the turbulence state recorded by Ulysses resulted to be more evolved than the situation seen at 0.3 AU and, perhaps, more similar to the turbulence state observed around 1 AU, as shown

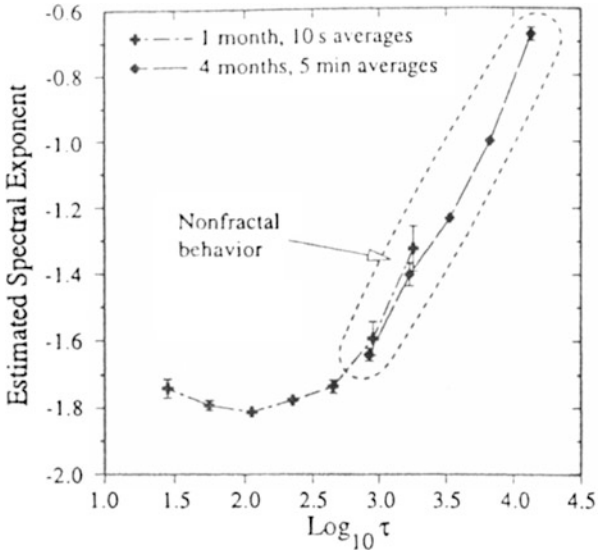

Fig. 4.16 Spectral exponents for the B_z component estimated from the length function computed from Ulysses magnetic field data, when the s/c was at about 4 AU and $\sim -50°$ latitude. *Different symbols* refer to different time intervals as reported in the graph. Image reproduced by permission from Horbury et al. (1995c)

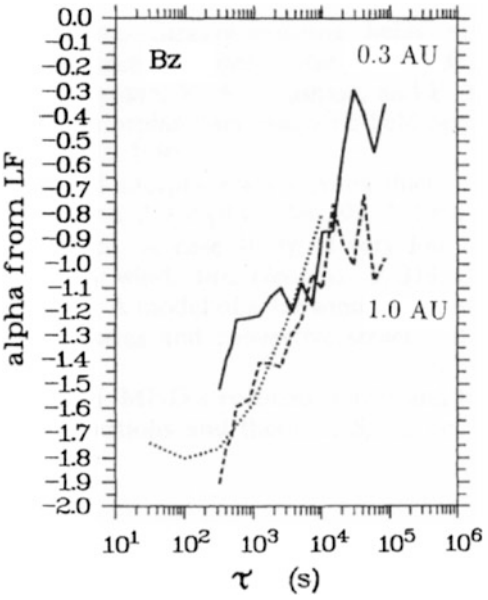

Fig. 4.17 Spectral exponents for the B_z component estimated from the length function computed from Helios and Ulysses magnetic field data. Ulysses length function (*dotted line*) is the same shown in the paper by Horbury et al. (1995c) when the s/c was at about 4 AU and $\sim -50°$ latitude. Image reproduced by permission from Marsch and Tu (1996), copyright by AGU

by Marsch and Tu (1996). These authors compared the spectral exponents, estimated using the same method of Horbury et al. (1995c), from Helios 2 magnetic field observations at two different heliocentric distances: 0.3 and 1.0 AU. The comparison with Ulysses results is shown in Fig. 4.17 where it appears rather clear that the slope of the B_z spectrum experiences a remarkable evolution during the wind expansion between 0.3 and 4 AU. Obviously, this comparison is meaningful in the reasonable hypothesis that fluctuations observed by Helios 2 at 0.3 AU are representative of out-of-the-ecliptic solar wind (Marsch and Tu 1996). This figure also shows that the degree of spectral evolution experienced by the fluctuations when observed at 4 AU at high latitude, is comparable to Helios observations at 1 AU in the ecliptic. Thus, the spectral evolution at high latitude is present although quite slower with respect to the ecliptic.

Forsyth et al. (1996) studied the radial dependence of the normalized hourly variances of the components B_R, B_T and B_N and the magnitude $|\mathbf{B}|$ of the magnetic field (see Sect. 3.3.6 to learn about the *RTN* reference system). The variance along the radial direction was computed as $\sigma_R{}^2 = \langle B_R{}^2 > - < B_R \rangle^2$ and successively normalized to $|\mathbf{B}|^2$ to remove the field strength dependence. Moreover, variances along the other two directions T and N were similarly defined. Fitting the radial dependence with a power law of the form $r^{-\alpha}$, but limiting the fit to the radial excursion between 1.5 and 3 AU (Fig. 4.18), these authors obtained $\alpha = 3.39 \pm 0.07$ for σ_r^2, $\alpha = 3.45 \pm 0.09$ for σ_T^2, $\alpha = 3.37 \pm 0.09$ for σ_N^2, and $\alpha = 2.48 \pm 0.14$ for σ_B^2. Thus, for hourly variances, the power associated with the components showed a radial dependence stronger than the one predicted by the WKB approximation, which would provide $\alpha = 3$. These authors also showed that including data between

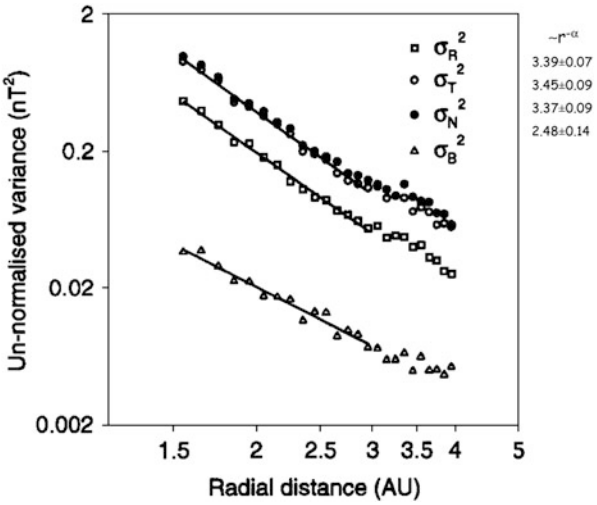

Fig. 4.18 Hourly variances of the components and the magnitude of the magnetic field vs. radial distance from the Sun. The meaning of the *different symbols* is also indicated in the *upper right corner*. Image reproduced by permission from Forsyth et al. (1996), copyright by AGU

3 and 4 AU, corresponding to intervals characterized by compressional features mainly due to high latitude CMEs, they would obtain less steep radial gradients, much closer to a WKB type. These results suggested that compressive effects can feed energy at the smallest scales, counteracting dissipative phenomena and mimicking a WKB-like behavior of the fluctuations. However, they concluded that for lower frequencies, below the frequency break point, fluctuations do follow the WKB radial evolution.

Horbury and Balogh (2001) presented a detailed comparison between Ulysses and Helios observations about the evolution of magnetic field fluctuations in high-speed solar wind. Ulysses results, between 1.4 and 4.1 AU, were presented as wave number dependence of radial and latitudinal power scaling. The first results of this analysis showed (Fig. 3 of their work) a general decrease of the power levels with solar distance, in both magnetic field components and magnitude fluctuations. In addition, the power associated with the radial component was always less than that of the transverse components, as already found by Forsyth et al. (1996). However, Horbury and Balogh (2001), supposing a possible latitude dependence, performed a multiple linear regression of the type:

$$\log_{10} w = A_p + B_p \log_{10} r + C_p \sin\theta, \tag{4.17}$$

where w is the power density integrated in a given spectral band, r is the radial distance and θ is the heliolatitude (0° at the equator). Moreover, the same procedure was applied to spectral index estimates α of the form $\alpha = A_\alpha + B_\alpha \log_{10} r + C_\alpha \sin\theta$. Results obtained for $B_p, C_p, B_\alpha, C_\alpha$ are shown in Fig. 4.19.

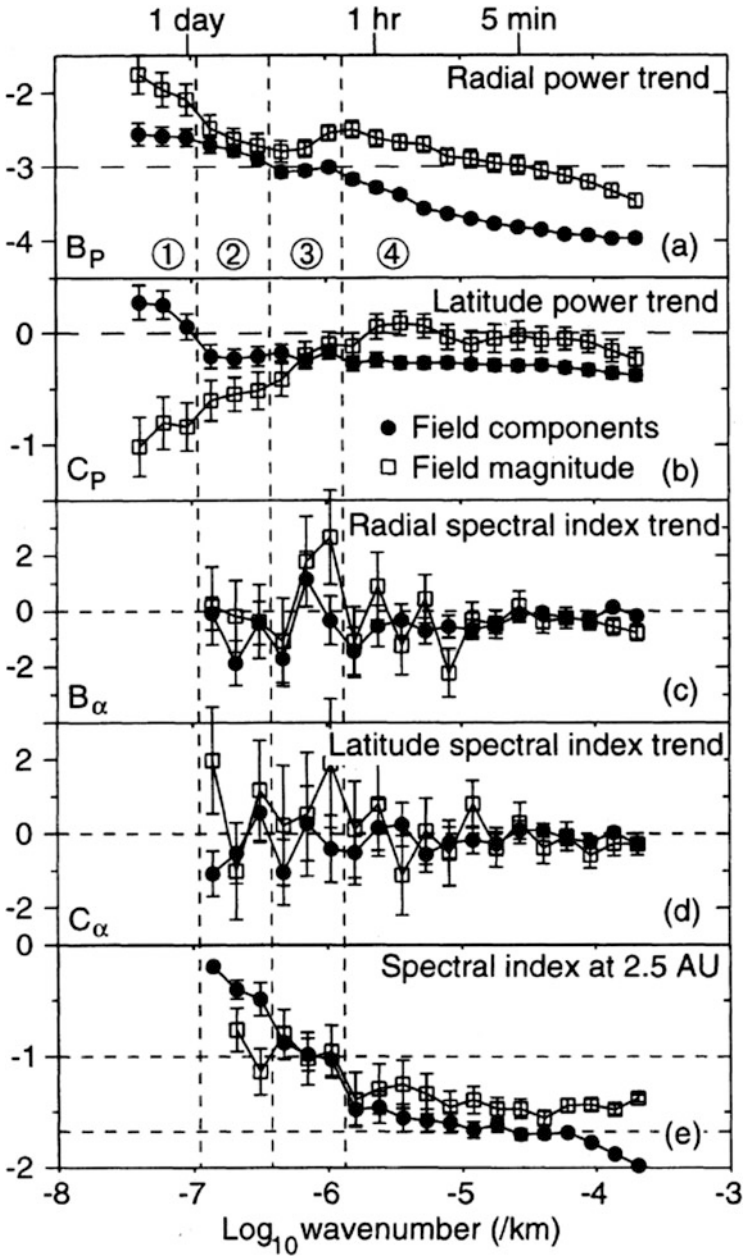

Fig. 4.19 (**a**) Scale dependence of radial power, (**b**) latitudinal power, (**c**) radial spectral index, (**d**) latitudinal spectral index, and (**e**) spectral index computed at 2.5 AU. *Solid circles* refer to the trace of the spectral matrix of the components, *open squares* refer to field magnitude. Correspondence between wave number scale and time scale is based on a wind velocity of 750 $\mathrm{km\,s^{-1}}$. Image reproduced by permission from Horbury and Balogh (2001), copyright by AGU

On the basis of variations of spectral index and radial and latitudinal dependencies, these authors were able to identify four wave number ranges as indicated by the circled numbers in the top panel of Fig. 4.19. Range 1 was characterized by a radial power decrease weaker than WKB (-3), positive latitudinal trend for components (more power at higher latitude) and negative for magnitude (less compressive events at higher latitudes). Range 2 showed a more rapid radial decrease of power for both magnitude and components and a negative latitudinal power trend, which implies less power at higher latitudes. Moreover, the spectral index of the components (bottom panel) is around 0.5 and tends to 0 at larger scales. Within range 3 the power of the components follows a WKB radial trend and the spectral index is around -1 for both magnitude and components. This hourly range has been identified as the most Alfvénic at low latitudes and its radial evolution has been recognized to be consistent with WKB radial index (Roberts 1989; Marsch and Tu 1990). Even within this range, and also within the next one, the latitude power trend is slightly negative for both components and magnitude. Finally, range 4 is clearly indicative of turbulent cascade with a radial power trend of the components much faster than WKB expectation and becoming even stronger at higher wave numbers. Moreover, the radial spectral index reveals that steepening is at work only for the previous wave number ranges as expected since the breakpoint moves to smaller wave number during spectrum evolution. The spectral index of the components tends to $-5/3$ with increasing wave number while that of the magnitude is constantly flatter. The same authors gave an estimate of the radial scale-shift of the breakpoint during the wind expansion around $k \propto r^{1.1}$, in agreement with earlier estimates (Horbury et al. 1996b).

Although most of these results support previous conclusions obtained for the ecliptic turbulence, the negative value of the latitudinal power trend that starts within the second range, is unexpected. As a matter of fact, moving towards more Alfénic regions like the polar regions, one would perhaps expect a positive latitudinal trend similarly to what happens in the ecliptic when moving from slow to fast wind.

Horbury and Balogh (2001) and Horbury and Tsurutani (2001) estimated that the power observed at 80° is about 30 % less than that observed at 30°. These authors proposed a possible effect due to the over-expansion of the polar coronal hole at higher latitudes. In addition, within the fourth range, field magnitude fluctuations radially decrease less rapidly than the fluctuations of the components, but do not show significant latitudinal variations. Finally, the smaller spectral index reveals that the high frequency range of the field magnitude spectrum shows a flattening.

The same authors investigated the anisotropy of these fluctuations as a function of radial and latitudinal excursion. Their results, reported in Fig. 4.20, show that, at 2.5 AU, the lowest compressibility is recorded within the hourly frequency band (third and part of the fourth band), which has been recognized as the most Alfvénic frequency range. The anisotropy of the components confirms that the power associated with the transverse components is larger than that associated with the radial one, and this difference slightly tends to decrease at higher wave numbers.

As already shown by Horbury et al. (1995a), around the 5 min range, magnetic field fluctuations are transverse to the mean field direction the majority of the time.

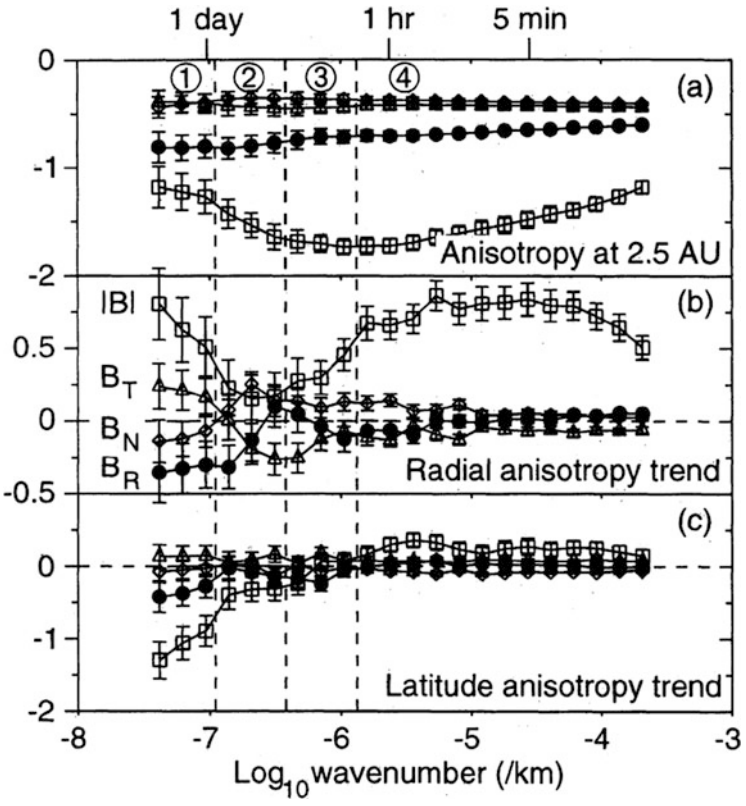

Fig. 4.20 (**a**) Scale dependence of power anisotropy at 2.5 AU plotted as the $\log_{10}$ of the ratio of B_R (*solid circles*), B_T (*triangles*), B_N (*diamonds*), and $|\mathbf{B}|$ (*squares*) to the trace of the spectral matrix; (**b**) the radial, and (**c**) latitudinal behavior of the same values, respectively. Image reproduced by permission from Horbury and Balogh (2001), copyright by AGU

The minimum variance direction lies mainly within an angle of about 26° from the average background field direction and fluctuations are highly anisotropic, such that the ratio between perpendicular to parallel power is about 30. Since during the observations reported in Horbury and Balogh (2001) and Horbury and Tsurutani (2001) the mean field resulted to be radially oriented most of the time, the radial minimum variance direction at short time scales is an effect induced by larger scales behavior.

Anyhow, radial and latitudinal anisotropy trends tend to disappear for higher frequencies. In the mean time, interesting enough, there is a strong radial increase of magnetic field compression (top panel of Fig. 4.20), defined as the ratio between the power density associated with magnetic field intensity fluctuations and that associated with the fluctuations of the three components (Bavassano et al. 1982b; Bruno and Bavassano 1991). The attempt to attribute this phenomenon to parametric

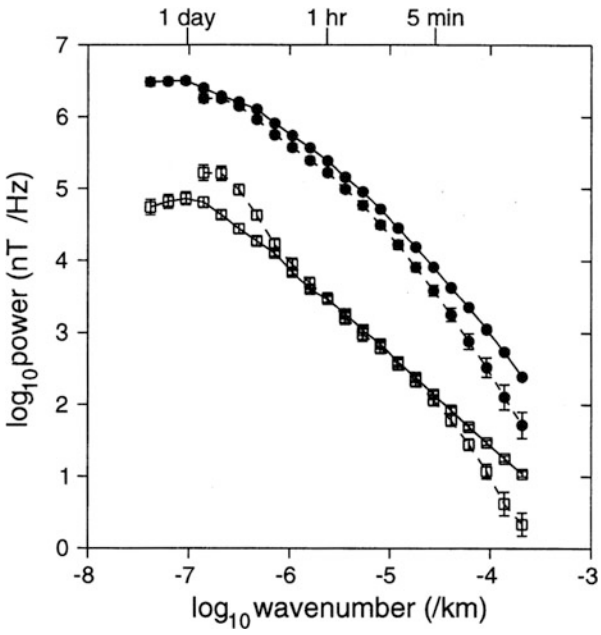

Fig. 4.21 Power spectra of magnetic field components (*solid circles*) and magnitude (*open squares*) from Ulysses (*solid line*) and Helios 1 (*dashed line*). Spectra have been extrapolated to 1 AU using radial trends in power scalings estimated from Ulysses between 1.4 and 4.1 AU and Helios between 0.3 and 1 AU. Image reproduced by permission from Horbury and Balogh (2001), copyright by AGU

decay of large amplitude Alfvén waves or dynamical interactions between adjacent flux tubes or interstellar pick-up ions was not satisfactory in all cases.

Comparing high latitude with low latitude results for high speed streams, Horbury and Balogh (2001) found remarkable good agreement between observations by Ulysses at 2.5 AU and by Helios at 0.7 AU. In particular, Fig. 4.21 shows Ulysses and Helios 1 spectra projected to 1 AU for comparison.

It is interesting to notice that the spectral slope of the spectrum of the components for Helios 1 is slightly higher than that of Ulysses, suggesting a slower radial evolution of turbulence in the polar wind (Bruno 1992; Bruno and Bavassano 1992). However, the faster spectral evolution at low latitudes does not lead to strong differences between the spectra.

4.3.2 Polar Turbulence Studied via Elsässer Variables

Goldstein et al. (1995) for the first time showed a spectral analysis of Ulysses observations based on Elsässer variables during two different time intervals, at

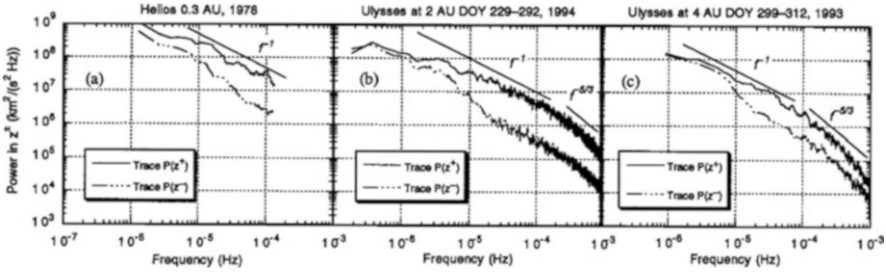

Fig. 4.22 Trace of e^+ (*solid line*) and e^- (*dash-dotted line*) power spectra. The *central and right panels* refer to Ulysses observations at 2 and 4 AU, respectively, when Ulysses was embedded in the fast southern polar wind during 1993–1994. The *leftmost panel* refers to Helios observations during 1978 at 0.3 AU. Image reproduced by permission from Goldstein et al. (1995), copyright by AGU

4 AU and close to −40°, and at 2 AU and around the maximum southern pass, as shown in Fig. 4.22. Comparing the two Ulysses observations it clearly appears that the spectrum closer to the Sun is less evolved than the spectrum measured farther out, as will be confirmed by the next Fig. 4.23, where these authors reported the normalized cross-helicity and the Alfvén ratio for the two intervals. Moreover, following these authors, the comparison between Helios spectra at 0.3 AU and Ulysses at 2 and 4 AU suggests that the radial scaling of e^+ at the low frequency end of the spectrum follows the WKB prediction of $1/r$ decrease (Heinemann and Olbert 1980). However, the selected time interval for Helios s/c was characterized by rather slow wind taken during the rising phase the solar cycle, two conditions which greatly differ from those referring to Ulysses data. As a consequence, comparing Helios results with Ulysses results obtained within the fast polar wind might be misleading. It would be better to choose Helios observations within high speed co-rotating streams which resemble much better solar wind conditions at high latitude.

Anyhow, results relative to the normalized cross-helicity σ_c (see Fig. 4.23) clearly show high values of σ_c, around 0.8, which normally we observe in the ecliptic at much shorter heliocentric distances (Tu and Marsch 1995). A possible radial effect would be responsible for the depleted level of σ_c at 4 AU. Moreover, a strong anisotropy can also be seen for frequencies between 10^{-6} and 10^{-5} Hz with the transverse σ_c much larger than the radial one. This anisotropy is somewhat lost during the expansion to 4 AU.

The Alfvén ratio (bottom panels of Fig. 4.23) has values around 0.5 for frequencies higher than roughly 10^{-5} Hz, with no much evolution between 2 and 4 AU. A result similar to what was originally obtained in the ecliptic at about 1 AU (Martin et al. 1973; Belcher and Solodyna 1975; Solodyna et al. 1977; Neugebauer et al. 1984; Bruno et al. 1985; Marsch and Tu 1990; Roberts et al. 1990). The low frequency extension of $r_{A\perp}$ together with $\sigma_{c\perp}$, where the subscript $\perp$ indicates that these quantities are calculated from the transverse components only, was interpreted by the authors as due to the sampling of Alfvénic features in longitude rather than to a real presence of Alfvénic fluctuations. However, by the time Ulysses reaches

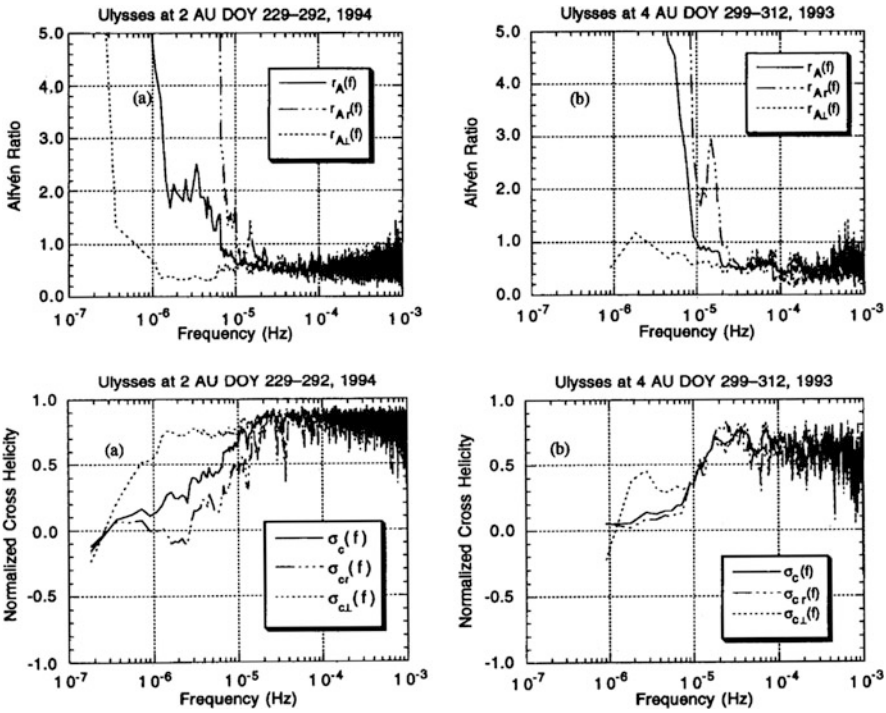

Fig. 4.23 Normalized cross-helicity and Alfvén ratio at 2 and 4 AU, as observed by Ulysses at −80° and −40° latitude, respectively. Image reproduced by permission from Goldstein et al. (1995), copyright by AGU

to 4 AU, $\sigma_{c\perp}$ has strongly decreased as expected while $r_{A\perp}$ gets closer to 1, making the situation less clear. Anyhow, these results suggest that the situation at 2 AU and, even more at 4 AU, can be considered as an evolution of what Helios 2 recorded in the ecliptic at shorter heliocentric distance. Ulysses observations at 2 AU resemble more the turbulence conditions observed by Helios at 0.9 AU rather than at 0.3 AU.

Bavassano et al. (2000b) studied in detail the evolution of the power e^+ and e^- associated with outward δz^+ and inward δz^- Alfvénic fluctuations, respectively. The study referred to the polar regions, during the wind expansion between 1.4 and 4.3 AU. These authors analyzed 1 h variances of $\delta z^\pm$ and found two different regimes, as shown in Fig. 4.24. Inside 2.5 AU outward modes e^+ decrease faster than inward modes e^-, in agreement with previous ecliptic observations performed within the trailing edge of co-rotating fast streams (Bruno and Bavassano 1991; Tu and Marsch 1990a; Grappin et al. 1989). Beyond this distance, the radial gradient of e^- becomes steeper and steeper while that of e^+ remains approximately unchanged. This change in e^- is rather fast and both species keep declining with the same rate beyond 2.5 AU. The radial dependence of e^+ between $r^{-1.39}$ and $r^{-1.48}$, reported by Bavassano et al. (2000b), indicate a radial decay faster than r^{-1} predicted by WKB

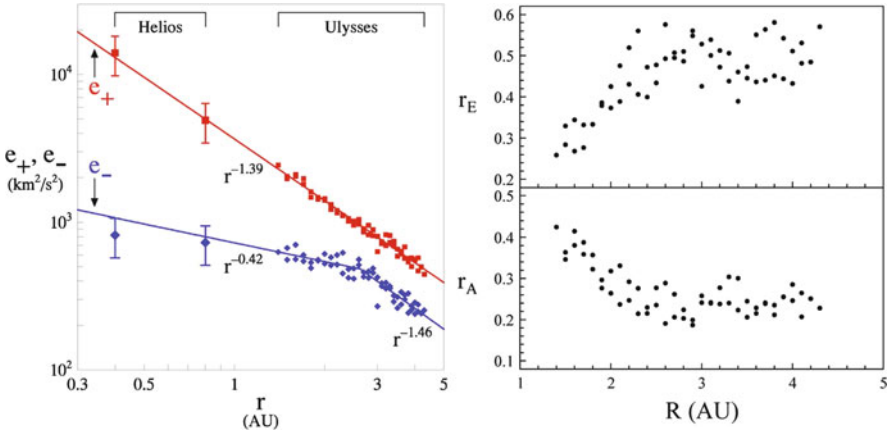

Fig. 4.24 *Left panel:* values of hourly variance of $\delta z^{\pm}$ (i.e., $e^{\pm}$) vs. heliocentric distance, as observed by Ulysses. Helios observations are shown for comparison and appear to be in good agreement. *Right panel:* Elsässer ratio (*top*) and Alfvén ratio (*bottom*) are plotted vs. radial distance while Ulysses is embedded in the polar wind. Image reproduced by permission from Bavassano et al. (2000b), copyright by AGU

approximation. This is in agreement with the analysis performed by Forsyth et al. (1996) using magnetic field observations only.

This different radial behavior is readily seen in the radial plot of the Elsässer ratio r_E shown in the top panel of the right column of Fig. 4.24. Before 2.5 AU this ratio continuously grows to about 0.5 near 2.5 AU. Beyond this region, since the radial gradient of the inward and outward components is approximately the same, r_E stabilizes around 0.5.

On the other hand, also the Alfvén ratio r_A shows a clear radial dependence that stops at about the same limit distance of 2.5 AU. In this case, r_A constantly decreases from ~ 0.4 at 1.4 AU to ~ 0.25 at 2.5 AU, slightly fluctuating around this value for larger distances. A different interpretation of these results was offered by Grappin (2002). For this author, since Ulysses has not explored the whole three-dimensional heliosphere, solar wind parameters experience different dependencies on latitude and distance which would result in the same radial distance variation along Ulysses trajectory as claimed in Bavassano's works. Another interesting feature observed in polar turbulence is unraveled by Fig. 4.25 from Bavassano et al. (1998, 2000a). The plot shows 2D histograms of normalized cross-helicity and normalized residual energy (see Sect. 4.1.1 for definition) for different heliospheric regions (ecliptic wind, mid-latitude wind with strong velocity gradients, polar wind). A predominance of outward fluctuations (positive values of σ_c) and of magnetic fluctuations (negative values of σ_r) seems to be a general feature. It results that the most Alfvénic region is the one at high latitude and at shorter heliocentric distances. However, in all the panels there is always a relative peak at $\sigma_c \simeq 0$ and $\sigma_r \simeq -1$,

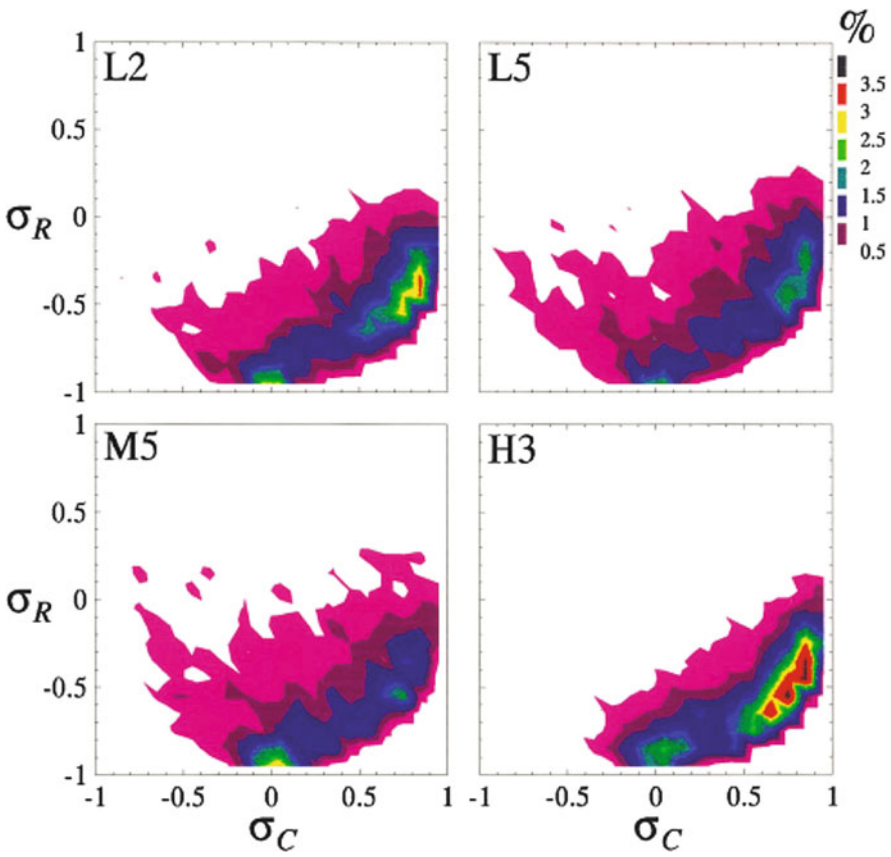

Fig. 4.25 2D histograms of normalized cross-helicity σ_c (here indicated by σ_C) and normalized residual energy σ_r (here indicated by σ_R) for different heliospheric regions (ecliptic wind, mid-latitude wind with strong velocity gradients, polar wind). Image reproduced by permission from Bavassano et al. (1998), copyright by AGU

which might well be due to magnetic structures like the MFDT found by Tu and Marsch (1991) in the ecliptic.

In a successive paper, Bavassano et al. (2002a) tested whether or not the radial dependence observed in $e^{\pm}$ was to be completely ascribed to the radial expansion of the wind or possible latitudinal dependencies also contributed to the turbulence evolution in the polar wind.

As already discussed in the previous section, Horbury and Balogh (2001), using Ulysses data from the northern polar pass, evaluated the dependence of magnetic field power levels on solar distance and latitude using a multiple regression analysis based on Eq. (4.17). In the Alfvénic range, the latitudinal coefficient "*C*" for power in field components was appreciably different from 0 (around 0.3). However, this analysis was limited to magnetic field fluctuations alone and cannot be transferred

sic et simpliciter to Alfvénic turbulence. In their analysis, Bavassano et al. (2002b) used the first southern and northern polar passes and removed from their dataset all intervals with large gradients in plasma velocity, and/or plasma density, and/or magnetic field magnitude, as already done in Bavassano et al. (2000b). As a matter of fact, the use of Elsässer variables (see Sect. 4.1.1) instead of magnetic field, and of selected data samples, leads to very small values of the latitudinal coefficient as shown in Fig. 4.26, where different contributions are plotted with different colors and where the top panel refers to the same dataset used by Horbury and Balogh (2001), while the bottom panel refers to a dataset omni-comprehensive of south and north passages free of strong compressive events (Bavassano et al. 2000b). Moreover, the latitudinal effect appears to be very weak also for the data sample

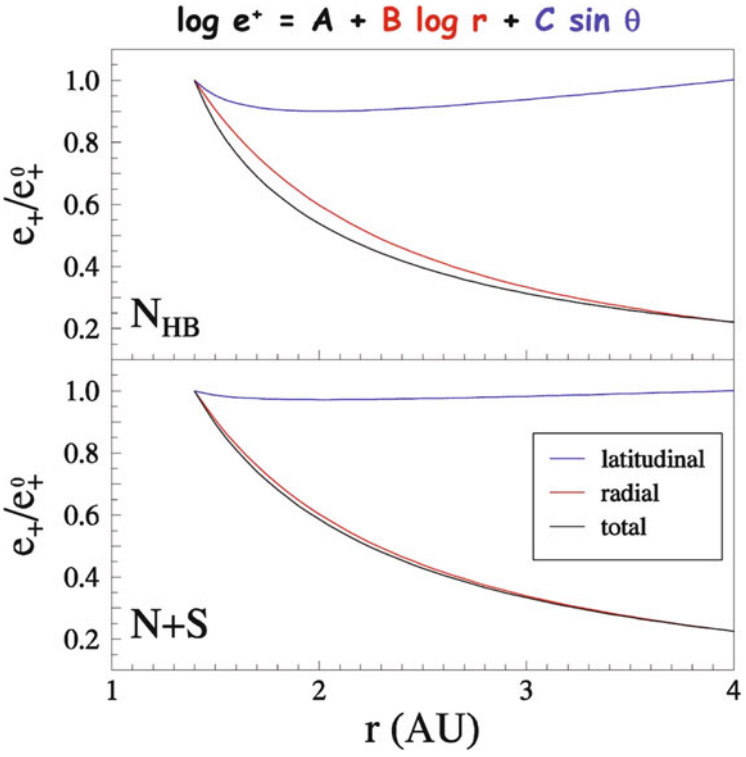

Fig. 4.26 Results from the multiple regression analysis showing radial and latitudinal dependence of the power e^+ associated with outward modes (see Sect. 4.1.1). The *top panel* refers to the same dataset used by Horbury and Balogh (2001). The *bottom panel* refers to a dataset omni-comprehensive of south and north passages free of strong compressive events (Bavassano et al. 2000b). Values of e_+ have been normalized to the value $e_+{}^\circ$ assumed by this parameter at 1.4 AU, closest approach to the Sun. The *black line* is the total regression, the *blue line* is the latitudinal contribution and the *red line* is the radial contribution. Image reproduced by permission from Bavassano et al. (2002a), copyright by AGU

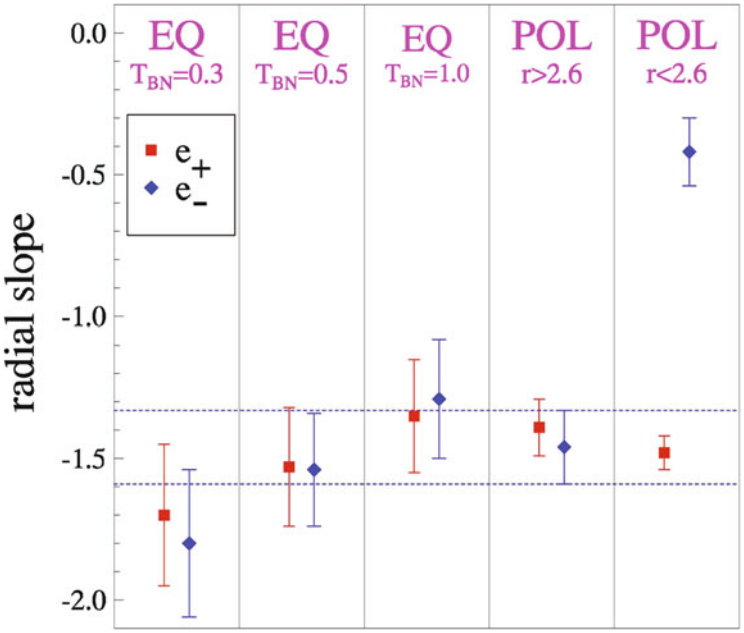

Fig. 4.27 e^+ (*red*) and e^- (*blue*) radial gradient for different latitudinal regions of the solar wind. The *first three columns*, labeled EQ, refer to ecliptic observations obtained with different values of the upper limit of TBN defined as the relative fluctuations of density and magnetic intensity. The *last two columns*, labeled POL, refer to observations of polar turbulence outside and inside 2.6 AU, respectively. Image reproduced by permission from Bavassano et al. (2001), copyright by AGU

used by Horbury and Balogh (2001), although this is the sample with the largest value of the "*C*" coefficient.

A further argument in favor of radial vs. latitudinal dependence is represented by the comparison of the radial gradient of e^+ in different regions, in the ecliptic and in the polar wind. These results, shown in Fig. 4.27, provide the radial slopes for e^+ (red squares) and e^- (blue diamonds) in different regions. The first three columns (labeled EQ) summarize ecliptic results obtained with different values of an upper limit (TBN) for relative fluctuations of density and magnetic intensity. The last two columns (labeled POL) refer to the results for polar turbulence (north and south passes) outside and inside 2.6 AU, respectively. A general agreement exists between slopes in ecliptic and in polar wind with no significant role left for latitude, the only exception being e^- in the region inside 2.6 AU. The behavior of the inward component cannot be explained by a simple power law over the range of distances explored by Ulysses. Moreover, a possible latitudinal effect has been clearly rejected by the results from a multiple regression analysis performed by Bavassano et al. (2002a) similar to that reported above for e^+.

4.3.3 Local Production of Alfvénic Turbulence at High Latitude

An interesting solution to the radial behavior of the minority modes might be represented by local generation mechanisms, like parametric decay (Malara et al. 2001b; Del Zanna et al. 2001), which might saturate and be inhibited beyond 2.5 AU.

Parametric instability has been studied in a variety of situations depending on the value of the plasma β (among others Sagdeev and Galeev 1969; Goldstein 1978; Hoshino and Goldstein 1989; Malara and Velli 1996).

Malara et al. (2000) and Del Zanna et al. (2001) recently studied the non-linear growth of parametric decay of a broadband Alfvén wave, and showed that the final state strongly depends on the value of the plasma β (thermal to magnetic pressure ratio). For $\beta < 1$ the instability completely destroys the initial Alfvénic correlation. For $\beta \sim 1$ (a value close to solar wind conditions) the instability is not able to go beyond some limit in the disruption of the initial correlation between velocity and magnetic field fluctuations, and the final state is $\sigma_c \sim 0.5$ as observed in the solar wind (see Sect. 4.3.2).

These authors solved numerically the fully compressible, non-linear MHD equations in a one-dimensional configuration using a pseudo-spectral numerical code. The simulation starts with a non-monochromatic, large amplitude Alfvén wave polarized on the yz plane, propagating in a uniform background magnetic field. Successively, the instability was triggered by adding some noise of the order 10^{-6} to the initial density level.

During the first part of the evolution of the instability the amplitude of unstable modes is small and, consequently, non-linear couplings are negligible. A subsequent exponential growth, predicted by the linear theory, increases the level of both e^- and density compressive fluctuations. During the second part of the development of the instability, non-linear couplings are not longer disregardable and their effect is firstly to slow down the exponential growth of unstable modes and then to saturate the instability to a level that depends on the value of the plasma β.

Spectra of $e^{\pm}$ are shown in Fig. 4.28 for different times during the development of the instability. At the beginning the spectrum of the mother-wave is peaked at $k = 10$, and before the instability saturation ($t \leq 35$) the back-scattered e^- and the density fluctuations e^{ρ} are peaked at $k = 1$ and $k = 11$, respectively. After saturation, as the run goes on, the spectrum of e^- approaches that of e^+ towards a common final state characterized by a Kolmogorov-like spectrum and e^+ slightly larger than e^-.

The behavior of outward and inward modes, density and magnetic magnitude variances and the normalized cross-helicity σ_c is summarized in the left column of Fig. 4.29. The evolution of σ_c, when the instability reaches saturation, can be qualitatively compared with Ulysses observations (courtesy of B. Bavassano) in the right panel of the same figure, which shows a similar trend.

Obviously, making this comparison, one has to take into account that this model has strong limitations like the presence of a peak in e^+ not observed in real polar

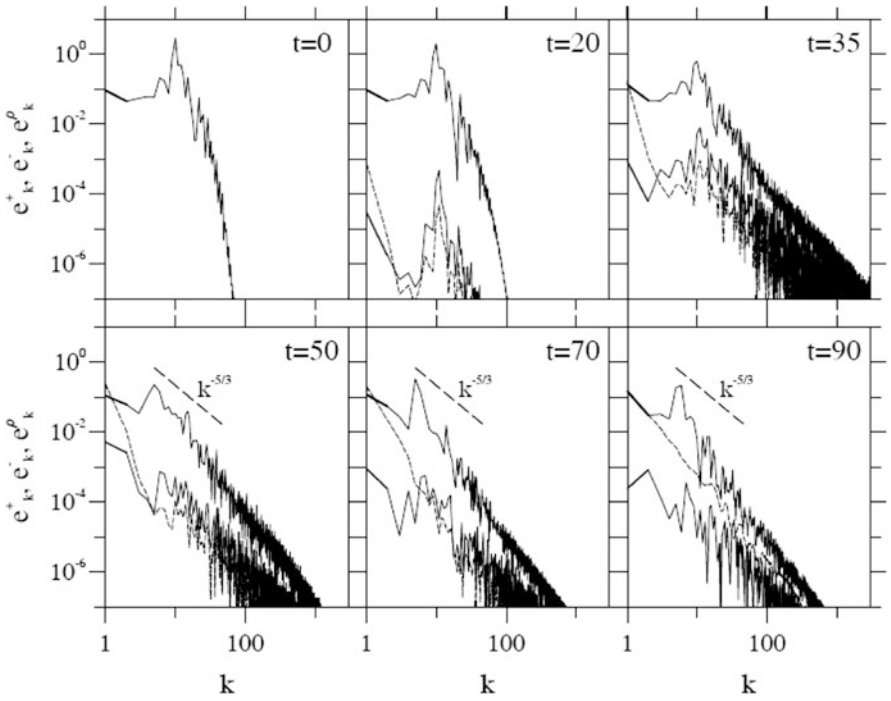

Fig. 4.28 Spectra of e^+ (*thick line*), e^- (*dashed line*), and e^ρ (*thin line*) are shown for six different times during the development of the instability. For $t \geq 50$ a typical Kolmogorov slope appears. These results refer to $\beta = 1$. Image reproduced by permission from Malara et al. (2001a), copyright by EGU

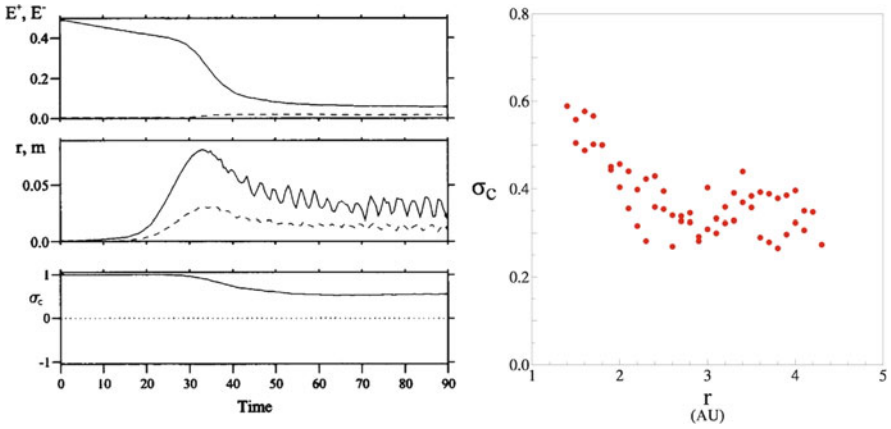

Fig. 4.29 *Top left panel:* time evolution of e^+ (*solid line*) and e^- (*dashed line*). *Middle left panel:* density (*solid line*) and magnetic magnitude (*dashed line*) variances. *Bottom left panel:* normalized cross helicity σ_c. *Right panel:* Ulysses observations of σ_c radial evolution within the polar wind (*left column* is from Malara et al. 2001a, *right panel* is a courtesy of B. Bavassano)

turbulence. Another limitation, partly due to dissipation that has to be included in the model, is that the spectra obtained at the end of the instability growth are steeper than those observed in the solar wind. Finally, a further limitation is represented by the fact that this code is 1D. However, although for an incompressible 1-D simulation we do not expect to have turbulence development, in this case, since parametric decay is based on compressive phenomena, an energy transfer along the spectrum might be at work.

In addition, Umeki and Terasawa (1992) studying the non-linear evolution of a large-amplitude incoherent Alfvén wave via 1D magnetohydrodynamic simulations, reported that while in a low beta plasma ($\beta \approx 0.2$) the growth of backscattered Alfvén waves, which are opposite in helicity and propagation direction from the original Alfvén waves, could be clearly detected, in a high beta plasma ($\beta \approx 2$) there was no production of backscattered Alfvén waves. Consequently, although numerical results obtained by Malara et al. (2001a) are very encouraging, the high beta plasma ($\beta \approx 2$), characteristic of fast polar wind at solar minimum, plays against a relevant role of parametric instability in developing solar wind turbulence as observed by Ulysses. However, these simulations do remain an important step forward towards the understanding of turbulent evolution in the polar wind until other mechanisms will be found to be active enough to justify the observations shown in Fig. 4.24.

4.4 The Transport of Low-Frequency Turbulent Fluctuations in Expanding Non-homogeneous Solar Wind

One of the most interesting and challenging problem in space physics is a detailed understanding of the transport of the low-frequency turbulent fluctuations in the expanding non-homogeneous magnetized solar wind flow. Since the beginning of in-situ solar wind observations, interplanetary fluctuations have been interpreted either as evidence of the turbulent nature of the solar wind (Coleman 1968) or as a superposition of outward propagating Alfvén waves (Belcher and Davis Jr 1971). The turbulence point of view relied on the fact that power spectra of both plasma and magnetic field parameters fluctuations clearly showed a typical turbulence spectrum with a frequency scaling between Kolmogorov's and Kraichnan's theoretical predictions (Kolmogorov 1941; Kraichnan 1974). On the other hand, the observed strong Alfvénic character of the fluctuations could not support the possibility that a simple superposition of non interacting Alfvén waves could produce the observed scaling unless nonlinear interactions between inward and outward Alfvénic fluctuations were present in order to produce a continuous energy cascade along the spectrum. Tu et al. (1984) interpreted the radial change of the spectral slope of the fluctuations reported by Denskat and Neubauer (1983) and Bavassano et al. (1982a) as evidence that nonlinear processes were at work.

However, a linear superposition of outward propagating Alfvén waves was the starting point to derive a manageable theory based on WKB approximation able to describe the radial evolution of the amplitude of interplanetary magnetic field fluctuations $< \delta B^2 >^{1/2}$ (see review by Barnes 1979). At the same time, in-situ observations suggested that the turbulence description was by far more appropriate and WKB theory could not incorporate dissipation processes necessary to explain the non-adiabatic expansion of the wind. On the other hand, WKB, assuming that the density decreases as r^{-2}, proved to be able to accurately predict a radial dependence of r^{-3} for the power associated to magnetic field fluctuations, as it had been found by Belcher and Burchsted (1974) between 0.7 and 1.6 AU.

All these considerations triggered the formulation of a new model (Tu et al. 1984) in which both inward and outward Alfvén modes, present in the solar wind in different amounts, interact nonlinearly producing an energy cascade which leads the fluctuations toward a fully developed turbulence. This model partially reconciled the views of Coleman (1968) and Belcher and Davis Jr (1971) and has been the basis of several other papers which shed further light on the nature of solar wind fluctuations. The model by Tu et al. (1984) was able to reproduce the radial behavior of the magnetic power spectrum as well as heating properties of the type suggested by Coleman (1968) although it was clear that the framework of the transport equations needed to be generalized (Zhou and Matthaeus 1989). In addition, successive analyses performed on the interplanetary data available at that time clearly highlighted significant departures from WKB radial evolution in the inner and outer heliosphere (Bavassano et al. 1982a; Roberts et al. 1987a,b; Bruno et al. 1985; Roberts et al. 1990; Zank et al. 1996; Matthaeus et al. 1999; Smith et al. 2001) and contributed to stimulate a different approach to the problem of the radial evolution of solar wind fluctuations, possibly comprehensive of all the phenomena contributing to the observed behavior.

Matthaeus et al. (1999) clearly showed that, on the basis of WKB approximation, it was impossible to explain the observed simultaneous behavior of energy density of the turbulent magnetic field, correlation length, and proton temperature from 1 AU to beyond 30 AU. Their turbulence theory included a simple closure for local anisotropic magnetohydrodynamic turbulence, spatial transport, and driving by large-scale shear and pickup ions. As a matter of fact, the non adiabatic expansion of the solar wind suggests that it is necessary to fully understand the driving, transport and dissipation of low frequency magnetohydrodynamic turbulence in order to understand the heating of the solar wind. The same authors concluded that similar models might be applied to both inner heliosphere and high latitude solar wind environments although it is likely that they might require extra efforts in order to include separate equations for the two Elsässer amplitudes where cross helicity effects are important and it is not possible to neglect Alfvén wave propagation effects which would limit an MHD nonlinear Taylor–Kármán approach to turbulent heating (Hossain et al. 1995).

Simulation of the evolution of turbulence, from the energy-containing range, up to the dissipative scales is a formidable task, due to the wide range of scales one needs to reproduce, the complexity of plasma physics phenomena involved and the

present-day capability of computers (Zank et al. 2012b; McComb and Watt 1990; Chassaing et al. 2002). These difficulties are superimposed on the non-homogeneity of the large-scales and the expansion of the solar wind. Very few numerical simulations exists describing turbulence in a non homogeneous flow, because they are so challenging numerically. This makes the MHD equations useless, so that, to work around the problem, it can be wise to introduce some modeling transport of turbulence in the presence of an expanding non-homogeneous field, identifying appropriate closures.

The first attempt in this direction and able to resolve the problems inherent in the WKB model was proposed by Zank et al. (1996). This model for the first time coupled together turbulence transport model of the power density of the magnetic field fluctuations and the associated correlation length by taking moments of the two scale-separated incompressible MHD equations (Marsch and Tu 1989; Zhou and Matthaeus 1990; Marsch and Tu 1990) expressed in terms of Elsässer variables. Later, Matthaeus et al. (1999) and Smith et al. (2001) took into account also plasma heating due to turbulence dissipation and the model was further improved when also cross helicity was included (Matthaeus et al. 2004; Breech et al. 2005, 2008). However, the resulting model could not be applied to the inner heliosphere because of not adequate assumption for this region and did not include yet the residual energy and the role played by the Alfvén velocity, particularly relevant for short heliocentric distances.

A more comprehensive model was formulated by Zank et al. (2012b,a) using a closure of the original MHD equations. These authors included also the energy corresponding to forward and backward propagating modes and their correlation lengths to model the dissipative term, the residual energy and its correlation length necessary to close the system of equations. The model was based on the two scale MHD equations describing the evolution of velocity and magnetic field fluctuations **u** and **b** about the inhomogeneous mean velocity field **U** and magnetic field **B** (Marsch and Tu 1989; Zhou and Matthaeus 1990), i.e., while **u** and **b** vary on both the slowly varying large-scale spatial coordinates and the fast small-scale coordinates, **U** and **B** depend only on the slowly varying large-scale spatial coordinates. These MHD equations, expressed in terms of Elsässer variables, are:

$$\frac{\partial \mathbf{Z}^{\pm}}{\partial t} + (\mathbf{U} \mp \mathbf{V}_A) \cdot \nabla \mathbf{Z}^{\pm} + \frac{1}{2} \nabla \cdot (\mathbf{U}/2 \pm \mathbf{V}_A) \mathbf{z}^{\pm} + \mathbf{z}^{\mp} \cdot \left[\nabla \mathbf{U} \pm \frac{\nabla \mathbf{B}}{\sqrt{4\pi\rho}} - \frac{1}{2} I \nabla \cdot (\mathbf{U}/2 \pm \mathbf{V}_A) \right] = \mathbf{N}\mathbf{L}_{\pm} + \mathbf{S}^{\pm} \tag{4.18}$$

where $\mathbf{z}^{\pm} \equiv \mathbf{u} \pm \mathbf{b}/\sqrt{4\pi\rho}$ are the Elsässer variables, $\mathbf{V}_A$ is the Alfvén velocity, ρ is the plasma density, I is the identity matrix, $NL_{\pm}$ are nonlinear dissipation terms and $S^{\pm}$ are source terms. $NL_{\pm}$ and $S^{\pm}$ are modeled separately for outward and inward modes. The model is then based on the following seven coupled turbulence transport equations, one for each of the parameters listed above plus one that describes the transport equation for the solar wind temperature in the super-Alfvénic solar wind.

$$\frac{\partial E^{\pm}}{\partial t} + \left[(\mathbf{U} \mp \mathbf{V}_A)\cdot\nabla + \nabla\cdot\left(\frac{1}{2}\mathbf{U} \pm \mathbf{V}_A\right)\right]E^{\pm} + \nabla\cdot\left(\frac{1}{2}\mathbf{U} - \Gamma \mp \mathbf{V}_A\right)E_D = -2\frac{E^{\pm}\sqrt{E^{\mp}}}{\lambda^{\pm}} + 2\langle \mathbf{S}^{\pm}\cdot\mathbf{z}^{\pm}\rangle \tag{4.19}$$

$$\frac{\partial E_D}{\partial t} + \mathbf{U}\cdot\nabla E_D + \frac{1}{2}\nabla\cdot\mathbf{U}E_D + \frac{1}{2}\sqrt{E^+E^-}\left(E^+\mathbf{V}_A\cdot\nabla E^- - E^-\mathbf{V}_A\cdot\nabla E^+\right) + \left(\frac{1}{2}\nabla\cdot\mathbf{U} - \Gamma\right)\frac{E^+ + E^-}{2} + \nabla\cdot\mathbf{V}_A\frac{E^+ - E^-}{2} = -E_D\left(\frac{\sqrt{E^+}}{\lambda^-} + \frac{\sqrt{E^-}}{\lambda^+}\right) + \langle \mathbf{S}^-\cdot\mathbf{z}^+\rangle + \langle \mathbf{S}^+\cdot\mathbf{z}^-\rangle \tag{4.20}$$

$$\frac{\partial \lambda^{\pm}}{\partial t} + \left[(\mathbf{U} \mp \mathbf{V}_A)\cdot\nabla\lambda^{\pm} + \frac{E_D}{E^{\pm}}\left[\frac{1}{4}\nabla\cdot\mathbf{U} \mp \frac{1}{2}\nabla\cdot\mathbf{V}_A - \Gamma/2\right](\lambda_D - 2\lambda^{\pm})\right] = 2\sqrt{E^{\mp}} - 2\frac{\langle \mathbf{S}^{\pm}\cdot\mathbf{z}^{\pm}\rangle}{E^{\pm}} \tag{4.21}$$

$$\frac{\partial \lambda_D}{\partial t} + (\mathbf{U}\cdot\nabla\lambda_D + 2\left(\frac{1}{4}\nabla\cdot\mathbf{U} - \Gamma/2\right)\left(\frac{E^+\lambda^+ + E^-\lambda^-}{E^+ + E^-} - \frac{\lambda_D}{2}\right)\frac{E^+ + E^-}{E_D} + \nabla\cdot\mathbf{V}_A\left(\frac{E^+\lambda^+ - E^-\lambda^-}{E^+ - E^-} - \frac{\lambda_D}{2}\right)\frac{E^+ - E^-}{E_D} + \frac{1}{2E_D\sqrt{E^+E^-}}\left(E^+\mathbf{V}_A\cdot\nabla E^- - E^-\mathbf{V}_A\cdot\nabla E^+\right)\left[2\sqrt{\lambda^+\lambda^-} - \lambda_D\right] + \frac{\sqrt{E^+E^-}}{E_D}\left[\sqrt{\frac{\lambda^+}{\lambda^-}}\mathbf{V}_A\cdot\nabla\lambda^- - \sqrt{\frac{\lambda^-}{\lambda^+}}\mathbf{V}_A\cdot\nabla\lambda^+\right] = \lambda_D\left[\frac{\sqrt{E^+}}{\lambda^-} + \frac{\sqrt{E^-}}{\lambda^+}\right] - \frac{\lambda_D}{E_D}\left[\langle \mathbf{S}^+\cdot\mathbf{z}^-\rangle + \langle \mathbf{S}^-\cdot\mathbf{z}^+\rangle\right] \tag{4.22, 4.23}$$

$$\frac{dT}{dt} + U\frac{dT}{dr} + (\gamma - 1)\frac{2UT}{r} = \frac{\alpha m_p}{9k_B}\left[\frac{E^+\sqrt{E^-}}{\lambda^+} + \frac{E^-\sqrt{E^+}}{\lambda^-} + E_D\left(\frac{\sqrt{E^+}}{\lambda^-} + \frac{\sqrt{E^-}}{\lambda^+}\right)\right] \tag{4.24}$$

Here, the angle brackets $\langle \mathbf{S}^{\pm} \cdot \mathbf{z}^{\pm} \rangle$ and $\langle \mathbf{S}^{\pm} \cdot \mathbf{z}^{\mp} \rangle$ represent sources of turbulence, Γ represents the shear mixing term. Other quantities are $\gamma = 5/3$ is the adiabatic index, m_p the proton mass, k_B the Boltzmann constant and α is the Kármán–Taylor parameter which has been set $\alpha = 1$. The l.h.s. of the temperature equation (4.24) describes the adiabatic temperature profile, the second term introduces the turbulent heating term.

The main unknown terms of these equations are the source terms which can be modeled according to phenomenological arguments. Adhikari et al. (2015) individuate three main sources of turbulence in the heliosphere, say: (1) turbulence driven by shear due to interaction between fast and slow streams; (2) stream–stream interactions and shock waves which generate compressional turbulence; (3) turbulence due to pickup ions created by charge exchange between solar wind protons and interstellar neutral hydrogen. Clearly, the importance of these sources of turbulence depends on the location in the heliosphere.

The first source of turbulence is due to velocity shear, which represents an indicator for the evolution of solar wind fluctuations. These sources can be modeled as a direct proportionality to the energies in the Elsässer modes and the residual energy (Zank et al. 1996)

$$\begin{aligned} \langle \mathbf{S}^{\pm} \cdot \mathbf{z}^{\pm} \rangle &= C_{shear}(E^{\pm}) \frac{\Delta U_{shear}}{r} E^{\pm} \\ \langle \mathbf{S}^{-} \cdot \mathbf{z}^{+} \rangle + \langle \mathbf{S}^{+} \cdot \mathbf{z}^{-} \rangle &= \left[C_{shear}(E^{+}) + C_s(E^{-}) \right] \frac{\Delta U_{shear}}{r} E_D \end{aligned} \tag{4.25}$$

where the parameters $C_{shear}(E^{\pm})$ represents the strength of the shear interaction which depend on energies for the backwards and forward propagating fluctuations, and $\Delta U_{shear} \simeq 350\,\mathrm{km/s}$ is the difference between slow and fast bulk solar wind speeds. The same phenomenological arguments can be used for shocks (Zank et al. 1996), that is the same relations (4.25) are used when the source of turbulence are shocks, where the strength of the shear interactions and the speed difference are C_{shock} and ΔU_{shock}.

As far as the pickup ions are concerned, phenomenological arguments lead to

$$\begin{aligned} \langle \mathbf{S}^{\pm} \cdot \mathbf{z}^{\pm} \rangle &= \frac{F(E^{\pm}) n_H U V_A}{n_{sw} \tau_{ion}} \exp\left[-\frac{\lambda \psi}{r \sin \psi} \right] \\ \langle \mathbf{S}^{-} \cdot \mathbf{z}^{+} \rangle + \langle \mathbf{S}^{+} \cdot \mathbf{z}^{-} \rangle &= 0 \end{aligned} \tag{4.26}$$

where $F(E^{+}) \simeq F(E^{-}) < 1$ are positive functions which determines the fraction of pickup ion energy transferred into excited waves. The parameters $n_H \simeq 0.1\,\mathrm{cm}^{-3}$ is the number density of interstellar neutrals, $\tau_{ions} \simeq 10^6\,\mathrm{s}$ is the neutral ionization time at 1 AU, ψ is the angle between the observation point and the upstream direction $\lambda\psi/\sin\psi \simeq 8\,\mathrm{AU}$ and λ is the ionization cavity length scale. The other parameters are $n_{sw} \simeq 5\,\mathrm{cm}^{-3}$ and $V_A \simeq 50\,\mathrm{km/s}$.

Numerical results of the above equations represent a formidable task. Recently, Adhikari et al. (2014, 2015) solved numerically the transport model for low

frequency MHD turbulence introduced by Zank et al. (2012b) in order to investigate theoretically the evolution of the various quantities forming the model. Equations are solved in a spherical 1D coordinate system by neglecting θ and ϕ coordinates. In the adopted idealized system all fields have been assumed to depend only on the radial component.

Adhikari et al. (2015) applied this 1D model (Zank et al. 2012b) to the super-Alfvénic solar wind firstly between 0.29 and 5 AU with and without the Alfvén velocity and successively between 0.29 and 100 AU without Alfvén velocity. This last choice was based on the fact that the use of 1D radially symmetric model cannot allow to include in a satisfactory way Alfvén wave propagation along the magnetic field especially in the outer heliosphere. In the inner heliosphere, since the comparison with in-situ measurements was based on Helios 2 within fast wind and Ulysses at high latitude, the assumption of radial IMF was less critical and allowed to test the model with and without the Alfvén velocity.

Figure 4.30 shows the comparison between model predictions, with (black curve) and without (red curve) Alfvén velocity, and in-situ measurements (blue crosses)

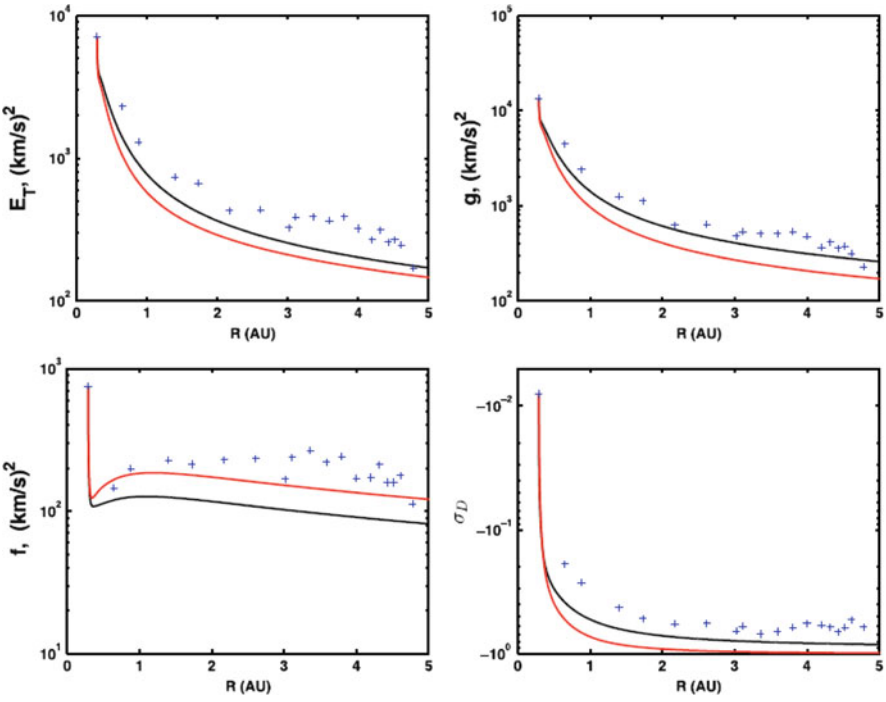

Fig. 4.30 Performance of the theoretical model wrt in-situ observations between 0.29 and 5 AU. Moving from *left to right* and *top to bottom*, the *solid black* and *red curves* in each panel show the model results, including or not the Alfvén velocity, for the total turbulent energy E_T, the energy in forward propagating modes g, the energy in backward propagating modes f, and the normalized residual energy σ_D, respectively. The *blue plus symbols* represent the corresponding observed values. Image adopted from Adhikari et al. (2015) and reproduced by permission of the AAS

imposing that the only source of turbulence is due to stream–shear interactions. The parameters represented in this Figure are, from left to right and top to bottom: the total turbulent energy E_T, the energy in forward propagating modes g, the energy in backward propagating modes f, and the normalized residual energy σ_D, respectively. The general behavior predicted by the model is a gradual decrease for E_T, g and σ_D and a more complex behavior for f. The general agreement with observations is quite satisfactory and becomes stronger when the Alfvén velocity is included in the model (black curve). It is interesting to note that in case of forward modes the better agreement is due to the fact that the presence of the Alfén velocity reduces the decay rate of the energy. On the other hand, the non monotonic behavior of the backward propagating modes f is due to both shear driving and the generation of backward propagating modes in the inner heliosphere and the agreement with the observations is worse when the Alfvén velocity is included.

Comparison with Voyager 2 observations is shown in Fig. 4.31 in the same format of Fig. 4.30 with the difference that only the red curve is shown since V_A is set $= 0$

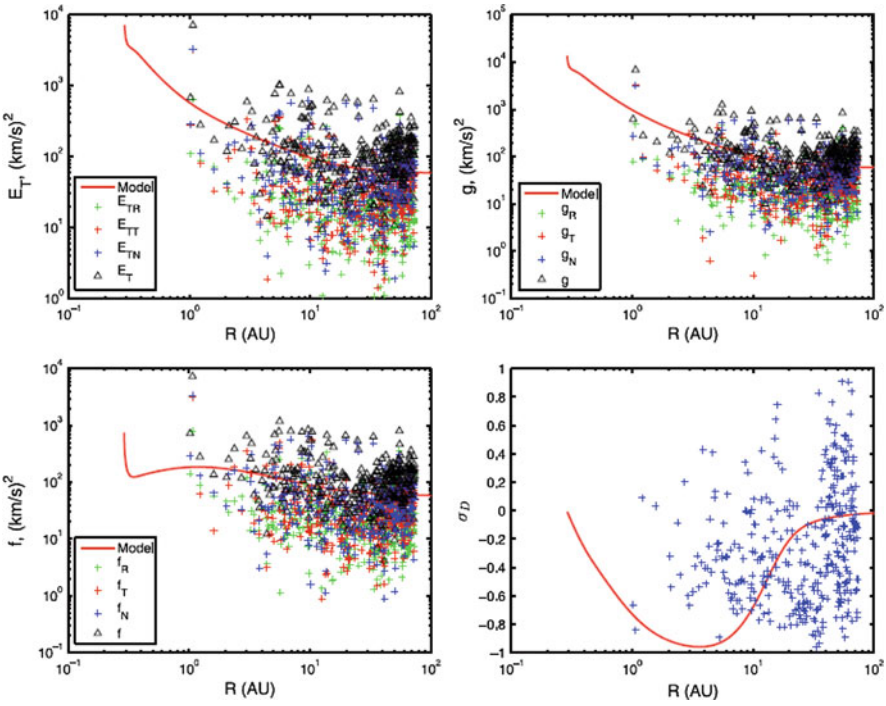

Fig. 4.31 Performance of the theoretical model wrt in-situ observations between 0.29 and 100 AU, from Adhikari et al. (2015). Moving from *left to right* and *top to bottom*, the *solid red curve* in each panel shows the model results having set $V_A = 0$, for the total turbulent energy E_T, the energy in forward propagating modes g, the energy in backward propagating modes f, and the residual energy σ_D, respectively. The suffix R, T, and N represent R-component, T-component, and N-component, respectively. Image adopted from Adhikari et al. (2015) and reproduced by permission of the AAS

and that, besides the estimates of E_T, g and f, also the corresponding R, T and N components are reported.

Similar monotonic decrease can be observed for theoretical and experimental results between 1 and 10 AU. Beyond this distance, pick-up ions play a role driving the turbulence and producing the observed flattening of E_T, g and f. The behavior of the normalized residual energy shows how, in the outer heliosphere, magnetic and kinetic energy compare to each other. However,the large scatter affecting the observations makes this test of the model difficult to perform. Finally, the same paper by Adhikari et al. (2015) reports also a quite satisfactory quantitative/qualitative agreement with observations, approximately up to 10 AU, for the correlation lengths of residual energy, forward and backward modes which monotonically increase with radial distance.

In summary, the model by Zank et al. (2012b) represents a quality leap towards a better understanding to a satisfactory level of the transport of turbulence in the super-Alfvénic solar wind since it is able to capture the overall radial trends shown in the measurements throughout the heliosphere.

References

L. Adhikari, G.P. Zank, Q. Hu, A. Dosch, Turbulence transport modeling of the temporal outer heliosphere. Astrophys. J **793**, 52 (2014). doi:10.1088/0004-637X/793/1/52

L. Adhikari, G.P. Zank, R. Bruno, D. Telloni, P. Hunana, A. Dosch, R. Marino, Q. Hu, The transport of low-frequency turbulence in astrophysical flows. ii. solutions for the super-Alfvénic solar wind. Astrophys. J. **805**, 63 (2015). doi:10.1088/0004-637X/805/1/63

A. Balogh, T.S. Horbury, R.J. Forsyth, E.J. Smith, Variances of the components and magnitude of the polar heliospheric magnetic field, in *Solar Wind Eight*, ed. by D. Winterhalter, J.T. Gosling, S.R. Habbal, W.S. Kurth, M. Neugebauer. AIP Conference Proceedings, vol. 382 (American Institute of Physics, Woodbury, 1995), pp. 38–43

A. Barnes, Hydromagnetic waves and turbulence in the solar wind, in *Solar System Plasma Physics*, vol. 1, ed. by E.N. Parker, C.F. Kennel, L.J. Lanzerotti (North-Holland, Amsterdam, 1979), pp. 249–319

A. Barnes, Interplanetary Alfvénic fluctuations: a stochastic model. J. Geophys. Res. **86**, 7498–7506 (1981). doi:10.1029/JA086iA09p07498

B. Bavassano, R. Bruno, Evidence of local generation of Alfvénic turbulence in the solar wind. J. Geophys. Res. **94**(13), 11977–11982 (1989). doi:10.1029/JA094iA09p11977

B. Bavassano, R. Bruno, On the role of interplanetary sources in the evolution of low-frequency Alfvénic turbulence in the solar wind. J. Geophys. Res. **97**(16), 19129–19137 (1992). doi:10.1029/92JA01510

B. Bavassano, M. Dobrowolny, F. Mariani, N.F. Ness, Radial evolution of power spectra of interplanetary Alfvénic turbulence. J. Geophys. Res. **87**, 3617–3622 (1982a). doi:10.1029/JA087iA05p03617

B. Bavassano, M. Dobrowolny, G. Fanfoni, F. Mariani, N.F. Ness, Statistical properties of MHD fluctuations associated with high-speed streams from Helios 2 observations. Solar Phys. **78**, 373–384 (1982b). doi:10.1007/BF00151617

B. Bavassano, E. Pietropaolo, R. Bruno, Cross-helicity and residual energy in solar wind turbulence. radial evolution and latitudinal dependence in the region from 1 to 5 AU. J. Geophys. Res. **103**(12), 6521–6530 (1998). doi:10.1029/97JA03029

B. Bavassano, E. Pietropaolo, R. Bruno, Alfvénic turbulence in the polar wind: a statistical study on cross helicity and residual energy variations. J. Geophys. Res. **105**(14), 12697–12704 (2000a). doi:10.1029/2000JA900004

B. Bavassano, E. Pietropaolo, R. Bruno, On the evolution of outward and inward Alfvénic fluctuations in the polar wind. J. Geophys. Res. **105**(14), 15959–15964 (2000b). doi:10.1029/1999JA000276

B. Bavassano, E. Pietropaolo, R. Bruno, Radial evolution of outward and inward Alfvénic fluctuations in the solar wind: A comparison between equatorial and polar observations by ulysses. J. Geophys. Res. **106**(15), 10659–10668 (2001). doi:10.1029/2000JA000453

B. Bavassano, E. Pietropaolo, R. Bruno, Alfvénic turbulence in high-latitude solar wind: Radial versus latitudinal variations. J. Geophys. Res. **107**(A12), 1452 (2002a). doi:10.1029/2002JA009267

B. Bavassano, E. Pietropaolo, R. Bruno, On parametric instability and MHD turbulence evolution in high-latitude heliosphere, in *Solspa 2001*, ed. by H. Sawaya-Lacoste ESA Conference Proceedings, vol. SP-477 (ESA Publications Division, Noordwijk, 2002b), pp. 313–316

J.W. Belcher, R. Burchsted, Energy densities of alfven waves between 0.7 and 1.6 AU. J. Geophys. Res. **79**, 4765–4768 (1974). doi:10.1029/JA079i031p04765

J.W. Belcher, L. Davis Jr, Large amplitude Alfvén waves in the interplanetary medium. J. Geophys. Res. **76**, 3534–3563 (1971). doi:10.1029/JA076i016p03534

J.W. Belcher, C.V. Solodyna, Alfvén waves and directional discontinuities in the interplanetary medium. J. Geophys. Res. **80**(9), 181–186 (1975). doi:10.1029/JA080i001p00181

D. Biskamp, *Nonlinear Magnetohydrodynamics*. Cambridge Monographs on Plasma Physics, vol. 1 (Cambridge University Press, Cambridge, 1993)

B. Breech, W.H. Matthaeus, J. Minnie, S. Oughton, S. Parhi, J.W. Bieber, B. Bavassano, Radial evolution of cross helicity in high-latitude solar wind. Geophys. Res. Lett. **32**, 06103 (2005). doi:10.1029/2004GL022321

B. Breech, W.H. Matthaeus, J. Minnie, J.W. Bieber, S. Oughton, C.W. Smith, P.A. Isenberg, Turbulence transport throughout the heliosphere. J. Geophys. Res. **113**, 08105 (2008). doi:10.1029/2007JA012711

R. Bruno, Inner heliosphere observations of MHD turbulence in the solar wind – challenges to theory, in *Solar Wind Seven*, ed. by E. Marsch, R. Schwenn. COSPAR Colloquia Series, vol. 3 (Pergamon Press, Oxford, 1992), pp. 423–428

R. Bruno, B. Bavassano, Origin of low cross-helicity regions in the solar wind. J. Geophys. Res. **96**, 7841–7851 (1991). doi:10.1029/91JA00144

R. Bruno, B. Bavassano, Evolution of the Alfvénic correlation in the solar wind. Nuovo Cimento C **15**, 599–605 (1992). doi:10.1007/BF02507833

R. Bruno, B. Bavassano, U. Villante, Evidence for long period Alfvén waves in the inner solar system. J. Geophys. Res. **90**(9), 4373–4377 (1985). doi:10.1029/JA090iA05p04373

R. Bruno, B. Bavassano, H. Rosenbauer, F. Mariani, On the local generation of interplanetary Alfvénic fluctuations. Adv. Space Res. **9**, 131–133 (1989). doi:10.1016/0273-1177(89)90106-3

R. Bruno, B. Bavassano, E. Pietropaolo, On the nature of Alfvénic 'inward' modes in the solar wind, in *Solar Wind Eight*, ed. by D. Winterhalter, J.T. Gosling, S.R. Habbal, W.S. Kurth, M. Neugebauer. AIP Conference Proceedings, vol. 382 (American Institute of Physics, Woodbury, 1996), pp. 229–232. doi:10.1063/1.51389

R. Bruno, R. D'Amicis, B. Bavassano, V. Carbone, L. Sorriso-Valvo, Magnetically dominated structures as an important component of the solar wind turbulence. Ann. Geophys. **25**, 1913–1927 (2007). doi:10.5194/angeo-25-1913-2007

L.F. Burlaga, Multifractal structure of the magnetic field and plasma in recurrent streams at 1 AU. J. Geophys. Res. **97**(16), 4283–4293 (1992a). doi:10.1029/91JA03027

L.F. Burlaga, Multifractals in the solar wind, in *Solar Wind Seven*, ed. by E. Marsch, R. Schwenn. COSPAR Colloquia Series, vol. 3 (Pergamon Press, Oxford, 1992b), pp. 429–432

L.F. Burlaga, L.W. Klein, Fractal structure of the interplanetary magnetic field. J. Geophys. Res. **91**(10), 347–350 (1986). doi:10.1029/JA091iA01p00347

V. Carbone, P. Veltri, A simplified cascade model for MHD turbulence. Astron. Astrophys. **188**, 239–250 (1987)
V. Carbone, P. Veltri, Relaxation processes in magnetohydrodynamics: a triad-interaction model. Astron. Astrophys. **259**, 359–372 (1992)
P. Chassaing, R.A. Antonia, F. Anselmet, L. Joly, S. Sarkar, *Variable Density Fluid Turbulence*. Fluid Mechanics and Its Applications, vol. 69 (Springer, Washington, 2002)
P.J. Coleman, Turbulence, viscosity, and dissipation in the solar-wind plasma. Astrophys. J. **153**, 371 (1968). doi:10.1086/149674
L. Del Zanna, Parametric decay of oblique arc-polarized Alfvén waves. Geophys. Res. Lett. **28**, 2585–2588 (2001). doi:10.1029/2001GL012911
L. Del Zanna, M. Velli, P. Londrillo, Parametric decay of circularly polarized Alfvén waves: multidimensional simulations in periodic and open domains. Astron. Astrophys. **367**, 705–718 (2001). doi:10.1051/0004-6361:20000455
K.U. Denskat, F.M. Neubauer, Observations of hydromagnetic turbulence in the solar wind, in *Solar Wind Five*, ed. by M. Neugebauer. NASA Conference Publication, vol. 2280 (NASA, Washington, 1983), pp. 81–91
N.F. Derby, Modulational instability of finite-amplitude, circularly polarized Alfvén waves. Astrophys. J. **224**, 1013–1016 (1978). doi:10.1086/156451
M. Dobrowolny, A. Mangeney, P. Veltri, Fully developed anisotropic hydromagnetic turbulence in interplanetary space. Phys. Rev. Lett. **45**, 144–147 (1980a). doi:10.1103/PhysRevLett.45.144
M. Dobrowolny, A. Mangeney, P. Veltri, Properties of magnetohydrodynamic turbulence in the solar wind. Astron. Astrophys. **83**, 26–32 (1980b)
W.M. Elsässer, The hydromagnetic equations. Phys. Rev. **79**, 183 (1950). doi:10.1103/PhysRev.79.183
R.J. Forsyth, T.S. Horbury, A. Balogh, E.J. Smith, Hourly variances of fluctuations in the heliospheric magnetic field out of the ecliptic plane. Geophys. Res. Lett. **23**, 595–598 (1996). doi:10.1029/96GL00416
A.A. Galeev, V.N. Oraevskii, The stability of Alfvén waves. Sov. Phys. Dokl. **7**, 988–1003 (1963)
S. Ghosh, W.H. Matthaeus, Relaxation processes in a turbulent compressible magnetofluid. Phys. Fluids B **2**, 1520–1534 (1990). doi:10.1063/1.859477
B.E. Goldstein, E.J. Smith, A. Balogh, T.S. Horbury, M.L. Goldstein, D.A. Roberts, Properties of magnetohydrodynamic turbulence in the solar wind as observed by ulysses at high heliographic latitudes. Geophys. Res. Lett. **22**, 3393–3396 (1995). doi:10.1029/95GL03183
M.L. Goldstein, An instability of finite amplitude circularly polarized Alfvén waves. Astrophys. J. **219**, 700–704 (1978). doi:10.1086/155829
M.L. Goldstein, D.A. Roberts, Magnetohydrodynamic turbulence in the solar wind. Phys. Plasmas **6**, 4154–4160 (1999). doi:10.1063/1.873680
M.L. Goldstein, D.A. Roberts, W.H. Matthaeus, Systematic errors in determining the propagation direction of interplanetary Alfvénic fluctuations. J. Geophys. Res. **91**(10), 13357–13365 (1986). doi:10.1029/JA091iA12p13357
M.L. Goldstein, D.A. Roberts, W.H. Matthaeus, Numerical simulation of interplanetary and magnetospheric phenomena: the Kelvin–Helmholtz instability, in *Solar System Plasma Physics*, ed. by J.H. Waite Jr, J.L. Burch, R.L. Moore Geophysical Monograph, vol. 54 (American Institute of Physics, Washington, 1989), p. 113
R. Grappin, Comment on 'Alfvénic turbulence in the polar wind: a statistical study on cross helicity and residual energy variations' by B. Bavassano et al. J. Geophys. Res. **107**, 1247 (2002). doi:10.1029/2001JA005058
R. Grappin, M. Velli, Waves and streams in the expanding solar wind. J. Geophys. Res. **101**, 425–444 (1996). doi:10.1029/95JA02147
R. Grappin, U. Frisch, A. Pouquet, J. Leorat, Alfvénic fluctuations as asymptotic states of MHD turbulence. Astron. Astrophys. **105**, 6–14 (1982)
R. Grappin, A. Mangeney, E. Marsch, On the origin of solar wind turbulence: Helios data revisited, in *Turbulence and Nonlinear Dynamics in MHD Flows*, ed. by M. Meneguzzi, A. Pouquet, P.L. Sulem (North-Holland, Amsterdam, 1989), pp. 81–86

R. Grappin, A. Mangeney, E. Marsch, On the origin of solar wind MHD turbulence – Helios data revisited. J. Geophys. Res. **95**(14), 8197–8209 (1990). doi:10.1029/JA095iA06p08197

R. Grappin, M. Velli, A. Mangeney, Alfvénic versus standard turbulence in the solar wind. Ann. Geophys. **9**, 416–426 (1991)

R. Grappin, A. Mangeney, M. Velli, MHD turbulence: theory/simulations, in *Solar Wind Seven*, ed. by E. Marsch, R. Schwenn. COSPAR Colloquia Series, vol. 3 (Pergamon Press, Oxford, 1992), pp. 451–456

M. Heinemann, S. Olbert, Non-WKB Alfvén waves in the solar wind. J. Geophys. Res. **85**(14), 1311–1327 (1980)

P. Hellinger, P.M. Trávníček, Oblique proton fire hose instability in the expanding solar wind: Hybrid simulations. J. Geophys. Res. **113**(12), 10109 (2008). doi:10.1029/2008JA013416

T.S. Horbury, A. Balogh, Evolution of magnetic field fluctuations in high-speed solar wind streams: Ulysses and Helios observations. J. Geophys. Res. **106**(A8), 15929–15940 (2001). doi:10.1029/2000JA000108

T.S. Horbury, B. Tsurutani, Ulysses measurements of waves, turbulence and discontinuities, in *The Heliosphere Near Solar Minimum: The Ulysses perspective*, ed. by A. Balogh, R.G. Marsden, E.J. Smith. Springer-Praxis Books in Astronomy and Space Sciences (Springer, Berlin, 2001), pp. 167–227

T.S. Horbury, A. Balogh, R.J. Forsyth, E.J. Smith, Anisotropy of inertial range turbulence in the polar heliosphere. Geophys. Res. Lett. **22**, 3405–3408 (1995a). doi:10.1029/95GL03012

T.S. Horbury, A. Balogh, R.J. Forsyth, E.J. Smith, Observations of evolving turbulence in the polar solar wind. Geophys. Res. Lett. **22**, 3401–3404 (1995b). doi:10.1029/95GL03550

T.S. Horbury, A. Balogh, R.J. Forsyth, E.J. Smith, Ulysses magnetic field observations of fluctuations within polar coronal flows. Ann. Geophys. **13**, 105–107 (1995c)

T.S. Horbury, A. Balogh, R.J. Forsyth, E.J. Smith, Magnetic field signatures of unevolved turbulence in solar polar flows. J. Geophys. Res. **101**(10), 405–414 (1996a). doi:10.1029/95JA01343

T.S. Horbury, A. Balogh, R.J. Forsyth, E.J. Smith, The rate of turbulent evolution over the sun's poles. Astron. Astrophys. **316**, 333–341 (1996b)

M. Hoshino, M.L. Goldstein, Time evolution from linear to nonlinear stages in magnetohydrodynamic parametric instabilities. Phys. Fluids B **1**, 1405–1415 (1989). doi:10.1063/1.858971

M. Hossain, P.C. Gray, D.H. Pontius Jr., W.H. Matthaeus, S. Oughton, Phenomenology for the decay of energy-containing eddies in homogeneous MHD turbulence. Phys. Fluids **7**, 2886–2904 (1995). doi:10.1063/1.868665

A.N. Kolmogorov, The local structure turbulence in incompressible viscous fluids for very large Reynolds numbers. Dokl. Akad. Nauk. SSSR **30**, 301–305 (1941)

R.H. Kraichnan, On Kolmogorov's inertial-range theories. J. Fluid Mech. **62**, 305–330 (1974). doi:10.1017/S002211207400070X

F. Malara, M. Velli, Parametric instability of a large-amplitude nonmonochromatic Alfvén wave. Phys. Plasmas **3**, 4427–4433 (1996). doi:10.1063/1.872043

F. Malara, P. Veltri, V. Carbone, Competition among nonlinear effects in tearing instability saturation. Phys. Fluids B **4**, 3070 (1992). doi:10.1063/1.860477

F. Malara, L. Primavera, P. Veltri, Compressive fluctuations generated by time evolution of Alfvénic perturbations in the solar wind current sheet. J. Geophys. Res. **101**(A10), 21597–21617 (1996). doi:10.1029/96JA01637

F. Malara, L. Primavera, P. Veltri, Nonlinear evolution of parametric instability of a large-amplitude nonmonochromatic Alfvén wave. Phys. Plasmas **7**, 2866–2877 (2000). doi:10.1063/1.874136

F. Malara, L. Primavera, P. Veltri, Nonlinear evolution of the parametric instability: numerical predictions versus observations in the heliosphere. Nonlinear Process. Geophys. **8**, 159–166 (2001a). doi:10.5194/npg-8-159-2001

F. Malara, L. Primavera, P. Veltri, Parametric instability of a broad-band Alfvén wave: nonlinear evolution and saturation, in *Recent Insights into the Physics of the Sun and Heliosphere: Highlights from SOHO and Other Space Missions*, ed. by P. Brekke, B. Fleck, J.B. Gurman. IAU Symposia, vol. 203 (Astronomical Society of the Pacific, San Francisco, 2001b), pp. 511–513

F. Malara, L. Primavera, P. Veltri, Parametric instability of Alfvénic fluctuations in high-latitude solar wind, in *Solspa 2001*, ed. by H. Sawaya-Lacoste. ESA Conference Proceedings, vol. SP-477 (ESA Publications Division, Noordwijk, 2002), pp. 309–312

F. Mariani, N.F. Ness, L.F. Burlaga, B. Bavassano, U. Villante, The large-scale structure of the interplanetary magnetic field between 1 and 0.3 AU during the primary mission of Helios 1. J. Geophys. Res. **83**(12), 5161–5166 (1978). doi:10.1029/JA083iA11p05161

E. Marsch, A. Mangeney, Ideal MHD equations in terms of compressive elsässer variables. J. Geophys. Res. **92**(11), 7363–7367 (1987). doi:10.1029/JA092iA07p07363

E. Marsch, C.-Y. Tu, Dynamics of correlation functions with elsässer variables for inhomogeneous MHD turbulence. J. Plasma Phys. **41**, 479–491 (1989). doi:10.1017/S0022377800014033

E. Marsch, C.-Y. Tu, On the radial evolution of MHD turbulence in the inner heliosphere. J. Geophys. Res. **95**(14), 8211–8229 (1990). doi:10.1029/JA095iA06p08211

E. Marsch, C.-Y. Tu, Correlations between the fluctuations of pressure, density, temperature and magnetic field in the solar wind. Ann. Geophys. **11**, 659–677 (1993a)

E. Marsch, C.-Y. Tu, Modeling results on spatial transport and spectral transfer of solar wind Alfvénic turbulence. J. Geophys. Res. **98**(17), 21045–21059 (1993b). doi:10.1029/93JA02365

E. Marsch, C.-Y. Tu, Spatial evolution of the magnetic field spectral exponent in the solar wind: Helios and ulysses comparison. J. Geophys. Res. **101**(10), 11149–11152 (1996). doi:10.1029/95JA03804

R.N. Martin, J.W. Belcher, A.J. Lazarus, Observation and analysis of abrupt changes in the interplanetary plasma velocity and magnetic field. J. Geophys. Res. **78**, 3653 (1973). doi:10.1029/JA078i019p03653

W.H. Matthaeus, M.L. Goldstein, D.A. Roberts, Evidence for the presence of quasi-two-dimensional nearly incompressible fluctuations in the solar wind. J. Geophys. Res. **95**, 20673–20683 (1990). doi:10.1029/JA095iA12p20673

W.H. Matthaeus, G.P. Zank, C.W. Smith, S. Oughton, Turbulence, spatial transport, and heating of the solar wind. Phys. Rev. Lett. **82**, 3444–3447 (1999). doi:10.1103/PhysRevLett.82.3444

W.H. Matthaeus, J. Minnie, B. Breech, S. Parhi, J.W. Bieber, S. Oughton, Transport of cross helicity and radial evolution of Alfvénicity in the solar wind. Geophys. Res. Lett. **31**, 12803 (2004). doi:10.1029/2004GL019645

D.J. McComas, S.J. Bame, B.L. Barraclough, W.C. Feldman, H.O. Funsten, J.T. Gosling, P. Riley, R.M. Skoug, A. Balogh, R.J. Forsyth, B.E. Goldstein, M. Neugebauer, Ulysses' return to the slow solar wind. Geophys. Res. Lett. **25**, 1–4 (1998). doi:10.1029/97GL03444

D.J. McComas, H.A. Elliott, N.A. Schwadron, J.T. Gosling, R.M. Skoug, B.E. Goldstein, The three-dimensional solar wind around solar maximum. Geophys. Res. Lett. **30**(10) (2003). doi:10.1029/2003GL017136

W.D. McComb, A.G. Watt, Conditional averaging procedure for the elimination of the small-scale modes from incompressible fluid turbulence at high Reynolds numbers. Phys. Rev. Lett. **65**, 3281–3284 (1990). doi:10.1103/PhysRevLett.65.3281

A.S. Monin, A.M. Yaglom, *Statistical Fluid Mechanics – Mechanics of Turbulence*, vol. 2 (MIT Press, Cambridge, 1975)

M. Neugebauer, D.R. Clay, B.E. Goldstein, B.T. Tsurutani, R.D. Zwickl, A reexamination of rotational and tangential discontinuities in the solar wind. J. Geophys. Res. **89**, 5395–5408 (1984). doi:10.1029/JA089iA07p05395

A. Pouquet, Magnetohydrodynamic turbulence, in *Les Houches Summer School on Astrophysical Fluid Dynamics*, ed. by J.-P. Zahn, J. Zinn-Justin (Elsevier, Amsterdam, 1993), p. 139

A. Pouquet, Turbulence, statistics and structures: an introduction, in *Plasma Astrophysics*, ed. by C. Chiuderi, G. Einaudi. Lecture Notes in Physics, vol. 468 (Springer, Berlin, 1996), pp. 163–212. doi:10.1007/BFb0102544

L. Primavera, F. Malara, P. Veltri, Parametric instability in the solar wind: numerical study of the nonlinear evolution, in *Solar Wind Ten*, ed. by M. Velli, R. Bruno, F. Malara. AIP Conference Proceedings, vol. 679 (American Institute of Physics, Melville, NY, 2003), pp. 505–508

D.A. Roberts, Interplanetary observational constraints on Alfvén wave acceleration of the solar wind. J. Geophys. Res. **94**(13), 6899–6905 (1989). doi:10.1029/JA094iA06p06899

D.A. Roberts, M.L. Goldstein, Simulation of interplanetary dynamical processes, in *Proceedings of the Third International Conference on Supercomputing*, ed. by L.P. Kartashev, S.I. Kartashev (International Supercomputing Institute, St. Petersburg, 1988), p. 370

D.A. Roberts, M.L. Goldstein, L.W. Klein, W.H. Matthaeus, The nature and evolution of magnetohydrodynamic fluctuations in the solar wind: Voyager observations. J. Geophys. Res. **92**(11), 11021–11040 (1987a)

D.A. Roberts, M.L. Goldstein, L.W. Klein, W.H. Matthaeus, Origin and evolution of fluctuations in the solar wind: Helios observations and Helios–Voyager comparisons. J. Geophys. Res. **92**(11), 12023–12035 (1987b). doi:10.1029/JA092iA11p12023

D.A. Roberts, M.L. Goldstein, L.W. Klein, The amplitudes of interplanetary fluctuations – stream structure, heliocentric distance, and frequency dependence. J. Geophys. Res. **95**(14), 4203–4216 (1990). doi:10.1029/JA095iA04p04203

D.A. Roberts, S. Ghosh, M.L. Goldstein, W.H. Matthaeus, Magnetohydrodynamic simulation of the radial evolution and stream structure of solar-wind turbulence. Phys. Rev. Lett. **67**, 3741–3744 (1991). doi:10.1103/PhysRevLett.67.3741

D.A. Roberts, M.L. Goldstein, W.H. Matthaeus, S. Ghosh, Velocity shear generation of solar wind turbulence. J. Geophys. Res. **97**(16), 17115–17130 (1992). doi:10.1029/92JA01144

A. Ruzmaikin, I.P. Lyannaya, V.A. Styashkin, E.A. Eroshenko, The spectrum of the interplanetary magnetic field near 1.3 AU. J. Geophys. Res. **98**(17), 13303–13306 (1993). doi:10.1029/92JA01522

A.A. Ruzmaikin, J. Feynman, B.E. Goldstein, E.J. Smith, A. Balogh, Intermittent turbulence in solar wind from the south polar hole. J. Geophys. Res. **100**(9), 3395–3403 (1995). doi:10.1029/94JA02808

R.Z. Sagdeev, A.A. Galeev, *Nonlinear Plasma Theory* (Benjamin, New York, 1969)

E.J. Smith, A. Balogh, M. Neugebauer, D.J. McComas, Ulysses observations of Alfvén waves in the southern and northern solar hemispheres. Geophys. Res. Lett. **22**, 3381–3384 (1995). doi:10.1029/95GL03268

C.W. Smith, W.H. Matthaeus, G.P. Zank, N.F. Ness, S. Oughton, J.D. Richardson, Heating of the low-latitude solar wind by dissipation of turbulent magnetic fluctuations. J. Geophys. Res. **106**, 8253–8272 (2001). doi:10.1029/2000JA000366

C.V. Solodyna, J.W. Belcher, J.W. Sari, Plasma field characteristics of directional discontinuities in the interplanetary medium. J. Geophys. Res. **82**, 10–14 (1977). doi:10.1029/JA082i001p00010

A.C. Ting, W.H. Matthaeus, D. Montgomery, Turbulent relaxation processes in magnetohydrodynamics. Phys. Fluids **29**, 3261–3274 (1986). doi:10.1063/1.865843

C.-Y. Tu, E. Marsch, Evidence for a 'background' spectrum of solar wind turbulence in the inner heliosphere. J. Geophys. Res. **95**(14), 4337–4341 (1990a). doi:10.1029/JA095iA04p04337

C.-Y. Tu, E. Marsch, Transfer equations for spectral densities of inhomogeneous MHD turbulence. J. Plasma Phys. **44**, 103–122 (1990b). doi:10.1017/S002237780001504X

C.-Y. Tu, E. Marsch, A case study of very low cross-helicity fluctuations in the solar wind. Ann. Geophys. **9**, 319–332 (1991)

C.-Y. Tu, E. Marsch, A model of solar wind fluctuations with two components: Alfvén waves and convective structures. J. Geophys. Res. **98**(17), 1257–1276 (1993). doi:10.1029/92JA01947

C.-Y. Tu, E. Marsch, MHD structures, waves and turbulence in the solar wind: Observations and theories. Space Sci. Rev. **73**(1/2), 1–210 (1995). doi:10.1007/BF00748891

C.-Y. Tu, E. Marsch, K.M. Thieme, Basic properties of solar wind MHD turbulence near 0.3 AU analyzed by means of elsässer variables. J. Geophys. Res. **94**(13), 11739–11759 (1989). doi:10.1029/JA094iA09p11739

C.-Y. Tu, Z.-Y. Pu, F.-S. Wei, The power spectrum of interplanetary Alfvénic fluctuations derivation of the governing equation and its solution. J. Geophys. Res. **89**(18), 9695–9702 (1984). doi:10.1029/JA089iA11p09695

C.-Y. Tu, D.A. Roberts, M.L. Goldstein, Spectral evolution and cascade constant of solar wind Alfvénic turbulence. J. Geophys. Res. **94**(13), 13575–13578 (1989). doi:10.1029/JA094iA10p13575

C.-Y. Tu, E. Marsch, H. Rosenbauer, The dependence of MHD turbulence spectra on the inner solar wind stream structure near solar minimum. Geophys. Res. Lett. **17**, 283–286 (1990). doi:10.1029/GL017i003p00283

H. Umeki, T. Terasawa, Decay instability of incoherent Alfvén waves in the solar wind. J. Geophys. Res. **97**(16), 3113–3119 (1992). doi:10.1029/91JA02967

M. Velli, R. Grappin, A. Mangeney, Turbulent cascade of incompressible unidirectional Alfvén waves in the interplanetary medium. Phys. Rev. Lett. **63**, 1807–1810 (1989). doi:10.1103/PhysRevLett.63.1807

M. Velli, R. Grappin, A. Mangeney, Solar wind expansion effects on the evolution of hydromagnetic turbulence in the interplanetary medium. Comput. Phys. Commun. **59**, 153–162 (1990). doi:10.1016/0010-4655(90)90165-W

P. Veltri, A. Mangeney, M. Dobrowolny, Cross-helicity effects in anisotropic MHD turbulence. Nuovo Cimento B **68**, 235–251 (1982). doi:10.1007/BF02890146

P. Veltri, F. Malara, L. Primavera, Correlation, anisotropy and compressibility of low frequency fluctuations in solar wind, in *Solar Wind Seven*, ed. by E. Marsch, R. Schwenn. COSPAR Colloquia Series, vol. 3 (Pergamon Press, Oxford, 1992), pp. 423–428

A.F. Viñas, M.L. Goldstein, Parametric instabilities of circularly polarized large-amplitude dispersive Alfvén waves: excitation of obliquely-propagating daughter and side-band waves. J. Plasma Phys. **46**, 129–152 (1991). doi:10.1017/S0022377800015993

G.P. Zank, W.H. Matthaeus, C.W. Smith, Evolution of turbulent magnetic fluctuation power with heliospheric distance. J. Geophys. Res. **101**, 17093–17108 (1996). doi:10.1029/96JA01275

G.P. Zank, N. Jetha, Q. Hu, P. Hunana, The transport of density fluctuations throughout the heliosphere. Astrophys. J. **756**, 21 (2012a). doi:10.1088/0004-637X/756/1/21

G.P. Zank, A. Dosch, P. Hunana, V. Florinski, W.H. Matthaeus, G.M. Webb, The transport of low-frequency turbulence in astrophysical flows. i. governing equations. Astrophys. J. **745**, 35 (2012b). doi:10.1088/0004-637X/745/1/35

Y. Zhou, W.H. Matthaeus, Non-WKB evolution of solar wind fluctuations: a turbulence modeling approach. Geophys. Res. Lett. **16**, 755–758 (1989). doi:10.1029/GL016i007p00755

Y. Zhou, W.H. Matthaeus, Transport and turbulence modeling of solar wind fluctuations. J. Geophys. Res. **95**(14), 10291–10311 (1990). doi:10.1029/JA095iA07p10291

Chapter 5
Compressive Turbulence

Interplanetary medium is slightly compressive, magnetic field intensity and proton number density experience fluctuations over all scales and the compression depends on both the scale and the nature of the wind. As a matter of fact, slow wind is generally more compressive than fast wind, as shown in Fig. 5.1 where, following Bavassano et al. (1982b) and Bruno and Bavassano (1991), we report the ratio between the power density associated with magnetic field intensity fluctuations and that associated with the fluctuations of the three components. In addition, as already shown by Bavassano et al. (1982b), this parameter increases with heliocentric distance for both fast and slow wind as shown in the bottom panel, where the ratio between the compression at 0.9 AU and that at 0.3 AU is generally greater than 1. It is also interesting to notice that within the Alfvénic fast wind, the lowest compression is observed in the middle frequency range, roughly between 10^{-4} and 10^{-3} Hz. On the other hand, this frequency range has already been recognized as the most Alfvénic one, within the inner heliosphere (Bruno et al. 1996).

As a matter of fact, it seems that high Alfvénicity is correlated with low compressibility of the medium (Bruno and Bavassano 1991; Klein et al. 1993; Bruno and Bavassano 1993) although compressibility is not the only cause for a low Alfvénicity (Roberts et al. 1991, 1992; Roberts 1992).

The radial dependence of the normalized number density fluctuations $\delta n/n$ for the inner and outer heliosphere were studied by Grappin et al. (1990) and Roberts et al. (1987) for the hourly frequency range, but no clear radial trend emerged from these studies. However, interesting enough, Grappin et al. (1990) found that values of e^- were closely associated with enhancements of $\delta n/n$ on scales longer than 1 h.

On the other hand, a spectral analysis of proton number density, magnetic field intensity, and proton temperature performed by Marsch and Tu (1990) and Tu et al. (1991) in the inner heliosphere, separately for fast and slow wind (see Fig. 5.2), showed that normalized spectra of the above parameters within slow wind were only marginally dependent on the radial distance. On the contrary, within fast wind, magnetic field and proton density normalized spectra showed not only a clear radial

R. Bruno, V. Carbone, *Turbulence in the Solar Wind*, Lecture Notes in Physics 928, DOI 10.1007/978-3-319-43440-7_5

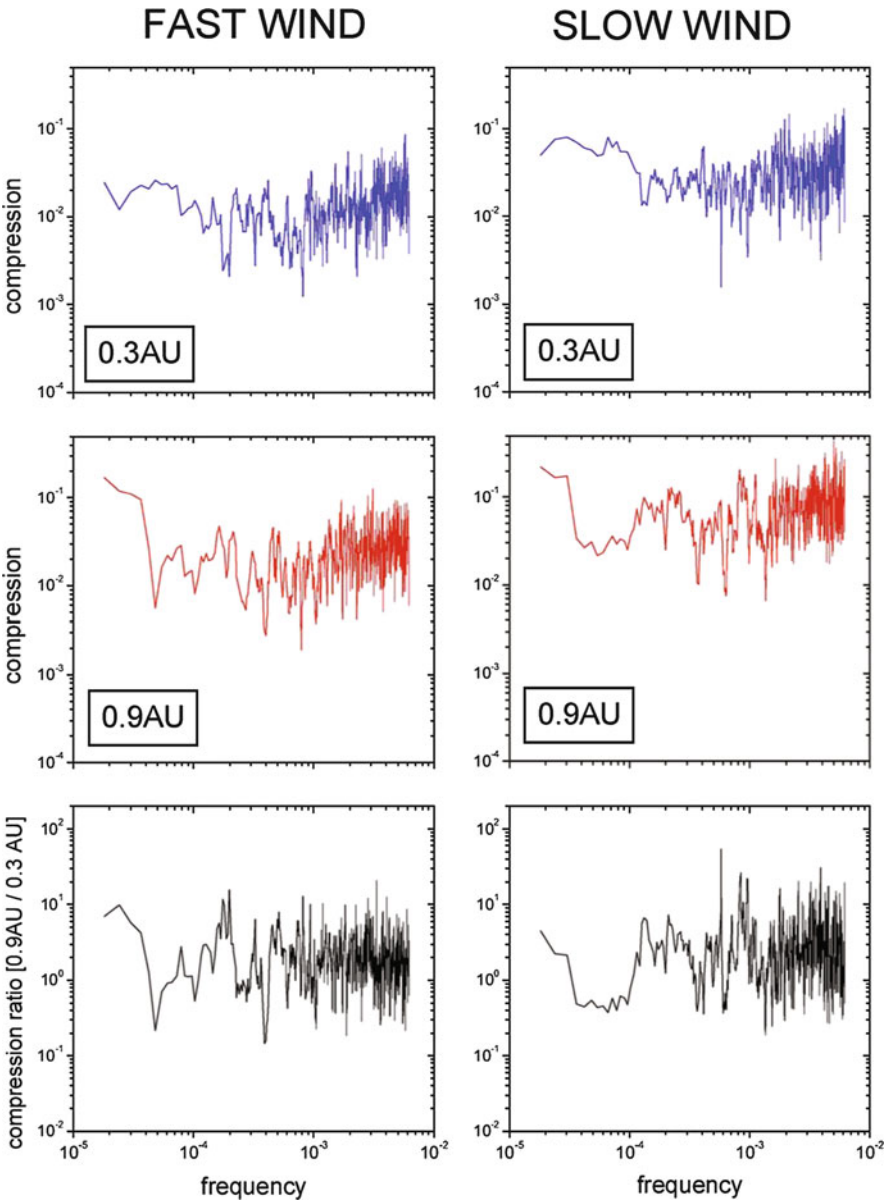

Fig. 5.1 The *first two rows* show magnetic field compression (see text for definition) for fast (*left column*) and slow (*right column*) wind at 0.3 AU (*upper row*) and 0.9 AU (*middle row*). The *bottom panels* show the ratio between compression at 0.9 AU and compression at 0.3 AU. This ratio is generally greater than 1 for both fast and slow wind

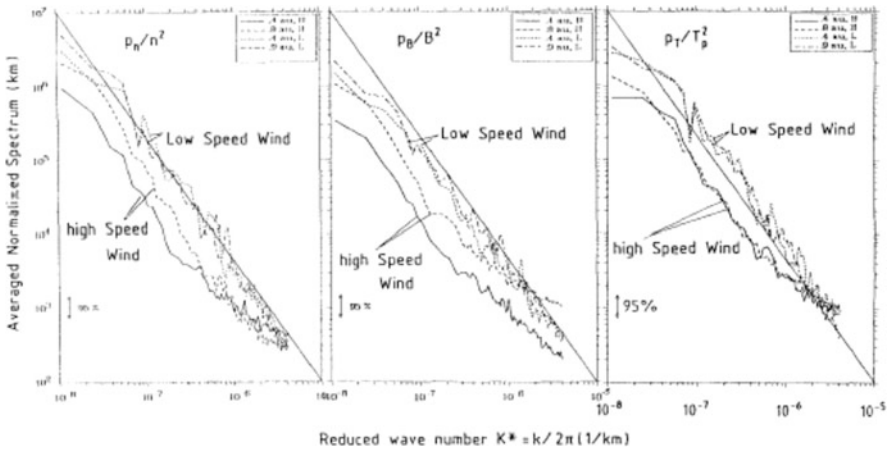

Fig. 5.2 *From left to right*: normalized spectra of proton temperature (from Tu et al. 1991), number density, and magnetic field intensity fluctuations (from Marsch and Tu 1990, copyright by AGU, reproduced by permission). *Different lines* refer to different heliocentric distances for both slow and fast wind

dependence but also similar level of power for $k < 4 \times 10^{-4}\,\mathrm{km\,s^{-1}}$. For larger k these spectra show a flattening that becomes steeper for increasing distance, as was already found by Bavassano et al. (1982a) for magnetic field intensity. Normalized temperature spectra does not suffer any radial dependence neither in slow wind nor in fast wind.

Spectral index is around $-5/3$ for all the spectra in slow wind while, fast wind spectral index is around $-5/3$ for $k < 4 \times 10^{-4}\,\mathrm{km^{-1}}$ and slightly less steep for larger wave numbers.

5.1 On the Nature of Compressive Turbulence

Considerable efforts, both theoretical and observational, have been made in order to disclose the nature of compressive fluctuations. It has been proposed (Montgomery et al. 1987; Matthaeus and Brown 1988; Zank et al. 1990; Zank and Matthaeus 1990; Matthaeus et al. 1991; Zank and Matthaeus 1992) that most of compressive fluctuations observed in the solar wind could be accounted for by the Nearly Incompressible (NI) model. Within the framework of this model, Montgomery et al. (1987) showed that a spectrum of small scale density fluctuations follows a $k^{-5/3}$ when the spectrum of magnetic field fluctuations follows the same scaling. Moreover, it was showed (Matthaeus and Brown 1988; Zank and Matthaeus 1992) that if compressible MHD equations are expanded in terms of small turbulent sonic Mach number, pressure balanced structures, Alfvénic and magnetosonic fluctuations naturally arise as solutions and, in particular, the RMS of small density fluctuations would scale like M^2, being $M = \delta v/C_s$ the turbulent sonic Mach number, δv the

RMS of velocity fluctuations and C_s the sound speed. In addition, if heat conduction is allowed in the approximation, temperature fluctuations dominate over magnetic and density fluctuations, temperature and density are anticorrelated and would scale like M. However, in spite of some examples supporting this theory (Matthaeus et al. (1991) reported 13 % of cases satisfied the requirements of NI-theory), wider statistical studies, conducted by Tu and Marsch (1994), Bavassano et al. (1995) and Bavassano and Bruno (1995), showed that NI theory is not generally applicable *sic et simpliciter* to the solar wind. The reason might be in the fact that interplanetary medium is highly inhomogeneous because of the presence of an underlying structure convected by the wind. As a matter of fact, Thieme et al. (1989) showed evidence for the presence of time intervals characterized by clear anti-correlation between kinetic pressure and magnetic pressure while the total pressure remained fairly constant. These pressure balance structures were for the first time observed by Burlaga and Ogilvie (1970) for a time scale of roughly 1–2 h. Later on, Vellante and Lazarus (1987) reported strong evidence for anti-correlation between field intensity and proton density, and between plasma and field pressure on time scales up to 10 h. The anti-correlation between kinetic and magnetic pressure is usually interpreted as indicative of the presence of a pressure balance structure since slow magnetosonic modes are readily damped (Barnes 1979).

These features, observed also in their dataset, were taken by Thieme et al. (1989) as evidence of stationary spatial structures which were supposed to be remnants of coronal structures convected by the wind. Different values assumed by plasma and field parameters within each structure were interpreted as a signature characterizing that particular structure and not destroyed during the expansion. These intervals, identifiable in Fig. 5.3 by vertical dashed lines, were characterized by pressure balance and a clear anti-correlation between magnetic field intensity and temperature.

These structures were finally related to the fine ray-like structures or plumes associated with the underlying chromospheric network and interpreted as the signature of interplanetary flow-tubes. The estimated dimension of these structures, back projected onto the Sun, suggested that they over-expand in the solar wind. In addition, Grappin et al. (2000) simulated the evolution of Alfvén waves propagating within such pressure equilibrium ray structures in the framework of global Eulerian solar wind approach and found that the compressive modes in these simulations are very much reduced within the ray structures, which indeed correspond to the observational findings (Buttighoffer et al. 1995, 1999).

The idea of filamentary structures in the solar wind dates back to Parker (1963), followed by other authors like McCracken and Ness (1966), Siscoe et al. (1968), and more recently has been considered again in the literature with new results (see Sect. 7.3). These interplanetary flow tubes would be of different sizes, ranging from minutes to several hours and would be separated from each other by tangential discontinuities and characterized by different values of plasma parameters and a different magnetic field orientation and intensity. This kind of scenario, because of some similarity to a bunch of tangled, smoking "spaghetti" lifted by a fork, was then named "spaghetti-model".

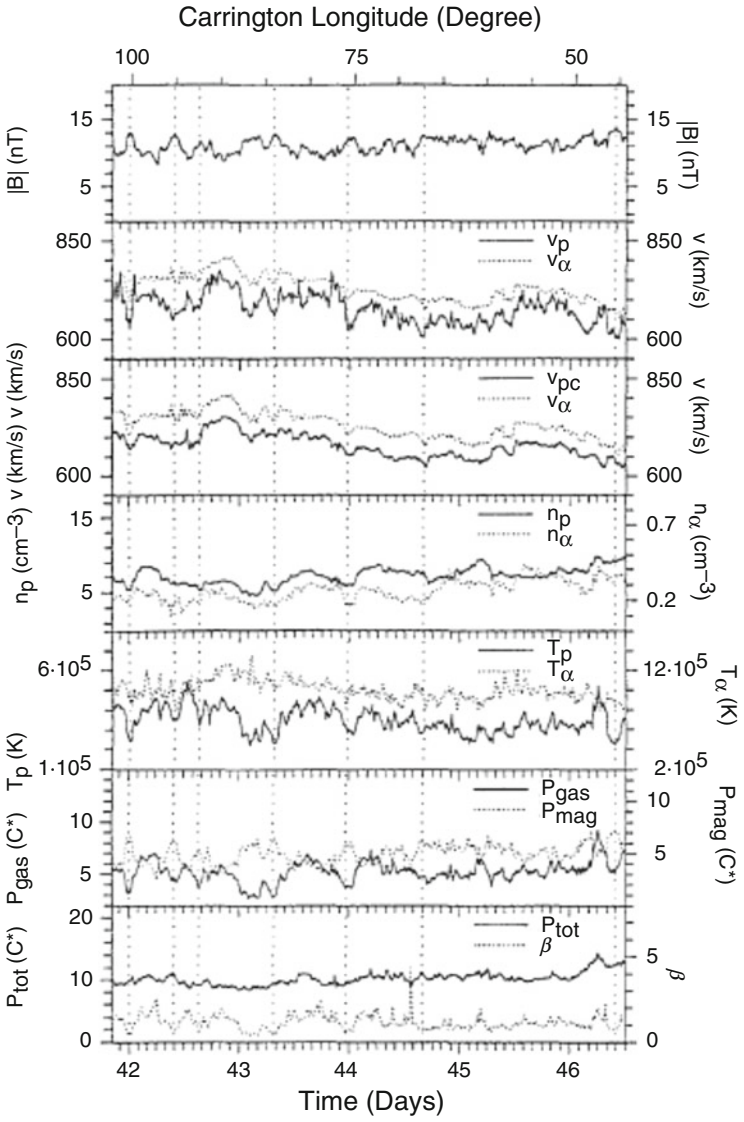

Fig. 5.3 *From top to bottom*: field intensity $|\mathbf{B}|$; proton and alpha particle velocity v_p and v_α; corrected proton velocity $v_{pc} = v_p - \delta v_A$, where v_A is the Alfvén speed; proton and alpha number density n_p and n_α; proton and alpha temperature T_p and T_α; kinetic and magnetic pressure P_k and P_m, which the authors call P_{gas} and P_{mag}; total pressure P_{tot} and $\beta = P_{\text{gas}}/P_{\text{mag}}$ (from Thieme et al. 1989)

A spectral analysis performed by Marsch and Tu (1993b) in the frequency range 6×10^{-3}–6×10^{-6} showed that the nature and intensity of compressive fluctuations systematically vary with the stream structure. They concluded that compressive fluctuations are a complex superposition of magnetoacoustic fluctuations and

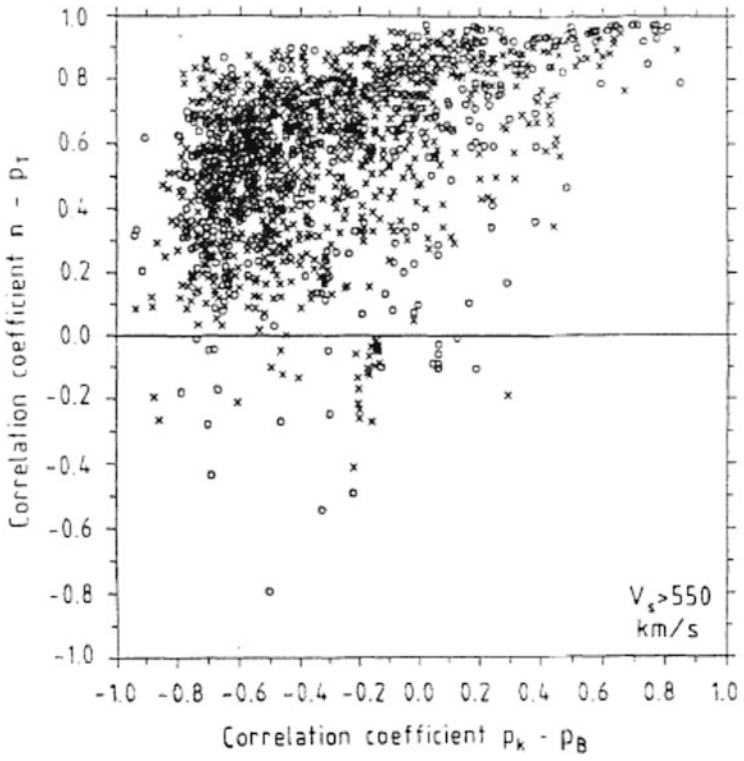

Fig. 5.4 Correlation coefficient between number density n and total pressure p_T plotted vs. the correlation coefficient between kinetic pressure and magnetic pressure for both Helios relatively to fast wind. Image reproduced by permission from Marsch and Tu (1993a)

pressure balance structures whose origin might be local, due to stream dynamical interaction, or of coronal origin related to the flow tube structure. These results are shown in Fig. 5.4 where the correlation coefficient between number density n and total pressure P_{tot} (indicated with the symbols p_T in the figure), and between kinetic pressure P_k and magnetic pressure P_m (indicated with the symbols p_k and p_b, respectively) is plotted for both Helios s/c relatively to fast wind. Positive values of correlation coefficients $C(n, p_T)$ and $C(p_k, p_b)$ identify magnetosonic waves, while positive values of $C(n, p_T)$ and negative values of $C(p_k, p_b)$ identify pressure balance structures. The purest examples of each category are located at the upper left and right corners.

Following these observations, Tu and Marsch (1994) proposed a model in which fluctuations in temperature, density, and field directly derive from an ensemble of small amplitude pressure balanced structures and small amplitude fast perpendicular magnetosonic waves. These last ones should be generated by the dynamical interaction between adjacent flow tubes due to the expansion and, eventually, they

would experience also a non-linear cascade process to smaller scales. This model was able to reproduce most of the correlations described by Marsch and Tu (1993b) for fast wind.

Later on, Bavassano et al. (1996a) characterized compressive fluctuations in terms of their polytropic index, which resulted to be a useful tool to study small scale variations in the solar wind. These authors followed the definition of polytropic fluid given by Chandrasekhar (1967): "a polytropic change is a quasi-static change of state carried out in such a way that the specific heat remains constant (at some prescribed value) during the entire process". For such a variation of state the adiabatic laws are still valid provided that the adiabatic index γ is replaced by a new adiabatic index $\gamma' = (c_P - c)/(c_V - c)$ where c is the specific heat of the polytropic variation, and c_P and c_V are the specific heat at constant pressure and constant volume, respectively. This similarity is lost if we adopt the definition given by Courant and Friedrichs (1976), for whom a fluid is polytropic if its internal energy is proportional to the temperature. Since no restriction applies to the specific heats, relations between temperature, density, and pressure do not have a simple form as in Chandrasekhar approach (Zank and Matthaeus 1991). Bavassano et al. (1996a) recovered the polytropic index from the relation between density n and temperature T changes for the selected scale $Tn^{1-\gamma'} = \text{const.}$ and used it to determine whether changes in density and temperature were isobaric ($\gamma' = 0$), isothermal ($\gamma' = 1$), adiabatic ($\gamma' = \gamma$), or isochoric ($\gamma' = \infty$). Although the role of the magnetic field was neglected, reliable conclusions could be obtained whenever the above relations between temperature and density were strikingly clear. These authors found intervals characterized by variations at constant thermal pressure P. They interpreted these intervals as a subset of total-pressure balanced structures where the equilibrium was assured by the thermal component only, perhaps tiny flow tubes like those described by Thieme et al. (1989) and Tu and Marsch (1994). Adiabatic changes were probably related to magnetosonic waves excited by contiguous flow tubes (Tu and Marsch 1994). Proton temperature changes at almost constant density were preferentially found in fast wind, close to the Sun. These regions were characterized by values of B and N remarkable stable and by strong Alfvénic fluctuations (Bruno et al. 1985). Thus, they suggested that these temperature changes could be remnants of thermal features already established at the base of the corona.

Thus, the polytropic index offers a very simple way to identify basic properties of solar wind fluctuations, provided that the magnetic field does not play a major role.

5.2 Compressive Turbulence in the Polar Wind

Compressive fluctuations in high latitude solar wind have been extensively studied by Bavassano et al. (2004) looking at the relationship between different parameters of the solar wind and comparing these results with predictions by existing models.

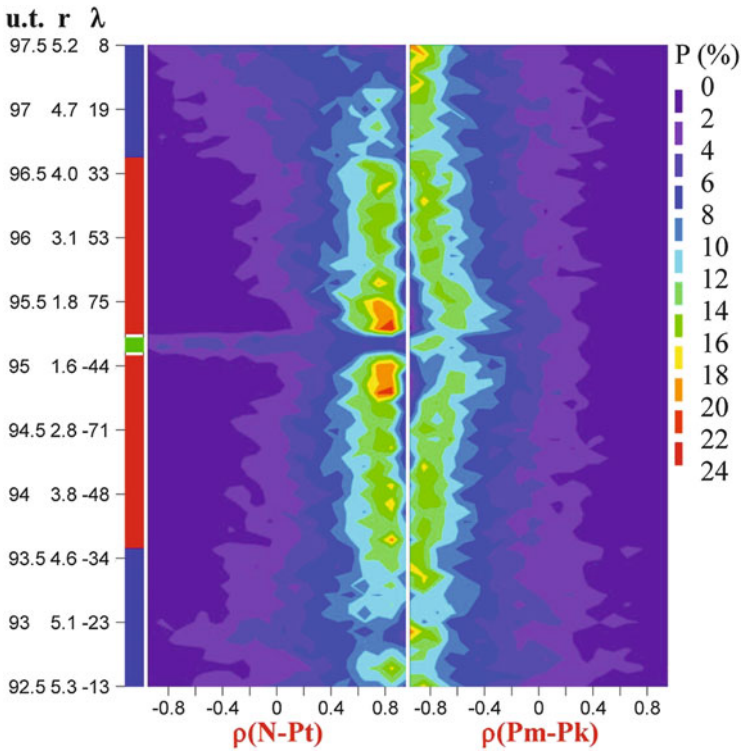

Fig. 5.5 Histograms of $\rho(N - P_t)$ and $\rho(P_m - P_k)$ per solar rotation. The *color bar* on the *left side* indicates polar (*red*), mid-latitude (*blue*), and low latitude (*green*) phases. Moreover, universal time UT, heliocentric distance, and heliographic latitude are also indicated on the *left side* of the plot. Occurrence frequency is indicated by the *color bar* shown on the *right hand side* of the figure. Image reproduced by permission from Bavassano et al. (2004), copyright EGU

These authors indicated with N, P_m, P_k, and P_t the proton number density n, magnetic pressure, kinetic pressure and total pressure ($P_{\text{tot}} = P_m + P_k$), respectively, and computed correlation coefficients ρ between these parameters. Figure 5.5 clearly shows that a pronounced positive correlation for $N - P_t$ and a negative pronounced correlation for $P_m - P_k$ is a constant feature of the observed compressive fluctuations. In particular, the correlation for $N - P_t$ is especially strong within polar regions at small heliocentric distance. In mid-latitude regions the correlation weakens, while almost disappears at low latitudes. In the case of $P_m - P_k$, the anticorrelation remains strong throughout the whole latitudinal excursion. For polar wind the anticorrelation appears to be less strong at small distances, just where the $N - P_t$ correlation is highest.

The role played by density and temperature in the anticorrelation between magnetic and thermal pressures is investigated in Fig. 5.6, where the magnetic field magnitude is directly compared with proton density and temperature. As regards the polar regions, a strong B-T anticorrelation is clearly apparent at all distances (right

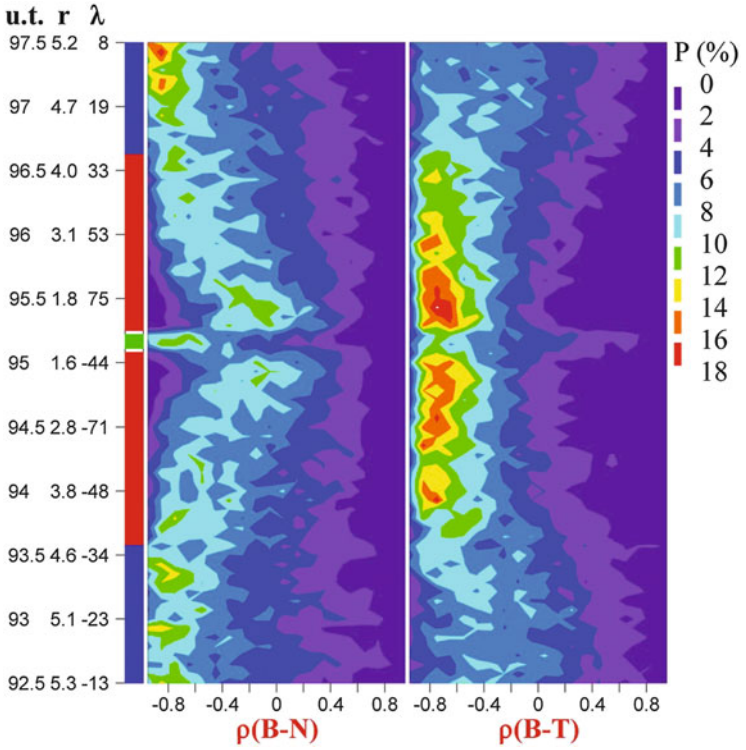

Fig. 5.6 Solar rotation histograms of B-N and B-T in the same format of Fig. 5.5. Image reproduced by permission from Bavassano et al. (2004), copyright EGU

panel). For B-N an anticorrelation tends to emerge when solar distance increases. This means that the magnetic-thermal pressure anticorrelation is mostly due to an anticorrelation of the magnetic field fluctuations with respect to temperature fluctuations, rather than density (see, e.g., Bavassano et al. 1996a,b). Outside polar regions the situation appears in part reversed, with a stronger role for the B-N anticorrelation.

In Fig. 5.7 scatter plots of total pressure vs. density fluctuations are used to test a model by Tu and Marsch (1994), based on the hypothesis that the compressive fluctuations observed in solar wind are mainly due to a mixture of pressure-balanced structures (PBS) and fast magnetosonic waves (W). Waves can only contribute to total pressure fluctuations while both waves and pressure-balanced structures may contribute to density fluctuations. A tunable parameter in the model is the relative PBS/W contribution to density fluctuations α. Straight lines in Fig. 5.7 indicate the model predictions for different values of α. It is easily seen that for all polar wind samples the great majority of experimental data fall in the $\alpha > 1$ region. Thus, pressure-balanced structures appear to play a major role with respect to magnetosonic waves. This is a feature already observed by Helios in the ecliptic

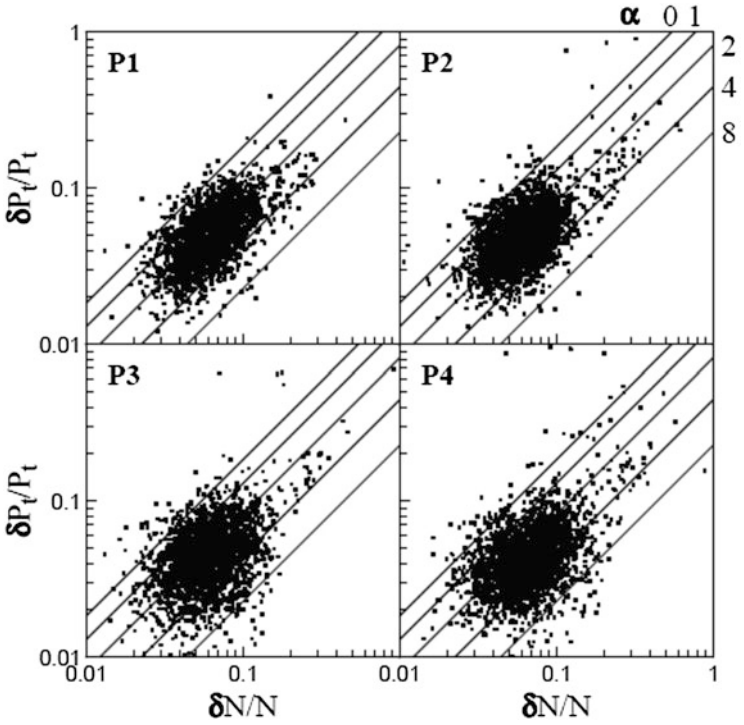

Fig. 5.7 Scatter plots of the relative amplitudes of total pressure vs. density fluctuations for polar wind samples P1 to P4. *Straight lines* indicate the Tu and Marsch (1994) model predictions for different values of α, the relative PBS/W contribution to density fluctuations. Image reproduced by permission from Bavassano et al. (2004), copyright EGU

wind (Tu and Marsch 1994), although in a less pronounced way. Different panels of Fig. 5.7 refer to different heliocentric distances within the polar wind. Namely, going from P1 to P4 is equivalent to move from 1.4 to 4 AU. A comparison between these panels indicates that the observed distribution tends to shift towards higher values of α (i.e., pressure-balanced structures become increasingly important), which probably is a radial distance effect.

Finally, the relative density fluctuations dependence on the turbulent Mach number M (the ratio between velocity fluctuation amplitude and sound speed) is shown in Fig. 5.8. The aim is to look for the presence, in the observed fluctuations, of nearly incompressible MHD behaviors. In the framework of the NI theory (Zank and Matthaeus 1991, 1993) two different scalings for the relative density fluctuations are possible, as M or as M^2, depending on the role that thermal conduction effects may play in the plasma under study (namely a heat-fluctuation-dominated or a heat-fluctuation-modified behavior, respectively). These scalings are shown in Fig. 5.8 as solid (for M) and dashed (for M^2) lines.

It is clearly seen that for all the polar wind samples no clear trend emerges in the data. Thus, NI-MHD effects do not seem to play a relevant role in driving the

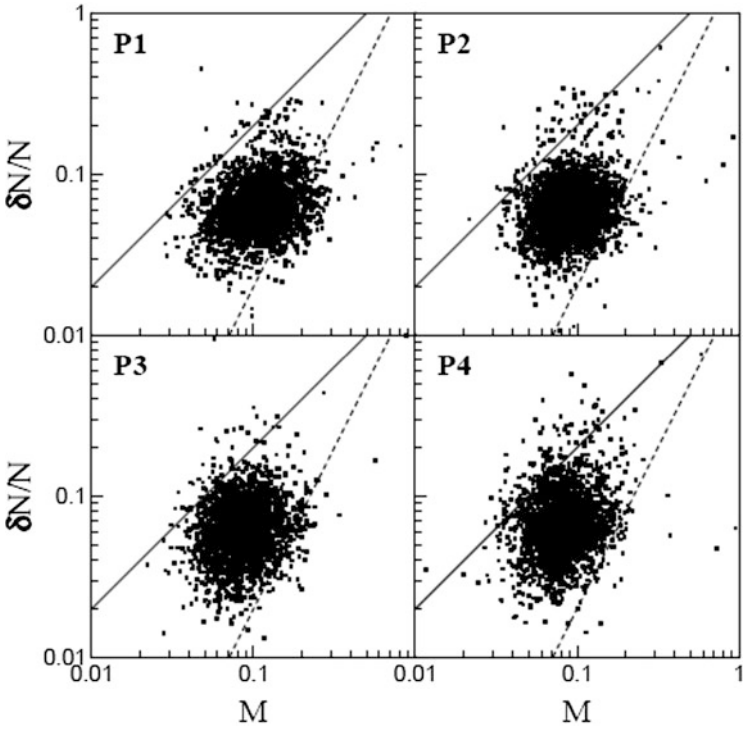

Fig. 5.8 Relative amplitude of density fluctuations vs. turbulent Mach number for polar wind. *Solid and dashed lines* indicate the M and M^2 scalings, respectively. Image reproduced by permission from Bavassano et al. (2004), copyright EGU

polar wind fluctuations. This confirms previous results in the ecliptic by Helios in the inner heliosphere (Bavassano et al. 1995; Bavassano and Bruno 1995) and by Voyagers in the outer heliosphere (Matthaeus et al. 1991). It is worthy of note that, apart from the lack of NI trends, the experimental data from Ulysses, Voyagers, and Helios missions in all cases exhibit quite similar distributions. In other words, for different heliospheric regions, solar wind regimes, and solar activity conditions, the behavior of the compressive fluctuations in terms of relative density fluctuations and turbulent Mach numbers seems almost to be an invariant feature.

The above observations fully support the view that compressive fluctuations in high latitude solar wind are a mixture of MHD modes and pressure balanced structures. It has to be reminded that previous studies (McComas et al. 1995, 1996; Reisenfeld et al. 1999) indicated a relevant presence of pressure balanced structures at hourly scales. Moreover, nearly-incompressible (see Sect. 5.1) effects do not seem to play any relevant role. Thus, polar observations do not show major differences when compared with ecliptic observations in fast wind, the only possible difference being a major role of pressure balanced structures.

5.3 The Effect of Compressive Phenomena on Alfvénic Correlations

A lack of $\delta\mathbf{V}-\delta\mathbf{B}$ correlation does not strictly indicate a lack of Alfvénic fluctuations since a superposition of both outward and inward oriented fluctuations of the same amplitude would produce a very low correlation as well. In addition, the rather complicated scenario at the base of the corona, where both kinetic and magnetic phenomena contribute to the birth of the wind, suggest that the imprints of such a structured corona is carried away by the wind during its expansion. At this point, we would expect that solar wind fluctuations would not solely be due to the ubiquitous Alfvénic and other MHD propagating modes but also to an underlying structure convected by the wind, not necessarily characterized by Alfvén-like correlations. Moreover, dynamical interactions between fast and slow wind, built up during the expansion, contribute to increase the compressibility of the medium.

It has been suggested that disturbances of the mean magnetic field intensity and plasma density act destructively on $\delta\mathbf{V} - \delta\mathbf{B}$ correlation. Bruno and Bavassano (1993) analyzed the loss of the Alfvénic character of interplanetary fluctuations in the inner heliosphere within the low frequency part of the Alfvénic range, i.e., between 2 and 10 h. Figure 5.9, from their work, shows the wind speed profile, σ_c, the correlation coefficients, phase and coherence for the three components (see Sect. 3.2.3), the angle between magnetic field and velocity minimum variance directions, and the heliocentric distance. Magnetic field sectors were rectified (see Sect. 4.1) and magnetic field and velocity components were rotated into the magnetic field minimum variance reference system (see Sect. 3.3.6). Although the three components behave in a similar way, the most Alfvénic ones are the two components Y and Z transverse to the minimum variance component X. As a matter of fact, for an Alfvén mode we would expect a high $\delta V - \delta B$ correlation, a phase close to zero for outward waves and a high coherence. Moreover, it is rather clear that the most Alfvénic intervals are located within the trailing edges of high velocity streams. However, as the radial distance increases, the Alfvénic character of the fluctuations decreases and the angle Θ_{bv} increases. The same authors found that high values of Θ_{bv} are associated with low values of σ_c and correspond to the most compressive intervals. They concluded that the depletion of the Alfvénic character of the fluctuations, within the hourly frequency range, might be driven by the interaction with static structures or magnetosonic perturbations able to modify the homogeneity of the background medium on spatial scales comparable to the wavelength of the Alfvénic fluctuations. A subsequent paper by Klein et al. (1993) showed that the $\delta\mathbf{V} - \delta\mathbf{B}$ decoupling increases with the plasma β, suggesting that in regions where the local magnetic field is less relevant, compressive events play a major role in this phenomenon.

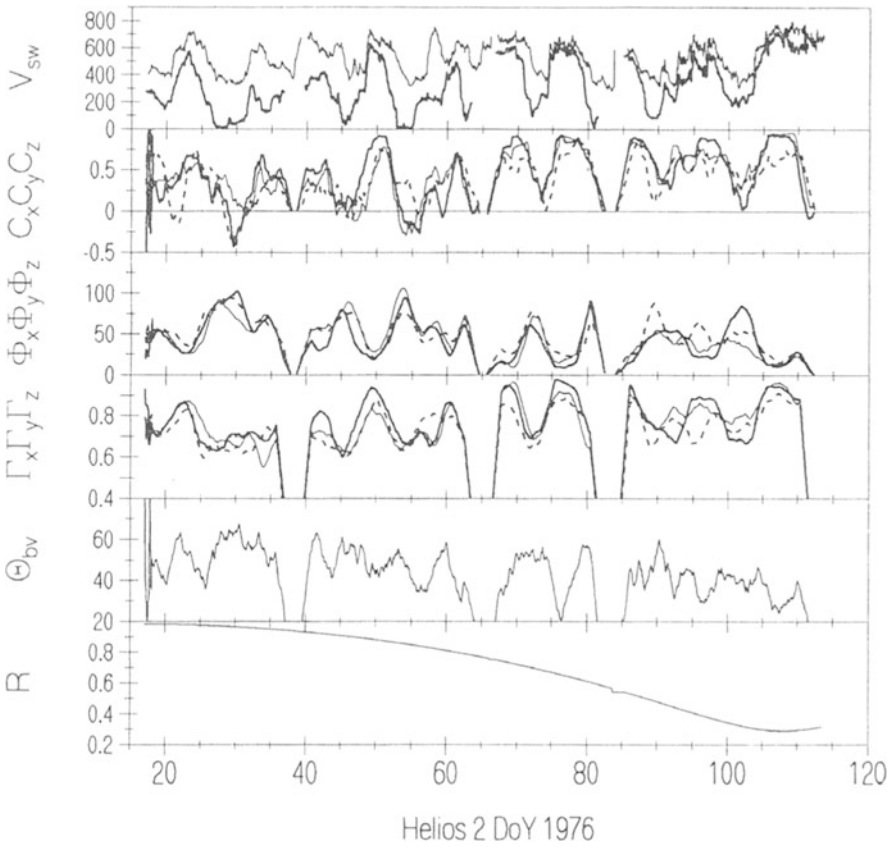

Fig. 5.9 Wind speed profile V and $|\sigma_c|V$ are shown in the *top panel*. The *lower three panels* refer to correlation coefficient, phase angle and coherence for the three components of δV and δB fluctuations, respectively. The *successive panel* indicates the value of the angle between magnetic field and velocity fluctuations minimum variance directions. The *bottom panel* refers to the heliocentric distance (from Bruno and Bavassano 1993)

References

A. Barnes, Hydromagnetic waves and turbulence in the solar wind, in *Solar System Plasma Physics*, vol. 1, ed. by E.N. Parker, C.F. Kennel, L.J. Lanzerotti (North-Holland, Amsterdam, 1979), pp. 249–319

B. Bavassano, R. Bruno, Density fluctuations and turbulent mach number in the inner solar wind. J. Geophys. Res. **100**, 9475–9480 (1995)

B. Bavassano, M. Dobrowolny, F. Mariani, N.F. Ness, Radial evolution of power spectra of interplanetary Alfvénic turbulence. J. Geophys. Res. **87**, 3617–3622 (1982a). doi:10.1029/JA087iA05p03617

B. Bavassano, M. Dobrowolny, G. Fanfoni, F. Mariani, N.F. Ness, Statistical properties of MHD fluctuations associated with high-speed streams from Helios 2 observations. Solar Phys. **78**, 373–384 (1982b). doi:10.1007/BF00151617

B. Bavassano, R. Bruno, L. Klein, Density–temperature correlation in solar wind MHD fluctuations: a test for nearly incompressible models. J. Geophys. Res. **100**, 5871–5875 (1995). doi:10.1029/94JA02571

B. Bavassano, R. Bruno, H. Rosenbauer, Compressive fluctuations in the solar wind and their polytropic index. Ann. Geophys. **14**(5), 510–517 (1996a). doi:10.1007/s00585-996-0510-z

B. Bavassano, R. Bruno, H. Rosenbauer, MHD compressive turbulence in the solar wind and the nearly incompressible approach. Astrophys. Space Sci. **243**, 159–169 (1996b). doi:10.1007/BF00644047

B. Bavassano, E. Pietropaolo, R. Bruno, Compressive fluctuations in high-latitude solar wind. Ann. Geophys. **22**(2), 689–696 (2004). doi:10.5194/angeo-22-689-2004

R. Bruno, B. Bavassano, Origin of low cross-helicity regions in the solar wind. J. Geophys. Res. **96**, 7841–7851 (1991). doi:10.1029/91JA00144

R. Bruno, B. Bavassano, Cross-helicity depletions in the inner heliosphere, and magnetic field and velocity fluctuation decoupling. Planet. Space Sci. **41**, 677–685 (1993). doi:10.1016/0032-0633(93)90052-4

R. Bruno, B. Bavassano, U. Villante, Evidence for long period Alfvén waves in the inner solar system. J. Geophys. Res. **90**(9), 4373–4377 (1985). doi:10.1029/JA090iA05p04373

R. Bruno, B. Bavassano, E. Pietropaolo, On the nature of Alfvénic 'inward' modes in the solar wind, in *Solar Wind Eight*, ed. by D. Winterhalter, J.T. Gosling, S.R. Habbal, W.S. Kurth, M. Neugebauer. AIP Conference Proceedings, vol. 382 (American Institute of Physics, Woodbury, 1996), pp. 229–232. doi:10.1063/1.51389

L.F. Burlaga, K.W. Ogilvie, Magnetic and thermal pressures in the solar wind. Solar Phys. **15**, 61–99 (1970). doi:10.1007/BF00149472

A. Buttighoffer, M. Pick, E.C. Roelof, S. Hoang, A. Mangeney, L.J. Lanzerotti, R.J. Forsyth, J.L. Phillips, Coronal electron stream and Langmuir wave detection inside a propagation channel at 4.3 AU. J. Geophys. Res. **100**, 3369–3381 (1995). doi:10.1029/94JA02033

A. Buttighoffer, L.J. Lanzerotti, D.J. Thomson, C.G. Maclennan, R.J. Forsyth, Spectral analysis of the magnetic field inside particle propagation channels detected by Ulysses. Astron. Astrophys. **351**, 385–392 (1999)

S. Chandrasekhar, *An Introduction to the Study of Stellar Structure* (Dover, New York, 1967)

R. Courant, K.O. Friedrichs, *Supersonic Flow and Shock Waves*. Applied Mathematical Sciences, vol. 21 (Springer, Berlin, 1976)

R. Grappin, A. Mangeney, E. Marsch, On the origin of solar wind MHD turbulence – Helios data revisited. J. Geophys. Res. **95**(14), 8197–8209 (1990). doi:10.1029/JA095iA06p08197

R. Grappin, J. Léorat, A. Buttighoffer, Alfvén wave propagation in the high solar corona. Astron. Astrophys. **362**, 342–358 (2000)

L. Klein, R. Bruno, B. Bavassano, H. Rosenbauer, Anisotropy and minimum variance of magnetohydrodynamic fluctuations in the inner heliosphere. J. Geophys. Res. **98**(17), 17461–17466 (1993). doi:10.1029/93JA01522

E. Marsch, C.-Y. Tu, Spectral and spatial evolution of compressible turbulence in the inner solar wind. J. Geophys. Res. **95**(14), 11945–11956 (1990). doi:10.1029/JA095iA08p11945

E. Marsch, C.-Y. Tu, Correlations between the fluctuations of pressure, density, temperature and magnetic field in the solar wind. Ann. Geophys. **11**, 659–677 (1993a)

E. Marsch, C.-Y. Tu, Modeling results on spatial transport and spectral transfer of solar wind Alfvénic turbulence. J. Geophys. Res. **98**(17), 21045–21059 (1993b). doi:10.1029/93JA02365

W.H. Matthaeus, M.R. Brown, Nearly incompressible magnetohydrodynamics at low mach number. Phys. Fluids **31**, 3634–3644 (1988). doi:10.1063/1.866880

W.H. Matthaeus, L.W. Klein, S. Ghosh, M.R. Brown, Nearly incompressible magnetohydrodynamics, pseudosound, and solar wind fluctuations. J. Geophys. Res. **96**(15), 5421–5435 (1991). doi:10.1029/90JA02609

D.J. McComas, B.L. Barraclough, J.T. Gosling, C.M. Hammond, J.L. Phillips, M. Neugebauer, A. Balogh, R.J. Forsyth, Structures in the polar solar wind: plasma and field observations from Ulysses. J. Geophys. Res. **100**(9), 19893–19902 (1995). doi:10.1029/95JA01634

D.J. McComas, G.W. Hoogeveen, J.T. Gosling, J.L. Phillips, M. Neugebauer, A. Balogh, R.J. Forsyth, Ulysses observations of pressure-balance structures in the polar solar wind. Astron. Astrophys. **316**, 368–373 (1996)

K.G. McCracken, N.F. Ness, The collimation of cosmic rays by the interplanetary magnetic field. J. Geophys. Res. **71**, 3315–3325 (1966)

D. Montgomery, M.R. Brown, W.H. Matthaeus, Density fluctuation spectra in magnetohydrodynamic turbulence. J. Geophys. Res. **92**(11), 282–284 (1987). doi:10.1029/JA092iA01p00282

E.N. Parker, Theory of solar wind, in *Proceedings of the International Conference on Cosmic Rays*. Solar Particles and Sun-Earth Relations, vol. 1 (Tata Institute of Fundamental Research, Bombay, 1963), p. 175

D.B. Reisenfeld, D.J. McComas, J.T. Steinberg, Evidence of a solar origin for pressure balance structures in the high-latitude solar wind. Geophys. Res. Lett. **26**, 1805–1808 (1999). doi:10.1029/1999GL900368

D.A. Roberts, Observation and simulation of the radial evolution and stream structure of solar wind turbulence, in *Solar Wind Seven*, ed. by E. Marsch, R. Schwenn. COSPAR Colloquia Series, vol. 3 (Pergamon Press, Oxford, 1992), pp. 533–538

D.A. Roberts, M.L. Goldstein, L.W. Klein, W.H. Matthaeus, Origin and evolution of fluctuations in the solar wind: Helios observations and Helios–Voyager comparisons. J. Geophys. Res. **92**(11), 12023–12035 (1987). doi:10.1029/JA092iA11p12023

D.A. Roberts, S. Ghosh, M.L. Goldstein, W.H. Matthaeus, Magnetohydrodynamic simulation of the radial evolution and stream structure of solar-wind turbulence. Phys. Rev. Lett. **67**, 3741–3744 (1991). doi:10.1103/PhysRevLett.67.3741

D.A. Roberts, M.L. Goldstein, W.H. Matthaeus, S. Ghosh, Velocity shear generation of solar wind turbulence. J. Geophys. Res. **97**(16), 17115– (1992). doi:10.1029/92JA01144

G.L. Siscoe, L. Davis, P.J. Coleman, E.J. Smith, D.E. Jones, Power spectra and discontinuities of the interplanetary magnetic field: Mariner 4. J. Geophys. Res. **73**(12), 61–99 (1968). doi:10.1029/JA073i001p00061

K.M. Thieme, R. Schwenn, E. Marsch, Are structures in high-speed streams signatures of coronal fine structures? Adv. Space Res. **9**, 127–130 (1989). doi:10.1016/0273-1177(89)90105-1

C.-Y. Tu, E. Marsch, On the nature of compressive fluctuations in the solar wind. J. Geophys. Res. **99**(18), 21481 (1994)

C.-Y. Tu, E. Marsch, H. Rosenbauer, Temperature fluctuation spectra in the inner solar wind. Ann. Geophys. **9**, 748–753 (1991)

M. Vellante, A.J. Lazarus, An analysis of solar wind fluctuations between 1 and 10 AU. J. Geophys. Res. **92**(17), 9893–9900 (1987). doi:10.1029/JA092iA09p09893

G.P. Zank, W.H. Matthaeus, Nearly incompressible hydrodynamics and heat conduction. Phys. Rev. Lett. **64**, 1243–1246 (1990). doi:10.1103/PhysRevLett.64.1243

G.P. Zank, W.H. Matthaeus, The equations of nearly incompressible fluids. i. Hydrodynamics, turbulence, and waves. Phys. Fluids A **3**, 69–82 (1991). doi:10.1063/1.857865

G.P. Zank, W.H. Matthaeus, Waves and turbulence in the solar wind. J. Geophys. Res. **97**(16), 17189–17194 (1992). doi:10.1029/92JA01734

G.P. Zank, W.H. Matthaeus, Nearly incompressible fluids. ii – magnetohydrodynamics, turbulence, and waves. Phys. Fluids **5**, 257–273 (1993)

G.P. Zank, W.H. Matthaeus, L.W. Klein, Temperature and density anti-correlations in solar wind fluctuations. Geophys. Res. Lett. **17**, 1239–1242 (1990). doi:10.1029/GL017i009p01239

Chapter 6
A Natural Wind Tunnel

The solar wind has been used as a wind tunnel by Burlaga who, at the beginning of the 1990s, started to investigate anomalous fluctuations (Burlaga 1991a,c,b, 1995) as observed by measurements in the outer heliosphere by the Voyager spacecraft. In 1991, Marsch (1992), in a review on solar wind turbulence given at the *Solar Wind Seven* conference, underlined the importance of investigating scaling laws in the solar wind and we like to report his sentence: "The recent work by Burlaga (1991a,c) opens in my mind a very promising avenue to analyze and understand solar wind turbulence from a new theoretical vantage point. ... This approach may also be useful for MHD turbulence. Possible connections between intermittent turbulence and deterministic chaos have recently been investigated ... We are still waiting for applications of these modern concepts of chaos theory to solar wind MHD fluctuations." (cf. Marsch 1992, p. 503). A few years later Carbone (1993) and, independently, Biskamp (1993) faced the question of anomalous scaling from a theoretical point of view. More than 10 years later the investigation of statistical mechanics of MHD turbulence from one side, and of low-frequency solar wind turbulence on the other side, has produced a lot of papers, and is now mature enough to be tentatively presented in a more organic way.

6.1 Scaling Exponents of Structure Functions

The phenomenology of turbulence developed by Kolmogorov (1941) deals with some statistical hypotheses for fluctuations. The famous footnote remark by Landau (Landau and Lifshitz 1971) pointed out a defect in the Kolmogorov theory, namely the fact that the theory does not take proper account of spatial fluctuations of local dissipation rate (Frisch 1995). This led different authors to investigate the features related to scaling laws of fluctuations and, in particular, to investigate the departure from the Kolmogorov's linear scaling of the structure functions (cf. Sect. 2.8). An

R. Bruno, V. Carbone, *Turbulence in the Solar Wind*, Lecture Notes in Physics 928, DOI 10.1007/978-3-319-43440-7_6

up-to-date comprehensive review of these theoretical efforts can be found in the book by Frisch (1995).

Here we are interested in understanding what we can learn from solar wind turbulence about the basic features of scaling laws for fluctuations. We use velocity and magnetic fields time series, and we investigate the scaling behavior of the high-order moments of stochastic variables defined as variations of fields separated by a time[1] interval τ. First of all, it is worthwhile to remark that scaling laws and, in particular, the exact relation (2.41) which defines the inertial range in fluid flows, is valid for longitudinal (streamwise) fluctuations. In common fluid flows the Kolmogorov linear scaling law is compared with the moments of longitudinal velocity differences. In the same way for the solar wind turbulence we investigate the scaling behavior of $\Delta u_\tau = u(t+\tau) - u(t)$, where $u(t)$ represents the component of the velocity field along the radial direction. As far as the magnetic differences are concerned $\Delta b_\tau = B(t+\tau) - B(t)$, we are free for different choices and, in some sense, this is more interesting from an experimental point of view. We can use the reference system where $B(t)$ represents the magnetic field projected along the radial direction, or the system where $B(t)$ represents the magnetic field along the local background magnetic field, or $B(t)$ represents the field along the minimum variance direction. As a different case we can simply investigate the scaling behavior of the fluctuations of the magnetic field intensity.

Let us consider the pth moment of both absolute values[2] of velocity fluctuations $R_p(\tau) = \langle |\Delta u_\tau|^p \rangle$ and magnetic fluctuations $S_p(\tau) = \langle |\Delta b_\tau|^p \rangle$, also called pth order structure function in literature (brackets being time average). Here we use magnetic fluctuations across structures at intervals τ calculated by using the magnetic field intensity. Typical structure functions of magnetic field fluctuations, for two different values of p, for both a slow wind and a fast wind at 0.9 AU, are shown in Fig. 6.1. The magnetic field we used is that measured by Helios 2 spacecraft. Structure functions calculated for the velocity fields have roughly the same shape. Looking at these figures the typical scaling features of turbulence can be observed. Starting from low values at small scales, the structure functions increase towards a region where $S_p \to$ const. at the largest scales. This means that at these scales the field fluctuations are uncorrelated. A kind of "inertial range", that is a region of intermediate scales τ

[1] Since the solar wind moves at supersonic speed V_{sw}, the usual Taylor's hypothesis is verified, and we can get information on spatial scaling laws ℓ by using time differences $\tau = \ell / V_{sw}$.

[2] Note that, according to the occurrence of the Yaglom's law, that is a third-order moment is different from zero, the fluctuations at a given scale in the inertial range must present some non-Gaussian features. From this point of view the calculation of structure functions with the absolute value is unappropriate because in this way we risk to cancel out non-Gaussian features. Namely we symmetrize the probability density functions of fluctuations. However, in general, the number of points at disposal is much lower than required for a robust estimate of odd structure functions, even in usual fluid flows. Then, as usually, we will obtain structure functions by taking the absolute value, even if some care must be taken in certain conclusions which can be found in literature.

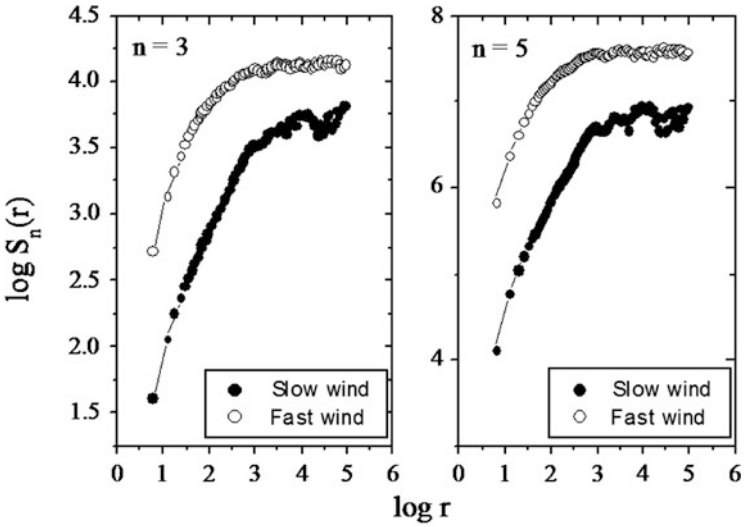

Fig. 6.1 Structure functions for the magnetic field intensity $S_n(r)$ for two different orders, $n = 3$ and $n = 5$, for both slow wind and fast wind, as a function of the time scale r. Data come from Helios 2 spacecraft at 0.9 AU

where a power law can be recognized for both

$$R_p(\tau) = \langle |\Delta u_\tau|^p \rangle \sim \tau^{\zeta_p}$$
$$S_p(\tau) = \langle |\Delta b_\tau|^p \rangle \sim \tau^{\xi_p} \tag{6.1}$$

is more or less visible only for the slow wind. In this range correlations exists, and we can obtain the scaling exponents ζ_p and ξ_p through a simple linear fit.

Since as we have seen, Yaglom's law is observed only in some few samples, the inertial range in the whole solar wind is not well defined. A look at Fig. 6.1 clearly shows that we are in a situation similar to a low-Reynolds number fluid flow. In order to compare scaling exponents of the solar wind turbulent fluctuations with other experiments, it is perhaps better to try to recover exponents using the Extended Self-Similarity (ESS), introduced some time ago by Benzi et al. (1993), and used here as a tool to determine relative scaling exponents. In the fluid-like case, the third-order structure function can be regarded as a generalized scaling using the inverse of Eq. (2.42) or of Eq. (2.41) (Politano et al. 1998). Then, we can plot the pth order structure function vs. the third-order one to recover at least relative scaling exponents ζ_p/ζ_3 and ξ_p/ξ_3 (6.1). Quite surprisingly (see Fig. 6.2), we find that the range where a power law can be recovered extends well beyond the inertial range, covering almost all the experimental range. In the fluid case the scaling exponents which can be obtained through ESS at low or moderate Reynolds numbers, coincide with the scaling exponents obtained for high Reynolds, where the inertial range is very well defined (Benzi et al. 1993). This is due to the fact that, since by definition

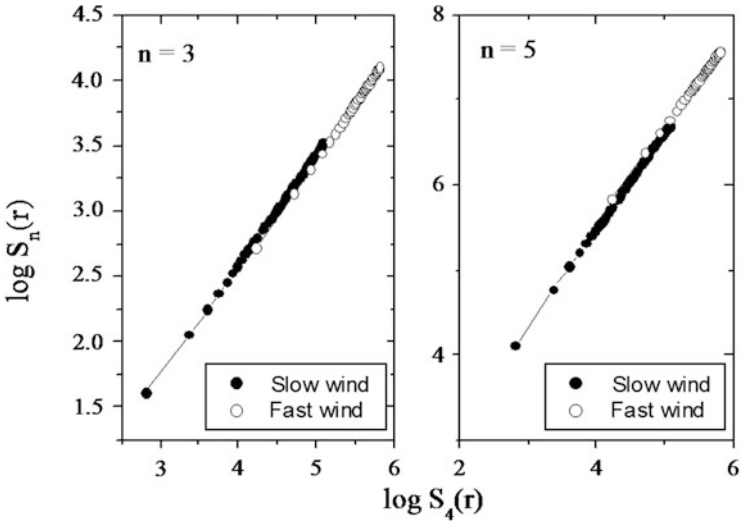

Fig. 6.2 Structure functions $S_n(r)$ for two different orders, $n = 3$ and $n = 5$, for both slow wind and high wind, as a function of the fourth-order structure function $S_4(r)$. Data come from Helios 2 spacecraft at 0.9 AU

$\zeta_3 = 1$ in the inertial range (Frisch 1995), whatever its extension might be. In our case scaling exponents obtained through ESS can be used as a surrogate, since we cannot be sure that an inertial range exists.

It is worthwhile to remark (as shown in Fig. 6.2) that we can introduce a general scaling relation between the qth order velocity structure function and the pth order structure function, with a relative scaling exponent $\alpha_p(q)$. It has been found that this relation becomes an exact relation

$$S_q(r) = \left[S_p(r)\right]^{\alpha_p(q)},$$

when the velocity structure functions are normalized to the average velocity within each period used to calculate the structure function (Carbone et al. 1996a). This is very interesting because it implies that the above relationship is satisfied by the following probability distribution function, if we assume that odd moments are much smaller than the even ones (Carbone et al. 1996a):

$$PDF(\Delta u_\tau) = \int_{-\infty}^{\infty} dk\, e^{ik\Delta u_\tau} \sum_{q=0}^{\infty} \frac{(ik)^{2q}}{2\pi(2q)!} \left[S_p(\tau)\right]^{\alpha_p(2q)}. \tag{6.2}$$

That is, for each scale τ the knowledge of the relative scaling exponents $\alpha_p(q)$ completely determines the probability distribution of velocity differences as a function of a single parameter $S_p(\tau)$.

Table 6.1 Scaling exponents for velocity ζ_p and magnetic ξ_p variables calculated through ESS

p	ζ_p	ξ_p	$u(t)$ (fluid)	$T(t)$ (fluid)
1	0.37 ± 0.06	0.56 ± 0.06	0.37	0.61
2	0.70 ± 0.05	0.83 ± 0.05	0.70	0.85
3	1.00	1.00	1.00	1.00
4	1.28 ± 0.02	1.14 ± 0.02	1.28	1.12
5	1.54 ± 0.03	1.25 ± 0.03	1.54	1.21
6	1.79 ± 0.05	1.35 ± 0.05	1.78	1.38

Errors represent the standard deviations of the linear fitting. The data used comes from a turbulent sample of slow wind at 0.9 AU from Helios 2 spacecraft. As a comparison we show the normalized scaling exponents of structure functions calculated in a wind tunnel on Earth (Ruíz-Chavarría et al. 1995) for velocity and temperature. The temperature is a passive scalar in this experiment

Relative scaling exponents, calculated by using data coming from Helios 2 at 0.9 AU, are reported in Table 6.1. As it can be seen, two main features can be noted:

1. There is a significant departure from the Kolmogorov linear scaling, that is, real scaling exponents are anomalous and seem to be non-linear functions of p, say $\zeta_p/\zeta_3 > p/3$ for $p < 3$, while $\zeta_p/\zeta_3 < p/3$ for $p > 3$. The same behavior can be observed for ξ_p/ξ_3. In Table 6.1 we report also the scaling exponents obtained in usual fluid flows for velocity and temperature, the latter being a passive scalar. Scaling exponents for velocity field are similar to scaling exponents obtained in turbulent flows on Earth, showing a kind of universality in the anomaly. This effect is commonly attributed to the phenomenon of *intermittency* in fully developed turbulence (Frisch 1995). Turbulence in the solar wind is intermittent, just like its fluid counterpart on Earth.
2. The degree of intermittency is measured through the distance between the curve ζ_p/ζ_3 and the linear scaling $p/3$. It can be seen that the magnetic field is more intermittent than the velocity field. The same difference is observed between the velocity field and a passive scalar (in our case the temperature) in ordinary fluid flows (Ruíz-Chavarría et al. 1995). That is the magnetic field, as long as intermittency properties are concerned, has the same scaling laws of a passive field. Of course *this does not mean that the magnetic field plays the same role as a passive field.* Statistical properties are in general different from dynamical properties.

In Table 6.1 we show scaling exponents up to the sixth order. Actually, a question concerns the validation of high-order moments estimates, say the maximum value of the order p which can be determined with a finite number of points of our dataset. As the value of p increases, we need an increasing number of points for an optimal determination of the structure function (Tennekes and Wyngaard 1972). Anomalous

scaling laws are generated by rare and intense events due to singularities in the gradients: the higher their intensity the more rare these events are. Of course, when the data set has a finite extent, the probability to get singularities stronger than a certain value approaches zero. In that case, scaling exponents ζ_p of order higher than a certain value become linear functions of p. Actually, the structure function $S_p(\tau)$ depends on the probability distribution function $\mathrm{PDF}(\Delta u_\tau)$ through

$$S_p(\tau) = \int \Delta u_\tau^p \, \mathrm{PDF}(\delta u_\tau) \, d\Delta u_\tau$$

and, the function S_p is determined only when the integral converges. As p increases, the function $F_p(\delta u_\tau) = \Delta u_\tau^p \, \mathrm{PDF}(\Delta u_\tau)$ becomes more and more disturbed, with some spikes, so that the integral becomes more and more undefined, as can be seen for example in Fig. 1 of the paper by Dudok de Wit (2004). A simple calculation (Dudok de Wit 2004) for the maximum value of the order p_m which can reliably be estimated with a given number N of points in the dataset, gives the empirical criterion $p_m \simeq \log N$. Structure functions of order $p > p_m$ cannot be determined accurately.

Only few large structures are enough to generate the anomalous scaling laws. In fact, as shown by Salem et al. (2009), by suppressing through wavelets analysis just a few percentage of large structures on all scales, the scaling exponents become linear functions of p, respectively $p/4$ and $p/3$ for the kinetic and magnetic fields.

As far as a comparison between different plasmas is concerned, the scaling exponents of magnetic structure functions, obtained from laboratory plasma experiments of a Reversed-Field Pinch at different distances from the external wall (Carbone et al. 2000) are shown in Table 6.2. In laboratory plasmas it is difficult to measure all the components of the vector field at the same time, thus, here we show only the scaling exponents obtained using magnetic field differences $B_r(t+\tau) - B_r(t)$ calculated from the radial component in a toroidal device where the z-axis is directed along the axis of the torus. As it can be seen, intermittency in magnetic turbulence is not so strong as it appears to be in the solar wind, actually the degree of intermittency

Table 6.2 Normalized scaling exponents ξ_p/ξ_3 for radial magnetic fluctuations in a laboratory plasma, as measured at different distances a/R ($R \simeq 0.45$ cm being the minor radius of the torus in the experiment) from the external wall

p	$a/R = 0.96$	$a/R = 0.93$	$a/R = 0.90$	$a/R = 0.86$
1	0.39 ± 0.01	0.38 ± 0.01	0.37 ± 0.01	0.36 ± 0.01
2	0.74 ± 0.01	0.73 ± 0.02	0.71 ± 0.01	0.70 ± 0.01
3	1.00	1.00	1.00	1.00
4	1.20 ± 0.02	1.24 ± 0.02	1.27 ± 0.01	1.28 ± 0.01
5	1.32 ± 0.03	1.41 ± 0.03	1.51 ± 0.03	1.55 ± 0.03
6	1.38 ± 0.04	1.50 ± 0.04	1.71 ± 0.03	1.78 ± 0.04

Errors represent the standard deviations of the linear fitting. Scaling exponents have been obtained using the ESS

Table 6.3 Normalized scaling exponents ξ_p/ξ_3 for Alfvénic, velocity, and magnetic fluctuations obtained from data of high resolution 2D MHD numerical simulations

p	Z^+	Z^-	v	B
1	0.36 ± 0.06	0.56 ± 0.06	0.37 ± 0.01	0.46 ± 0.02
2	0.70 ± 0.05	0.83 ± 0.05	0.70 ± 0.01	0.78 ± 0.01
3	1.00	1.00	1.00	1.00
4	1.28 ± 0.02	1.14 ± 0.02	1.28 ± 0.02	1.18 ± 0.02
5	1.53 ± 0.03	1.25 ± 0.03	1.54 ± 0.03	1.31 ± 0.03
6	1.79 ± 0.05	1.35 ± 0.05	1.78 ± 0.05	1.40 ± 0.03

Scaling exponents have been calculated from spatial fluctuations; different times, in the statistically stationary state, have been used to improve statistics. The scaling exponents have been calculated by ESS using Eq. (2.41) as characteristic scale rather than the third-order structure function (cf. Politano et al. 1998, for details

increases when going toward the external wall. This last feature appears to be similar to what is currently observed in channel flows, where intermittency also increases when going towards the external wall (Pope 2000).

Scaling exponents of structure functions for Alfvén variables, velocity, and magnetic variables have been calculated also for high resolution 2D incompressible MHD numerical simulations (Politano et al. 1998). In this case, we are freed from the constraint of the Taylor hypothesis when calculating the fluctuations at a given scale. From 2D simulations we recover the fields $\mathbf{u}(\mathbf{r}, t)$ and $\mathbf{b}(\mathbf{r}, t)$ at some fixed times. We calculate the longitudinal fluctuations directly in space at a fixed time, namely $\Delta u_\ell = [\mathbf{u}(\mathbf{r} + \ell, t) - \mathbf{u}(\mathbf{r}, t)] \cdot \ell/\ell$ (the same are made for different fields, namely the magnetic field or the Elsässer fields). Finally, averaging both in space and time, we calculate the scaling exponents through the structure functions. These scaling exponents are reported in Table 6.3. Note that, even in numerical simulations, intermittency for magnetic variables is stronger than for the velocity field.

6.2 Probability Distribution Functions and Self-Similarity of Fluctuations

The presence of scaling laws for fluctuations is a signature of the presence of self-similarity in the phenomenon. A given observable $u(\ell)$, which depends on a scaling variable ℓ, is invariant with respect to the scaling relation $\ell \to \lambda\ell$, when there exists a parameter $\mu(\lambda)$ such that $u(\ell) = \mu(\lambda)u(\lambda\ell)$. The solution of this last relation is a power law $u(\ell) = C\ell^h$, where the scaling exponent is $h = -\log_\lambda \mu$.

Since, as we have just seen, turbulence is characterized by scaling laws, this must be a signature of self-similarity for fluctuations. Let us see what this means. Let us consider fluctuations at two different scales, namely $\Delta z_\ell^\pm$ and $\Delta z_{\lambda\ell}^\pm$. Their ratio $\Delta z_{\lambda\ell}^\pm / \Delta z_\ell^\pm \sim \lambda^h$ depends only on the value of h, and this should imply that fluctuations are self-similar. This means that PDFs are related through

$$P(\Delta z_{\lambda\ell}^\pm) = \mathrm{PDF}(\lambda^h \Delta z_\ell^\pm).$$

Let us consider the normalized variables

$$y_\ell^\pm = \frac{\Delta z_\ell^\pm}{\langle (\Delta z_\ell^\pm)^2 \rangle^{1/2}}.$$

When h is unique or in a pure self-similar situation, PDFs are related through $P(y_\ell^\pm) = \mathrm{PDF}(y_{\lambda\ell}^\pm)$, say by changing scale PDFs coincide.

The PDFs relative to the normalized magnetic fluctuations $\delta b_\tau = \Delta b_\tau / \langle \Delta b_\tau^2 \rangle^{1/2}$, at three different scales τ, are shown in Fig. 6.3. It appears evident that the global self-similarity in real turbulence is broken. PDFs do not coincide at different scales,

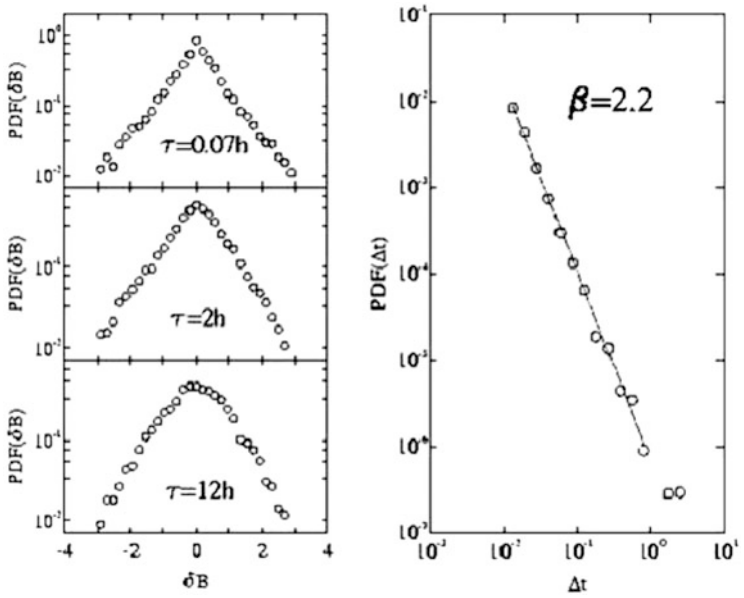

Fig. 6.3 *Left panel*: normalized PDFs for the magnetic fluctuations observed in the solar wind turbulence by using Helios data. *Right panel*: distribution function of waiting times Δt between structures at the smallest scale. The parameter β is the scaling exponent of the scaling relation $\mathrm{PDF}(\Delta t) \sim \Delta t^{-\beta}$ for the distribution function of waiting times

rather their shape seems to depend on the scale τ. In particular, at large scales PDFs seem to be almost Gaussian, but they become more and more stretched as τ decreases. At the smallest scale PDFs are stretched exponentials. This scaling dependence of PDFs is a different way to say that scaling exponents of fluctuations are anomalous, or can be taken as a different definition of intermittency. Note that the wings of PDFs are higher than those of a Gaussian function. This implies that intense fluctuations have a probability of occurrence higher than that they should have if they were Gaussianly distributed. Said differently, intense stochastic fluctuations are less rare than we should expect from the point of view of a Gaussian approach to the statistics. These fluctuations play a key role in the statistics of turbulence. The same statistical behavior can be found in different experiments related to the study of the atmosphere (see Fig. 6.4) and the laboratory plasma (see Fig. 6.5).

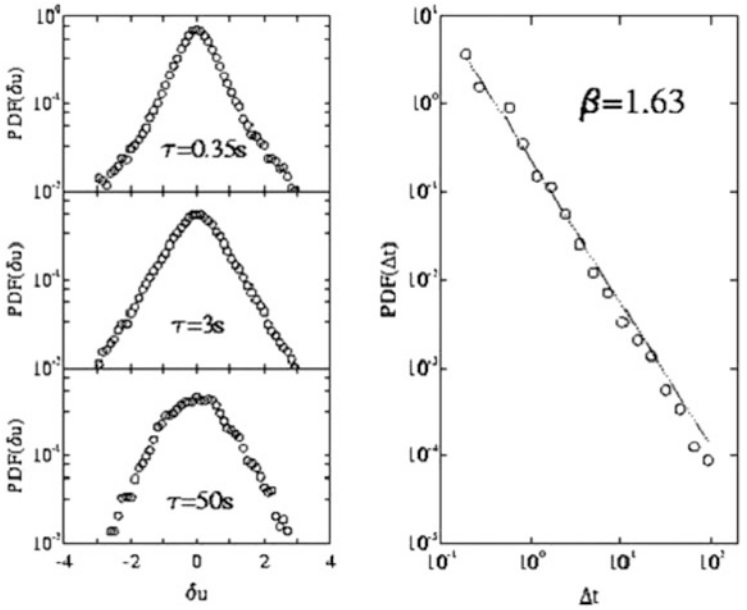

Fig. 6.4 *Left panel*: normalized PDFs of velocity fluctuations in atmospheric turbulence. *Right panel*: distribution function of waiting times Δt between structures at the smallest scale. The parameter β is the scaling exponent of the scaling relation $\mathrm{PDF}(\Delta t) \sim \Delta t^{-\beta}$ for the distribution function of waiting times. The turbulent samples have been collected above a grass-covered forest clearing at 5 m above the ground surface and at a sampling rate of 56 Hz (Katul et al. 1997)

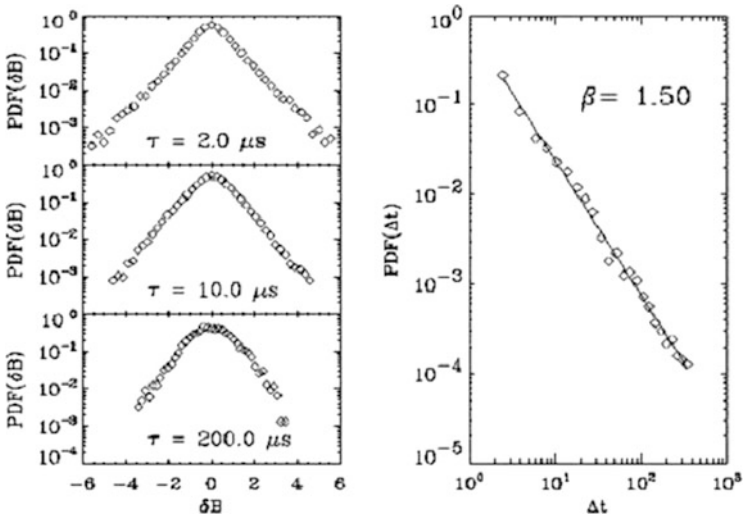

Fig. 6.5 *Left panel*: normalized PDFs of the radial magnetic field collected in RFX magnetic turbulence (Carbone et al. 2000). *Right panel*: distribution function of waiting times Δt between structures at the smallest scale. The parameter β is the scaling exponent of the scaling relation $\mathrm{PDF}(\Delta t) \sim \Delta t^{-\beta}$ for the distribution function of waiting times

6.3 What is Intermittent in the Solar Wind Turbulence? The Multifractal Approach

Time dependence of Δu_τ and Δb_τ for three different scales τ is shown in Figs. 6.6 and 6.7, respectively. These plots show that, as τ becomes small, intense fluctuations become more and more important, and they dominate the statistics. Fluctuations at large scales appear to be smooth while, as the scale becomes smaller, intense fluctuations becomes visible. These dominating fluctuations represent relatively rare events. Actually, at the smallest scales, the time behavior of both Δu_τ and Δb_τ is dominated by regions where fluctuations are low, in between regions where fluctuations are intense and turbulent activity is very high. Of course, this behavior cannot be described by a global self-similar behavior. Allowing the scaling laws to vary with the region of turbulence we are investigating would be more convincing.

The behavior we have just described is at the heart of the multifractal approach to turbulence (Frisch 1995). In that description of turbulence, even if the small scales of fluid flow cannot be globally self-similar, self-similarity can be reintroduced as a local property. In the multifractal description it is conjectured that turbulent flows can be made by an infinite set of points $S_h(\mathbf{r})$, each set being characterized by a scaling law $\Delta Z_\ell^\pm \sim \ell^{h(\mathbf{r})}$, that is, the scaling exponent can depend on the position $\mathbf{r}$. The usual dimension of that set is then not constant, but depends on the local value of h, and is quoted as $D(h)$ in literature.

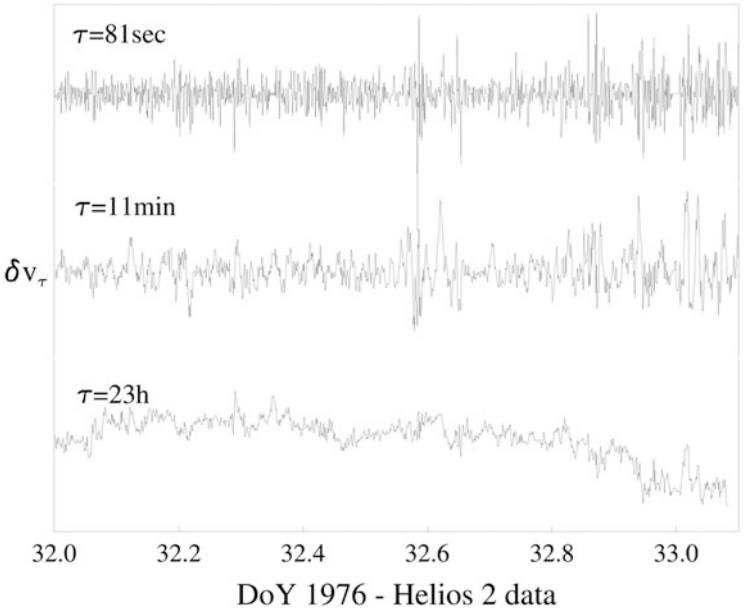

Fig. 6.6 Differences for the longitudinal velocity $\delta u_\tau = u(t+\tau) - u(t)$ at three different scales τ, as shown in the figure

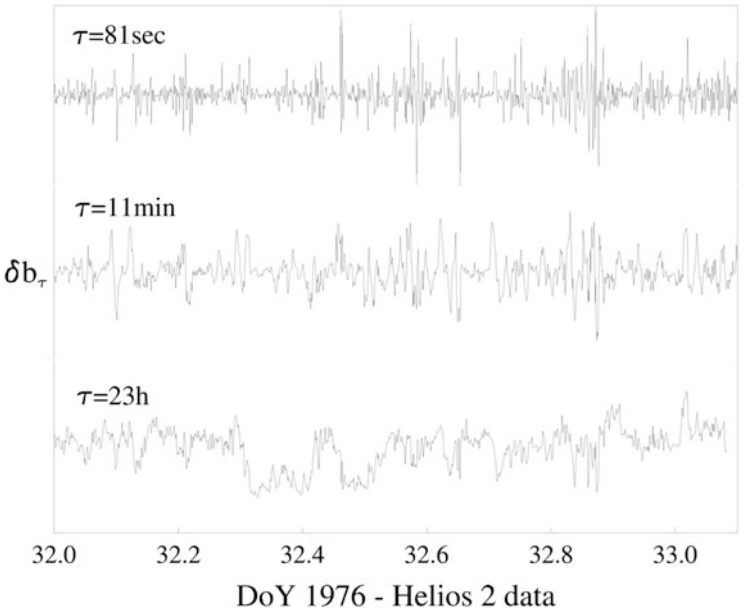

Fig. 6.7 Differences for the magnetic intensity $\Delta b_\tau = B(t+\tau) - B(t)$ at three different scales τ, as shown in the figure

Then, the probability of occurrence of a given fluctuation can be calculated through the weight the fluctuation assumes within the whole flow, i.e.,

$$P(\Delta Z_\ell^\pm) \sim (\Delta Z_\ell^\pm)^h \times \text{volume occupied by fluctuations},$$

and the pth order structure function is immediately written through the integral over all (continuous) values of h weighted by a smooth function $\mu(h) \sim 0(1)$, i.e.,

$$S_p(\ell) = \int \mu(h)(\Delta Z_\ell^\pm)^{ph}(\Delta Z_\ell^\pm)^{3-D(h)}dh.$$

A moment of reflection allows us to realize that in the limit $\ell \to 0$ the integral is dominated by the minimum value (over h) of the exponent and, as shown by Frisch (1995), the integral can be formally solved using the usual saddle-point method. The scaling exponents of the structure function can then be written as

$$\zeta_p = \min_h[ph + 3 - D(h)].$$

In this way, the departure of ζ_p from the linear Kolmogorov scaling and thus intermittency, can be characterized by the continuous changing of $D(h)$ as h varies. That is, as p varies we are probing regions of fluid where even more rare and intense events exist. These regions are characterized by small values of h, that is, by stronger singularities of the gradient of the field.

Owing to the famous Landau footnote on the fact that fluctuations of the energy transfer rate must be taken into account in determining the statistics of turbulence, people tried to interpret the non-linear energy cascade typical of turbulence theory, within a geometrical framework. The old Richardson's picture of the turbulent behavior as the result of a hierarchy of eddies at different scales has been modified and, as realized by Kraichnan (1974), once we leave the idea of a constant energy cascade rate we open a "Pandora's box" of possibilities for modeling the energy cascade. By looking at scaling laws for $\Delta z_\ell^\pm$ and introducing the scaling exponents for the energy transfer rate $\langle \epsilon_\ell^p \rangle \sim r^{\tau_p}$, it can be found that $\zeta_p = p/m + \tau_{p/m}$ (being $m = 3$ when the Kolmogorov-like phenomenology is taken into account, or $m = 4$ when the Iroshnikov-Kraichnan phenomenology holds). In this way the intermittency correction are determined by a cascade model for the energy transfer rate. When τ_p is a non-linear function of p, the energy transfer rate can be described within the multifractal geometry (see, e.g., Meneveau 1991, and references therein) characterized by the generalized dimensions $D_p = 1 - \tau_p/(p-1)$ (Hentschel and Procaccia 1983). The scaling exponents of the structure functions are then related to D_p by

$$\zeta_p = \left(\frac{p}{m} - 1\right) D_{p/m} + 1.$$

The correction to the linear scaling p/m is positive for $p < m$, negative for $p > m$, and zero for $p = m$. A fractal behavior where $D_p = \text{const.} < 1$ gives a linear correction with a slope different from $1/m$.

6.4 Fragmentation Models for the Energy Transfer Rate

Cascade models view turbulence as a collection of fragments at a given scale ℓ, which results from the fragmentation of structures at the scale $\ell' > \ell$, down to the dissipative scale (Novikov 1969). Sophisticated statistics are applied to obtain scaling exponents ζ_p for the pth order structure function.

The starting point of fragmentation models is the old β-model, a "pedagogical" fractal model introduced by Frisch et al. (1978) to account for the modification of the cascade in a simple way. In this model, the cascade is realized through the conjecture that active eddies and non-active eddies are present at each scale, the space-filling factor for the fragments being fixed for each scale. Since it is a fractal model, the β-model gives a *linear* modification to ζ_p. This can account for a fit on the data, as far as small values of p are concerned. However, the whole curve ζ_p is clearly nonlinear, and a multifractal approach is needed.

The random-β model (Benzi et al. 1984), a multifractal modification of the β-model, can be derived by invoking that the space-filling factor for the fragments at a given scale in the energy cascade is not fixed, but is given by a random variable β. The probability of occurrence of a given β is assumed to be a bimodal distribution where the eddies fragmentation process generates either space-filling eddies with probability ξ or planar sheets with probability $(1-\xi)$ (for conservation $0 \leq \xi \leq 1$). It can be found that

$$\zeta_p = \frac{p}{m} - \log_2\left[1 - \xi + \xi 2^{p/m-1}\right], \tag{6.3}$$

where the free parameter ξ can be fixed through a fit on the data.

The p-model (Meneveau 1991; Carbone 1993) consists in an eddies fragmentation process described by a two-scale Cantor set with equal partition intervals. An eddy at the scale ℓ, with an energy derived from the transfer rate ϵ_r, breaks down into two eddies at the scale $\ell/2$, with energies $\mu\epsilon_r$ and $(1-\mu)\epsilon_r$. The parameter $0.5 \leq \mu \leq 1$ is not defined by the model, but is fixed from the experimental data. The model gives

$$\zeta_p = 1 - \log_2\left[\mu^{p/m} + (1-\mu)^{p/m}\right]. \tag{6.4}$$

In the model by She and Leveque (see, e.g., She and Leveque 1994; Politano and Pouquet 1998) one assumes an infinite hierarchy for the moments of the energy transfer rates, leading to $\epsilon_r^{(p+1)} \sim [\epsilon_r^{(p)}]^{\beta}[\epsilon_r^{(\infty)}]^{1-\beta}$, and a divergent scaling law for

the infinite-order moment $\epsilon_r^{(\infty)} \sim r^{-x}$, which describes the most singular structures within the flow. The model reads

$$\zeta_p = \frac{p}{m}(1-x) + \mathrm{C}\left[1 - \left(1 - \frac{x}{\mathrm{C}}\right)^{p/m}\right]. \tag{6.5}$$

The parameter $\mathrm{C} = x/(1-\beta)$ is identified as the codimension of the most singular structures. In the standard MHD case (Politano and Pouquet 1995) $x = \beta = 1/2$, so that $\mathrm{C} = 1$, that is, the most singular dissipative structures are planar sheets. On the contrary, in fluid flows $\mathrm{C} = 2$ and the most dissipative structures are filaments. The large p behavior of the p-model is given by $\zeta_p \sim (p/m)\log_2(1/\mu) + 1$, so that Eqs. (6.4) and (6.5) give the same results providing $\mu \simeq 2^{-x}$. As shown by Carbone et al. (1996b) all models are able to capture intermittency of fluctuations in the solar wind. The agreement between the curves ζ_p and normalized scaling exponents is excellent, and this means that we realistically cannot discriminate between the models we reported above. The main problem is that all models are based on a conjecture which gives a curve ζ_p as a function of a single free parameter, and that curve is able to fit the smooth observed behavior of ζ_p. Statistics cannot prove, just disprove. We can distinguish between the fractal model and multifractal models, but we cannot realistically distinguish among the various multifractal models.

6.5 A Model for the Departure from Self-Similarity

Besides the idea of self-similarity underlying the process of energy cascade in turbulence, a different point of view can be introduced. The idea is to characterize the behavior of the PDFs through the scaling laws of the parameters, which describe how the shape of the PDFs changes when going towards small scales. The model, originally introduced by Castaing et al. (2001), is based on a multiplicative process describing the cascade. In its simplest form the model can be introduced by saying that PDFs of increments $\delta Z_\ell^\pm$, at a given scale, are made as a sum of Gaussian distributions with different widths $\sigma = \langle(\delta Z_\ell^\pm)^2\rangle^{1/2}$. The distribution of widths is given by $G_\lambda(\sigma)$, namely

$$P(\delta Z_\ell^\pm) = \frac{1}{2\pi}\int_0^\infty G_\lambda(\sigma)\exp\left(-\frac{(\delta Z_\ell^\pm)^2}{2\sigma^2}\right)\frac{d\sigma}{\sigma}. \tag{6.6}$$

In a purely self-similar situation, where the energy cascade generates only a trivial variation of σ with scales, the width of the distribution $G_\lambda(\sigma)$ is zero and, invariably, we recover a Gaussian distribution for $P(\delta Z_\ell^\pm)$. On the contrary, when the cascade is not strictly self-similar, the width of $G_\lambda(\sigma)$ is different from zero and the scaling behavior of the width λ^2 of $G_\lambda(\sigma)$ can be used to characterize intermittency.

6.6 Intermittency Properties Recovered via a Shell Model

Shell models have remarkable properties which closely resemble those typical of MHD phenomena (Gloaguen et al. 1985; Biskamp 1994; Giuliani and Carbone 1998; Plunian et al. 2012). However, the presence of a constant forcing term always induces a dynamical alignment, unless the model is forced appropriately, which invariably brings the system towards a state in which velocity and magnetic fields are strongly correlated, that is, where $Z_n^{\pm} \neq 0$ and $Z_n^{\mp} = 0$. When we want to compare statistical properties of turbulence described by MHD shell models with solar wind observations, this term should be avoided. It is possible to replace the constant forcing term by an exponentially time-correlated Gaussian random forcing which is able to destabilize the Alfvénic fixed point of the model (Giuliani and Carbone 1998), thus assuring the energy cascade. The forcing is obtained by solving the following Langevin equation:

$$\frac{dF_n}{dt} = -\frac{F_n}{\tau} + \mu(t), \tag{6.7}$$

where $\mu(t)$ is a Gaussian stochastic process δ-correlated in time $\langle \mu(t)\mu(t') \rangle = 2D\delta(t' - t)$. This kind of forcing will be used to investigate statistical properties.

A statistically stationary state is reached by the system (Gloaguen et al. 1985; Biskamp 1994; Giuliani and Carbone 1998; Plunian et al. 2012), with a well defined inertial range, say a region where Eq. (2.49) is verified. Spectra for both the velocity $|u_n(t)|^2$ and magnetic $|b_n(t)|^2$ variables, as a function of k_n, obtained in the stationary state using the GOY MHD shell model, are shown in Figs. 6.8 and 6.9. Fluctuations are averaged over time. The Kolmogorov spectrum is also reported as a solid line. It is worthwhile to remark that, by adding a random term like $ik_nB_0(t)Z_n^{\pm}$ to a little modified version of the MHD shell models (B_0 is a random function with some

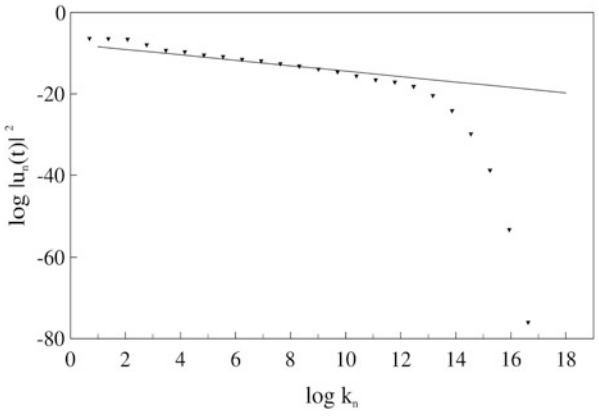

Fig. 6.8 We show the kinetic energy spectrum $|u_n(t)|^2$ as a function of $\log_2 k_n$ for the MHD shell model. The *full line* refer to the Kolmogorov spectrum $k_n^{-2/3}$

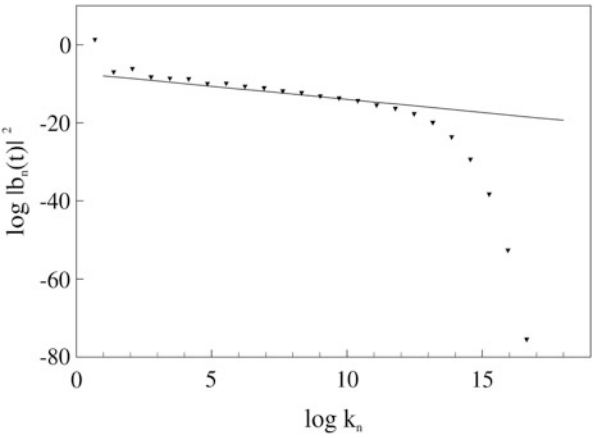

Fig. 6.9 We show the magnetic energy spectrum $|b_n(t)|^2$ as a function of $\log_2 k_n$ for the MHD shell model. The *full line* refer to the Kolmogorov spectrum $k_n^{-2/3}$

statistical characteristics), a Kraichnan spectrum, say $E(k_n) \sim k_n^{-3/2}$, where $E(k_n)$ is the total energy, can be recovered (Biskamp 1994; Hattori and Ishizawa 2001). The term added to the model could represent the effect of the occurrence of a large-scale magnetic field.

Intermittency in the shell model is due to the time behavior of shell variables. It has been shown (Okkels 1997) that the evolution of GOY model consists of short bursts traveling through the shells and long period of oscillations before the next burst arises. In Figs. 6.10 and 6.11 we report the time evolution of the real part of both velocity variables $u_n(t)$ and magnetic variables $b_n(t)$ at three different shells. It can be seen that, while at smaller k_n variables seems to be Gaussian, at larger k_n variables present very sharp fluctuations in between very low fluctuations.

The time behavior of variables at different shells changes the statistics of fluctuations. In Fig. 6.12 we report the probability distribution functions $P(\delta u_n)$ and $P(\delta B_n)$, for different shells n, of normalized variables

$$\delta u_n = \frac{\Re e(u_n)}{\sqrt{\langle |u_n|^2 \rangle}} \quad \text{and} \quad \delta B_n = \frac{\Re e(b_n)}{\sqrt{\langle |b_n|^2 \rangle}},$$

where $\Re e$ indicates that we take the real part of u_n and b_n. Typically we see that PDFs look differently at different shells: At small k_n fluctuations are quite Gaussian distributed, while at large k_n they tend to become increasingly non-Gaussian, by developing fat tails. Rare fluctuations have a probability of occurrence larger than a Gaussian distribution. This is the typical behavior of intermittency as observed in usual fluid flows and described in previous sections.

The same phenomenon gives rise to the departure of scaling laws of structure functions from a Kolmogorov scaling. Within the framework of the shell model the

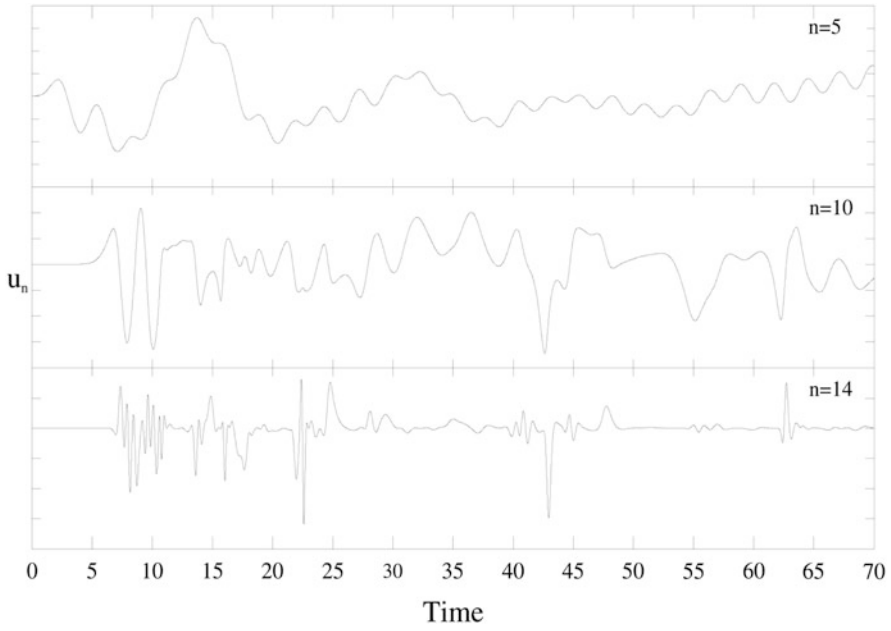

Fig. 6.10 Time behavior of the real part of velocity variable $u_n(t)$ at three different shells n, as indicated in the different panels

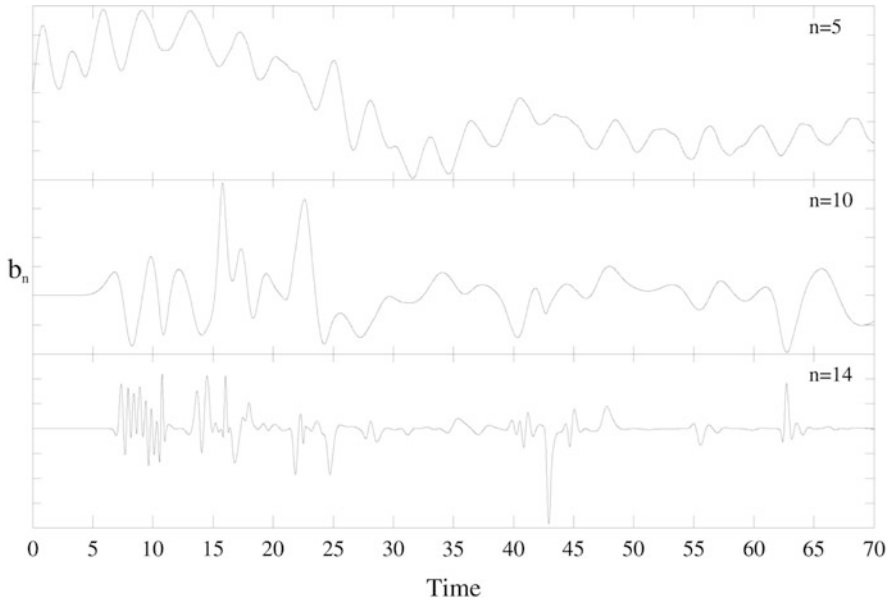

Fig. 6.11 Time behavior of the real part of magnetic variable $b_n(t)$ at three different shells n, as indicated in the different panels

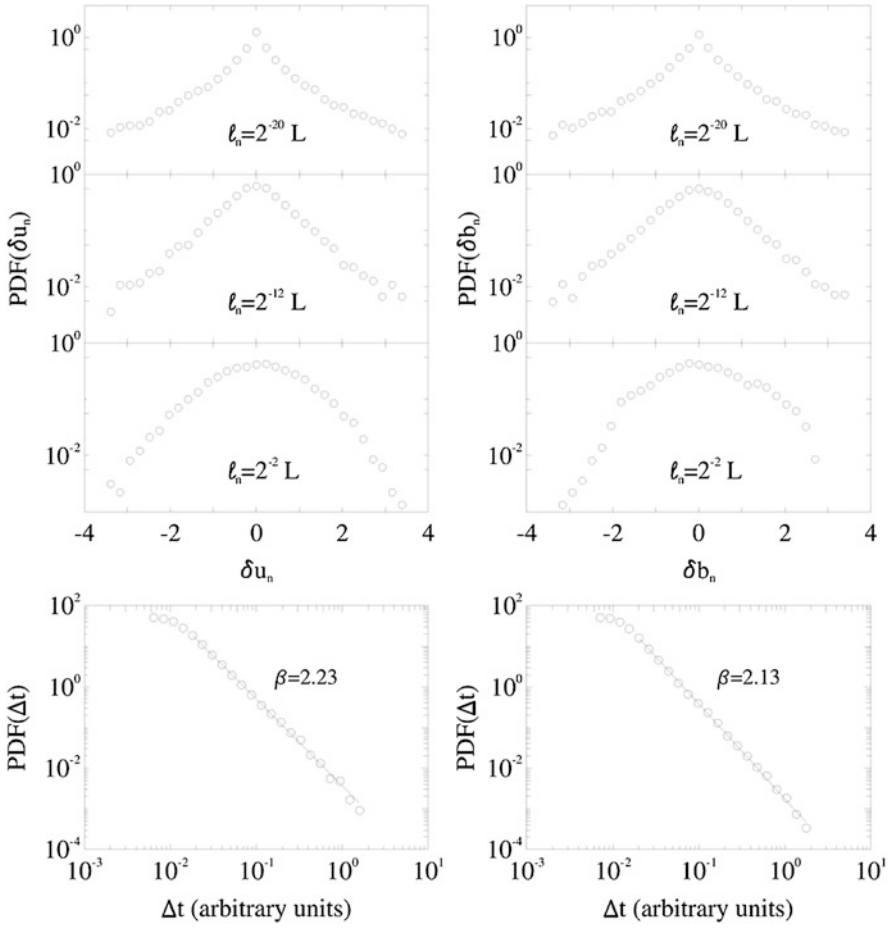

Fig. 6.12 In the *first three panels* we report PDFs of both velocity (*left column*) and magnetic (*right column*) shell variables, at three different shells ℓ_n. The *bottom panels* refer to probability distribution functions of waiting times between intermittent structures at the shell $n = 12$ for the corresponding velocity and magnetic variables

analogous of structure functions are defined as

$$\langle |u_n|^p \rangle \sim k_n^{-\xi_p}; \qquad \langle |b_n|^p \rangle \sim k_n^{-\eta_p}; \qquad \langle |Z_n^{\pm}|^p \rangle \sim k_n^{-\xi_p^{\pm}}.$$

For MHD turbulence it is also useful to report mixed correlators of the flux variables, i.e.,

$$\langle [T_n^{\pm}]^{p/3} \rangle \sim k_n^{-\beta_p^{\pm}}.$$

Table 6.4 Scaling exponents for velocity and magnetic variables, Elsässer variables, and fluxes. Errors on $\beta_p^{\pm}$ are about one order of magnitude smaller than the errors shown

p	ζ_p	η_p	ξ_p^+	ξ_p^-	β_p^+	β_p^-
1	0.36 ± 0.01	0.35 ± 0.01	0.35 ± 0.01	0.36 ± 0.01	0.326	0.318
2	0.71 ± 0.02	0.69 ± 0.03	0.70 ± 0.02	0.70 ± 0.03	0.671	0.666
3	1.03 ± 0.03	1.01 ± 0.04	1.02 ± 0.04	1.02 ± 0.04	1.000	1.000
4	1.31 ± 0.05	1.31 ± 0.06	1.30 ± 0.05	1.32 ± 0.06	1.317	1.323
5	1.57 ± 0.07	1.58 ± 0.08	1.54 ± 0.07	1.60 ± 0.08	1.621	1.635
6	1.80 ± 0.08	1.8 ± 0.10	1.79 ± 0.09	1.87 ± 0.10	1.91	1.94

Scaling exponents have been determined from a least square fit in the inertial range $3 \leq n \leq 12$. The values of these exponents are reported in Table 6.4. It is interesting to notice that, while scaling exponents for velocity are the same as those found in the solar wind, scaling exponents for the magnetic field found in the solar wind reveal a more intermittent character. Moreover, we notice that velocity, magnetic and Elsässer variables are more intermittent than the mixed correlators and we think that this could be due to the cancelation effects among the different terms defining the mixed correlators.

Time intermittency in the shell model generates rare and intense events. These events are the result of the chaotic dynamics in the phase-space typical of the shell model (Okkels 1997). That dynamics is characterized by a certain amount of memory, as can be seen through the statistics of waiting times between these events. The distributions $P(\delta t)$ of waiting times is reported in the bottom panels of Fig. 6.12, at a given shell $n = 12$. The same statistical law is observed for the bursts of total dissipation (Boffetta et al. 1999).

6.7 Observations of Yaglom's Law in Solar Wind Turbulence

To avoid the risk of misunderstanding, let us start by recalling that Yaglom's law (2.40) has been derived from a set of equations (MHD) and under assumptions which are far from representing an exact mathematical model for the solar wind plasma. Yaglom's law is valid in MHD under the hypotheses of incompressibility, stationarity, homogeneity, and isotropy. Also, the form used for the dissipative terms of MHD equations is only valid for collisional plasmas, characterized by quasi-Maxwellian distribution functions, and in case of equal kinematic viscosity and magnetic diffusivity coefficients (Biskamp 2003). In solar wind plasmas the above hypotheses are only rough approximations, and MHD dissipative coefficients are not even defined (Tu and Marsch 1995). At frequencies higher than the ion cyclotron frequency, kinetic processes are indeed present, and a number of possible dissipation mechanisms can be discussed. When looking for the Yaglom's law in the SW, the strong conjecture that the law remains valid for any form of the dissipative term is needed.

Despite the above considerations, Yaglom's law results surprisingly verified in some solar wind samples. Results of the occurrence of Yaglom's law in the ecliptic plane, has been reported by MacBride et al. (2008, 2010) and Smith et al. (2009) and, independently, in the polar wind by Sorriso-Valvo et al. (2007). It is worthwhile to note that, the occurrence of Yaglom's law in polar wind, where fluctuations are Alfvénic, represents a double surprising feature because, according to the usual phenomenology of MHD turbulence, a nonlinear energy cascade should be absent for Alfénic turbulence.

In a first attempt to evaluate phenomenologically the value of the energy dissipation rate, MacBride et al. (2008) analyzed the data from ACE to evaluate the occurrence of both the Kolmogorov's 4/5-law and their MHD analog (2.40). Although some words of caution related to spikes in wind speed, magnetic field strength caused by shocks and other imposed heliospheric structures that constitute inhomogeneities in the data, authors found that both relations are more or less verified in solar wind turbulence. They found a distribution for the energy dissipation rate, defined in the above paper as $\epsilon = (\epsilon_{ii}^{+} + \epsilon_{ii}^{-})/2$, with an average of about $\epsilon \simeq 1.22 \times 10^4\,\mathrm{J/kg\,s}$.

In order to avoid variations of the solar activity and ecliptic disturbances (like slow wind sources, coronal mass ejections, ecliptic current sheet, and so on), and mainly mixing between fast and slow wind, Sorriso-Valvo et al. (2007) used high speed polar wind data measured by the Ulysses spacecraft. In particular, authors analyze the first 7 months of 1996, when the heliocentric distance slowly increased from 3 to 4 AU, while the heliolatitude decreased from about 55° to 30°. The third-order mixed structure functions have been obtained using 10-days moving averages, during which the fields can be considered as stationary. A linear scaling law, like the one shown in Fig. 6.13, has been observed in a significant fraction of samples in the examined period, with a linear range spanning more than two decades. The linear law generally extends from few minutes up to 1 day or more, and is present in about 20 periods of a few days in the 7 months considered. This probably reflects different regimes of driving of the turbulence by the Sun itself, and it is certainly an indication of the nonstationarity of the energy injection process. According to the formal definition of *inertial range* in the usual fluid flows, authors attribute to the range where Yaglom's law appear the role of inertial range in the solar wind turbulence (Sorriso-Valvo et al. 2007). This range extends on scales larger than the usual range of scales where a Kolmogorov relation has been observed, say up to about few hours (cf. Fig. 3.4).

Several other periods are found where the linear scaling range is reduced and, in particular, the sign of $Y_\ell^{\pm}$ is observed to be either positive or negative. In some other periods the linear scaling law is observed either for Y_ℓ^{+} or Y_ℓ^{-} rather than for both quantities. It is worth noting that in a large fraction of cases the sign switches from negative to positive (or viceversa) at scales of about 1 day, roughly indicating the scale where the small scale Alfvénic correlations between velocity and magnetic fields are lost. This should indicate that the nature of fluctuations changes across the break. The values of the pseudo-energies dissipation rates $\epsilon^{\pm}$ has been found to be

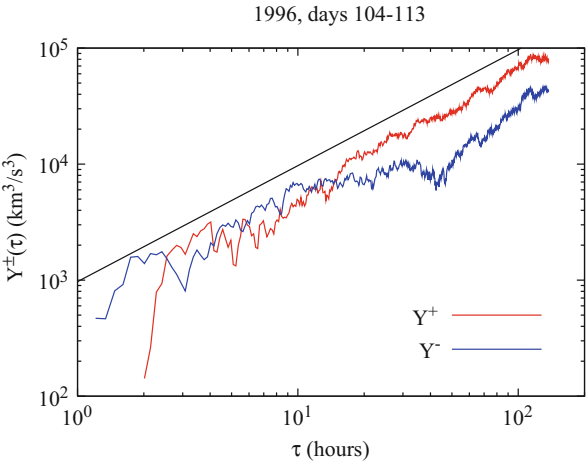

Fig. 6.13 An example of the linear scaling for the third-order mixed structure functions $Y^{\pm}$, obtained in the polar wind using Ulysses measurements. A linear scaling law represents a range of scales where Yaglom's law is satisfied. Image reproduced by permission from Sorriso-Valvo et al. (2007), copyright by APS

of the order of magnitude about few hundreds of J/kg s, higher than that found in usual fluid flows which result of the order of $1 \div 50\,\mathrm{J/kg\,s}$.

The occurrence of Yaglom's law in solar wind turbulence has been evidenced by a systematic study by MacBride et al. (2010), which, using ACE data, found a reasonable linear scaling for the mixed third-order structure functions, from about 64 s. to several hours at 1 AU in the ecliptic plane. Assuming that the third-order mixed structure function is perpendicular to the mean field, or assuming that this function varies only with the component of the scale ℓ_α that is perpendicular to the mean field, and is cylindrically symmetric, the Yaglom's law would reduce to a 2D state. On the other hand, if the third-order function is parallel to the mean field or varies only with the component of the scale that is parallel to the mean field, the Yaglom's law would reduce to a 1D-like case. In both cases the result will depend on the angle between the average magnetic field and the flow direction. In both cases the energy cascade rate varies in the range $10^3 \div 10^4\,\mathrm{J/kg\,s}$ (see MacBride et al. 2010, for further details).

Quite interestingly, Smith et al. (2009) found that the pseudo-energy cascade rates derived from Yaglom's scaling law reveal a strong dependence on the amount of cross-helicity. In particular, they showed that when the correlation between velocity and magnetic fluctuations are higher than about 0.75, the third-order moment of the outward-propagating component, as well as of the total energy and cross-helicity are negative. As already made by Sorriso-Valvo et al. (2007), they attribute this phenomenon to a kind of inverse cascade, namely a back-transfer of energy from small to large scales within the inertial range of the dominant component. We should point out that experimental values of energy transfer rate

in the incompressive case, estimated with different techniques from different data sets (Vasquez et al. 2007; MacBride et al. 2010), are only partially in agreement with that obtained by Sorriso-Valvo et al. (2007). However, the different nature of wind (ecliptic vs. polar, fast vs. slow, at different radial distances from the Sun) makes such a comparison only indicative.

As far as the scaling law (2.47) is concerned, Carbone et al. (2009) found that a linear scaling for $W_\ell^\pm$ as defined in (2.47), appears almost in all Ulysses dataset. In particular, the linear scaling for $W_\ell^\pm$ is verified even when there is no scaling at all for $Y_\ell^\pm$ (2.40). In particular, it has been observed (Carbone et al. 2009) that a linear scaling for W_ℓ^+ appears in about half the whole signal, while W_ℓ^- displays scaling on about a quarter of the sample. The linear scaling law generally extends on about two decades, from a few minutes up to 1 day or more, as shown in Fig. 6.14. At variance to the incompressible case, the two fluxes $W_\ell^\pm$ coexist in a large number of cases. The pseudo-energies dissipation rates so obtained are considerably larger than the relative values obtained in the incompressible case. In fact it has been found that on average $\epsilon^+ \simeq 3 \times 10^3$ J/kg s. This result shows that the nonlinear energy cascade in solar wind turbulence is considerably enhanced by density fluctuations, despite their small amplitude within the Alfvénic polar turbulence. Note that the new variables $\Delta w_i^\pm$ are built by coupling the Elsässer fields with the density, before computing the scale-dependent increments. Moreover, the third-order moments are very sensitive to intense field fluctuations, that could arise when density fluctuations are correlated with velocity and magnetic field. Similar results, but with a considerably smaller effect, were found in numerical simulations of compressive MHD (Mac Low and Klessen 2004).

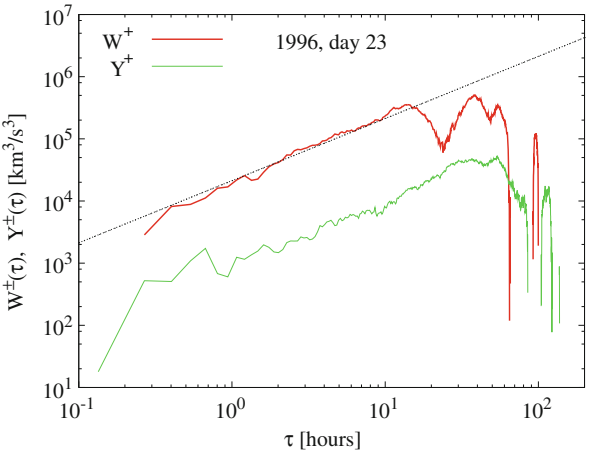

Fig. 6.14 The linear scaling relation is reported for both the usual third-order structure function Y_ℓ^+ and the same quantity build up with the density-mediated variables W_ℓ^+. A linear relation full line is clearly observed. Data refer to the Ulysses spacecraft. Image reproduced by permission from Carbone et al. (2009), copyright by APS

Finally, it is worth reporting that the presence of Yaglom's law in solar wind turbulence is an interesting theoretical topic, because this is the first real experimental evidence that the solar wind turbulence, at least at large-scales, can be described within the magnetohydrodynamic model. In fact, Yaglom's law is an exact law derived from MHD equations and, let us say once more, their occurrence in a medium like the solar wind is a welcomed surprise. By the way, the presence of the law in the polar wind solves the paradox of the presence of Alfvénic turbulence as first pointed out by Dobrowolny et al. (1980). Of course, the presence of Yaglom's law generates some controversial questions about data selection, reliability and a brief discussion on the extension of the inertial range. The interested reader can find some questions and relative answers in *Physical Review Letters* (Forman et al. 2010; Sorriso-Valvo et al. 2010).

References

R. Benzi, G. Paladin, A. Vulpiani, G. Parisi, On the multifractal nature of fully developed turbulence and chaotic systems. J. Phys. A: Math. Gen. **17**, 3521–3531 (1984). doi:10.1088/0305-4470/17/18/021

R. Benzi, S. Ciliberto, R. Tripiccione, C. Baudet, F. Massaioli, S. Succi, Extended self-similarity in turbulent flows. Phys. Rev. E **48**, 29–35 (1993). doi:10.1103/PhysRevE.48.R29

D. Biskamp, *Nonlinear Magnetohydrodynamics*. Cambridge Monographs on Plasma Physics, vol. 1 (Cambridge University Press, Cambridge, 1993)

D. Biskamp, Cascade models for magnetohydrodynamic turbulence. Phys. Rev. E **50**, 2702–2711 (1994). doi:10.1103/PhysRevE.50.2702

D. Biskamp, *Magnetohydrodynamic Turbulence* (Cambridge University Press, Cambridge, 2003)

G. Boffetta, V. Carbone, P. Giuliani, P. Veltri, A. Vulpiani, Power laws in solar flares: self-organized criticality or turbulence? Phys. Rev. Lett. **83**, 4662–4665 (1999). doi:10.1103/PhysRevLett.83.4662

L.F. Burlaga, Intermittent turbulence in the solar wind. J. Geophys. Res. **96**(15), 5847–5851 (1991a). doi:10.1029/91JA00087

L.F. Burlaga, Multifractal structure of speed fluctuations in recurrent streams at 1 AU and near 6 AU. Geophys. Res. Lett. **18**, 1651–1654 (1991b). doi:10.1029/91GL01221

L.F. Burlaga, Multifractal structure of the interplanetary magnetic field: Voyager 2 observations near 25 AU, 1987–1988. Geophys. Res. Lett. **18**, 69–72 (1991c). doi:10.1029/90GL02596

L.F. Burlaga, *Interplanetary Magnetohydrodynamics*. International Series on Astronomy and Astrophysics, vol. 3 (Oxford University Press, New York, 1995)

V. Carbone, Cascade model for intermittency in fully developed magnetohydrodynamic turbulence. Phys. Rev. Lett. **71**, 1546–1548 (1993). doi:10.1103/PhysRevLett.71.1546

V. Carbone, R. Bruno, P. Veltri, Evidences for extended self-similarity in hydromagnetic turbulence. Geophys. Res. Lett. **23**, 121–124 (1996a). doi:10.1029/95GL03777

V. Carbone, P. Veltri, R. Bruno, Solar wind low-frequency magnetohydrodynamic turbulence: extended self-similarity and scaling laws. Nonlinear Process. Geophys. **3**, 247–261 (1996b). doi:10.5194/npg-3-247-1996

V. Carbone, L. Sorriso-Valvo, E. Martines, V. Antoni, P. Veltri, Intermittency and turbulence in a magnetically confined fusion plasma. Phys. Rev. E **62**, 49–56 (2000). doi:10.1103/PhysRevE.62.R49

V. Carbone, R. Marino, L. Sorriso-Valvo, A. Noullez, R. Bruno, Scaling laws of turbulence and heating of fast solar wind: the role of density fluctuations. Phys. Rev. Lett. **103**(6) (2009). doi:10.1103/PhysRevLett.103.061102

B. Castaing, Y. Gagne, V. Hopfinger, Velocity probability density functions of high Reynolds number turbulence. Physica D **46**, 177–200 (2001)

M. Dobrowolny, A. Mangeney, P. Veltri, Fully developed anisotropic hydromagnetic turbulence in interplanetary space. Phys. Rev. Lett. **45**, 144–147 (1980). doi:10.1103/PhysRevLett.45.144

T. Dudok de Wit, Can high-order moments be meaningfully estimated from experimental turbulence measurements? Phys. Rev. E **70** (2004). doi:10.1103/PhysRevE.70.055302

M.A. Forman, C.W. Smith, B.J. Vasquez, Comment on 'scaling laws of turbulence and heating of fast solar wind: the role of density fluctuations'. Phys. Rev. Lett. **104**(18) (2010). doi:10.1103/PhysRevLett.104.189001

U. Frisch, *Turbulence: The Legacy of A.N. Kolmogorov* (Cambridge University Press, Cambridge, 1995)

U. Frisch, P.-L. Sulem, M. Nelkin, A simple dynamical model of intermittent fully developed turbulence. J. Fluid Mech. **87**, 719–736 (1978). doi:10.1017/S0022112078001846

P. Giuliani, V. Carbone, A note on shell models for MHD turbulence. Europhys. Lett. **43**, 527–532 (1998). doi:10.1209/epl/i1998-00386-y

C. Gloaguen, J. Léorat, A. Pouquet, R. Grappin, A scalar model for MHD turbulence. Physica D **17**, 154–182 (1985). doi:10.1016/0167-2789(85)90002-8

Y. Hattori, A. Ishizawa, Characteristic time scales and energy transfer in MHD turbulence, in *IUTAM Symposium on Geometry and Statistics of Turbulence*, ed. by T. Kambe, T. Nakano, T. Miyauchi. Fluid Mechanics and Its Applications, vol. 59 (Kluwer, Dordrecht, 2001), pp. 89–94

H.G.E.F. Hentschel, I. Procaccia, The infinite number of generalized dimensions of fractals and strange attractor. Physica D **8**, 435–444 (1983). doi:10.1016/0167-2789(83)90235-X

G.G. Katul, C.I. Hsieh, J. Sigmon, Energy-inertial scale interaction for temperature and velocity in the unstable surface layer. Bound.-Layer Meteorol. **82**, 49–80 (1997). doi:10.1023/A:1000178707511

A.N. Kolmogorov, The local structure turbulence in incompressible viscous fluids for very large Reynolds numbers. Dokl. Akad. Nauk. SSSR **30**, 301–305 (1941)

R.H. Kraichnan, On Kolmogorov's inertial-range theories. J. Fluid Mech. **62**, 305–330 (1974). doi:10.1017/S002211207400070X

L.D. Landau, E.M. Lifshitz, *Physique Théorique*. Mécanique des fluides, vol. 6 (Editions MIR, Moscow, 1971)

M.-M. Mac Low, R.S. Klessen, Control of star formation by supersonic turbulence. Rev. Mod. Phys. **76**, 125–194 (2004). doi:10.1103/RevModPhys.76.125

B.T. MacBride, C.W. Smith, M.A. Forman, The turbulent cascade at 1 AU: energy transfer and the third-order scaling for MHD. Astrophys. J. **679**, 1644–1660 (2008). doi:10.1086/529575

B.T. MacBride, C.W. Smith, B.J. Vasquez, Inertial-range anisotropies in the solar wind from 0.3 to 1 AU: Helios 1 observations. J. Geophys. Res. **115**(A14), 7105 (2010). doi:10.1029/2009JA014939

E. Marsch, Introduction to kinetic physics, waves and turbulence in the solar wind, in *Solar Wind Seven*, ed. by E. Marsch, R. Schwenn. COSPAR Colloquia Series, vol. 3 (Pergamon Press, Oxford, 1992), pp. 499–504

C. Meneveau, Analysis of turbulence in the orthonormal wavelet representation. J. Fluid Mech. **232**, 469–520 (1991). doi:10.1017/S0022112091003786

E.A. Novikov, Scale similarity for random fields. Sov. Phys. Dokl. **14**, 104–107 (1969)

F. Okkels, The intermittent dynamics in turbulent shell models, Master's Thesis, University of Copenhagen, Copenhagen, 1997

F. Plunian, R. Stepanov, P. Frick, Shell models of magnetohydrodynamic turbulence. Phys. Rep. **523**, 1–60 (2012)

H. Politano, A. Pouquet, Model of intermittency in magnetohydrodynamic turbulence. Phys. Rev. E **52**, 636–641 (1995). doi:10.1103/PhysRevE.52.636

H. Politano, A. Pouquet, von Kármán–Howarth equation for magnetohydrodynamics and its consequences on third-order longitudinal structure and correlation functions. Phys. Rev. E **57**, 21–25 (1998). doi:10.1103/PhysRevE.57.R21

H. Politano, A. Pouquet, V. Carbone, Determination of anomalous exponents of structure functions in two-dimensional magnetohydrodynamic turbulence. Europhys. Lett. **43**, 516–521 (1998). doi:10.1209/epl/i1998-00391-2

S.B. Pope, *Turbulent Flows* (Cambridge University Press, Cambridge, 2000)

G. Ruíz-Chavarría, C. Baudet, S. Ciliberto, Extended self similarity of passive scalars in fully developed turbulence. Europhys. Lett. **32**, 319 (1995)

C. Salem, A. Mangeney, S.D. Bale, P. Veltri, Solar wind magnetohydrodynamics turbulence: anomalous scaling and role of intermittency. Astrophys. J. **702**, 537–553 (2009). doi:10.1088/0004-637X/702/1/537

Z.-S. She, E. Leveque, Universal scaling laws in fully developed turbulence. Phys. Rev. Lett. **72**, 336–339 (1994). doi:10.1103/PhysRevLett.72.336

C.W. Smith, J.E. Stawarz, B.J. Vasquez, M.A. Forman, B.T. MacBride, Turbulent cascade at 1 AU in high cross-helicity flows. Phys. Rev. Lett. **103**(20) (2009). doi:10.1103/PhysRevLett.103.201101

L. Sorriso-Valvo, R. Marino, V. Carbone, A. Noullez, F. Lepreti, P. Veltri, R. Bruno, B. Bavassano, E. Pietropaolo, Observation of inertial energy cascade in interplanetary space plasma. Phys. Rev. Lett. **99**(11) (2007). doi:10.1103/PhysRevLett.99.115001

L. Sorriso-Valvo, V. Carbone, R. Marino, A. Noullez, R. Bruno, P. Veltri, Sorriso-valvo et al. reply. Phys. Rev. Lett. **104**(18) (2010). doi:10.1103/PhysRevLett.104.189002

H. Tennekes, J. Wyngaard, The intermittent small-scale structure of turbulence: data-processing hazards. J. Fluid Mech. **55**, 93 (1972). doi:10.1017/S0022112072001661

C.-Y. Tu, E. Marsch, MHD structures, waves and turbulence in the solar wind: observations and theories. Space Sci. Rev. **73**(1/2), 1–210 (1995). doi:10.1007/BF00748891

B.J. Vasquez, C.W. Smith, K. Hamilton, B.T. MacBride, R.J. Leamon, Evaluation of the turbulent energy cascade rates from the upper inertial range in the solar wind at 1 AU. J. Geophys. Res. **112**(A11), 7101 (2007). doi:10.1029/2007JA012305

Chapter 7
Intermittency Properties in the 3D Heliosphere

In this section, we present a reasoned look at the main aspect of what has been reported in literature about the problem of intermittency in the solar wind turbulence. In particular, we present results from data analysis.

7.1 Structure Functions

Apart from the earliest investigations on the fractal structure of magnetic field as observed in interplanetary space (Burlaga and Klein 1986), the starting point for the investigation of intermittency in the solar wind dates back to 1991, when Burlaga (1991a) started to look at the scaling of the bulk velocity fluctuations at 8.5 AU using Voyager 2 data. This author found that anomalous scaling laws for structure functions could be recovered in the range $0.85 \leq r \leq 13.6$ h. This range of scales has been arbitrarily identified as a kind of "inertial range", say a region were a linear scaling exists between $\log S_r^{(p)}$ and $\log r$, and the scaling exponents have been calculated as the slope of these curves. However, structure functions of order $p \leq 20$ were determined on the basis of only about 4500 data points. Nevertheless the scaling was found to be quite in agreement with that found in ordinary fluid flows. Although the data might be in agreement with the random-β model, from a theoretical point of view Carbone (1993, 1994b) showed that normalized scaling exponents ζ_p/ζ_4 calculated by Burlaga (1991a) would be better fitted by using a p-model derived from the Kraichnan phenomenology (Kraichnan 1965; Carbone 1993), and considering the parameter $\mu \simeq 0.77$. The same author Burlaga (1991c) investigated the multifractal structure of the interplanetary magnetic field near 25 AU and analyzed positive defined fields as magnetic field strength, temperature, and density using the multifractal machinery of dissipation fields (Paladin and Vulpiani 1987; Meneveau 1991). Burlaga (1991b) showed that intermittent events

R. Bruno, V. Carbone, *Turbulence in the Solar Wind*, Lecture Notes in Physics 928, DOI 10.1007/978-3-319-43440-7_7

observed in co-rotating streams at 1 AU should be described by a multifractal geometry. Even in this case the number of points used was very low to assure the reliability of high-order moments.

Marsch and Liu (1993) investigated the structure of intermittency of the turbulence observed in the inner heliosphere by using Helios 2 data. They analyzed both bulk velocity and Alfvén speed to calculate structure functions in the whole range 40.5 s (the instrument resolution) up to 24 h to estimate the pth order scaling exponents. Note that also in this analysis the number of data points used was too small to assure a reliability for order $p = 20$ structure functions as reported by Marsch and Liu (1993). From the analysis analogous to Burlaga (1991a), authors found that anomalous scaling laws are present. A comparison between fast and slow streams at two heliocentric distances, namely 0.3 and 1 AU, allows authors to conjecture a scenario for high speed streams were Alfvénic turbulence, originally self-similar (or poorly intermittent) near the Sun, "...loses its self-similarity and becomes more multifractal in nature" (Marsch and Liu 1993), which means that intermittent corrections increase from 0.3 to 1 AU. No such behavior seems to occur in the slow solar wind. From a phenomenological point of view, Marsch and Liu (1993) found that data can be fitted with a piecewise linear function for the scaling exponents ζ_p, namely a β-model $\zeta_p = 3 - D + p(D-2)/3$, where $D \simeq 3$ for $p \leq 6$ and $D \simeq 2.6$ for $p > 6$. Authors say that "We believe that we see similar indications in the data by Burlaga, who still prefers to fit his whole ζ_p dataset with a single fit according to the non-linear random β-model.". We like to comment that the impression by Marsch and Liu (1993) is due to the fact that the number of data points used was very small. As a matter of fact, only structure functions of order $p \leq 4$ are reliably described by the number of points used by Burlaga (1991a).

However, the data analyses quoted above, which in some sense present some contradictory results, are based on high order statistics which is not supported by an adequate number of data points and the range of scales, where scaling laws have been recovered, is not easily identifiable. To overcome these difficulties Carbone et al. (1996) investigated the behavior of the normalized ratios ζ_p/ζ_3 through the ESS procedure described above, using data coming from low-speed streams measurements of Helios 2 spacecraft. Using ESS the whole range covered by measurements is linear, and scaling exponent ratios can be reliably calculated. Moreover, to have a dataset with a high number of points, authors mixed in the same statistics data coming from different heliocentric distances (from 0.3 AU up to 1 AU). This is not correct as far as fast wind fluctuations are taken into account, because, as found by Marsch and Liu (1993) and Bruno et al. (2003b), there is a radial evolution of intermittency. Results showed that intermittency is a real characteristic of turbulence in the solar wind, and that the curve ζ_p/ζ_3 is a non-linear function of p as soon as values of $p \leq 6$ are considered.

Marsch et al. (1996) for the first time investigated the geometrical and scaling properties of the energy flux along the turbulent cascade and dissipation rate of kinetic energy. They showed the multifractal nature of the dissipation field and estimated, for the first time in solar wind MHD turbulence, the associated singularity spectrum which resulted to be very similar to those obtained for ordinary fluid

turbulence (Meneveau and Sreenivasan 1987). They also estimated the energy dissipation rate for time scales of 10^2 s to be around 5.4×10^{-16} erg cm^{-3} s^{-1}. This value was similar to the theoretical heating rate required in the model by Tu (1988) with Alfvén waves to explain the radial temperature dependence observed in fast solar wind. Looking at the literature, it can be realized that often scaling exponents ζ_p, as observed mainly in the high-speed streams of the inner solar wind, cannot be explained properly by any cascade model for turbulence. This feature has been attributed to the fact that this kind of turbulence is not in a fully-developed state with a well defined spectral index. Models developed by Tu et al. (1984) and Tu (1988) were successful in describing the evolution of the observed power spectra. Using the same idea Tu et al. (1996) and Marsch and Tu (1997) investigated the behavior of an extended cascade model developed on the base of the p-model (Meneveau and Sreenivasan 1987; Carbone 1993). Authors conjectured that: (1) the scaling laws for fluctuations are still valid in the form $\delta Z_\ell^\pm \sim \ell^h$, even when turbulence is not fully developed; (2) the energy cascade rate is not constant, its moments rather depend not only on the generalized dimensions D_p but also on the spectral index α of the power spectrum, say $\langle \epsilon_r^p \rangle \sim \epsilon^p(\ell, \alpha)\ell^{(p-1)D_p}$, where the averaged energy transfer rate is assumed to be

$$\epsilon(\ell, \alpha) \sim \ell^{-(m/2+1)} P_\ell^{\alpha/2},$$

being $P_\ell \sim \ell^\alpha$ the usual energy spectrum ($\ell \sim 1/k$). The model gives

$$\zeta_p = 1 + \left(\frac{p}{m} - 1\right) D_{p/m} + \left[\alpha \frac{m}{2} - \left(1 + \frac{m}{2}\right)\right] \frac{p}{m}, \tag{7.1}$$

where the generalized dimensions are recovered from the usual p-model

$$D_p = \frac{\log_2 \left[\mu^p + (1-\mu)^p\right]}{(1-p)}.$$

In the limit of "fully developed turbulence", say when the spectral slope is $\alpha = 2/m + 1$ the usual Eq. (6.4) is recovered. The Helios 2 data are consistent with this model as far as the parameters are $\mu \simeq 0.77$ and $\alpha \simeq 1.45$, and the fit is relatively good (Tu et al. 1996). Recently, Horbury et al. (1997) and Horbury and Balogh (1997) studied the magnetic field fluctuations of the polar high-speed turbulence from Ulysses measurements at 3.1 AU and at 63° heliolatitude. These authors showed that the observed magnetic field fluctuations were in agreement with the intermittent turbulence p-model of Meneveau and Sreenivasan (1987). They also showed that the scaling exponents of structure functions of order $p \leq 6$, in the scaling range $20 \leq r \leq 300$ s followed the Kolmogorov scaling instead of Kraichnan scaling as expected. In addition, the same authors Horbury et al. (1997) estimated the applicability of the model by Tu et al. (1996) and Marsch and Tu (1997) to the spectral transition range where the spectral index changes during the

spectral evolution and concluded that this model was able to fit the observations much better than the p-model when values of the parameters p change continuously with the scale.

Analysis of scaling exponents of pth order structure functions has been performed using different spacecraft datasets of Ulysses spacecraft. Horbury et al. (1995b) and Horbury et al. (1995a) investigated the structure functions of magnetic field as obtained from observations recorded between 1.7 and 4 AU, and covering a heliographic latitude between 40° and 80° south. By investigating the spectral index of the second order structure function, they found a decrease with heliocentric distance attributed to the radial evolution of fluctuations. Further investigations (see, e.g., Ruzmaikin et al. 1995) were obtained using structure functions to study the Ulysses magnetic field data in the range of scales $1 \leq r \leq 32$ min. Ruzmaikin et al. (1995) showed that intermittency is at work and developed a bi-fractal model to describe Alfvénic turbulence. They found that intermittency may change the spectral index of the second order structure function and this modifies the calculation of the spectral index (Carbone 1994a). Ruzmaikin et al. (1995) found that polar Alfvénic turbulence should be described by a Kraichnan phenomenology (Kraichnan 1965). However, the same data can be fitted also with a fluid-like scaling law (Tu et al. 1996) and, due to the relatively small amount of data, it is difficult to decide, on the basis of the second order structure function, which scaling relation describes appropriately intermittency in the solar wind.

In a further paper Carbone et al. (1995) provided evidence for differences in the ESS scaling laws between ordinary fluid flows and solar wind turbulence. Through the analysis of different datasets collected in the solar wind and in ordinary fluid flows, it was shown that normalized scaling exponents ζ_p/ζ_3 are the same as far as $p \leq 8$ are considered. This indicates a kind of universality in the scaling exponents for the velocity structure functions. Differences between scaling exponents calculated in ordinary fluid flows and solar wind turbulence are confined to high-order moments. Nevertheless, the differences found in the datasets were related to different kind of singular structures in the model described by Eq. (6.5). Solar wind data can be fitted by that model as soon as the most intermittent structures are assumed to be planar sheets $\mathrm{C} = 1$ and $m = 4$, that is a Kraichnan scaling is used. On the contrary, ordinary fluid flows can be fitted only when $\mathrm{C} = 2$ and $m = 3$, that is, structures are filaments and the Kolmogorov scaling have been used. However it is worthwhile to remark that differences have been found for high-order structure functions, just where measurements are unreliable.

7.2 Probability Distribution Functions

As said in Sect. 6.2 the statistics of turbulent flows can be characterized by the PDF of field differences over varying scales. At large scales PDFs are Gaussian, while tails become higher than Gaussian (actually, PDFs decay as $\exp[-\delta Z_\ell^{\pm}]$) at smaller scales.

Marsch and Tu (1994) started to investigate the behavior of PDFs of fluctuations against scales and they found that PDFs are rather spiky at small scales and quite Gaussian at large scales. The same behavior have been obtained by Sorriso-Valvo et al. (1999, 2001) who investigated Helios 2 data for both velocity and magnetic field.

In order to make a quantitative analysis of the energy cascade leading to the scaling dependence of PDFs just described, the distributions obtained in the solar wind have been fitted (Sorriso-Valvo et al. 1999) by using the log-normal ansatz

$$G_\lambda(\sigma) = \frac{1}{\sqrt{2\pi}\lambda} \exp\left(-\frac{\ln^2 \sigma/\sigma_0}{2\lambda^2}\right). \tag{7.2}$$

The width of the log-normal distribution of σ is given by $\lambda^2(\ell) = \sqrt{\langle(\delta\sigma)^2\rangle}$, while σ_0 is the most probable value of σ.

The Eq. (6.6) has been fitted to the experimental PDFs of both velocity and magnetic intensity, and the corresponding values of the parameter λ have been recovered. In Fig. 7.1 the solid lines show the curves relative to the fit. It can be seen that the scaling behavior of PDFs, in all cases, is very well described by Eq. (6.6). At every scale r, we get a single value for the width $\lambda^2(r)$, which can be approximated by a power law $\lambda^2(r) = \mu r^{-\gamma}$ for $r < 1$ h, as it can be seen in Fig. 7.2. The values of parameters μ and γ obtained in the fit, along with the values of σ_0, are reported in Table 7.1. The fits have been obtained in the range of scales $\tau \leq 0.72$ h for the magnetic field, and $\tau \leq 1.44$ h for the velocity field. The analysis of PDFs shows once more that magnetic field is more intermittent than the velocity field.

The same analysis has been repeated by Forman and Burlaga (2003). These authors used 64 s averages of radial solar wind speed reported by the SWEPAM instrument on the ACE spacecraft, increments have been calculated over a range of

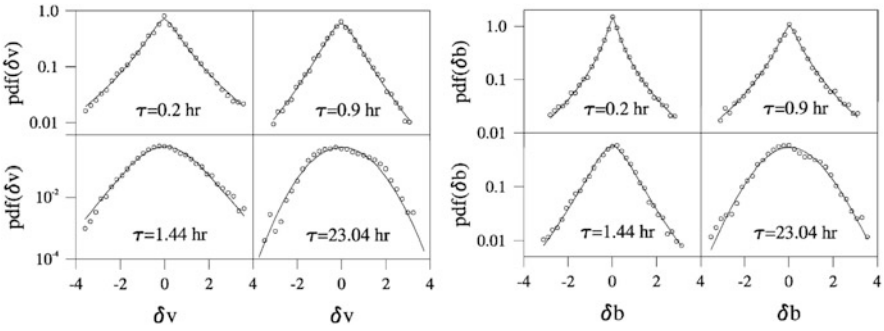

Fig. 7.1 *Left*: normalized PDFs of fluctuations of the longitudinal velocity field at four different scales τ. *Right*: normalized PDFs of fluctuations of the magnetic field magnitude at four different scales τ. *Solid lines* represent the fit made by using the log-normal model. Image reproduced by permission from Sorriso-Valvo et al. (1999), copyright by AGU

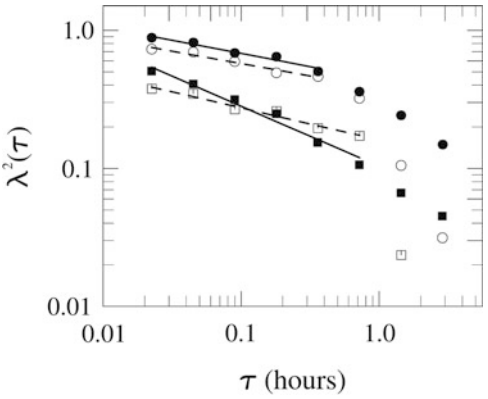

Fig. 7.2 Scaling laws of the parameter $\lambda^2(\tau)$ as a function of the scales τ, obtained by the fits of the PDFs of both velocity and magnetic variables (see Fig. 7.1). *Solid lines* represent fits made by power laws. Image reproduced by permission from Sorriso-Valvo et al. (1999), copyright by AGU

Table 7.1 The values of the parameters σ_0, μ, and γ, in the fit of $\lambda^2(\tau)$ [see Eq. (7.2) as a kernel for the scaling behavior of PDFs]

Parameter	B field (SW)	V field (SW)	B field (FW)	V field (FW)
σ_0	0.90 ± 0.05	0.95 ± 0.05	0.85 ± 0.05	0.90 ± 0.05
μ	0.75 ± 0.03	0.38 ± 0.02	0.90 ± 0.03	0.54 ± 0.03
γ	0.18 ± 0.03	0.20 ± 0.04	0.19 ± 0.02	0.44 ± 0.05

FW and SW refer to fast and slow wind, respectively, as obtained from the Helios 2 spacecraft, by collecting in a single dataset all periods

lag times from 64 s to several days. From the PDF obtained through the Eq. (7.2) authors calculated the structure functions and compared the free parameters of the model with the scaling exponents of the structure functions. Then a fit on the scaling exponents allows to calculate the values of λ^2 and σ_0. Once these parameters have been calculated, the whole PDF is evaluated. The same authors found that the PDFs do not precisely fit the data, at least for large values of the moment order. Interesting enough, Forman and Burlaga (2003) investigated the behavior of PDFs when different kernels $G_\lambda(\sigma)$, derived from different cascade models, are taken into account in Eq. (6.6). They discussed the physical content of each model, concluding that a cascade model derived from lognormal or log-Lévy theories,[1] modified by self-organized criticality proposed by Schertzer et al. (1997), seems to avoid all problems present in other cascade models.

[1]The lognormal model is derived by using a multiplicative process, where random variable generates the cascade. Then, according to the Central Limit Theorem, the process converges to a lognormal distribution of finite variance. The log-Lévy model is a modification of the lognormal model. In such case, the Central Limit Theorem is used to derive the limit distribution of an infinite sum of random variables by relaxing the hypothesis of finite variance usually used. The resulting limit function is a Lévy function.

7.3 Turbulent Structures

The non-linear energy cascade towards smaller scales accumulates fluctuations only in relatively small regions of space, where gradients become singular. As a rather different point of view (see Farge 1992) these regions can be viewed as localized zones of fluid where phase correlation exists, in some sense *coherent structures*. These structures, which dominate the statistics of small scales, occur as isolated events with a typical lifetime greater than that of stochastic fluctuations surrounding them. The idea of a turbulence in the solar wind made by a mixture of structures convected by the wind and stochastic fluctuations is not particularly new (see, e.g., Tu and Marsch 1995). However, these large-scale structures cannot be considered as intermittent structures at all scales. Structures continuously appear and disappear apparently in a random fashion, at some random location of fluid, and carry a great quantity of energy of the flow. In this framework intermittency can be considered as the result of the occurrence of coherent (non-Gaussian) structures at all scales, within the sea of stochastic Gaussian fluctuations.

This point of view is the result of data analysis of scaling laws of turbulent fluctuations made by using wavelets filters (see Sect. 7.3.1) instead of the usual Fourier transform. Unlike the Fourier basis, wavelets allow a decomposition both in time and frequency (or space and scale). In analyzing intermittent structures it is useful to introduce a measure of local intermittency, as for example the Local Intermittency Measure (LIM) introduced by Farge (1992) and described below.

7.3.1 Local Intermittency Measure

Following Farge et al. (1990) and Farge (1992), intermittent events can be viewed as localized zones of fluid where phase correlation exists, in some sense *coherent structures*. These structures, which dominate the statistics of small scales, occur as isolated events with a typical lifetime which is greater than that of stochastic fluctuations surrounding them. Structures continuously appear and disappear, apparently in a random fashion, at some random location of fluid, and they carry most of the flow energy. In this framework, intermittency can be considered as the result of the occurrence of coherent (non-Gaussian) structures at all scales, within the sea of stochastic Gaussian fluctuations.

It follows that, since these structures are well localized in spatial scale and time, it would be advisable to analyze them using wavelets filter instead of the usual Fourier transform. Unlike the Fourier basis, wavelets allow a decomposition both in time and frequency (or space and scale). The wavelet transform $W\{f(t)\}$ of a function $f(t)$ consists of the projection of $f(t)$ on a wavelet basis to obtain wavelet coefficients $w(\tau, t)$. These coefficients are obtained through a convolution between

the analyzed function and a shifted and scaled version of an optional wavelet base

$$w(\tau, t) = \int f(t') \frac{1}{\sqrt{\tau}} \Psi \left(\frac{t - t'}{\tau} \right) dt', \tag{7.3}$$

where the wavelet function

$$\Psi_{t',\tau}(t) = \frac{1}{\sqrt{\tau}} \Psi \left(\frac{t - t'}{\tau} \right)$$

has zero mean and compact support. Some examples of translated and scaled version of this function for a particular wavelet called "charro", because its profile resembles the Mexican hat "El Charro", are given in Fig. 7.3, and the analytical expression for this wavelet is

$$\Psi_{t',\tau}(t) = \frac{1}{\sqrt{\tau}} \left[\left(1 - \left(\frac{t - t'}{\tau} \right)^2 \right) \exp \left(-\frac{1}{2} \left(\frac{t - t'}{\tau} \right)^2 \right) \right].$$

Since the Parceval's theorem exists, the square modulus $|w(\tau, t)|^2$ represents the energy content of fluctuations $f(t + \tau) - f(t)$ at the scale τ at position t.

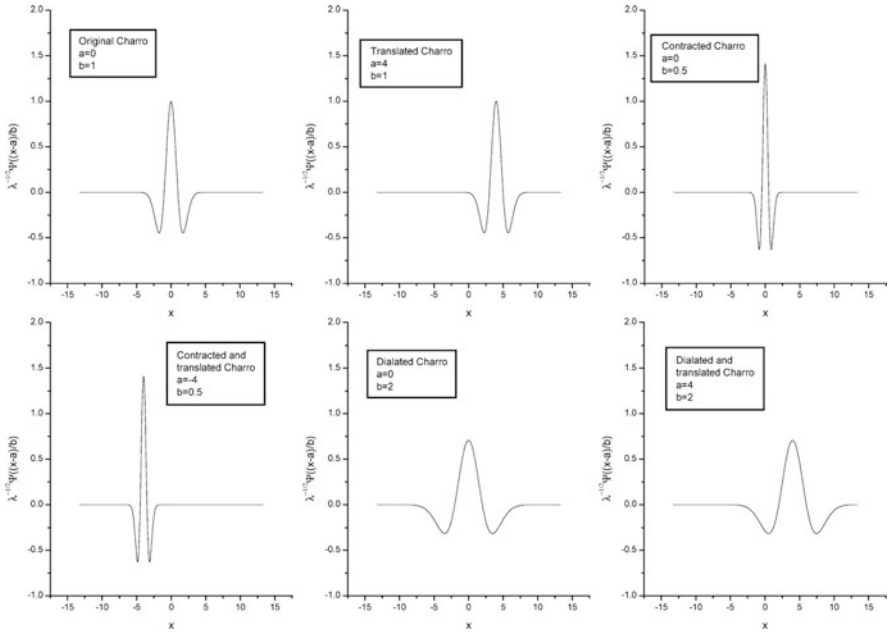

Fig. 7.3 Some examples of *Mexican Hat* wavelet, for different values of the parameters τ and t'

In analyzing intermittent structures it is useful to introduce a measure of local intermittency, as for example the Local Intermittency Measure (LIM) introduced by Farge (see, e.g., Farge et al. 1990; Farge 1992)

$$\mathrm{LIM} = \frac{|w(\tau,t)|^2}{\langle |w(\tau,t)|^2 \rangle_t} \tag{7.4}$$

(averages are made over all positions at a given scale τ). The quantity from Eq. (7.4) represents the energy content of fluctuations at a given scale with respect to the standard deviation of fluctuations at that scale. The whole set of wavelets coefficients can then be split in two sets: a set which corresponds to "Gaussian" fluctuations $w_g(\tau,t)$, and a set which corresponds to "structure" fluctuations $w_s(\tau,t)$, that is, the whole set of coefficients $w(\tau,t) = w_g(\tau,t) \oplus w_s(\tau,t)$ (the symbol $\oplus$ stands here for the union of disjoint sets). A coefficient at a given scale and position will belong to a structure or to the Gaussian background according whether LIM will be respectively greater or lesser than a threshold value. An inverse wavelets transform performed separately on both sets, namely $f_g(t) = W^{-1}\{w_g(\tau,t)\}$ and $f_s(t) = W^{-1}\{w_s(\tau,t)\}$, gives two separate fields: a field $f_g(t)$ where the Gaussian background is collected, and the field $f_s(t)$ where only the non-Gaussian fluctuations of the original turbulent flow are taken into account. Looking at the field $f_s(t)$ one can investigate the spatial behavior of structures generating intermittency. The Haar basis have been applied to time series of 13 months of velocity and magnetic data from ISEE space experiment for the first time by Veltri and Mangeney (1999).

In our analyses we adopted a recursive method (Bianchini et al. 1999; Bruno et al. 1999b) similar to the one introduced by Onorato et al. (2000) to study experimental turbulent jet flows. The method consists in eliminating, for each scale, those events which cause LIM to exceed a given threshold. Subsequently, the flatness value for each scale is checked and, in case this value exceeds the value of 3 (characteristic of a Gaussian distribution), the threshold is lowered, new events are eliminated and a new flatness is computed. The process is iterated until the flatness is equal to 3, or reaches some constant value, for each scale of the wavelet decomposition. This process is usually accomplished eliminating only a few percent of the wavelet coefficients for each scale, and this percentage reduces moving from small to large scales.

The black curve in Fig. 7.4 shows the original profile of the magnetic field intensity observed by Helios 2 between day 50 and 52 within a highly velocity stream at 0.9 AU. The overlapped red profile refers to the same time series after intermittent events have been removed using the LIM method. Most of the peaks, present in the original time series, are not longer present in the LIMed curve. The intermittent component that has been removed can be observed as the blue curve centered around zero.

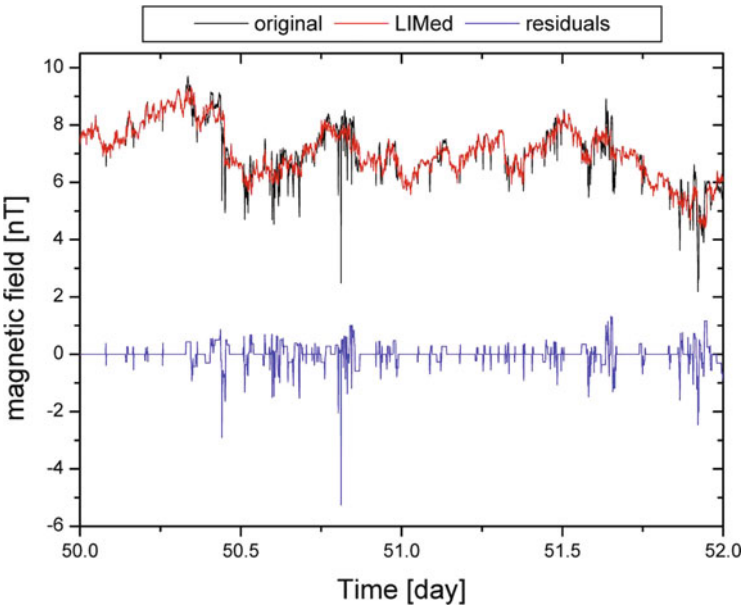

Fig. 7.4 The *black curve* indicates the original time series, the *red* one refers to the LIMed data, and the *blue* one shows the difference between these two curves

7.3.2 On the Nature of Intermittent Events

The spatial structures generating intermittency have been investigated by Veltri and Mangeney (1999), using the Haar basis applied to time series of 13 months of velocity and magnetic data from ISEE s/c. Analyzing intermittent events, they found that intermittent events occur on time scale of the order of few minutes and that they are one-dimensional structures (in agreement with Carbone et al. 1995). In particular, they found different types of structures which can represent two different categories:

1. Some of the structures are the well known one-dimensional current sheets, characterized by pressure balance and almost constant density and temperature. When a minimum variance analysis is made on the magnetic field near the structure, it can be seen that the most variable component of the magnetic field changes sign. This component is perpendicular to the average magnetic field, the third component being zero. An interesting property of these structures is that the correlation between velocity and magnetic field within them is opposite with respect to the rest of fluctuations. That is, when they occur during Alfvénic periods velocity and magnetic field correlation is low; on the contrary, during non-Alfvénic periods the correlation of structure increases.
2. A different kind of structures looks like a shock wave. They can be parallel shocks or slow-mode shocks. In the first case they are observed on the radial

component of the velocity field, but are also seen on the magnetic field intensity, proton temperature, and density. In the second case they are characterized by a very low value of the plasma β parameter, constant pressure, anti-correlation between density and proton temperature, no magnetic fluctuations, and velocity fluctuations directed along the average magnetic field.

However, Salem et al. (2009), as already anticipated in Sect. 3.3.1, demonstrated that a monofractal can be recovered and intermittency eliminated simply by subtracting a small subset of the events at small scales.

Given a turbulent time series, as derived in the solar wind, a very interesting statistics can be made on the time separation between the occurrence of two consecutive structures. Let us consider a signal, for example $u(t)$ or $b(t)$ derived from solar wind, and let us define the wavelets set $w_s(r,t)$ as the set which captures, at time t, the occurrence of structures at the scale r. Then define the waiting times δt, as that time between two consecutive structures at the scale r, that is, between $w_s(r,t)$ and $w_s(r,t+\delta t)$. The PDFs of waiting times $P(\delta t)$ are reported in Fig. 6.3. As it can be seen, waiting times are distributed according to a power law $P(\delta t) \sim \delta t^{-\beta}$ extended over at least two decades. This property is very interesting, because this means that the underlying process for the energy cascade is non-Poissonian. Waiting times occurring between isolated Poissonian events, must be distributed according to an exponential function. The power law for $P(\delta t)$ represents the asymptotic behavior of a Lévy function with characteristic exponent $\alpha = \beta - 1$. This describes self-affine processes and are obtained from the central limit theorem by relaxing the hypothesis that the variance of variables is finite. The power law for waiting times we found is a clear evidence that long-range correlation (or in some sense "memory") exists in the underlying cascade process.

On the other hand, Bruno et al. (2001), analyzing the statistics of the occurrence of waiting times of magnetic field intensity and wind speed intermittent events for a short time interval within the trailing edge of a high velocity stream, found a possible Poissonian-like behavior with a characteristic time around 30 min for both magnetic field and wind speed. These results are to be compared with previous estimates of the occurrence of interplanetary discontinuities performed by Tsurutani and Smith (1979), who found a waiting time around 14 min. In addition, Bruno et al. (2001), taking into account the wind speed and the orientation of the magnetic field vector at the site of the observation, in the hypothesis of spherical expansion, estimated the corresponding size at the Sun surface that resulted to be of the order of the photospheric structures estimated also by Thieme et al. (1989). Obviously, the Poissonian statistics found by these authors does not agree with the clear power law shown in Fig. 6.3. However, Bruno et al. (2001) included intermittent events found at all scales while results shown in Fig. 6.3 refer to waiting times between intermittent events extracted at the smallest scale, which results to be about an order of magnitude smaller than the time resolution used by Bruno et al. (2001). A detailed study on this topic would certainly clarify possible influences on the waiting time statistics due to the selection of intermittent events according to the corresponding scale.

In the same study by Bruno et al. (2001), these authors analyzed in detail an event characterized by a strong intermittent signature in the magnetic field intensity. A comparative study was performed choosing a close-by time interval which, although intermittent in velocity, was not characterized by strong magnetic intermittency. This time interval was located a few hours apart from the previous one. These two intervals are indicated in Fig. 7.5 by the two vertical boxes labeled 1 and 2,

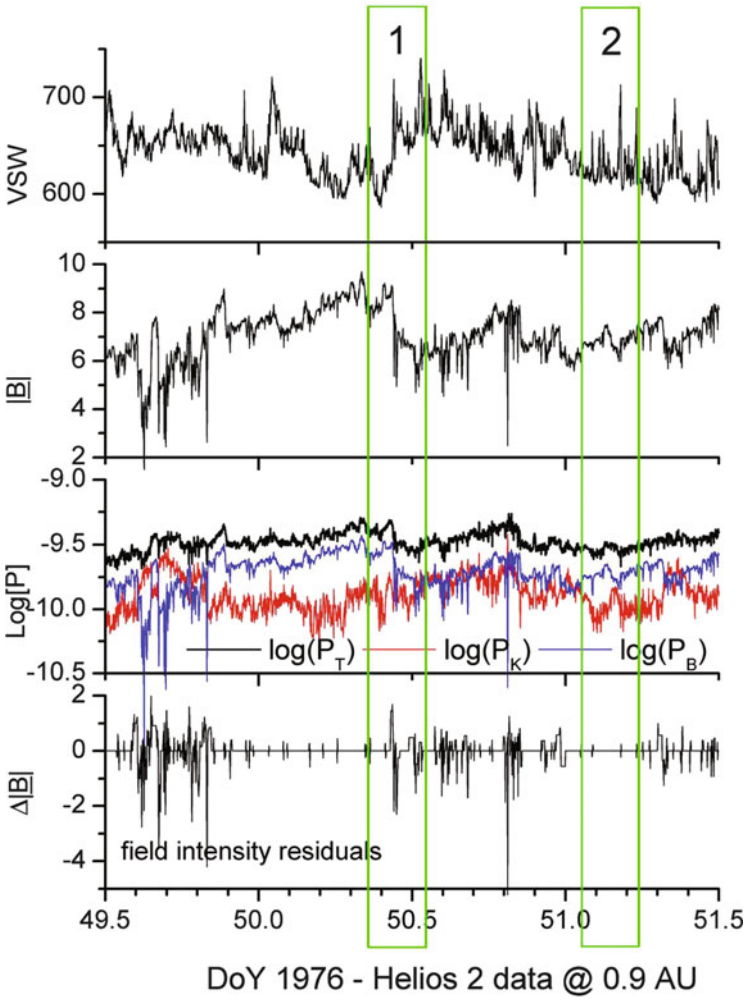

Fig. 7.5 *From top to bottom*: 81 s averages of velocity wind profile in km s^{-1}, magnetic field intensity in nT, the logarithmic value of magnetic (*blue line*), thermal (*red line*), and total pressure (*black line*) in dyne/cm^2 and field intensity residuals in nT. The *two vertical boxes* delimit the two time intervals #1 and #2 which were chosen for comparison. While the first interval shows strong magnetic intermittency, the second one does not. Image reproduced by permission from Bruno et al. (2001), copyright by Elsevier

respectively. Wind speed profile and magnetic field magnitude are shown in the first two panels. In the third panel, the blue line refers to the logarithmic value of the magnetic pressure P_m, here indicated by P_B; the red line refers to the logarithmic value of the thermal pressure P_k, here indicated by P_K and the black line refers to the logarithmic value of the total pressure P_{tot}, here indicated by $P_{\text{T}} = P_B + P_K$, including an average estimate of the electrons and αs contributions. Magnetic field intensity residuals, obtained from the LIM technique, are shown in the bottom panel. The first interval is characterized by strong magnetic field intermittency while the second one is not. In particular, the first event corresponds to a relatively strong field discontinuity which separates two regions characterized by a different bulk velocity and different level of total pressure. While kinetic pressure (red trace) does not show any major jump across the discontinuity but only a light trend, magnetic pressure (blue trace) clearly shows two distinct levels.

A minimum variance analysis further reveals the intrinsic different nature of these two intervals as shown in Fig. 7.6 where original data have been rotated into the field minimum variance reference system (see Sect. 3.3.4) where maximum, intermediate and minimum variance components are identified by λ_3, λ_2, and λ_1, respectively. Moreover, at the bottom of the column we show the hodogram on the maximum variance plane $\lambda_3 - \lambda_2$, as a function of time on the vertical axis.

The good correlation existing between magnetic and velocity variations for both time intervals highlights the presence of Alfvénic fluctuations. However, only within the first interval the magnetic field vector describes an arc-like structure larger than 90° on the maximum variance plane (see rotation from A to B on the 3D graph at the bottom of the left column in Fig. 7.6) in correspondence with the time interval identified in the profile of the magnetic field components by the thick line. At this location, the magnetic field intensity shows a clear discontinuity, $B[\lambda_3]$ changes sign, $B[\lambda_2]$ shows a hump whose maximum is located where the previous component changes sign and, finally, $B[\lambda_1]$ keeps its value close to zero across the discontinuity. Velocity fluctuations are well correlated with magnetic field fluctuations and, in particular, the minimum variance component $V[\lambda_1]$ has the same value on both sides of the discontinuity, approximately $350\,\text{km}\,\text{s}^{-1}$, indicating that there is no mass flux through the discontinuity. During this interval, which lasts about 26 min, the minimum variance direction lies close to the background magnetic field direction at 11.9° so that the arc is essentially described on a plane perpendicular to the average background magnetic field vector. However, additional although smaller and less regular arc-like structures can be recognized on the maximum variance plane $\lambda_2 - \lambda_3$, and they tend to cover the whole 2π interval.

Within the second interval, magnetic field intensity is rather constant and the three components do not show any particular fluctuation, which could resemble any sort of rotation. In other words, the projection on the maximum variance plane does not show any coherent path. Even in this case, these fluctuations happen to be in a plane almost perpendicular to the average field direction since the angle between this direction and the minimum variance direction is about 9.3°.

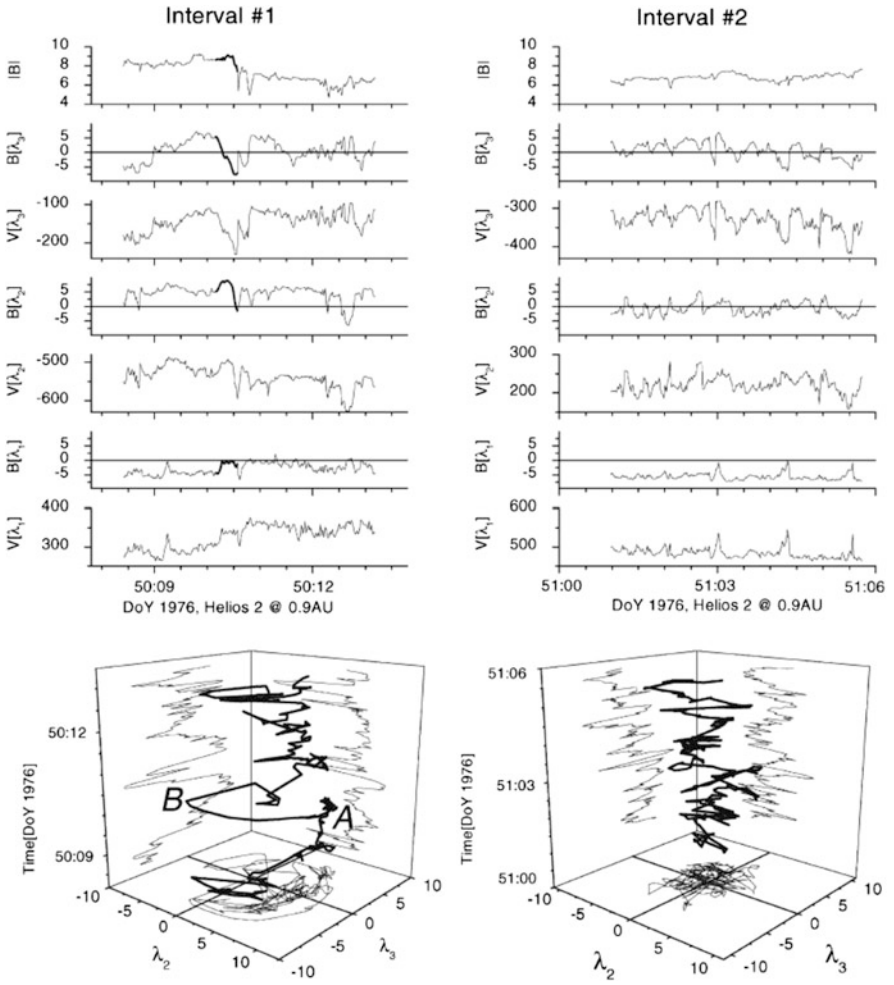

Fig. 7.6 *Left column, from top to bottom*: we show magnetic field intensity, maximum λ_3, intermediate λ_2 and minimum λ_1 variance components for magnetic field and wind velocity relative to the time interval #1 shown in Fig. 7.5. *Right below*, we show the hodogram on the maximum variance plane $\lambda_3 - \lambda_2$, as a function of time. Projections onto the side planes are also shown. The large arc, from *A* to *B*, corresponds to the thick segment in the profile of the magnetic field components shown in the *upper panel*. The same parameters are shown for interval #2 (Fig. 7.5), in the same format, on the *right hand side* of the figure. The time resolution of the data is 81 s. Image reproduced by permission from Bruno et al. (2001), copyright by Elsevier

Further insights about differences between these two intervals can be obtained when we plot the trajectory followed by the tip of the magnetic field vector in the minimum variance reference system, as shown in Fig. 7.7. The main difference

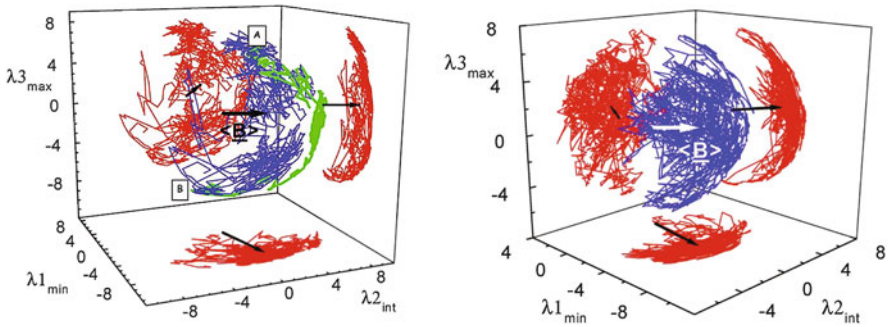

Fig. 7.7 Trajectory followed by the tip of the magnetic field vector (*blue color line*) in the minimum variance reference system for interval #1 (*left*) and #2 (*right*). Projections on the three planes (*red color lines*) formed by the three eigenvectors $\lambda_1, \lambda_2, \lambda_3$, and the average magnetic field vector, with its projections on the same planes, are also shown. The *green line* extending from label *A* to label *B* refers to the arc-like discontinuity shown in Fig. 7.6. The time resolution of the magnetic field averages is 6 s. Image reproduced by permission from Bruno et al. (2001), copyright by Elsevier

between these two plots is that the one relative to the first interval shows a rather patchy trajectory with respect to the second interval. As a matter of fact, if we follow the displacements of the tip of the vector as the time goes by, we observe that the two intervals have a completely different behavior.

Within the first time interval, the magnetic field vector experiences for some time small displacements around a given direction in space and then it suddenly performs a much larger displacement towards another direction in space, about which it starts to wander again. This process keeps on going several times within this time interval. In particular, the thick green line extending from label A to label B refers to the arc-like discontinuity shown in Fig. 7.6, which is also the largest directional variation within this time interval. Within the second interval, the vector randomly fluctuates in all direction and, as a consequence, both the 3D trajectory and its projection on the maximum variance plane do not show any large empty spot. In practice, the second time interval, although longer, is similar to any sub-interval corresponding to one of the trajectory patches recognizable in the left hand side panel. As a matter of fact, selecting a single patch from the first interval and performing a minimum variance analysis, the maximum variance plane would result to be perpendicular to the local average magnetic field direction and the tip of the vector would randomly fluctuate in all directions. The first interval can be seen as a collection of several sub-intervals similar to interval #2 characterized by different field orientations and, possibly, intensities. Thus, magnetic field intermittent events mark the border between adjacent intervals populated by stochastic Alfvénic fluctuations.

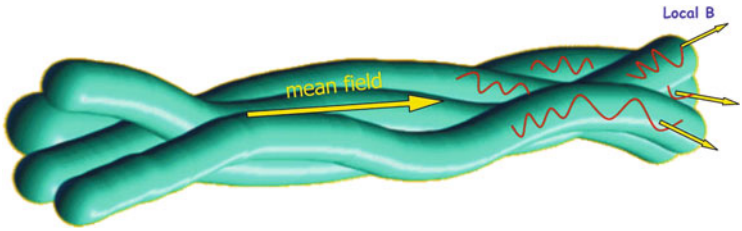

Fig. 7.8 Simple visualization of hypothetical flux tubes which tangle up in space. Each flux tube is characterized by a local field direction, and within each flux tube the presence of Alfvénic fluctuations makes the magnetic field vector randomly wander about this direction. Moreover, the large scale is characterized by an average background field direction aligned with the local interplanetary magnetic field. Moving across different flux-tubes, characterized by a different values of $|B|$, enhances the intermittency level of the magnetic field intensity time series (from Bruno et al. 2001)

The observations reported above suggested these authors to draw the sketch shown in Fig. 7.8 that shows a simple visualization of hypothetical flux tubes, convected by the wind, which tangle up in space. Each flux tube is characterized by a local field direction and intensity, and within each flux tube the presence of Alfvénic fluctuations makes the magnetic field vector randomly wander bout this direction. Moreover, the large scale is characterized by an average background field direction aligned with the local interplanetary magnetic field. This view, based on the idea that solar wind fluctuations are a superposition of propagating Alfvén waves and convected structures (Bavassano and Bruno 1989), strongly recalls the work by Tu and Marsch (1990, 1993) who suggested the solar wind fluctuations being a superposition of pressure balance structure (PBS) type flux tubes and Alfvén waves. In the inner heliosphere these PBS-type flux tubes are embedded in the large structure of fast solar wind streams and would form a kind of spaghetti-like sub-structure, which probably has its origin t the base of the solar atmosphere.

The border between these flux tubes can be a tangential discontinuity where the total pressure on both sides of the discontinuity is in equilibrium or, as in the case of interval #1, the discontinuity is located between two regions not in pressure equilibrium. If the observer moves across these tubes he will record the patchy configuration shown in Fig. 7.7, panel (A). Within each flux tube he will observe a local average field direction and the magnetic field vector would mainly fluctuate on a plane perpendicular to this direction. Moving to the next tube, the average field direction would rapidly change and magnetic vector fluctuations would cluster around this new direction. Moreover, if we imagine a situation with many flux tubes, each one characterized by a different magnetic field intensity, moving across them would possibly increase the intermittent level of the fluctuations. On the contrary, moving along a single flux tube, the same observer would constantly be in the situation typical of interval #2, which is mostly characterized by a rather constant magnetic field intensity and directional stochastic fluctuations mainly on a

plane quasi perpendicular to the average magnetic field direction. In such a situation, magnetic field intensity fluctuations would not increase their intermittency.

A theoretical effort by Chang et al. (2004), Chang (2003), and Chang and Wu (2002) was dedicated to model MHD turbulence in a way that recalls the interpretation of the interplanetary observations given by Bruno et al. (2001) and, at the same time, reminds also the point of view expressed by Farge (1992) in this section. These authors stress the fact that propagating modes and coherent, convected structures share a common origin within the general view described by the physics of complexity. Propagating modes experience resonances which generate coherent structures, possibly flux tubes, which, in turn, will migrate, interact, and, eventually, generate new modes. This process, schematically represented in Fig. 7.9, which favors the local generation of coherent structures in the solar wind, fully complement the possible solar origin of the convected component of interplanetary MHD turbulence.

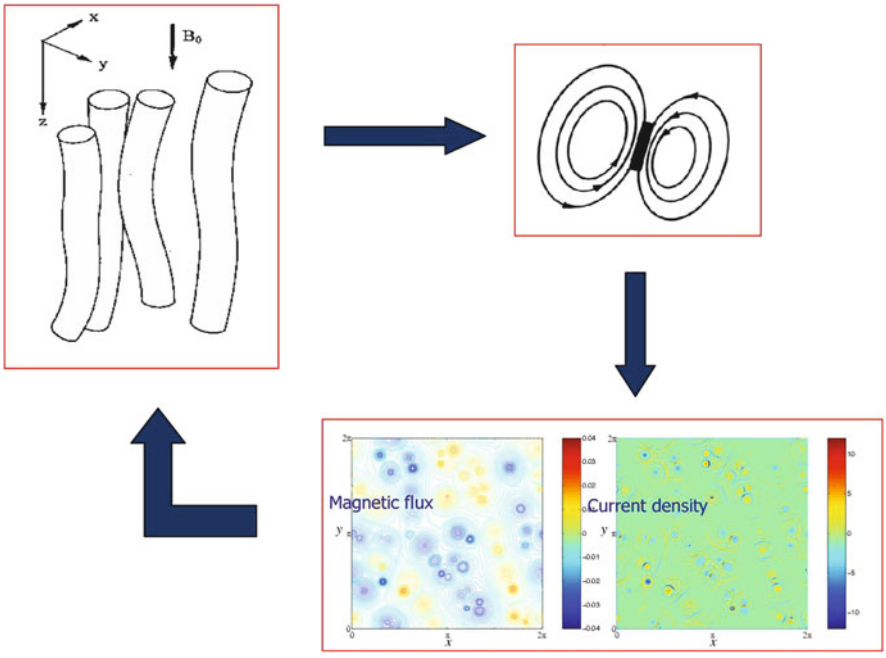

Fig. 7.9 Composite figure made adapting original figures from the paper by Chang et al. (2004). The first element on the *upper left corner* represents field-aligned spatio-temporal coherent structures. A cross-section of two of these structures of the same polarity is shown in the *upper right corner*. Magnetic flux iso-contours and field polarity are also shown. The *darkened area* represents intense current sheet during strong magnetic shear. The bottom element of the figure is the result of 2D MHD simulations of interacting coherent structures, and shows intermittent spatial distribution of intense current sheets. In this scenario, new fluctuations are produced which can provide new resonance sites, possibly nucleating new coherent structures

7.3.3 *On the Statistics of Magnetic Field Directional Fluctuations*

Interesting enough is to look at the statistics of the angular jumps relative to the orientation of the magnetic field vector. Studies of this kind can help to infer the relevance of modes and advected structures within MHD turbulent fluctuations. Bruno et al. (2004) found that PDFs of interplanetary magnetic field vector angular displacements within high velocity streams can be reasonably fitted by a double log-normal distribution, reminiscent of multiplicative processes following turbulence evolution (Fig. 7.10). As a matter of fact, the *multiplicative cascade* notion was introduced by Kolmogorov into his statistical theory (Kolmogorov 1941, 1991, 1962) of turbulence as a phenomenological framework to accommodate extreme behavior observed in real turbulent fluids.

The same authors, studying the radial behavior of the two lognormal components of this distribution concluded that they could be associated with Alfvénic fluctuations and advected structures, respectively. In particular, it was also suggested that the nature of these advected structures could be intimately connected to tangential discontinuities separating two contiguous flux tubes (Bruno et al. 2001). Whether or not these fluctuations should be identified with the 2D turbulence was uncertain since their relative PDF, differently from the one associated with Alfvénic fluctuations, did not show a clear radial evolution. As a matter of fact, since 2D turbulence is characterized by having its k vectors perpendicular to the local field it should experience a remarkable evolution given that the turbulent cascade acts preferably on wave numbers perpendicular to the ambient magnetic field direction, as suggested by the three-wave resonant interaction (Shebalin et al. 1983). Obviously, an alternative solution would be the solar origin of these fluctuations. However, it is still unclear whether these structures come directly from the Sun or are locally generated by some mechanism. Some theoretical results (Primavera et al. 2003) would indicate that coherent structures causing intermittency in the solar wind (Bruno et al. 2003a), might be locally created by parametric decay of Alfvén waves. As a matter of fact, coherent structures like current sheets are continuously created when the instability is active (Primavera et al. 2003).

A more recent analysis (Borovsky 2008) on changes in the field direction experienced by the solar wind magnetic field vector reproposed the picture that the inner heliosphere is filled with a network of entangled magnetic flux tubes (Bruno et al. 2001) and interpreted these flux tubes like fossil structures that originate at the solar surface. These tubes are characterized by strong changes in the magnetic field direction as shown by the distribution illustrated in Fig. 7.11 that refers to the occurrence of changes in the magnetic field direction observed by ACE for about 7 years for a time scale of roughly 2 min. Two exponential curves have been used to fit the distribution, one for the small angular change population and one for the large angular change population. The small angular-change population is associated with

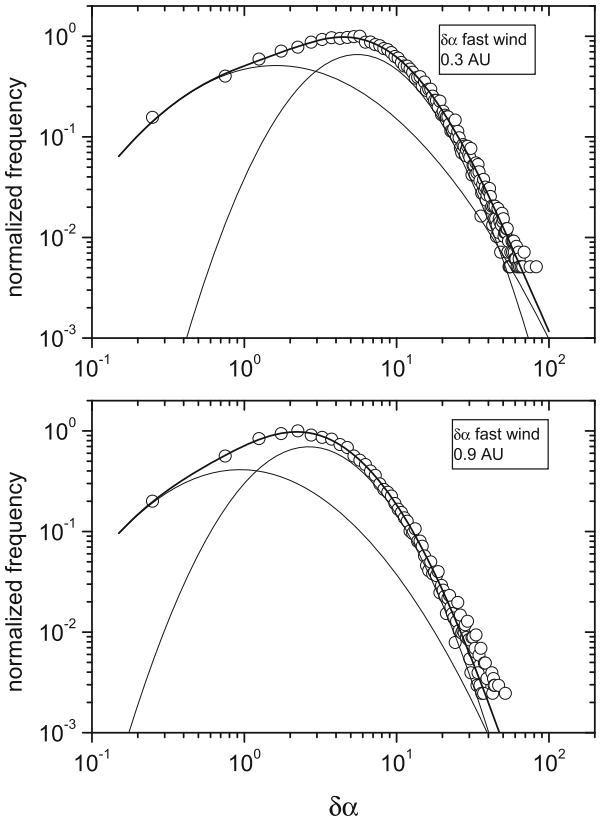

Fig. 7.10 Probability distributions of the angular displacements experienced by magnetic vector on a time scale of 6 s at 0.3 and 0.9 AU, for a fast wind, respectively. *Solid curves* refer to lognormals contributing to form the *thick solid curve* which best fits the distribution. Image reproduced by permission from Bruno et al. (2004), copyright EGU

fluctuations active within the flux tube while, the second population would be due to large directional jumps identifying the crossing of the border between adjacent flux tubes. The same authors performed similar analyses on several plasma and magnetic field parameters like velocity fluctuations, alpha to proton ratio, proton and electron entropies, and found that also for these parameters small/large changes of these parameters are associated with small/large angular changes confirming the different nature of these two populations. Larger flux tubes, originating at the Sun, thanks to wind expansion which would inhibit reconnection, would eventually reach 1 AU.

In another recent paper, Li (2008) developed a genuine data analysis method to localize individual current sheets from a turbulent solar wind magnetic field sample. He noticed that, in the presence of a current sheet, a scaling law appears for the cumulative distribution function of the angle between two magnetic field vectors

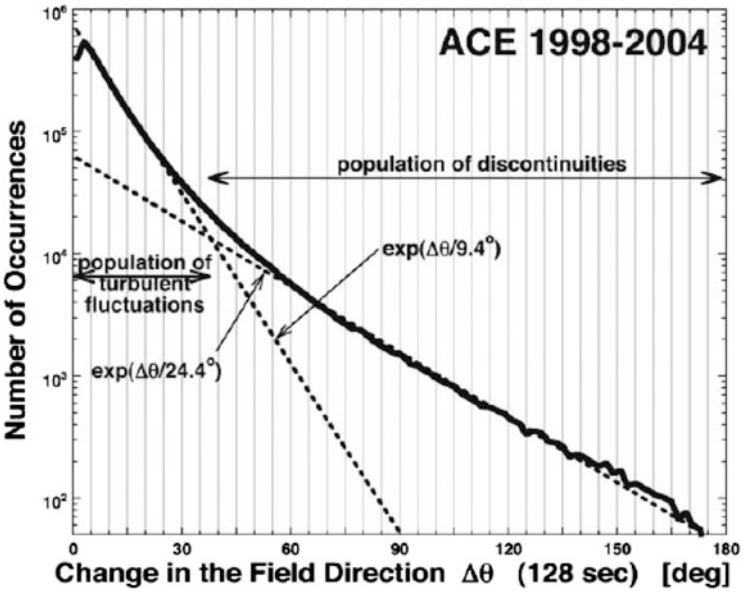

Fig. 7.11 Measurements of angular differences of magnetic field direction on time scale of 128 s. Data set is from ACE measurements for the years 1998–2004. Exponential fits to two portions of the distribution are shown as *dashed curves*. Images reproduced by permission from Borovsky (2008), copyright by AGU

separated by some time lags. In other words, if we define the function $F(\theta, \zeta)$ to represent the frequency of having the measured angle between magnetic vectors separated by a time lag ζ larger than θ we expect to have the following scaling relation:

$$F(\theta, N\zeta) \sim NF(\theta, \zeta). \tag{7.5}$$

As a matter of fact, if the distribution function $F(\theta, \zeta)$ above a certain critical angle θ_0 is dominated by current-sheet crossing separating two adjacent flux tubes, we expect to find the scaling represented by relation (7.5). On the contrary, if we are observing these fluctuations within the same side of the current sheet $F(\theta, \zeta)$ is dominated by small angular fluctuations and we do not expect to find any scaling.

Using the same methodology, Li et al. (2008) also studied fluctuations in the Earth's magnetotail to highlight the absence of similar structures and to conclude that most of those advected structures observed in the solar wind must be of solar origin (Fig. 7.12).

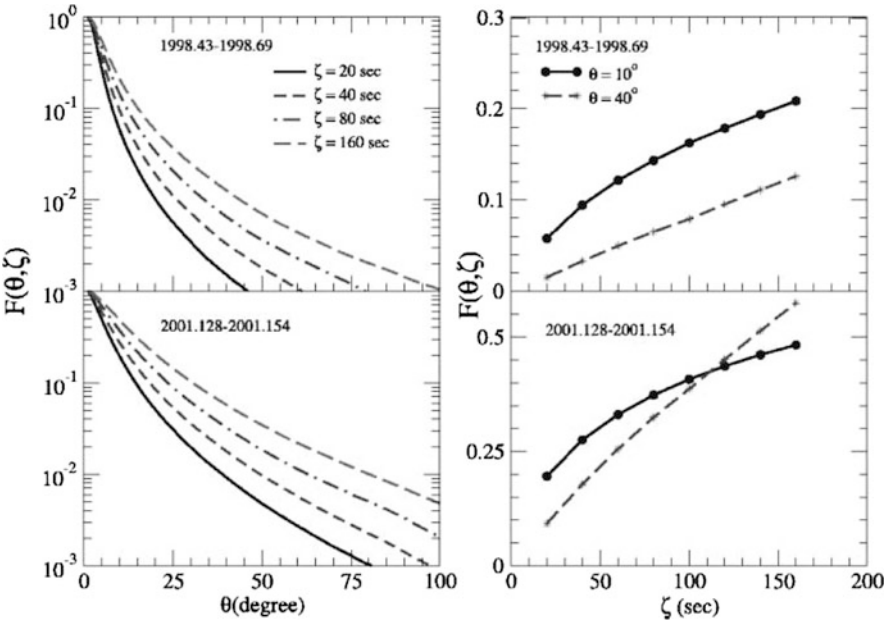

Fig. 7.12 Distribution function for two time periods. The *left panels* show the dependence of $F(\theta, \zeta)$ on θ, and the *right panels* show the dependence of $F(\theta, \zeta)$ on ζ. The presence of a current sheet makes $F(\theta, \zeta)$ to increases linearly with ζ (*dashed lines* in the *right panels*). Image reproduced by permission from Li (2008), copyright by AAS

7.4 Radial Evolution of Intermittency in the Ecliptic

Marsch and Liu (1993) investigated for the first time solar wind scaling properties in the inner heliosphere. These authors provided some insights on the different intermittent character of slow and fast wind, on the radial evolution of intermittency, and on the different scaling characterizing the three components of velocity. In particular, they found that fast streams were less intermittent than slow streams and the observed intermittency showed a weak tendency to increase with heliocentric distance. They also concluded that the Alfvénic turbulence observed in fast streams starts from the Sun as self-similar but then, during the expansion, decorrelates becoming more multifractal. This evolution was not seen in the slow wind, supporting the idea that turbulence in fast wind is mainly made of Alfvén waves and convected structures (Tu and Marsch 1993), as already inferred by looking at the radial evolution of the level of cross-helicity in the solar wind (Bruno and Bavassano 1991).

Bruno et al. (2003a) investigated the radial evolution of intermittency in the inner heliosphere, using the behavior of the flatness of the PDF of magnetic field and velocity fluctuations as a function of scale. As a matter of fact, probability distribution functions of fluctuating fields affected by intermittency become more

and more peaked at smaller and smaller scales. Since the peakedness of a distribution is measured by its flatness factor, they studied the behavior of this parameter at different scales to estimate the degree of intermittency of their time series, as suggested by Frisch (1995).

In order to study intermittency they computed the following estimator of the flatness factor $\mathscr{F}$:

$$\mathscr{F}(\tau) = \frac{\langle S_\tau^4 \rangle}{\langle S_\tau^2 \rangle^2}, \tag{7.6}$$

where τ is the scale of interest and $S_\tau^p = \langle |V(t+\tau) - V(t)|^p \rangle$ is the structure function of order p of the generic function $V(t)$. They considered a given function to be intermittent if the factor $\mathscr{F}$ increased when considering smaller and smaller scales or, equivalently, higher and higher frequencies.

In particular, vector field, like velocity and magnetic field, encompasses two distinct contributions, a compressive one due to intensity fluctuations that can be expressed as $\delta|\mathbf{B}(t,\tau)| = |\mathbf{B}(t+\tau)| - |\mathbf{B}(t)|$, and a directional one due to changes in the vector orientation $\delta\mathbf{B}(t,\tau) = \sqrt{\sum_{i=x,y,z}(B_i(t+\tau) - B_i(t))^2}$. Obviously, relation $\delta\mathbf{B}(t,\tau)$ takes into account also compressive contributions, and the expression $\delta\mathbf{B}(t,\tau) \geq |\delta|\mathbf{B}(t,\tau)||$ is always true.

Looking at Figs. 7.13 and 7.14, taken from the work of Bruno et al. (2003a), the following conclusions can be drawn:

- Magnetic field fluctuations are more intermittent than velocity fluctuations.
- Compressive fluctuations are more intermittent than directional fluctuations.
- Slow wind intermittency does not show appreciable radial dependence.
- Fast wind intermittency, for both magnetic field and velocity, clearly increases with distance.
- Magnetic and velocity fluctuations have a rather Gaussian behavior at large scales, as expected, regardless of type of wind or heliocentric distance.

Moreover, they also found that the intermittency of the components rotated into the mean field reference system (see Sect. 3.3.4) showed that the most intermittent component of the magnetic field is the one along the mean field, while the other two show a similar level of intermittency within the associated uncertainties. Finally, with increasing the radial distance, the component along the mean field becomes more and more intermittent with respect to the transverse components. These results agree with conclusions drawn by Marsch and Tu (1994) who, analyzing fast and slow wind at 0.3 AU in Solar Ecliptic (SE hereafter) coordinate system, found that the PDFs of the fluctuations of transverse components of both velocity and magnetic fields, constructed for different time scales, were appreciably more Gaussian-like than fluctuations observed for the radial component, which resulted to be more and more spiky for smaller and smaller scales.

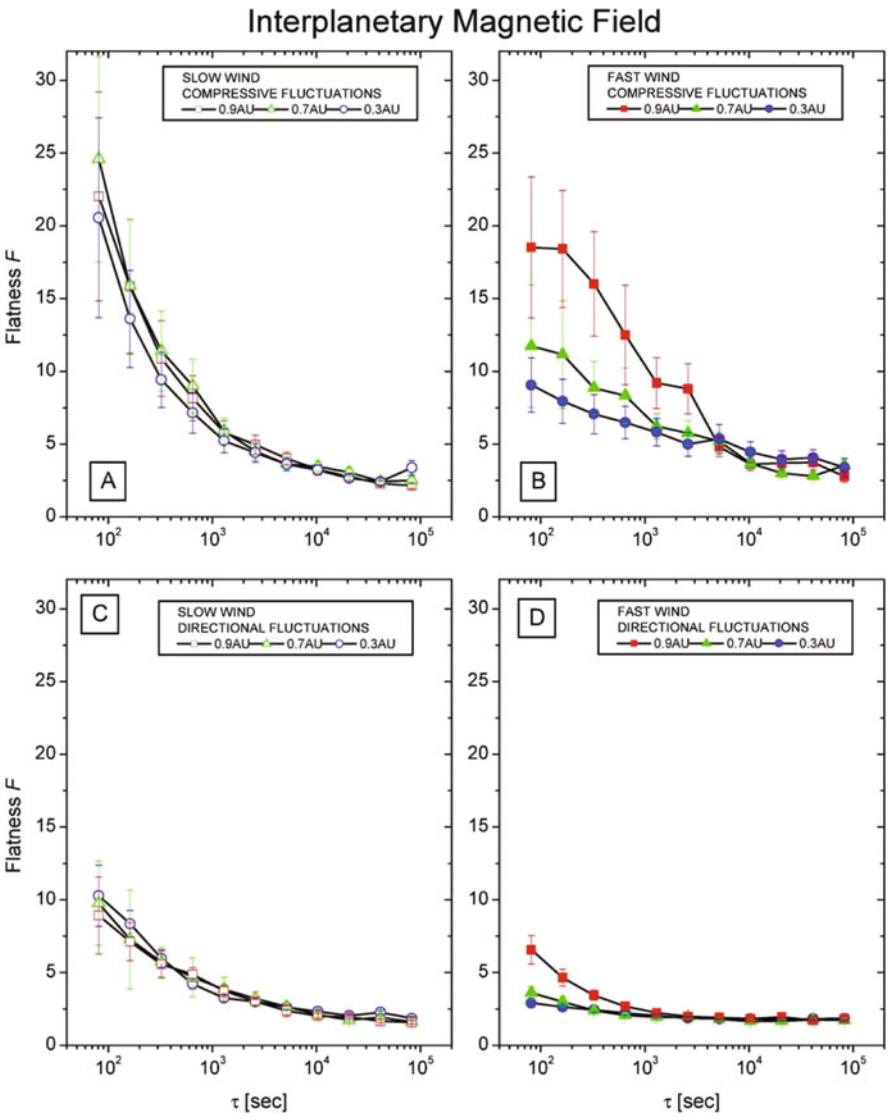

Fig. 7.13 Flatness $\mathscr{F}$ vs. time scale τ relative to magnetic field fluctuations. The *left column* [panels (**a**) and (**c**)] refers to slow wind and the *right column* [panels (**b**) and (**d**)] refers to fast wind. The *upper panels* refer to compressive fluctuations and the *lower panels* refer to directional fluctuations. *Vertical bars* represent errors associated with each value of $\mathscr{F}$. The *three different symbols* in each panel refer to different heliocentric distances as reported in the legend. Image reproduced by permission from Bruno et al. (2003b), copyright by AGU

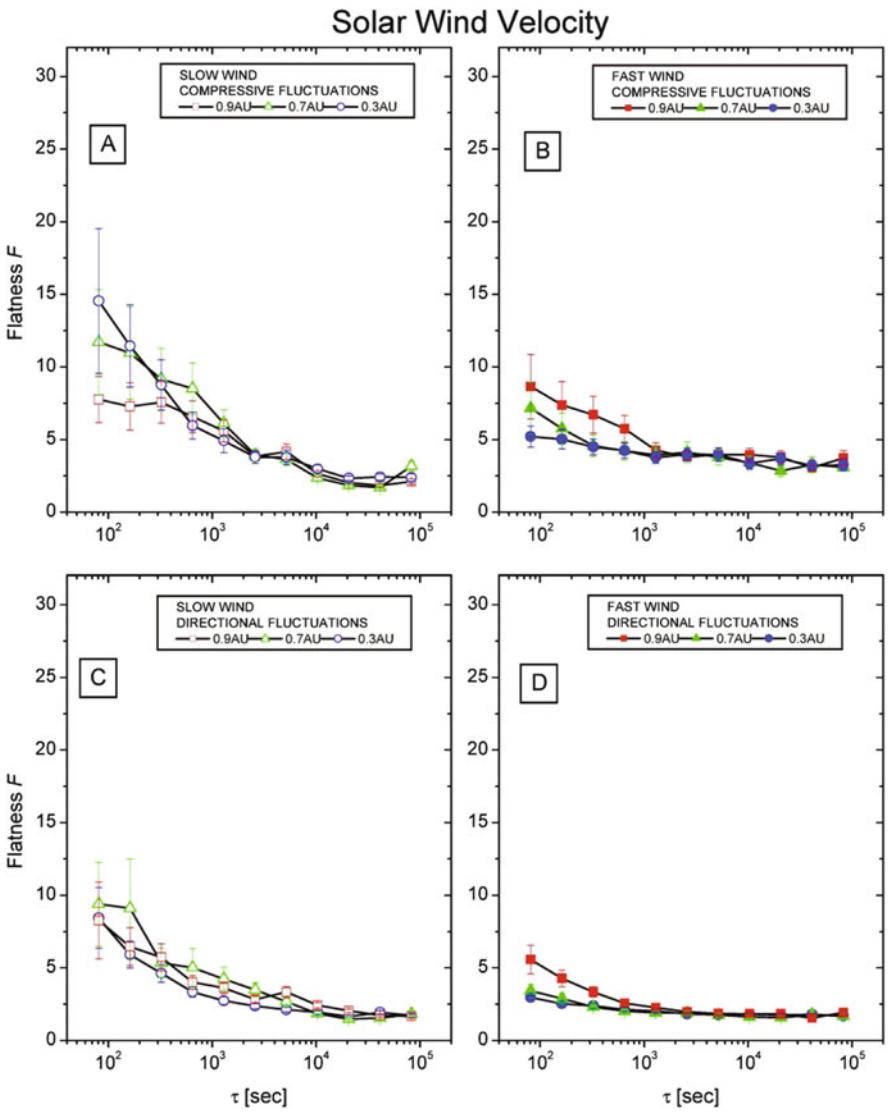

Fig. 7.14 Flatness $\mathscr{F}$ vs. time scale τ relative to wind velocity fluctuations. In the same format of Fig. 7.13 panels (**a**) and (**c**) refer to slow wind and panels (**b**) and (**d**) refer to fast wind. The *upper panels* refer to compressive fluctuations and the *lower panels* refer to directional fluctuations. *Vertical bars* represent errors associated with each value of $\mathscr{F}$. Image reproduced by permission from Bruno et al. (2003b), copyright by AGU

However, at odds with Bruno et al. (2003a), Tu et al. (1996) could not establish any radial dependence since their analysis was performed in the SE reference system instead of the mean field reference system (see Sect. 3.1) as in the analysis of Bruno et al. (2003a). As a matter of fact, the mean field reference system is a more natural reference system where to study magnetic field fluctuations.

The reason is that components normal to the mean field direction are more influenced by Alfvénic fluctuations and, as a consequence, their fluctuations are more stochastic and less intermittent. This effect largely reduces during the radial excursion mainly because in the SE reference system cross-talking between different components is artificially introduced. As a matter of fact, the presence of the large scale spiral magnetic field breaks the spatial symmetry introducing a preferential direction parallel to the mean field. The same Bruno et al. (2003b) showed that it was not possible to find a clear radial trend unless magnetic field data were rotated into this more natural reference system.

On the other hand, it looks more difficult to reconcile the radial evolution of intermittency found by Bruno et al. (2003b) and Marsch and Liu (1993) in fast wind with conclusions drawn by Tu et al. (1996), who stated that "Neither a clear radial evolution nor a clear anisotropy can be established. The value of P1 in high-speed and low-speed wind are not prominent different.". However, it is very likely that the conclusions given above are related with how to deal with the flat slope of the spectrum in fast wind near 0.3 AU. Tu et al. (1996) concluded, indeed: "It should be pointed out that the extended model cannot be used to analyze the intermittency of such fluctuations which have a flat spectrum. If the index of the power spectrum is near or less than unity ... P1 would be 0.5. However, this does not mean there is no intermittency. The model simply cannot be used in this case, because the structure function(1) does not represent the effects of intermittency adequately for those fluctuations which have a flat spectrum and reveal no clear scaling behavior".

Bruno et al. (2003a) suggested that, depending on the type of solar wind sample and on the heliocentric distance, the observed scaling properties would change accordingly. In particular, as the radial distance increases, convected, coherent structures of the wind assume a more relevant role since the Alfvénic component of the fluctuations is depleted. This would be reflected in the increased intermittent character of the fluctuations. The coherent nature of the convected structures would contribute to increase intermittency while the stochastic character of the Alfvénic fluctuations would contribute to decrease it. This interpretation would also justify why compressive fluctuations are always more intermittent than directional fluctuations. As a matter of fact, coherent structures would contribute to the intermittency of compressive fluctuations and, at the same time, would also produce intermittency in directional fluctuations. However, since directional fluctuations are greatly influenced by Alfvénic stochastic fluctuations, their intermittency will be more or less reduced depending on the amplitude of the Alfvén waves with respect to the amplitude of compressive fluctuations.

The radial dependence of the intermittency behavior of solar wind fluctuations stimulated Bruno et al. (1999a) to reconsider previous investigations on fluctuations anisotropy reported in Sect. 3.3.4. These authors studied magnetic field and velocity

fluctuations anisotropy for the same co-rotating, high velocity stream observed by Bavassano et al. (1982) within the framework of the dynamics of non-linear systems. Using the Local Intermittency Measure Farge et al. (1990), Farge (1992) and Bruno et al. (1999a) were able to justify the controversy between results by Klein et al. (1991) in the outer heliosphere and Bavassano et al. (1982) in the inner heliosphere. Exploiting the possibility offered by this technique to locate in space and time those events which produce intermittency, these authors were able to remove intermittent events and perform again the anisotropy analysis. They found that intermittency strongly affected the radial dependence of magnetic fluctuations while it was less effective on velocity fluctuations. In particular, after intermittency removal, the average level of anisotropy decreased for both magnetic and velocity field at all distances. Although magnetic fluctuations remained more anisotropic than their kinetic counterpart, the radial dependence was eliminated. On the other hand, the velocity field anisotropy showed that intermittency, although altering the anisotropic level of the fluctuations, does not markedly change its radial trend.

7.5 Radial Evolution of Intermittency at High Latitude

Recently, Pagel and Balogh (2003) studied intermittency in the outer heliosphere using Ulysses observations at high heliographic latitude, well within high speed solar wind. In particular, these authors used Castaing distribution (Castaing et al. 2001) to study the Probability Distribution Functions (PDF) of the fluctuations of magnetic field components (see Sect. 7.2 for description of Castaing distribution and related governing parameters definition λ and σ). They found that intermittency of small scales fluctuations, within the inertial range, increased with increasing the radial distance from the Sun as a consequence of the growth to larger scales of the inertial range.

As a matter of fact, using the scaling found by Horbury et al. (1996) between the transition scale (the inverse of the frequency corresponding to the break-point in the magnetic field spectrum) $T_B \sim r^{1.1\pm0.1}$, Pagel and Balogh (2003) quantitatively evaluated how the top of the inertial range in their data should shift to larger time scales with increasing heliocentric distance. Moreover, taking into account that inside the inertial range $\lambda^2 \sim \tau^{-\beta} \Longrightarrow \lambda^2 = a\tau^{-\beta}$ and that the proposed scaling from Castaing et al. (2001) would be $\lambda^2 \sim \text{const.}(\tau/T)^{-\beta}$, we should expect that for $\tau = T$ the parameter $\lambda^2 = \text{const}$. Thus, these authors calculated σ^2 and λ^2 at different heliocentric distances and made the hypothesis of a similar scaling for σ^2 and λ^2, although this is not assured by the model. Figure 7.15 reports values of λ^2 and σ^2 vs. distance calculated for the top of the inertial range at that distance using the above procedure. The radial behavior shown in this figure suggests that there is no radial dependence for these parameters for all the three components (indicated by different symbols), as expected if the observed radial increase of intermittency in the inertial range is due to a broadening of the inertial range itself.

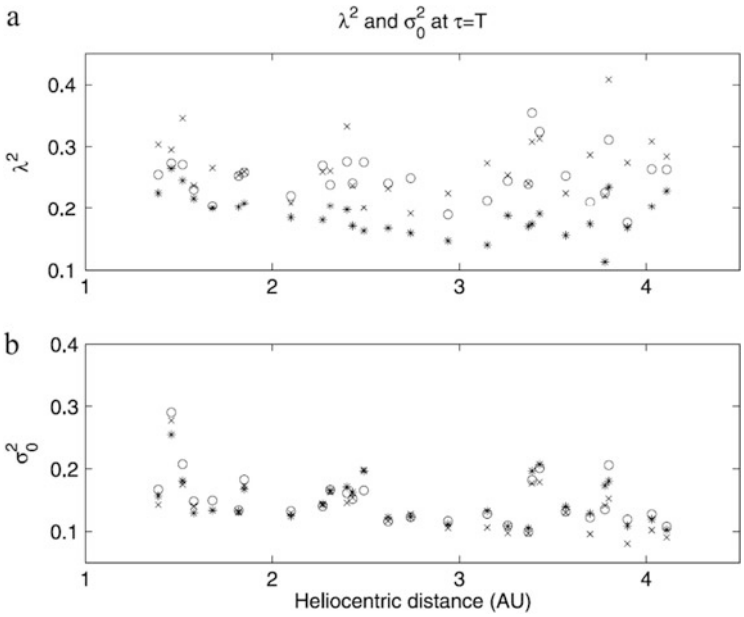

Fig. 7.15 Values of λ^2 (*upper panel*) and σ^2 (*lower panel*) vs. heliocentric distance (see Sect. 7.2 for description of Castaing distribution and definition of λ and σ). These values have been calculated for the projected low frequency beginning of the inertial range relative to each distance (see text for details). R, T, and N components are indicated by *asterisks*, *crosses* and *circles*, respectively. Image reproduced by permission from Pagel and Balogh (2003), copyright by AGU

They also found that, in the RTN reference system, transverse magnetic field components exhibit less Gaussian behavior with respect to the radial component. This result should be compared with results from similar studies by Marsch and Tu (1994) and Bruno et al. (2003b) who, studying the radial evolution of intermittency in the ecliptic, found that the components transverse to the local magnetic field direction, are the most Gaussian ones. Probably, the above discrepancy depends totally on the reference system adopted in these different studies and it would be desirable to perform a new comparison between high and low latitude intermittency in the mean-field reference system.

Pagel and Balogh (2002) focused also on the different intermittent level of magnetic field fluctuations during two fast latitudinal scans which happened to be during solar minimum the first one, and during solar maximum the second one. Their results showed a strong latitudinal dependence but were probably not, or just slightly, affected by radial dependence given the short heliocentric radial variations during these time intervals. They analyzed the anomalous scaling of the third order magnetic field structure functions looking at the value of the parameter μ obtained from the best fit performed using the p-model (see Sect. 6.4). In a previous analysis of the same kind, but focalized on the first latitudinal scan, the same authors tested three intermittency models, namely: "lognormal", "p" and "G-

infinity" models. In particular, this last model was an empirical model introduced by Pierrehumbert (1999) and Cho et al. (2000) and was not intended for turbulent systems. Anyhow, the best fits were obtained with the lognormal and Kolmogorov-p model. These authors concluded that magnetic field components display a very high level of intermittency throughout minimum and maximum phases of solar cycle, and slow wind shows a lower level of intermittency compared with the Alfvénic polar flows. These results do not seem to agree with ecliptic observations (Marsch and Liu 1993; Bruno et al. 2003a) which showed that fast wind is generally less intermittent than slow wind not only for wind speed and magnetic field magnitude, but also for the components. At this point, since it has been widely recognized that low latitude fast wind collected within co-rotating streams and fast polar wind share many common turbulence features, they should be expected to have many similarities also as regards intermittency. Thus, it is possible that also in this case the reference system in which the analysis is performed plays some role in determining some of the results regarding the behavior of the components. In any case, further analyses should clarify the reasons for this discrepancy.

References

B. Bavassano, R. Bruno, Evidence of local generation of Alfvénic turbulence in the solar wind. J. Geophys. Res. **94**(13), 11977–11982 (1989). doi:10.1029/JA094iA09p11977

B. Bavassano, M. Dobrowolny, G. Fanfoni, F. Mariani, N.F. Ness, Statistical properties of MHD fluctuations associated with high-speed streams from Helios 2 observations. Solar Phys. **78**, 373–384 (1982). doi:10.1007/BF00151617

L. Bianchini, E. Pietropaolo, R. Bruno, An improved method for local intermittency recognition, in *Magnetic Fields and Solar Processes*, ed. by A. Wilson. ESA Conference Proceedings, vol. SP-448 (ESA Publications Division, Noordwijk, 1999), pp. 1141–1146

J.E. Borovsky, Flux tube texture of the solar wind: Strands of the magnetic carpet at 1 AU? J. Geophys. Res. **113** (2008). doi:10.1029/2007JA012684

R. Bruno, B. Bavassano, Origin of low cross-helicity regions in the solar wind. J. Geophys. Res. **96**, 7841–7851 (1991). doi:10.1029/91JA00144

R. Bruno, B. Bavassano, E. Pietropaolo, V. Carbone, P. Veltri, Effects of intermittency on interplanetary velocity and magnetic field fluctuations anisotropy. Geophys. Res. Lett. **26**, 3185–3188 (1999a). doi:10.1029/1999GL010668

R. Bruno, B. Bavassano, L. Bianchini, E. Pietropaolo, U. Villante, V. Carbone, P. Veltri, Solar wind intermittency studied via local intermittency measure, in *Magnetic Fields and Solar Processes*, ed. by A. Wilson. ESA Conference Proceedings, vol. SP-448 (ESA, Noordwijk, 1999b), pp. 1147–1152

R. Bruno, V. Carbone, P. Veltri, E. Pietropaolo, B. Bavassano, Identifying intermittent events in the solar wind. Planet. Space Sci. **49**, 1201–1210 (2001). doi:10.1016/S0032-0633(01)00061-7

R. Bruno, V. Carbone, L. Sorriso-Valvo, B. Bavassano, On the role of coherent and stochastic fluctuations in the evolving solar wind MHD turbulence: intermittency, in *Solar Wind Ten*, ed. by M. Velli, R. Bruno, F. Malara. AIP Conference Proceedings, vol. 679 (American Institute of Physics, Melville, 2003a), pp. 453–456

R. Bruno, V. Carbone, L. Sorriso-Valvo, B. Bavassano, Radial evolution of solar wind intermittency in the inner heliosphere. J. Geophys. Res. **108**(3), 8–24 (2003b). doi:10.1029/2002JA009615

R. Bruno, V. Carbone, L. Primavera, F. Malara, L. Sorriso-Valvo, B. Bavassano, P. Veltri, On the probability distribution function of small-scale interplanetary magnetic field fluctuations. Ann. Geophys. **22**, 3751–3769 (2004). doi:10.5194/angeo-22-3751-2004

L.F. Burlaga, Intermittent turbulence in the solar wind. J. Geophys. Res. **96**(15), 5847–5851 (1991a). doi:10.1029/91JA00087

L.F. Burlaga, Multifractal structure of speed fluctuations in recurrent streams at 1 AU and near 6 AU. Geophys. Res. Lett. **18**, 1651–1654 (1991b). doi:10.1029/91GL01221

L.F. Burlaga, Multifractal structure of the interplanetary magnetic field: Voyager 2 observations near 25 AU, 1987–1988. Geophys. Res. Lett. **18**, 69–72 (1991c). doi:10.1029/90GL02596

L.F. Burlaga, L.W. Klein, Fractal structure of the interplanetary magnetic field. J. Geophys. Res. **91**(10), 347–350 (1986). doi:10.1029/JA091iA01p00347

V. Carbone, Cascade model for intermittency in fully developed magnetohydrodynamic turbulence. Phys. Rev. Lett. **71**, 1546–1548 (1993). doi:10.1103/PhysRevLett.71.1546

V. Carbone, Scale similarity of the velocity structure functions in fully developed magnetohydrodynamic turbulence. Phys. Rev. E **50**, 671–674 (1994a). doi:10.1103/PhysRevE.50.R671

V. Carbone, Scaling exponents of the velocity structure functions in the interplanetary medium. Ann. Geophys. **12**(7), 585–590 (1994b). doi:10.1007/s00585-994-0585-3

V. Carbone, P. Veltri, R. Bruno, Experimental evidence for differences in the extended self-similarity scaling laws between fluid and magnetohydrodynamic turbulent flows. Phys. Rev. Lett. **75**, 3110–3113 (1995). doi:10.1103/PhysRevLett.75.3110

V. Carbone, R. Bruno, P. Veltri, Evidences for extended self-similarity in hydromagnetic turbulence. Geophys. Res. Lett. **23**, 121–124 (1996). doi:10.1029/95GL03777

B. Castaing, Y. Gagne, V. Hopfinger, Velocity probability density functions of high Reynolds number turbulence. Physica D **46**, 177–200 (2001)

T. Chang, Complexity induced plasma turbulence in coronal holes and the solar wind, in *Solar Wind Ten*, ed. by M. Velli, R. Bruno, F. Malara. AIP Conference Proceedings, vol. 679 (American Institute of Physics, Melville, 2003), pp. 481–484

T. Chang, C. Wu, Complexity and anomalous transport in space plasmas. Phys. Plasmas **9**, 3679–3684 (2002). doi:10.1063/1.1499115

T. Chang, S.W.Y. Tam, C. Wu, Complexity induced anisotropic bimodal intermittent turbulence in space plasmas. Phys. Plasmas **11**, 1287–1299 (2004). doi:10.1063/1.1667496

J.Y.N. Cho, R.E. Newell, G.W. Sachse, Anomalous scaling of mesoscale tropospheric humidity fluctuations. Geophys. Res. Lett. **27**, 377–380 (2000). doi:10.1029/1999GL010846

M. Farge, Wavelet transforms and their applications to turbulence. Annu. Rev. Fluid Mech. **24**, 395–457 (1992). doi:10.1146/annurev.fl.24.010192.002143

M. Farge, M. Holschneider, J.F. Colonna, Wavelet analysis of coherent structures in two-dimensional turbulent flows, in *Topological Fluid Mechanics*, ed. by H.K. Moffat (Cambridge University Press, Cambridge, 1990), pp. 765–766

M.A. Forman, L.F. Burlaga, Exploring the Castaing distribution function to study intermittence in the solar wind at L1 in June 2000, in *Solar Wind Ten*, ed. by M. Velli, R. Bruno, F. Malara. AIP Conference Proceedings, vol. 679 (American Institute of Physics, Melville, 2003), pp. 554–557

U. Frisch, *Turbulence: The Legacy of A.N. Kolmogorov* (Cambridge University Press, Cambridge, 1995)

T.S. Horbury, A. Balogh, Structure function measurements of the intermittent MHD turbulent cascade. Nonlinear Process. Geophys. **4**, 185–199 (1997). doi:10.5194/npg-4-185-1997

T.S. Horbury, A. Balogh, R.J. Forsyth, E.J. Smith, Observations of evolving turbulence in the polar solar wind. Geophys. Res. Lett. **22**, 3401–3404 (1995a). doi:10.1029/95GL03550

T.S. Horbury, A. Balogh, R.J. Forsyth, E.J. Smith, Ulysses magnetic field observations of fluctuations within polar coronal flows. Ann. Geophys. **13**, 105–107 (1995b)

T.S. Horbury, A. Balogh, R.J. Forsyth, E.J. Smith, The rate of turbulent evolution over the sun's poles. Astron. Astrophys. **316**, 333–341 (1996)

T.S. Horbury, A. Balogh, R.J. Forsyth, E.J. Smith, Ulysses observations of intermittent heliospheric turbulence. Adv. Space Res. **19**, 847–850 (1997). doi:10.1016/S0273-1177(97)00290-1

L.W. Klein, D.A. Roberts, M.L. Goldstein, Anisotropy and minimum variance directions of solar wind fluctuations in the outer heliosphere. J. Geophys. Res. **96**(15), 3779–3788 (1991). doi:10.1029/90JA02240

A.N. Kolmogorov, The local structure turbulence in incompressible viscous fluids for very large Reynolds numbers. Dokl. Akad. Nauk. SSSR **30**, 301–305 (1941)

A.N. Kolmogorov, A refinement of previous hypotheses concerning the local structure of turbulence in a viscous incompressible fluid at high Reynolds number. J. Fluid Mech. **13**, 82–85 (1962). doi:10.1017/S0022112062000518

A.N. Kolmogorov, The local structure of turbulence in incompressible viscous fluid for very large Reynolds numbers. Proc. R. Soc. London, Ser. A **434**, 9–13 (1991)

R.H. Kraichnan, Inertial range spectrum of hydromagnetic turbulence. Phys. Fluids **8**, 1385–1387 (1965)

G. Li, Identifying current-sheet-like structures in the solar wind. Astrophys. J. **672**, 65–68 (2008). doi:10.1086/525847

G. Li, E. Lee, G. Parks, Are there current-sheet-like structures in the earth's magnetotail as in the solar wind—results and implications from high time resolution magnetic field measurements by cluster. Ann. Geophys. **26**, 1889–1895 (2008). doi:10.5194/angeo-26-1889-2008

E. Marsch, S. Liu, Structure functions and intermittency of velocity fluctuations in the inner solar wind. Ann. Geophys. **11**, 227–238 (1993)

E. Marsch, C.-Y. Tu, Non-Gaussian probability distributions of solar wind fluctuations. Ann. Geophys. **12**(12), 1127–1138 (1994). doi:10.1007/s00585-994-1127-8

E. Marsch, C.-Y. Tu, Intermittency, non-gaussian statistics and fractal scaling of MHD fluctuations in the solar wind. Nonlinear Process. Geophys. **4**, 101–124 (1997). doi:10.5194/npg-4-101-1997

E. Marsch, C.-Y. Tu, H. Rosenbauer, Multifractal scaling of the kinetic energy flux in solar wind turbulence. Ann. Geophys. **14**(3), 259–269 (1996). doi:10.1007/s00585-996-0259-4

C. Meneveau, Analysis of turbulence in the orthonormal wavelet representation. J. Fluid Mech. **232**, 469–520 (1991). doi:10.1017/S0022112091003786

C. Meneveau, K.R. Sreenivasan, Simple multifractal cascade model for fully developed turbulence. Phys. Rev. Lett. **59**, 1424–1427 (1987). doi:10.1103/PhysRevLett.59.1424

M. Onorato, R. Camussi, G. Iuso, Anomalous scaling and bursting process in an experimental turbulent channel flow. Phys. Rev. E **61**, 1447–1460 (2000). doi:10.1103/PhysRevE.61.1447

C. Pagel, A. Balogh, Intermittency in the solar wind: a comparison between solar minimum and maximum using Ulysses data. J. Geophys. Res. **107**(A8), 1178 (2002). doi:10.1029/2002JA009331

C. Pagel, A. Balogh, Radial dependence of intermittency in the fast polar solar wind magnetic field using Ulysses. J. Geophys. Res. **108**(A1), 1012 (2003). doi:10.1029/2002JA009498

G. Paladin, A. Vulpiani, Anomalous scaling laws in multifractal objects. Phys. Rep. **156**, 147–225 (1987). doi:10.1016/0370-1573(87)90110-4

R.T. Pierrehumbert, Huascaran δ^{18}o as an indicator of tropical climate during the last glacial maximum. Geophys. Res. Lett. **26**, 1345–1348 (1999). doi:10.1029/1999GL900183

L. Primavera, F. Malara, P. Veltri, Parametric instability in the solar wind: numerical study of the nonlinear evolution, in *Solar Wind Ten*, ed. by M. Velli, R. Bruno, F. Malara. AIP Conference Proceedings, vol. 679 (American Institute of Physics, Melville, 2003), pp. 505–508

A.A. Ruzmaikin, J. Feynman, B.E. Goldstein, E.J. Smith, A. Balogh, Intermittent turbulence in solar wind from the south polar hole. J. Geophys. Res. **100**(9), 3395–3403 (1995). doi:10.1029/94JA02808

C. Salem, A. Mangeney, S.D. Bale, P. Veltri, Solar wind magnetohydrodynamics turbulence: Anomalous scaling and role of intermittency. Astrophys. J. **702**, 537–553 (2009). doi:10.1088/0004-637X/702/1/537

D. Schertzer, S. Lovejoy, F. Schmitt, Y. Chigirinskaya, D. Marsan, Multifractal cascade dynamics and turbulent intermittency. Fractals **5**, 427–471 (1997). doi:10.1142/S0218348X97000371

J.V. Shebalin, W.H. Matthaeus, D. Montgomery, Anisotropy in MHD turbulence due to a mean magnetic field. J. Plasma Phys. **29**, 525–547 (1983). doi:10.1017/S0022377800000933

L. Sorriso-Valvo, V. Carbone, P. Veltri, G. Consolini, R. Bruno, Intermittency in the solar wind turbulence through probability distribution functions of fluctuations. Geophys. Res. Lett. **26**, 1801–1804 (1999). doi:10.1029/1999GL900270

L. Sorriso-Valvo, V. Carbone, P. Giuliani, P. Veltri, R. Bruno, V. Antoni, E. Martines, Intermittency in plasma turbulence. Planet. Space Sci. **49**, 1193–1200 (2001). doi:10.1016/S0032-0633(01)00060-5

K.M. Thieme, R. Schwenn, E. Marsch, Are structures in high-speed streams signatures of coronal fine structures? Adv. Space Res. **9**, 127–130 (1989). doi:10.1016/0273-1177(89)90105-1

B.T. Tsurutani, E.J. Smith, Interplanetary discontinuities - temporal variations and the radial gradient from 1 to 8.5 AU. J. Geophys. Res. **84**(13), 2773–2787 (1979). doi:10.1029/JA084iA06p02773

C.-Y. Tu, Z.-Y. Pu, F.-S. Wei, The power spectrum of interplanetary Alfvénic fluctuations derivation of the governing equation and its solution. J. Geophys. Res. **89**(18), 9695–9702 (1984). doi:10.1029/JA089iA11p09695

C.-Y. Tu, The damping of interplanetary Alfvénic fluctuations and the heating of the solar wind. J. Geophys. Res. **93**, 7–20 (1988). doi:10.1029/JA093iA01p00007

C.-Y. Tu, E. Marsch, Transfer equations for spectral densities of inhomogeneous MHD turbulence. J. Plasma Phys. **44**, 103–122 (1990). doi:10.1017/S002237780001504X

C.-Y. Tu, E. Marsch, A model of solar wind fluctuations with two components: Alfvén waves and convective structures. J. Geophys. Res. **98**(17), 1257–1276 (1993). doi:10.1029/92JA01947

C.-Y. Tu, E. Marsch, MHD structures, waves and turbulence in the solar wind: Observations and theories. Space Sci. Rev. **73**(1/2), 1–210 (1995). doi:10.1007/BF00748891

C.-Y. Tu, E. Marsch, H. Rosenbauer, An extended structure-function model and its application to the analysis of solar wind intermittency properties. Ann. Geophys. **14**(3), 270–285 (1996). doi:10.1007/s00585-996-0270-9

P. Veltri, A. Mangeney, Scaling laws and intermittent structures in solar wind MHD turbulence, in *Solar Wind Nine*, ed. by S.R. Habbal, J.V. Hollweg, P.A. Isenberg. AIP Conference Proceedings, vol. 471 (American Institute of Physics, Woodbury, 1999), pp. 543–546. doi:10.1063/1.58809

Chapter 8
Solar Wind Heating by the Turbulent Energy Cascade

The Parker theory (Parker 1958; Parker 1963) predicts an adiabatic expansion of the solar wind from the hot corona without further heating. For such a model, the proton temperature $T(r)$ should decrease with the heliocentric distance r as $T(r) \sim r^{-4/3}$. The radial profile of proton temperature have been obtained from measurements by the Helios spacecraft at 0.3 AU (Marsch et al. 1982; Marsch 1983; Schwenn 1983; Freeman 1988; Goldstein 1996), up to 100 AU or more by Voyager and Pioneer spacecrafts (Gazis 1984; Gazis et al. 1994; Richardson et al. 1995). These measurements show that the temperature decay, at least within fast and Alfvénic wind, is in fact considerably slower than expected. Fits of the radial temperature profile gave an effective decrease $T \sim T_0(r_0/r)^{\xi}$ in the ecliptic plane, with the exponent $\xi \in [0.7; 1]$, much smaller than the adiabatic case. Actually $\xi \simeq 1$ within 1 AU, while ξ flattens to $\xi \simeq 0.7$ beyond 30 AU, where pickup ions probably contribute significantly (Richardson et al. 1995; Zank et al. 1996; Smith et al. 2001a). These observations imply that some heating mechanism must be at work within the wind plasma to supply the energy required to slow down the decay. The nature of the heating process of solar wind is an open problem.

The primary process governing the solar wind heating is probably active locally in the wind. However, since collisions are very rare in the solar wind plasma, the usual viscous coefficients have no meaning, say energy must be transferred to very small scales before it can be efficiently dissipated, perhaps by kinetic processes. As a consequence, the presence of a turbulent energy flux is the crucial first step towards the understanding of solar wind heating (Coleman 1968; Tu and Marsch 1995a) because, as said in Sect. 2.4, the turbulent energy cascade represents nothing but the way for energy to be efficiently dissipated in a high-Reynolds number flow.[1] In other words, before to face the problem of what actually be the physical mechanisms responsible for energy dissipation, if we conjecture that these processes happens at

[1] For a discussion on non-turbulent mechanism of solar wind heating cf. Tu and Marsch (1995a).

R. Bruno, V. Carbone, *Turbulence in the Solar Wind*, Lecture Notes in Physics 928, DOI 10.1007/978-3-319-43440-7_8

small scales, the turbulent energy flux towards small scales must be of the same order of the heating rate.

Using the hypothesis that the energy dissipation rate is equal to the heat addition, one can use the omnidirectional power law spectrum derived by Kolmogorov

$$P(k) = C_K \epsilon_P^{2/3} k^{-5/3}$$

(C_K is the Kolmogorov constant that can be obtained from measurements) to infer the energy dissipation rate (Leamon et al. 1999)

$$\epsilon_P = \left[\frac{5}{3} P(k) C_K^{-1}\right]^{3/2} k^{5/2}, \tag{8.1}$$

where $k = 2\pi f/V$ (f is the frequency in the spacecraft frame and V is the solar wind speed). The same conjecture can be made by using Elsässer variables, thus obtaining a generalized Kolmogorov phenomenology for the power spectra $P^{\pm}(k)$ of the Elsässer variables (Zhou and Matthaeus 1989, 1990; Marsch 1991)

$$\epsilon_P^{\pm} = C_k^{-3/2} P^{\pm}(k) \sqrt{P^{\mp}(k)} k^{5/2}. \tag{8.2}$$

Even if the above expressions are affected by the presence of intermittency, namely extreme fluctuations of the energy transfer rate, and an estimated value for the Kolmogorov constant is required, the estimated energy dissipation rates roughly agree with the heating rates derived from gradients of the thermal proton distribution (MacBride et al. 2010).

A different estimate for the energy dissipation rate in spherical symmetry can be derived from an expression that uses the adiabatic cooling in combination with local heating rate ϵ. In a steady state situation the equation for the radial profile of ions temperature can be written as (Verma et al. 1995)

$$\frac{dT(r)}{dr} + \frac{4}{3}\frac{T(r)}{r} = \frac{m_p \epsilon}{(3/2) V_{\rm SW}(r) k_B}, \tag{8.3}$$

where m_p is the proton mass and $V_{\rm SW}(r)$ is the radial profile of the bulk wind speed in km s^{-1}. (k_B is the Boltzmann constant). Equation (8.3) can be solved using the actual radial profile of temperature thus obtaining an expression for the radial profile of the heating rate needed to heat the wind at the actual value (Vasquez et al. 2007)

$$\epsilon(r) = \frac{3}{2}\left(\frac{4}{3} - \xi\right) \frac{V_{\rm SW}(r) k_B T(r)}{r m_p}. \tag{8.4}$$

This relation is obtained by considering a polytropic index $\gamma = 5/3$ for the adiabatic expansion of the solar wind plasma, the protons being the only particles heated in the process. Such assumptions are only partially correct, since the electrons could play a relevant role in the heat exchange. Heating rates obtained using Eq. (8.4) should

thus be only seen as a first approximation that could be improved with better models of the heating processes. Using the expected solar wind parameters at 1 AU, the expected heating rate ranges from 10^2 J/kg s for cold wind to 10^4 J/kg s in hot wind. Cascade rates estimated from the energy-containing scale of turbulence at 1 AU obtained by evaluating triple correlations of fluctuations and the correlation length scale of turbulence give values in this range (Smith et al. 2001b, 2006; Isenberg 2005; Vasquez et al. 2007)

Rather than estimating the heating rate by typical solar wind fluctuations and the Kolmogorov constant, it is perhaps much more convenient to get a direct estimate of the energy dissipation rate by measurements of the turbulent energy cascade using the Yaglom's law, say from measurements of the third-order mixed moments of fluctuations. In fact, the roughly constant values of $Y_\ell^\pm/\ell$, or alternatively their compressible counterpart $W_\ell^\pm/\ell$ will result in an estimate for the pseudo-energy dissipation rates $\epsilon^\pm$ (at least within a constant of order unity), over a range of scales ℓ, which by definition is unaffected by intermittency. This has been done both in the ecliptic plane (MacBride et al. 2008, 2010) and in polar wind (Marino et al. 2009; Carbone et al. 2009). Preliminary attempts (MacBride et al. 2008) already estimated that the energy dissipation rate ϵ_E was close to the value required for the heating of solar wind. However, refined analysis (MacBride et al. 2010) indicated that at 1 AU, in the ecliptic plane, the solar wind can be sufficiently heated by a turbulent energy cascade. As a different approach, Marino et al. (2009), using data from the Ulysses spacecraft in the polar wind, calculated values of the pseudo-energies from the relation $Y_\ell^\pm/\ell$, and compared these values with the radial profile of the heating rate (8.4) required to maintain the observed temperature against the adiabatic cooling. The Ulysses database provides two different estimates for the temperature, T_1, indicated as $T_{\rm large}$ in literature, and T_2, known as $T_{\rm small}$. In general, T_1 and T_2 are known to give sometimes an overestimate and an underestimate of the true temperature, respectively, so that the analysis was performed using both temperatures (Marino et al. 2008; Marino et al. 2009; Marino et al. 2011). The heating rate was estimated at the same locations where the energy cascade was observed. As shown in Fig. 8.1, results indicate that turbulent transfer rate represents a significant amount of the expected heating, say the MHD turbulent cascade contributes to the in situ heating of the wind from 8 to 50 % (for T_1 and T_2 respectively), up to 100 % in some cases. The authors concluded that, although the turbulent cascade in the polar wind must be considered an important ingredient of the heating, the turbulent cascade alone seems unable to provide all the heating needed to explain the observed slowdown of the temperature decrease, in the framework of the model profile given in Eq. (8.4). The situation is completely different as far as compressibility is taken into account. In fact, when the pseudo-energy transfer rates have been calculated through $W_\ell^\pm/\ell$, the radial profile of energy dissipation rate is well described thus indicating that the turbulent energy cascade provides the amount of energy required to locally heat the solar wind to the observed values.

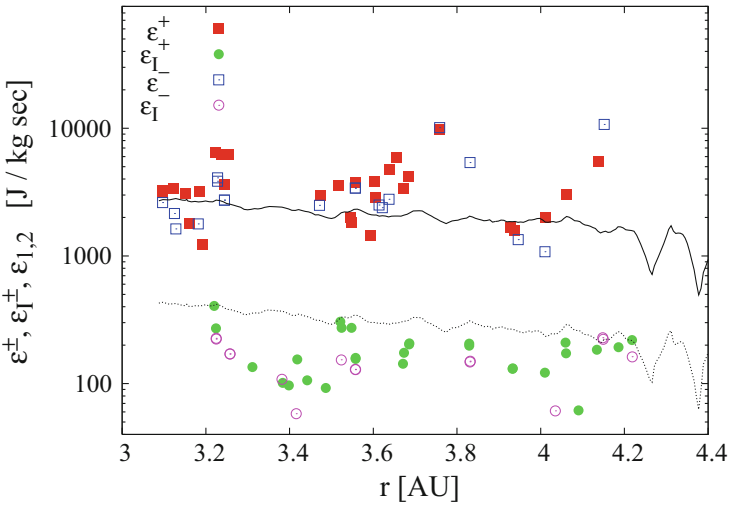

Fig. 8.1 Radial profile of the pseudoenergy transfer rates obtained from the turbulent cascade rate through the Yaglom relation, for both the compressive and the incompressive case. The *solid lines* represent the radial profiles of the heating rate required to obtain the observed temperature profile. Figure adapted from Marino et al. (2011)

8.1 Dissipative/Dispersive Range in the Solar Wind Turbulence

As we saw in Sect. 6.7, the energy cascade in turbulence can be recognized by looking at Yaglom's law. The presence of this law in the solar wind turbulence showed that an energy cascade is at work, thus transferring energy to small scales where it is dissipated by some mechanism. While, as we showed before, the inertial range of turbulence in solar wind can be described more or less in a fluid framework, the small scales dissipative region can be much more (perhaps completely) different. The main motivation for this is the fact that the collision length in the solar wind, as a rough estimate the thermal velocity divided by the collision frequency, results to be of the order of 1 AU. Then the solar wind behaves formally as a collisionless plasma, that is the usual viscous dissipation is negligible. At the same time, in a magnetized plasma there are a number of characteristic scales, then understanding the physics of the generation of the small-scale region of turbulence in solar wind is a challenging topic from the point of view of basic plasma physics. With small-scales we mean scales ranging between the ion-cyclotron frequency $f_{\rm ci} = eB/m_i$ (which in the solar wind at 1 AU is about $f_{\rm ci} \simeq 0.1$ Hz, see Table 1.3), or the ion inertial length $\lambda_i = c/\omega_{pi}$, and the electron-cyclotron frequency $f_{\rm ce} = eB/m_e$. At these scales the usual MHD approximation breaks down in favour of a more complex description of plasma where kinetic processes take place.

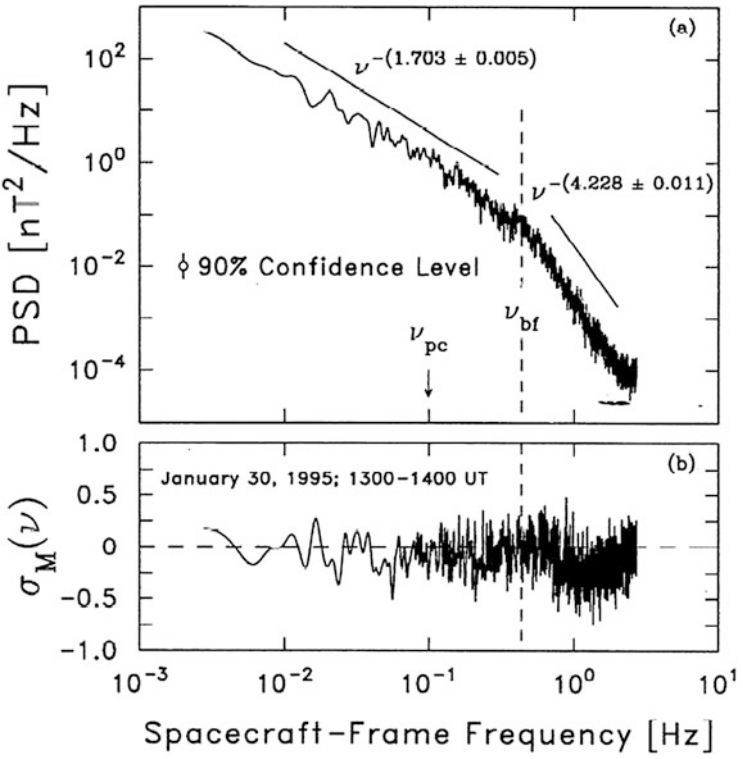

Fig. 8.2 (**a**) Typical interplanetary magnetic field power spectrum obtained from the trace of the spectral matrix. A spectral break at about ~ 0.4 Hz is clearly visible. (**b**) Corresponding magnetic helicity spectrum. Image reproduced by permission from Leamon et al. (1998), copyright by AGU

Some time ago, Leamon et al. (1998) analyzed small-scales magnetic field measurements at 1 AU, by using 33 1-h intervals of the MFI instrument on board Wind spacecraft. Figure 8.2 shows the trace of the power spectral density matrix for hour 13:00 on day 30 of 1995, which is a typical interplanetary magnetic field power spectrum representative of those analysed by Leamon et al. (1998). It is evident that a spectral break exists at about $f_{\rm br} \simeq 0.44$ Hz, slightly above to the ion-cyclotron frequency. Below the ion-cyclotron frequency, the spectrum follows the usual power law $f^{-\alpha}$, where the spectral index is close to the Kolmogorov value $\alpha \simeq 5/3$. At small-scales, namely at frequencies above $f_{\rm br}$, the spectrum steepens significantly, but is still described by a power law with a slope in the range $\alpha \in [2\text{–}4]$ (Leamon et al. 1998; Smith et al. 2006). As a direct analogy to hydrodynamics where the steepening of the inertial range spectrum corresponds to the onset of dissipation, the authors attribute the steepening of the spectrum to the occurrence of a "dissipative" range (Leamon et al. 1998).

In this respect, Smith et al. (2006) performed a wide statistical study on the spectral index in the dissipation range using about 900 intervals of interplanetary

magnetic field recorded by ACE spacecraft at 1 AU. These authors found that while within the inertial range the distribution of the values of the spectral index was quite narrow and peaked between $-5/3$ and $-3/2$ that corresponding to the dissipation range was much broader, roughly varying between -1 and -4 with a broad peak between -2 and -3. These authors were able to correlate this power-law index to the rate of the magnetic energy cascade ϵ. They found steeper dissipation range spectra associated with higher cascade rates. In particular, they found ϵ following $\sim -1.05\epsilon^{0.09}$. These results corroborated previous findings by Leamon et al. (1998) who found that the spectral slope in the dissipation range was directly correlated to the thermal proton temperature, i.e. steeper slopes would imply greater heating rates. Markovskii et al. (2006) found that turbulence spectra often have power-law dissipation ranges with an average spectral index of -3 and suggested that this fact is a consequence of a marginal state of the instability in the dissipation range. However, they concluded that their mechanism, acting together with the Landau damping, would produce an entire range of spectral indices, not just -3, in better agreement with the observations.

Later, Bruno et al. (2014), similarly to previous analyses reported in literature, investigated the behavior of the spectral index within the first frequency decade beyond the spectral break analyzing different solar wind samples along the speed profile of several high velocity streams within the inner heliosphere. They found the same large variability already reported in literature (Leamon et al. 1998; Smith et al. 2006) but were able to highlight a robust tendency for this parameter to indicate steeper spectra within the trailing edge of fast streams and lower values within the subsequent slow wind, following a gradual transition between these two states. These results were successively confirmed also for the parallel and perpendicular spectra (Bruno and Telloni 2015). The value of the spectral index seems to depend firmly on the power associated to the fluctuations within the inertial range, higher the power steeper the slope (see also Smith et al. 2006). In particular, the spectral index tends to approach $-5/3$, typical of the inertial range, within the slow wind while, a simple fit of all the estimates recorded at 1 AU, would suggest a limiting value of roughly -4.2 ± 0.43 within the fast wind. These same authors suggested also that it would be interesting to investigate whether not only the power level of the fluctuations but also their Alfvénic character might play a role in the observed behavior of the spectral index at ion scales in the framework of ion-cyclotron resonance mechanism (see Marsch 2006, and references therein).

Further properties of turbulence in the high-frequency region have been evidenced by looking at solar wind observations by the FGM (flux-gate magnetometer) instrument onboard Cluster satellites (Alexandrova et al. 2008) spanning a $0.02 \div 0.5$ Hz frequency range. The authors found that the same spectral break by Leamon et al. (1998) exists when different datasets (Helios for large-scales and Cluster for small scales) are used. The break (cf. Fig. 1 of Alexandrova et al. 2008) has been found at about $f_{\rm br} \simeq 0.3$ Hz, near the ion cyclotron frequency $f_{\rm ci} \simeq 0.1$ Hz, which roughly corresponds to spatial scales of about 1900 km $\simeq 15\lambda_i$ (being $\lambda_i \simeq 130$ km the ion-skin-depth). However, as shown in Fig. 1 of Alexandrova et al. (2008), the compressible magnetic fluctuations, measured by magnetic field

parallel spectrum $S_\parallel$, are enhanced at small-scales (see Bruno and Telloni 2015; Podesta 2009, and references therein). This means that, after the break compressible fluctuations become much more important than in the low-frequency part. The parameter $\langle S_\parallel \rangle / \langle S \rangle / \simeq 0.03$ in the low-frequency range (S is the total power spectrum density and brackets means averages value over the whole range) while compressible fluctuations are increased to about $\langle S_\parallel \rangle / \langle S \rangle / \simeq 0.26$ in the high-frequency part. The increase of the above ratio were already noted in the paper by Leamon et al. (1998). Moreover, Alexandrova et al. (2008) found that, similarly to the low-frequency region (cf. Sect. 6.2), intermittency is a basic property also in the high-frequency range. In fact, the authors found that PDFs of normalized magnetic field increments strongly depend on the scale (Alexandrova et al. 2008), a typical signature of intermittency in fully developed turbulence (cf. Sect. 6.2). More quantitatively, the behavior of the fourth-order moment of magnetic fluctuations at different frequencies $K(f)$ is shown in Fig. 8.3.

It is evident that this quantity increases with frequency, indicating the presence of intermittency. However the rate at which $K(f)$ increases is pronounced above the ion cyclotron frequency, meaning that intermittency in the high-frequency range is much more effective than in the low-frequency region. Recently, analyzing a different datasets recorded by Cluster spacecraft, it was found that the intermittent character of magnetic fluctuations within the kinetic range persists at least to electron scales (Perri et al. 2012; Wan et al. 2012; Karimabadi et al. 2013) and this was ascribed to the presence of small scale coherent magnetic structures. Further

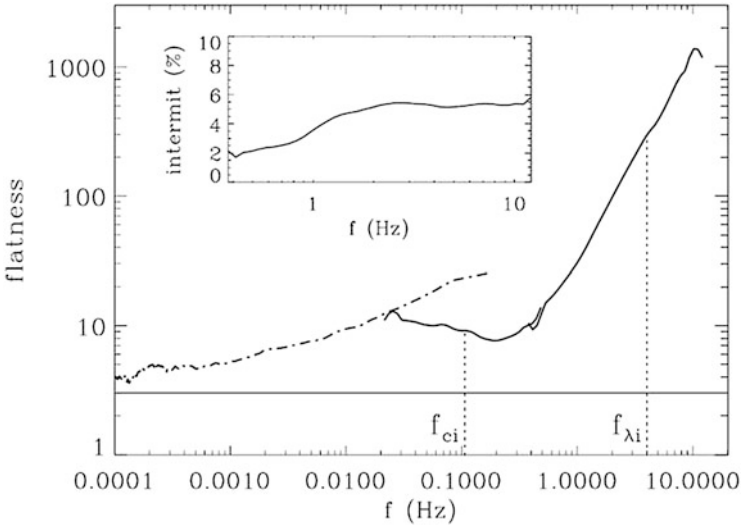

Fig. 8.3 The fourth-order moment $K(f)$ of magnetic fluctuations as a function of frequency f is shown. *Dashed line* refers to data from Helios spacecraft while full line refers to data from Cluster spacecrafts at 1 AU. The *inset* refers to the number of intermittent structures revealed as da function of frequency. Image reproduced by permission from Alexandrova et al. (2008), copyright by AAS

analyses associated elevated plasma temperature and anisotropy events with these structures, suggesting that inhomogeneous dissipation was at work (Servidio et al. 2012).

Different results were obtained by Wu et al. (2013) who, using both flux-gate and search-coil magnetometers on board Cluster, found kinetic scales that are much less intermittent than fluid scales. These authors recorded a remarkable and sudden decrease back to near-Gaussian values of intermittency around scales of about ten times the ion inertial scale (see also results by Telloni et al. 2015; Bruno and Telloni 2015), followed by a modest increase moving toward electron scales, in agreement with Kiyani et al. (2009). These last authors, using high-order statistics of magnetic differences, showed that the scaling exponents of structure functions, evaluated at small scales, are no more anomalous like the low-frequency range, even if Yordanova et al. (2008, 2009) showed that the situation is not so clear.

The above results provide a good example of absence of universality in turbulence, a topic which received renewed attention in the last years (Chapman et al. 2009; Lee et al. 2010; Matthaeus 2009).

8.2 The Origin of the High-Frequency Region

How is the high-frequency region of the spectrum generated? This has become the urgent topic which must be addressed. Ghosh et al. (1996) appeals to change of invariants in controlling the flow of spectral energy transfer in the cascade process, and in this picture no dissipation is required to explain the steepening of the magnetic power spectrum. Furthermore it is believed that the high-frequency region is highly anisotropic, with a significant fraction of turbulent energy cascades mostly in the quasi 2D structures, perpendicular to the background magnetic field. How magnetic energy is dissipated in the anisotropic energy cascade still remains an unsolved and fascinating question.

8.2.1 A Dissipation Range

As we already said, in their analysis of Wind data, Leamon et al. (1998) attribute the presence of the region at frequencies higher than the ion-cyclotron frequency to a kind of dissipative range. Besides analyzing the power spectrum, the authors examined also the normalized reduced magnetic helicity $\sigma_m(f)$ and, they found an excess of negative values at high frequencies. Since this quantity is a measure of the spatial handedness of the magnetic field (Moffatt 1978) and can be related to the polarization in the plasma frame once the propagation direction is known (Smith et al. 1983), the above observations were consistent with the ion-cyclotron damping of Alfvén waves which would leave an excess of kinetic Alfvén waves responsible for the observed value of magnetic helicity. In particular, using a reference system

relative to the mean magnetic field direction $\mathbf{e}_B$ and radial direction $\mathbf{e}_R$ as $(\mathbf{e}_B \times \mathbf{e}_R, \mathbf{e}_B \times (\mathbf{e}_B \times \mathbf{e}_R), \mathbf{e}_B)$, they conclude that transverse fluctuations are less dominant than in the inertial range and the high frequency range is best described by a mixture of 46 % slab waves and of 54 % 2D geometry. Since in the low-frequency range they found 11 and 89 % respectively, the increased slab fraction my be explained by the preferential dissipation of oblique structures. Thermal particles interactions with the 2D slab component may be responsible for the formation of dissipative range, even if the situation seems to be more complicated. In fact they found that also kinetic Alfvén waves propagating at large angles with the background magnetic field might be consistent with the observations and form some portion of the 2D component.

Recently the question of the increased power anisotropy of the high-frequency region has been addressed by Perri et al. (2009) who investigated the scaling behavior of the eigenvalues of the variance matrix of magnetic fluctuations, which provide information on the anisotropy due to different polarizations of fluctuations. These authors investigated data coming from Cluster spacecraft when these satellites orbited in front of the Earth's parallel Bow Shock. Their results showed that magnetic turbulence in the high-frequency region is strongly anisotropic, the minimum variance direction being almost parallel to the background magnetic field at scales larger than the ion cyclotron scale. A very interesting result is the fact that the eigenvalues of the variance matrix have a strong intermittent behavior, with very high localized fluctuations below the ion cyclotron scale. This behavior, never investigated before, generates a cross-scale effect in magnetic turbulence. Indeed, PDFs of eigenvalues evolve with the scale, namely they are almost Gaussian above the ion cyclotron scale and become power laws at scales smaller than the ion cyclotron scale. As a consequence it is not possible to define a characteristic value (as the average value) for the eigenvalues of the variance matrix at small scales. Since the wave-vector spectrum of magnetic turbulence is related to the characteristic eigenvalues of the variance matrix (Carbone et al. 1995), the absence of a characteristic value means that a typical power spectrum at small-scales cannot be properly defined. This is a feature which received little attention, and represents a further indication for the absence of universal characteristics of turbulence at small-scales.

8.2.2 A Dispersive Range

The presence of a frequency range of the magnetic power density spectrum characterized by a clear spectral slope, whose value fluctuates between -2 and -4, (Leamon et al. 1998; Smith et al. 2006; Bruno et al. 2014; Bruno and Telloni 2015), suggests that the high-frequency region above the ion-cyclotron frequency might be interpreted as a kind of different energy cascade due to dispersive effects. Then turbulence in this region can be described through the Hall-MHD models, which is the simplest model apt to investigate dispersive effects in a fluid-like framework. In fact, at variance with the usual MHD, where the effect of ion inertia is taken into

account, the generalized Ohm's law reads

$$\mathbf{E} = -\mathbf{V} \times \mathbf{B} + \frac{m_i}{\rho e}(\nabla \times \mathbf{B}) \times \mathbf{B},$$

where the second term on the r.h.s. of this equation represents the Hall term (m_i being the ion mass). This means that MHD equations are enriched by a new term in the equation describing the magnetic field and derived from the induction equation

$$\frac{\partial \mathbf{B}}{\partial t} = \nabla \times \left[\mathbf{V} \times \mathbf{B} - \frac{m_i}{\rho e}(\nabla \times \mathbf{B}) \times \mathbf{B} + \eta \nabla \times \mathbf{B} \right], \tag{8.5}$$

which is quadratic in the magnetic field. The above equation contains three different physical processes characterized by three different times. By introducing a length scale ℓ and characteristic fluctuations ρ_ℓ, B_ℓ, and u_ℓ, we can define an eddy-turnover time $T_{NL} \sim \ell/u_\ell$, related to the convective process, a Hall time $T_H \sim \rho_\ell \ell^2/B_\ell$ which characterizes typical processes related to the presence of the Hall term, and a dissipative time $T_D \sim \ell^2/\eta$. At large scales the first term on the r.h.s. of Eq. (8.5) describes the Alfvénic turbulent cascade, realized in a time T_{NL}. At very small scales, the dissipative time becomes the smallest timescale, and dissipation takes place.[2] However, one can conjecture that at intermediate scales a cascade is realized in a time which is no more T_{NL} and not yet T_D, rather the cascade is realized in a time T_H. This happens when $T_H \sim T_{NL}$. Since at these scales density fluctuations become important, the mean volume rate of energy transfer can be defined as $\epsilon_V \sim B_\ell^2/T_H \sim B_\ell^3/\ell^2 \rho_\ell$, where T_H is used as a characteristic time for the cascade. Using the usual Richardson's cartoon for the energy cascade which is viewed as a hierarchy of eddies at different scales, and following von Weizsäcker (1951), the ratio of the mass density ρ_ℓ at two successive levels $\ell_v > \ell_{v+1}$ of the hierarchy is related to the corresponding scale size by

$$\frac{\rho_v}{\rho_{v+1}} \sim \left(\frac{\ell_v}{\ell_{nu+1}} \right)^{-3r}, \tag{8.6}$$

where $0 \leq |r| \leq 1$ is a measure of the degree of compression at each level ℓ_v. Using a scaling law for compressive effects $\rho_\ell \sim \ell^{-3r}$ and assuming a constant spectrum energy transfer rate, we have $B_\ell \sim \ell^{(2/3-2r)}$, from which the spectral energy density

$$E(k) \sim k^{-7/3+r}. \tag{8.7}$$

[2] Of course, this is based on classical turbulence. As said before, in the solar wind the dissipative term is unknown, even if it might happens at very small kinetic scales.

The observed range of scaling exponents observed in solar wind $\alpha \in [2\,,4]$ (Smith et al. 2006; Bruno et al. 2014), can then be reproduced by different degree of compression of the solar wind plasma $-5/6 \leq r \leq 1/6$.

8.3 Further Questions About Small-Scale Turbulence

The most "conservative" way to describe the presence of a dissipative/dispersive region in the solar wind turbulence, as we reported before, is for example through the Hall-MHD model. While when dealing with large-scale we can successfully approach the problem of turbulence by saying that some form of dissipation must exist at small-scales, the dissipationless character of solar wind cannot be avoided when we deal with small-scales. The full understanding of the physical mechanisms that allow the dissipation of energy in the absence of collisional viscosity would be a step of crucial importance in the problem of high frequency turbulence in space plasmas. Another fundamental question concerns the dispersive properties of small-scale turbulence beyond the spectral break. This last question has been reformulated by saying: what are the principal constituent modes of small-scale turbulence? This approach explicitly assumes that small-scale fluctuations in solar wind can be described through a weak turbulence framework. In other words, a dispersion relation, namely a precise relationship between the frequency ω and the wave-vector k, is assumed.

As it is well known from basic plasma physics, linear theory for homogeneous, collisionless plasma yields three kind of modes at and below the proton cyclotron frequency Ω_p. At wave-vectors transverse to the background magnetic field and $\Omega_p > \omega_r$ (being ω_r the real part of the frequency of fluctuation), two modes are present, namely a left-hand polarized Alfvén cyclotron mode and a right-hand polarized magnetosonic mode. A third ion-acoustic (slow) mode exists but is damped, except when $T_e \gg T_p$, which is not common in solar wind turbulence. At quasi-perpendicular propagation the Alfvénic branch evolves into Kinetic Alfvén Waves (KAW) (Hollweg 1999), while magnetosonic modes may propagate at $\Omega_p \ll \omega_r$ as whistler modes. As the wave-vector becomes oblique to the background magnetic field both modes develop a nonzero magnetic compressibility where parallel fluctuations become important. There are two distinct scenarios for the subsequent energy cascade of KAW and whistlers (Gary and Smith 2009).

8.3.1 Whistler Modes Scenario

This scenario involves a two-mode cascade process, both Alfvénic and magnetosonic modes which are only weakly damped as the plasma $\beta \leq 1$, transfer energy to quasi-perpendicular propagating wave-vectors. The KAW are damped by Landau damping which is proportional to $k_\perp^2$, so that they cannot contribute to the formation

of dispersive region (unless for fluctuations propagating along the perpendicular direction). Even left-hand polarized Alfvén modes at quasi-parallel propagation suffer for proton cyclotron damping at scales $k_\parallel \sim \omega_p/c$ and do not contribute. Quasi-parallel magnetosonic modes are not damped at the above scale, so that a weak cascade of right-hand polarized fluctuations can generate a dispersive region of whistler modes (Stawicki et al. 2001; Gary and Borovsky 2004, 2008; Goldstein et al. 1994). The cascade of weakly damped whistler modes has been reproduced through electron MHD numerical simulations (Biskamp et al. 1996, 1999; Wareing and Hollerbach 2009; Cho and Lazarian 2004) and Particle-in-Cell (PIC) codes (Gary et al. 2008; Saito et al. 2008).

8.3.2 *Kinetic Alfvén Waves and Ion-Cyclotron Waves Scenario*

In the KAWs scenario (Howes 2008; Schekochihin et al. 2009) long-wavelength Alfvénic turbulence transfer energy to quasi-perpendicular propagation for the primary turbulent cascade up to the thermal proton gyroradius where fluctuations are subject to the proton Landau damping. The remaining fluctuation energy continues the cascade to small-scales as KAWs at quasi-perpendicular propagation and at frequencies $\omega_r > \Omega_p$ (Bale et al. 2005; Sahraoui et al. 2009). Fluctuations are completely damped via electron Landau resonance at wavelength of the order of the electron gyroradius. This scenario has been observed through gyrokinetic numerical simulations (Howes et al. 2008b), where the spectral breakpoint $k_\perp \sim \Omega_p/v_{th}$ (being v_{th} the proton thermal speed) has been observed. In addition, Salem et al. (2012), using Cluster observations in the solar wind, showed that the properties of the small-scale fluctuations are inconsistent with the whistler wave model, but strongly agree with the prediction of a spectrum of KAWs with nearly perpendicular wavevectors.

Several other authors studied the nature of the fluctuations at proton scales near the frequency break f_b (He et al. 2011, 2012b,a; Podesta and Gary 2011; Telloni et al. 2015) adopting new data analysis techniques (Horbury et al. 2008; Bruno et al. 2008). These techniques allowed to infer the polarization of the magnetic fluctuations in a plane perpendicular to the sampling direction and for different sampling directions with respect to the local mean magnetic field orientation, for each scale of interest. These analyses showed the simultaneous signature of polarized fluctuations identified as right-handed KAWs propagating at large angles with the local mean magnetic field and left-handed Alfvén ion-cyclotron waves outward propagating at small angles from the local field. However, Podesta and Gary (2011) remarked that also inward-propagating whistler waves, in the case of a field-aligned drift instability, would give the same left-handed signature like outward-propagating Alfvén ion-cyclotron waves. The presence of KAWs had been already suggested by previous data analyses (Goldstein et al. 1994; Leamon et al. 1998; Hamilton et al. 2008) which, on the other hand, were not able to unravel the simultaneous presence also of left-handed polarized Alfvén ion-cyclotron waves. Figure 8.4 from Telloni et al. (2015) shows the distribution of the normalized

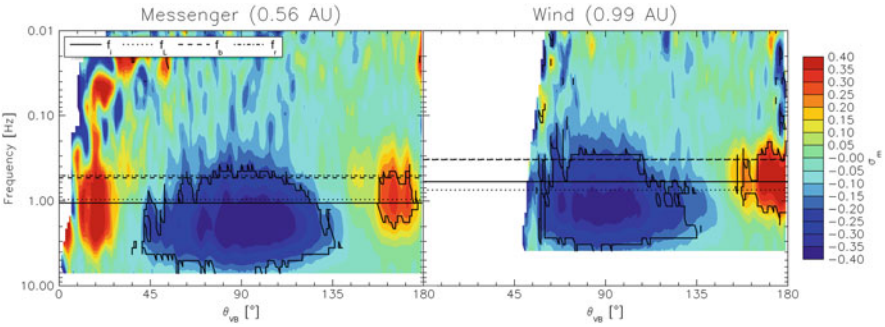

Fig. 8.4 Normalized magnetic helicity, scale by scale, vs the pitch angle θ_{VB} between the local mean magnetic field and the flow direction. Data were collected during a radial alignment between MESSENGER and WIND spacecraft, at 0.56 AU (*left*) and 0.99 AU (*right*), respectively. The *black contour lines* represent the 99 % confidence levels. Characteristic frequencies corresponding to proton inertial length f_i, proton Larmor radius f_L, the observed spectral break f_b and, the resonance condition for parallel propagating Alfvén waves f_r are represented by the *horizontal solid*, *dotted*, *dashed* and *dot-dashed lines*, respectively. Figure adopted from Telloni et al. (2015)

magnetic helicity with respect to the local field pitch angle at MESSENGER (left panel) and WIND (right panel) distances, 0.56 and 0.99 AU, respectively. The frequencies corresponding to the proton inertial length f_i, to the proton Larmor radius f_L, to the observed spectral break f_b, and to the resonance condition for parallel propagating Alfvén waves f_r (Leamon et al. 1998; Bruno and Trenchi 2014), are shown as horizontal solid, dotted, dashed and dot-dashed lines, respectively.

Two populations with opposite polarization can be identified at frequencies right beyond the location of the spectral break. Right-handed polarized KAWs are found for sampling directions highly oblique with respect to the local magnetic field, while left-handed polarized Alfvén ion-cyclotron fluctuations are observed for quasi anti-parallel directions. The same authors found that KAWs dominate the overall energy content of magnetic fluctuations in this frequency range and are largely more compressive than Alfvén ion-cyclotron waves. The compressive character of the KAWs is expected since they generate magnetic fluctuations $\delta B_{\parallel}$ parallel to the local field, particularly for low plasma beta, $\beta \lesssim 1$ (TenBarge and Howes 2012).

Finally, it is interesting to remark that during the wind expansion from Messenger's to WIND's location, the spectral break moved to a lower frequency (Bruno and Trenchi 2014), and both KAWs and Alfvén ion-cyclotron waves shifted accordingly. This observation, per se, is an experimental evidence that relates the location of the frequency break to the presence of these fluctuations (Fig. 8.4).

8.4 Where Does the Fluid-Like Behavior Break Down in Solar Wind Turbulence?

Till now spacecraft observations do not allow us to unambiguously distinguish between both previous scenarios. As stated by Gary and Smith (2009) at our present level of understanding of linear theory, the best we can say is that quasi-parallel whistlers, quasi-perpendicular whistlers, and KAW all probably could contribute to dispersion range turbulence in solar wind. Thus, the critical question is not which mode is present (if any exists in a nonlinear, collisionless medium as solar wind), but rather, what are the conditions which favor one mode over the others. On the other hand, starting from observations, we cannot rule out the possibility that strong turbulence rather than "modes" are at work to account for the high-frequency part of the magnetic energy spectrum. One of the most striking observations of small-scale turbulence is the fact that the electric field is strongly enhanced after the spectral break (Bale et al. 2005). This means that turbulence at small scales is essentially electrostatic in nature, even if weak magnetic fluctuations are present. The enhancement of the electrostatic part has been viewed as a strong indication for the presence of KAW, because gyrokinetic simulations show the same phenomenon (Howes et al. 2008b). However, as pointed out by Matthaeus et al. (2008) (see also the Reply by Howes et al. 2008a to the comment by Matthaeus et al. 2008), the enhancement of electrostatic fluctuations can be well reproduced by Hall-MHD turbulence, without the presence of KAW modes. Actually, the enhancement of the electric field turns out to be a statistical property of the inviscid Hall MHD (Servidio et al. 2008), that is in the absence of viscous and dissipative terms the statistical equilibrium ensemble of Hall-MHD equations in the wave-vectors space is built up with an enhancement of the electric field at large wave-vectors. This represents a thermodynamic equilibrium property of equations, and has little to do with a non-equilibrium turbulent cascade.[3] This would mean that the enhancement of the electrostatic part of fluctuations cannot be seen as a proof firmly establishing that KAW are at work in the dispersive region.

One of the most peculiar possibility from the Cluster spacecraft was the possibility to separate the time domain from the space domain, using the tetrahedral formation of the four spacecrafts which form the Cluster mission (Escoubet et al. 2001). This allows us to obtain a 3D wavevector spectrum and the possibility to identify the actual dispersion relation of solar wind turbulence, if any exists, at small scales. This can be made by using the k-filtering technique which is based on the

[3] It is worthwhile to remark that a turbulent fluid flows is out of equilibrium, say the cascade requires the injection of energy (input) and a dissipation mechanism (output), usually lying on well separated scales, along with a transfer of energy. Without input and output, the nonlinear term of equations works like an energy redistribution mechanism towards an equilibrium in the wave vectors space. This generates an equilibrium energy spectrum which should in general be the same as that obtained when the cascade is at work (cf., e.g., Frisch et al. 1975). However, even if the turbulent spectra could be anticipated by looking at the equilibrium spectra, the physical mechanisms are different. Of course, this should also be the case for the Hall MHD.

strong assumption of plane-wave propagation (Glassmeier et al. 2001). Of course, due to the relatively small distances between spacecrafts, this cannot be applied to large-scale turbulence.

Apart for the spectral break identified by Leamon et al. (1998), a new break has been identified in the solar wind turbulence using high-frequency Cluster data, at about few tens of Hz. In fact, Cluster data in burst mode can reach the characteristic electron inertial scale λ_e and the electron Larmor radius ρ_e. Using the Flux Gate Magnetometer (FGM) (Balogh et al. 2001) and the STAFF-Search Coil (SC) (Cornilleau-Wehrlin et al. 2003) magnetic field data and electric field data from the Electric Field and Wave experiment (EFW) (Gustafsson et al. 2001), Sahraoui et al. (2009) showed that the turbulent spectrum changes shape at wavevectors of about $k\rho_e \sim k\lambda_e \simeq 1$. This result, which perhaps identifies the occurrence of a dissipative range in solar wind turbulence, has been obtained in the upstream solar wind magnetically connected to the bow shock. However, in these studies the plasma β was of the order of $\beta_e \simeq 1$, thus not allowing the separation between both scales. Alexandrova et al. (2009), using three instruments onboard Cluster spacecrafts operating in different frequency ranges, resolved the spectrum up to 300 Hz. They confirmed the presence of the high-frequency spectral break at about $k\rho_e \sim [0.1, 1]$ and, interesting enough, they fitted this part of the spectrum through an exponential decay $\sim \exp[-\sqrt{k\rho_e}]$, thus indicating the onset of dissipation.

The 3D spectral shape reveals poor surprise, that is the energy distribution exhibits anisotropic features characterized by a prominently extended structure perpendicular to the mean magnetic field preferring the ecliptic north direction and also by a moderately extended structure parallel to the mean field (Narita et al. 2010). Results of the 3D energy distribution suggest the dominance of quasi 2D turbulence toward smaller spatial scales, overall symmetry to changing the sign of the wave vector (reflectional symmetry) and absence of spherical and axial symmetry. This last was one of the main hypothesis for the Maltese Cross (Matthaeus et al. 1990), even if bias due to satellite fly through can generate artificial deviations from axisymmetry (Turner et al. 2011).

More interestingly, Sahraoui et al. (2010a) investigated the occurrence of a dispersion relation. They claimed that the energy cascade should be carried by highly oblique KAW with doppler-shifted plasma frequency $\omega_{\text{plas}} \leq 0.1\omega_{ci}$ down to $k_\perp \rho_i \sim 2$. Each wavevector spectrum in the direction perpendicular to an "average" magnetic field $\mathbf{B}_0$ shows two scaling ranges separated by a breakpoint in the interval $[0.1, 1]k_\perp \rho_i$, say a Kolmogorov scaling followed by a steeper scaling. The authors conjectured that the turbulence undergoes a transition-range, where part of energy is dissipated into proton heating via Landau damping, and the remaining energy cascades down to electron scales where Electron Landau damping may dominate. The dispersion relation, compared with linear solutions of the Maxwell–Vlasov equations (Fig. 8.5), seems to identify KAW as responsible for the cascade at small scales. However, the conjecture by Sahraoui et al. (2010a) does not take into account the fact that Landau damping is rapidly saturating under solar wind conditions (Marsch 2006; Valentini et al. 2008).

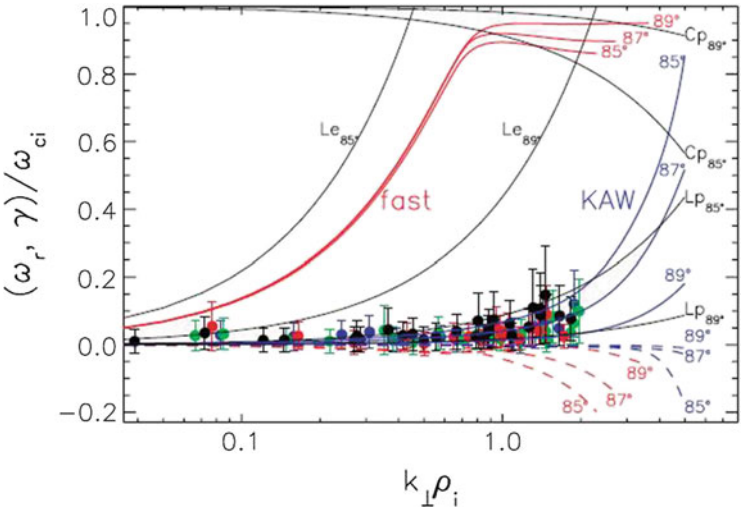

Fig. 8.5 Observed dispersion relations (*dots*), with estimated error bars, compared to linear solutions of the Maxwell–Vlasov equations for three observed angles between the k vector and the local magnetic field direction (damping rates are represented by the *dashed lines*). Proton and electron Landau resonances are represented by the *black curves* $L_{p,e}$. Proton cyclotron resonance are shown by the curves C_p. (the electron cyclotron resonance lies out of the plotted frequency range). Image reproduced by permission from Sahraoui et al. (2010b), copyright by APS

The question of the existence of a dispersion relation was investigated by Narita et al. (2011), who considered three selected time intervals of magnetic field data of CLUSTER FGM in the solar wind. They used a refined version of the *k*-filtering technique, called MSR technique, to obtain high-resolution energy spectra in the wavevector domain. Like the wave telescope, the MSR technique performs fitting of the measured data with a propagating plane wave as a function of frequency and wave vector. The main result is the strong spread in the frequency-wavevector domain, namely none of the three intervals exhibits a clear organization of dispersion relation (see Fig. 8.6). Frequencies and wave vectors appear to be strongly scattered, thus not allowing for the identification of wave-like behavior.

The above discussed papers shed some "darkness" on the scenario of small scales solar wind turbulence as only made by "modes", or at least they indicate that solar wind turbulence, at least at small scales, is far from universality.

Another grey area of investigation is related to the frequency locations of the spectral break separating fluid from kinetic regime.

This break is found at scales of the order of the proton inertial length $\lambda_i = c/\omega_p$ and the proton Larmor radius $\lambda_L = v_{th}/\Omega_p$, where ω_p is the local plasma frequency while Ω_p is the local gyro-frequency, with v_{th} and c the thermal speed and the speed of light, respectively. Several authors tried to match the location of the frequency break with λ_i or λ_L (Perri et al. 2011; Leamon et al. 1998; Bourouaine et al. 2012) with little success. In particular, Markovskii et al. (2008) showed that

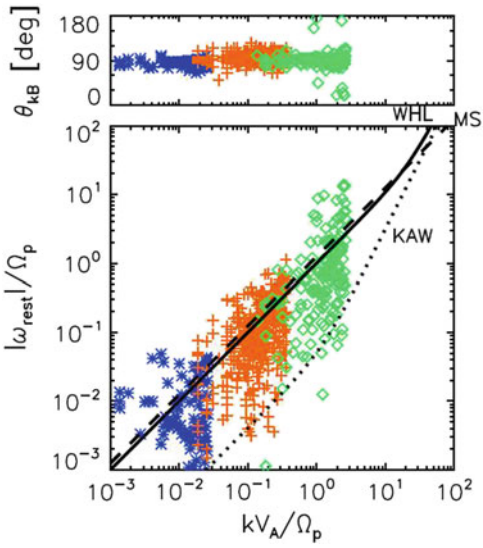

Fig. 8.6 *Top*: Angles between the wave vectors and the mean magnetic field as a function of the wave number. *Bottom*: Frequency-wave number diagram of the identified waves in the plasma rest frame. Magnetosonic (MS), whistler (WHL), and kinetic Alfvén waves (KAW) dispersion relations are represented by *dashed*, *solid*, and *dotted lines*, respectively. Image reproduced by permission from Narita et al. (2011), copyright by AGU

none of the available model could predict a value for the frequency break in good agreement with the observations. Landau damping of obliquely propagating kinetic Alfvén waves (KAW) was proposed by Leamon et al. (1999) and, in this case, the frequency break would correspond to the scale of the Larmor radius λ_L; for Dmitruk et al. (2004) 2-D turbulence dissipation through turbulence reconnection process and generation of current sheets of the order of the ion inertial length λ_i enhances the role of this scale which is the most relevant one also in the framework of incompressible Hall MHD used by Galtier (2006) to explain the break. Only recently, Bruno and Trenchi (2014), using higher time resolution magnetic field data and exploiting selected radial alignments between Messenger, WIND and Ulysses, to restrict the analysis as much as possible to the same fast wind plasma samples, were able to observe a large frequency shift of the high frequency break of about one decade between Messenger location at about 0.42 AU and Ulysses at about 5.3 AU. The same authors found that the resonant condition for outward parallel propagating Alfvén ion-cyclotron waves (ICWs) was the mechanism able to provide the best agreement with the observations, as shown in Fig. 8.7 panel a. Moreover, they showed that this agreement held even taking into account the angle between the background field and the sampling direction, as shown in panel b of the same figure. However, this result was not expected on the basis of anisotropy predictions by any turbulent cascade (Chen et al. 2014) and remains a point which needs to be understood if the ion-cyclotron resonance mechanism for parallel propagating waves is discharged on a theoretical basis.

At this point, having shown that also the high frequency break experiences a shift with distance towards lower frequency, Telloni et al. (2015) proposed a new version of Fig. 3.21 as shown in Fig. 8.8 which unravels the radial behaviour of the whole spectrum between injection and the kinetic scales. Low and high frequency spectral

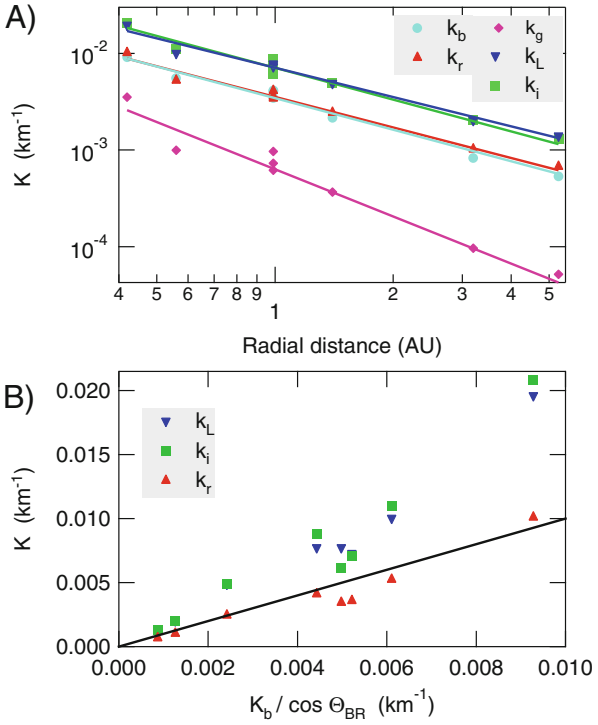

Fig. 8.7 Panel (**a**): radial dependence of wavenumbers associated with the scales corresponding to the observed frequency break κ_b (*cyan circles*), the local proton inertial length κ_i (*blue circles*), the proton Larmor radius κ_L (*green circles*), the wavenumber κ_r corresponding to the resonant condition and the one corresponding to the local cyclotron frequency κ_g (*magenta circles*). The relative best fit curves are shown in the same corresponding colors. Panel (**b**): Wavenumbers associated with the local proton inertial length κ_i (*blue circles*), the proton Larmor radius κ_L (*green circles*) and the wavenumber κ_r (*red circles*) are displayed versus $\kappa_b/\cos(\theta_{BR})$. Figure adopted from Bruno and Trenchi (2014)

breaks move to lower and lower frequencies as the wind expands but their radial dependence is different. The low frequency break has a faster radial evolution $R^{-1.5}$ compared with the high frequency break $R^{-1.1}$. Therefore, the inertial range grows with increasing the heliocentric distance and this confirms previous inferences suggesting that magnetic fluctuations in high speed streams become more and more turbulent with distance (see references in Tu and Marsch 1995b; Bruno and Carbone 2013).

Since the low and high frequency breaks are strictly related to the correlation length λ_C and to the Taylor scale λ_T (see Sect. 3.2.1), respectively, they can be used to determine empirically the effective magnetic Reynolds number R_m^{eff} as (Matthaeus et al. 2005):

$$R_m^{eff} = \left(\frac{\lambda_C}{\lambda_T}\right)^2. \tag{8.8}$$

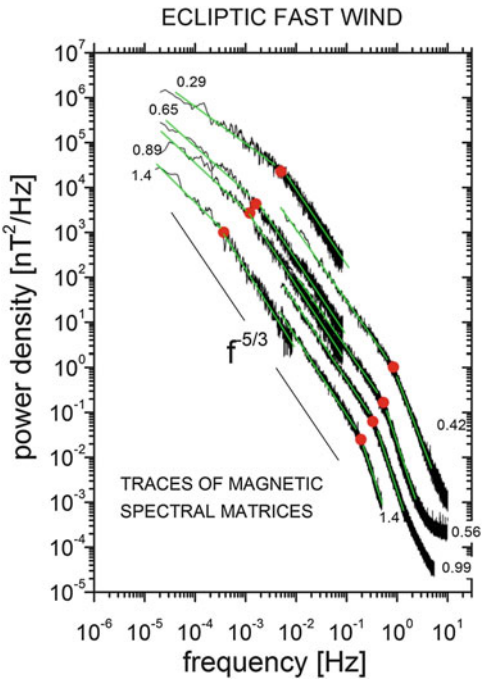

Fig. 8.8 Magnetic field spectral densities for different heliocentric distance as observed by different s/c: MESSENGER (at 0.42 and 0.56 AU), Helios 2 (at 0.29, 0.65 and 0.89 AU), WIND at the Lagrangian point L1 and, ULYSSES at 1.4 AU. Data refer to high speed streams observed in the ecliptic. Low and high frequency breaks are marked by *red dots*. The *solid line* shows, for reference, the Kolmogorov-like spectral slope ($f^{-5/3}$). Figure adopted from Telloni et al. (2015)

In doing so, Telloni et al. (2015) obtained the following values: 3×10^4 at about 0.35 AU, 1.1×10^5 at about 0.65 AU, 1.5×10^5 at about 0.95 AU and, finally, 3.2×10^5 at 1.4 AU. The same authors remarked that the estimate at about 1 AU was in good agreement with the value of 2.3×10^5 provided by Matthaeus et al. (2005) who, using simultaneous measurements of interplanetary magnetic field from the WIND, ACE, and Cluster spacecrafts, were able to build the canonical two-point correlation function.

8.5 What Physical Processes Replace "Dissipation" in a Collisionless Plasma?

As we said before, the understanding of the small-scale termination of the turbulent energy cascade in collisionless plasmas is nowadays one of the outstanding unsolved problem in space plasma physics. In the absence of collisional viscosity and resistivity the dynamics of small-scales is kinetic in nature and must be described by the kinetic theory of plasma. The identification of the physical mechanism that "replaces" dissipation in the collisionless solar wind plasma and establishes a link between the macroscopic and the microscopic scales would open new scenarios in the study of the turbulent heating in space plasmas. This problem is yet in its infancy. Kinetic theory is known since long time from plasma physics, the interested

reader can read the excellent review by Marsch (2006). However, it is restricted mainly to linear theoretical arguments. The fast technological development of supercomputers gives nowadays the possibility of using kinetic Eulerian Vlasov codes that solve the Vlasov–Maxwell equations in multi-dimensional phase space. The only limitation to the "dream" of solving 3D-3V problems (3D in real space and 3D in velocity space) resides in the technological development of fast enough solvers. The use of almost noise-less codes is crucial and allows for the first time the possibility of analyzing kinetic nonlinear effects as the nonlinear evolution of particles distribution function, nonlinear saturation of Landau damping, etc. Of course, faster numerical way to solve the dissipation issue in collisionless plasmas might consist in using intermediate gyrokinetic descriptions (Brizard and Hahm 2007) based on a gyrotropy and strong anisotropy assumptions $k_{\parallel} \ll k_{\perp}$.

As we said before, observations of small-scale turbulence showed the presence of a significant level of electrostatic fluctuations (Gurnett and Anderson 1977; Gurnett and Frank 1978; Gurnett et al. 1979; Bale et al. 2005). Old observations of plasma wave measurements on the Helios 1 and 2 spacecrafts (Gurnett and Anderson 1977; Gurnett and Frank 1978; Gurnett et al. 1979) revealed the occurrence of electric field wave-like turbulence in the solar wind at frequencies between the electron and ion plasma frequencies. Wavelength measurements using the IMP 6 spacecraft provided strong evidence for the presence of electric fluctuations which were identified as ion acoustic waves which are Doppler-shifted upward in frequency by the motion of the solar wind (Gurnett and Frank 1978). Comparison of the Helios results showed that the ion acoustic wave-like turbulence detected in interplanetary space has characteristics essentially identical to those of bursts of electrostatic turbulence generated by protons streaming into the solar wind from the earth's bow shock (Gurnett and Frank 1978; Gurnett et al. 1979). Gurnett and Frank (1978) observed that in a few cases of Helios data, ion acoustic wave intensities are enhanced in direct association with abrupt increases in the anisotropy of the solar wind electron distribution. This relationship strongly suggests that the ion acoustic wave-like structures detected by Helios far from the earth are produced by an electron heat flux instability or by protons streaming into the solar wind from the earth's bow shock. Further evidences (Marsch 2006) revealed the strong association between the electrostatic peak and nonthermal features of the velocity distribution function of particles like temperature anisotropy and generation of accelerated beams.

Araneda et al. (2008) using Vlasov kinetic theory and one-dimensional Particle-in-Cell hybrid simulations provided a novel explanation of the bursts of ion-acoustic activity occurring in the solar wind. These authors studied the effect on the proton velocity distributions in a low-β plasma of compressible fluctuations driven by the parametric instability of Alfvén-cyclotron waves. Simulations showed that field-aligned proton beams are generated during the saturation phase of the wave-particle interaction, with a drift speed which is slightly greater than the Alfvén speed. As a consequence, the main part of the distribution function becomes anisotropic due to phase mixing (Heyvaerts and Priest 1983). This observation is relevant, because the same anisotropy is typically observed in the velocity distributions measured in the fast solar wind (Marsch 2006).

In recent papers, Valentini et al. (2008) and Valentini and Veltri (2009) used hybrid Vlasov–Maxwell model where ions are considered as kinetic particles, while electrons are treated as a fluid. Numerical simulations have been obtained in 1D-3V phase space (1D in the physical space and 3D in the velocity space) where a turbulent cascade is triggered by the nonlinear coupling of circularly left-hand polarized Alfvén waves, in the perpendicular plane and in parallel propagation, at plasma-β of the order of unity. Numerical results show that energy is transferred to short scales in longitudinal electrostatic fluctuations of the acoustic form. The numerical dispersion relation in the $k - \omega$ plane displays the presence of two branches of electrostatic waves. The upper branch, at higher frequencies, consists of ion-acoustic waves while the new lower frequency branch consists of waves propagating with a phase speed of the order of the ion thermal speed. This new branch is characterized by the presence of a plateau around the thermal speed in the ion distribution function, which is a typical signature of the nonlinear saturation of wave-particle interaction process.

Numerical simulations show that energy should be "dissipated" at small-scales through the generation of an ion-beam in the velocity distribution function as a consequence of the trapping process and the nonlinear saturation of Landau damping. This mechanism would produce bursts of electrostatic activity. Whether or not this picture, which seems to be confirmed by recent numerical simulations (Araneda et al. 2008; Valentini et al. 2008; Valentini and Veltri 2009), represents the final fate of the *real* turbulent energy cascade observed at macroscopic scales, requires further investigations. Available plasma measurements in the interplanetary space, even using Cluster spacecrafts, do not allow analysis at typical kinetic scales.

References

O. Alexandrova, V. Carbone, P. Veltri, L. Sorriso-Valvo, Small-scale energy cascade of the solar wind turbulence. Astrophys. J. **674**, 1153–1157 (2008). doi:10.1086/524056

O. Alexandrova, J. Saur, C. Lacombe, A. Mangeney, J. Mitchell, S.J. Schwartz, P. Robert, Universality of solar-wind turbulent spectrum from MHD to electron scales. Phys. Rev. Lett. **103**(16) (2009). doi:10.1103/PhysRevLett.103.165003

J.A. Araneda, E. Marsch, A. F.-Viñas, Proton core heating and beam formation via parametrically unstable Alfvén-cyclotron waves. Phys. Rev. Lett. **100** (2008). doi:10.1103/PhysRevLett.100.125003

S.D. Bale, P.J. Kellogg, F.S. Mozer, T.S. Horbury, H. Reme, Measurement of the electric fluctuation spectrum of magnetohydrodynamic turbulence. Phys. Rev. Lett. **94** (2005). doi:10.1103/PhysRevLett.94.215002

A. Balogh, C.M. Carr, M.H. Acuña, M.W. Dunlop, T.J. Beek, P. Brown, K.-H. Fornaçon, E. Georgescu, K.-H. Glassmeier, J. Harris, G. Musmann, T. Oddy, K. Schwingenschuh, The cluster magnetic field investigation: overview of in-flight performance and initial results. Ann. Geophys. **19**, 1207–1217 (2001). doi:10.5194/angeo-19-1207-2001

D. Biskamp, E. Schwarz, J.F. Drake, Two-dimensional electron magnetohydrodynamic turbulence. Phys. Rev. Lett. **76**, 1264–1267 (1996). doi:10.1103/PhysRevLett.76.1264

D. Biskamp, E. Schwarz, A. Zeiler, A. Celani, J.F. Drake, Electron magnetohydrodynamic turbulence. Phys. Plasmas **6**, 751–758 (1999). doi:10.1063/1.873312

S. Bourouaine, O. Alexandrova, E. Marsch, M. Maksimovic, On spectral breaks in the power spectra of magnetic fluctuations in fast solar wind between 0.3 and 0.9 AU. Astrophys. J. **749**, 102 (2012). doi:10.1088/0004-637X/749/2/102

A.J. Brizard, T.S. Hahm, Foundations of nonlinear gyrokinetic theory. Rev. Mod. Phys. **79**, 421–468 (2007). doi:10.1103/RevModPhys.79.421

R. Bruno, V. Carbone, The solar wind as a turbulence laboratory. Living Rev. Sol. Phys. **10** (2013). doi:10.12942/lrsp-2013-2

R. Bruno, L. Trenchi, Radial dependence of the frequency break between fluid and kinetic scales in the solar wind fluctuations. Astrophys. J. Lett. **787**, 24 (2014). doi:10.1088/2041-8205/787/2/L24

R. Bruno, D. Telloni, Spectral analysis of magnetic fluctuations at proton scales from fast to slow solar wind. Astrophys. J. Lett. **811**, 17 (2015). doi:10.1088/2041-8205/811/2/L17

R. Bruno, E. Pietropaolo, S. Servidio, A. Greco, W.H. Matthaeus, R. D'Amicis, L. Sorriso-Valvo, V. Carbone, A. Balogh, B. Bavassano, Spatial and temporal analysis of magnetic helicity in the solar wind, in *AGU Fall Meeting Abstracts* (2008)

R. Bruno, L. Trenchi, D. Telloni, Spectral slope variation at proton scales from fast to slow solar wind. Astrophys. J. Lett. **793**, 15 (2014). doi:10.1088/2041-8205/793/1/L15

V. Carbone, F. Malara, P. Veltri, A model for the three-dimensional magnetic field correlation spectra of low-frequency solar wind fluctuations during Alfvénic periods. J. Geophys. Res. **100**(9), 1763–1778 (1995). doi:10.1029/94JA02500

V. Carbone, R. Marino, L. Sorriso-Valvo, A. Noullez, R. Bruno, Scaling laws of turbulence and heating of fast solar wind: the role of density fluctuations. Phys. Rev. Lett. **103**(6) (2009). doi:10.1103/PhysRevLett.103.061102

S.C. Chapman, R.M. Nicol, E. Leonardis, K. Kiyani, V. Carbone, Observation of universality in the generalized similarity of evolving solar wind turbulence as seen by Ulysses. Astrophys. J. Lett. **695**, 185–188 (2009). doi:10.1088/0004-637X/695/2/L185

C.H.K. Chen, L. Leung, S. Boldyrev, B.A. Maruca, S.D. Bale, Ion-scale spectral break of solar wind turbulence at high and low beta. Geophys. Res. Lett. **41**, 8081–8088 (2014). doi:10.1002/2014GL062009

J. Cho, A. Lazarian, The anisotropy of electron magnetohydrodynamic turbulence. Astrophys. J. Lett. **615**, 41–44 (2004). doi:10.1086/425215

P.J. Coleman, Turbulence, viscosity, and dissipation in the solar-wind plasma. Astrophys. J. **153**, 371 (1968). doi:10.1086/149674

N. Cornilleau-Wehrlin, G. Chanteur, S. Perraut, L. Rezeau, P. Robert, A. Roux, C. de Villedary, P. Canu, M. Maksimovic, Y. de Conchy, D.H.C. Lacombe, F. Lefeuvre, M. Parrot, J.L. Pinçon, P.M.E. Décréau, C.C. Harvey, P. Louarn, O. Santolik, H.S.C. Alleyne, M. Roth, T. Chust, O. Le Contel, Staff Team, First results obtained by the cluster staff experiment. Ann. Geophys. **21**, 437–456 (2003). doi:10.5194/angeo-21-437-2003

P. Dmitruk, W.H. Matthaeus, N. Seenu, Test particle energization by current sheets and nonuniform fields in magnetohydrodynamic turbulence. Astrophys. J. **617**, 667–679 (2004). doi:10.1086/425301

C.P. Escoubet, M. Fehringer, M. Goldstein, Introduction: the cluster mission. Ann. Geophys. **19**, 1197–1200 (2001). doi:10.5194/angeo-19-1197-2001

J.W. Freeman, Estimates of solar wind heating inside 0.3 AU. Geophys. Res. Lett. **15**, 88–91 (1988). doi:10.1029/GL015i001p00088

U. Frisch, A. Pouquet, J. Leorat, A. Mazure, Possibility of an inverse cascade of magnetic helicity in magnetohydrodynamic turbulence. J. Fluid Mech. **68**, 769–778 (1975). doi:10.1017/S002211207500122X

S. Galtier, Wave turbulence in incompressible hall magnetohydrodynamics. J. Plasma Phys. **72**, 721–769 (2006). doi:10.1017/S0022377806004521

S.P. Gary, J.E. Borovsky, Alfvén-cyclotron fluctuations: linear Vlasov theory. J. Geophys. Res. **109** (2004). doi:10.1029/2004JA010399

S.P. Gary, J.E. Borovsky, Damping of long-wavelength kinetic Alfvén fluctuations: linear theory. J. Geophys. Res. **113** (2008). doi:10.1029/2008JA013565

S.P. Gary, C.W. Smith, Short-wavelength turbulence in the solar wind: Linear theory of whistler and kinetic Alfvén fluctuations. J. Geophys. Res. **114** (2009). doi:10.1029/2009JA014525

S.P. Gary, S. Saito, H. Li, Cascade of whistler turbulence: particle-in-cell simulations. Geophys. Res. Lett. **35** (2008). doi:10.1029/2007GL032327

P.R. Gazis, Observations of plasma bulk parameters and the energy balance of the solar wind between 1 and 10 AU. J. Geophys. Res. **89**, 775–785 (1984). doi:10.1029/JA089iA02p00775

P.R. Gazis, A. Barnes, J.D. Mihalov, A.J. Lazarus, Solar wind velocity and temperature in the outer heliosphere. J. Geophys. Res. **99**, 6561–6573 (1994). doi:10.1029/93JA03144

S. Ghosh, E. Siregar, D.A. Roberts, M.L. Goldstein, Simulation of high-frequency solar wind power spectra using hall magnetohydrodynamics. J. Geophys. Res. **101**, 2493–2504 (1996). doi:10.1029/95JA03201

K.-H. Glassmeier, U. Motschmann, M. Dunlop, A. Balogh, M.H. Acuña, C. Carr, G. Musmann, K.-H. Fornaçon, K. Schweda, J. Vogt, E. Georgescu, S. Buchert, Cluster as a wave telescope - first results from the fluxgate magnetometer. Ann. Geophys. **19**, 1439–1447 (2001). doi:10.5194/angeo-19-1439-2001

M.L. Goldstein, D.A. Roberts, C.A. Fitch, Properties of the fluctuating magnetic helicity in the inertial and dissipation ranges of solar wind turbulence. J. Geophys. Res. **99**, 11519–11538 (1994). doi:10.1029/94JA00789

M.L. Goldstein, Turbulence in the solar wind: kinetic effects, in *Solar Wind Eight*, ed. by D. Winterhalter, J.T. Gosling, S.R. Habbal, W.S. Kurth, M. Neugebauer. AIP Conference Proceedings, vol. 382 (American Institute of Physics, Woodbury, 1996), pp. 239–244. doi:10.1063/1.51391

D.A. Gurnett, R.R. Anderson, Plasma wave electric fields in the solar wind: Initial results from Helios 1. J. Geophys. Res. **82**, 632–650 (1977). doi:10.1029/JA082i004p00632

D.A. Gurnett, L.A. Frank, Ion acoustic waves in the solar wind. J. Geophys. Res. **83**, 58–74 (1978). doi:10.1029/JA083iA01p00058

D.A. Gurnett, E. Marsch, W. Pilipp, R. Schwenn, H. Rosenbauer, Ion acoustic waves and related plasma observations in the solar wind. J. Geophys. Res. **84**, 2029–2038 (1979). doi:10.1029/JA084iA05p02029

G. Gustafsson, M. André, T. Carozzi, A.I. Eriksson, C.-G. Fälthammar, R. Grard, G. Holmgren, J.A. Holtet, N. Ivchenko, T. Karlsson, Y. Khotyaintsev, S. Klimov, H. Laakso, P.-A. Lindqvist, B. Lybekk, G. Marklund, F. Mozer, K. Mursula, A. Pedersen, B. Popielawska, S. Savin, K. Stasiewicz, P. Tanskanen, A. Vaivads, J.-E. Wahlund, First results of electric field and density observations by cluster EFW based on initial months of operation. Ann. Geophys. **19**, 1219–1240 (2001). doi:10.5194/angeo-19-1219-2001

K. Hamilton, C.W. Smith, B.J. Vasquez, R.J. Leamon, Anisotropies and helicities in the solar wind inertial and dissipation ranges at 1 AU. J. Geophys. Res. (Space Phys.) **113**, 01106 (2008). doi:10.1029/2007JA012559

J. He, E. Marsch, C. Tu, S. Yao, H. Tian, Possible evidence of Alfvén-cyclotron waves in the angle distribution of magnetic helicity of solar wind turbulence. Astrophys. J. **731**, 85 (2011). doi:10.1088/0004-637X/731/2/85

J. He, C. Tu, E. Marsch, S. Yao, Do oblique Alfvén/ion-cyclotron or fast-mode/whistler waves dominate the dissipation of solar wind turbulence near the proton inertial length? Astrophys. J. Lett. **745**, 8 (2012a). doi:10.1088/2041-8205/745/1/L8

J. He, C. Tu, E. Marsch, S. Yao, Reproduction of the observed two-component magnetic helicity in solar wind turbulence by a superposition of parallel and oblique Alfvén waves. Astrophys. J. **749**, 86 (2012b). doi:10.1088/0004-637X/749/1/86

J. Heyvaerts, E.R. Priest, Coronal heating by phase-mixed shear Alfven waves. Astron. Astrophys. **117**, 220–234 (1983)

J.V. Hollweg, Kinetic Alfvén wave revisited. J. Geophys. Res. **104**, 14811–14820 (1999). doi:10.1029/1998JA900132

T.S. Horbury, M.A. Forman, S. Oughton, Anisotropic scaling of magnetohydrodynamic turbulence. Phys. Rev. Lett. **807**(17) (2008). doi:10.1103/PhysRevLett.101.175005

G.G. Howes, Inertial range turbulence in kinetic plasmas. Phys. Plasmas **15**(5) (2008). doi:10.1063/1.2889005

G.G. Howes, S.C. Cowley, W. Dorland, G.W. Hammett, E. Quataert, A.A. Schekochihin, T. Tatsuno, Howes et al. reply. Phys. Rev. Lett. **101**(14) (2008a). doi:10.1103/PhysRevLett.101.149502

G.G. Howes, W. Dorland, S.C. Cowley, G.W. Hammett, E. Quataert, A.A. Schekochihin, T. Tatsuno, Kinetic simulations of magnetized turbulence in astrophysical plasmas. Phys. Rev. Lett. **100** (2008b). doi:10.1103/PhysRevLett.100.065004

P.A. Isenberg, Turbulence-driven solar wind heating and energization of pickup protons in the outer heliosphere. Astrophys. J. **623**, 502–510 (2005). doi:10.1086/428609

H. Karimabadi, V. Roytershteyn, M. Wan, W.H. Matthaeus, W. Daughton, P. Wu, M. Shay, B. Loring, J. Borovsky, E. Leonardis, S.C. Chapman, T.K.M. Nakamura, Coherent structures, intermittent turbulence, and dissipation in high-temperature plasmas. Phys. Plasmas **20**(1), 012303 (2013). doi:10.1063/1.4773205

K.H. Kiyani, S.C. Chapman, Y.V. Khotyaintsev, M.W. Dunlop, F. Sahraoui, Global scale-invariant dissipation in collisionless plasma turbulence. Phys. Rev. Lett. **103**(7) (2009). doi:10.1103/PhysRevLett.103.075006

R.J. Leamon, C.W. Smith, N.F. Ness, W.H. Matthaeus, H.K. Wong, Observational constraints on the dynamics of the interplanetary magnetic field dissipation range. J. Geophys. Res. **103**, 4775–4787 (1998). doi:10.1029/97JA03394

R.J. Leamon, C.W. Smith, N.F. Ness, H.K. Wong, Dissipation range dynamics: kinetic Alfvén waves and the importance of β_e. J. Geophys. Res. **104**, 22331–22344 (1999). doi:10.1029/1999JA900158

E. Lee, M.E. Brachet, A. Pouquet, P.D. Mininni, D. Rosenberg, Lack of universality in decaying magnetohydrodynamic turbulence. Phys. Rev. E **81**(1) (2010). doi:10.1103/PhysRevE.81.016318

B.T. MacBride, C.W. Smith, M.A. Forman, The turbulent cascade at 1 AU: energy transfer and the third-order scaling for MHD. Astrophys. J. **679**, 1644–1660 (2008). doi:10.1086/529575

B.T. MacBride, C.W. Smith, B.J. Vasquez, Inertial-range anisotropies in the solar wind from 0.3 to 1 AU: Helios 1 observations. J. Geophys. Res. **115**(A14), 7105 (2010). doi:10.1029/2009JA014939

R. Marino, L. Sorriso-Valvo, V. Carbone, A. Noullez, R. Bruno, B. Bavassano, Heating the solar wind by a magnetohydrodynamic turbulent energy cascade. Astrophys. J. **677**, 71 (2008). doi:10.1086/587957

R. Marino, L. Sorriso-Valvo, V. Carbone, A. Noullez, R. Bruno, B. Bavassano, The energy cascade in solar wind MHD turbulence. Earth Moon Planet. **104**, 115–119 (2009). doi:10.1007/s11038-008-9253-z

R. Marino, L. Sorriso-Valvo, V. Carbone, P. Veltri, A. Noullez, R. Bruno, The magnetohydrodynamic turbulent cascade in the ecliptic solar wind: study of Ulysses data. Planet. Space Sci. **59**, 592–597 (2011). doi:10.1016/j.pss.2010.06.005

S.A. Markovskii, B.J. Vasquez, C.W. Smith, J.V. Hollweg, Dissipation of the perpendicular turbulent cascade in the solar wind. Astrophys. J. **639**, 1177–1185 (2006). doi:10.1086/499398

S.A. Markovskii, B.J. Vasquez, C.W. Smith, Statistical analysis of the high-frequency spectral break of the solar wind turbulence at 1 AU. Astrophys. J. **675**, 1576–1583 (2008). doi:10.1086/527431

E. Marsch, Radial evolution of ion distribution functions, in *Solar Wind Five*, ed. by M. Neugebauer. NASA Conference Publication, vol. 2280 (NASA, Washington, 1983), pp. 355–367

E. Marsch, Turbulence in the solar wind, in *Reviews in Modern Astronomy*, ed. by G. Klare Reviews in Modern Astronomy, vol. 4 (Springer, Berlin, 1991), pp. 145–156

E. Marsch, Kinetic physics of the solar corona and solar wind. Living Rev. Sol. Phys. **3** (2006a). doi:10.12942/lrsp-2006-1

E. Marsch, R. Schwenn, H. Rosenbauer, K. Muehlhaeuser, W. Pilipp, F.M. Neubauer, Solar wind protons: three-dimensional velocity distributions and derived plasma parameters measured between 0.3 and 1 AU. J. Geophys. Res. **87**, 52–72 (1982). doi:10.1029/JA087iA01p00052

W.H. Matthaeus, Prospects for universality in MHD turbulence with cross helicity, anisotropy and shear (invited). Eos Trans. AGU **90**(52), 21–05 (2009)

W.H. Matthaeus, M.L. Goldstein, D.A. Roberts, Evidence for the presence of quasi-two-dimensional nearly incompressible fluctuations in the solar wind. J. Geophys. Res. **95**, 20673–20683 (1990). doi:10.1029/JA095iA12p20673

W.H. Matthaeus, S. Dasso, J.M. Weygand, L.J. Milano, C.W. Smith, M.G. Kivelson, Spatial correlation of solar-wind turbulence from two-point measurements. Phys. Rev. Lett. **95**(23) (2005). doi:10.1103/PhysRevLett.95.231101

W.H. Matthaeus, S. Servidio, P. Dmitruk, Comment on 'kinetic simulations of magnetized turbulence in astrophysical plasmas'. Phys. Rev. Lett. **101**(14) (2008). doi:10.1103/PhysRevLett.101.149501

H.K. Moffatt, *Magnetic Field Generation in Electrically Conducting Fluids*. Cambridge Monographs on Mechanics and Applied Mathematics (Cambridge University Press, Cambridge, 1978)

Y. Narita, K.-H. Glassmeier, F. Sahraoui, M.L. Goldstein, Wave-vector dependence of magnetic-turbulence spectra in the solar wind. Phys. Rev. Lett. **104**(17) (2010). doi:10.1103/PhysRevLett.104.171101

Y. Narita, S.P. Gary, S. Saito, K.-H. Glassmeier, U. Motschmann, Dispersion relation analysis of solar wind turbulence. Geophys. Res. Lett. **38** (2011). doi:10.1029/2010GL046588

E.N. Parker, Dynamics of the interplanetary gas and magnetic fields. Astrophys. J **128**, 664 (1958). doi:10.1086/146579

E.N. Parker, Theory of solar wind, in *Proceedings of the International Conference on Cosmic Rays, Vol. 1: Solar Particles and Sun-Earth Relations* (Tata Institute of Fundamental Research, Bombay, 1963), p. 175

S. Perri, E. Yordanova, V. Carbone, P. Veltri, L. Sorriso-Valvo, R. Bruno, M. André, Magnetic turbulence in space plasmas: scale-dependent effects of anisotropy. J. Geophys. Res. **114**(A13), 2102 (2009). doi:10.1029/2008JA013491

S. Perri, V. Carbone, E. Yordanova, R. Bruno, A. Balogh, Scaling law of the reduced magnetic helicity in fast streams. Planet. Space Sci. **59**, 575–579 (2011). doi:10.1016/j.pss.2010.04.017

S. Perri, M.L. Goldstein, J.C. Dorelli, F. Sahraoui, Detection of small-scale structures in the dissipation regime of solar-wind turbulence. Phys. Rev. Lett. **109**(19), 191101 (2012). doi:10.1103/PhysRevLett.109.191101

J.J. Podesta, Dependence of solar-wind power spectra on the direction of the local mean magnetic field. Astrophys. J. **698**, 986–999 (2009). doi:10.1088/0004-637X/698/2/986

J.J. Podesta, S.P. Gary, Magnetic helicity spectrum of solar wind fluctuations as a function of the angle with respect to the local mean magnetic field. Astrophys. J. **734**, 15 (2011). doi:10.1088/0004-637X/734/1/15

J.D. Richardson, K.I. Paularena, A.J. Lazarus, J.W. Belcher, Radial evolution of the solar wind from IMP 8 to voyager 2. Geophys. Res. Lett. **22**, 325–328 (1995). doi:10.1029/94GL03273

F. Sahraoui, M.L. Goldstein, P. Robert, Y.V. Khotyaintsev, Evidence of a cascade and dissipation of solar-wind turbulence at the electron gyroscale. Phys. Rev. Lett. **102**(23) (2009). doi:10.1103/PhysRevLett.102.231102

F. Sahraoui, M.L. Goldstein, G. Belmont, P. Canu, L. Rezeau, Three dimensional anisotropic k spectra of turbulence at subproton scales in the solar wind. Phys. Rev. Lett. **105**(13), 131101 (2010a). doi:10.1103/PhysRevLett.105.131101

F. Sahraoui, M.L. Goldstein, G. Belmont, P. Canu, L. Rezeau, Three dimensional anisotropic k spectra of turbulence at subproton scales in the solar wind. Phys. Rev. Lett. **105**(13) (2010b). doi:10.1103/PhysRevLett.105.131101

S. Saito, S.P. Gary, H. Li, Y. Narita, Whistler turbulence: particle-in-cell simulations. Phys. Plasmas **15**(10) (2008). doi:10.1063/1.2997339

C.S. Salem, G.G. Howes, D. Sundkvist, S.D. Bale, C.C. Chaston, C.H.K. Chen, F.S. Mozer, Identification of kinetic Alfvén wave turbulence in the solar wind. Astrophys. J. Lett. **745**, 9 (2012). doi:10.1088/2041-8205/745/1/L9

A.A. Schekochihin, S.C. Cowley, W. Dorland, G.W. Hammett, G.G. Howes, E. Quataert, T. Tatsuno, Astrophysical gyrokinetics: kinetic and fluid turbulent cascades in magnetized weakly collisional plasmas. Astrophys. J. Suppl. Ser. **182**, 310–377 (2009). doi:10.1088/0067-0049/182/1/310

R. Schwenn, The 'average' solar wind in the inner heliosphere: structures and slow variations, in *Solar Wind Five*, ed. by M. Neugebauer. NASA Conference Publication, vol. 2280 (NASA, Washington, 1983), pp. 489–507

S. Servidio, W.H. Matthaeus, V. Carbone, Statistical properties of ideal three-dimensional hall magnetohydrodynamics: The spectral structure of the equilibrium ensemble. Phys. Plasmas **15**(4) (2008). doi:10.1063/1.2907789

S. Servidio, F. Valentini, F. Califano, P. Veltri, Local kinetic effects in two-dimensional plasma turbulence. Phys. Rev. Lett. **108**(4), 045001 (2012). doi:10.1103/PhysRevLett.108.045001

C.W. Smith, M.L. Goldstein, W.H. Matthaeus, Turbulence analysis of the Jovian upstream 'wave' phenomenon. J. Geophys. Res. **88**(17), 5581–5593 (1983). doi:10.1029/JA088iA07p05581

C.W. Smith, D.J. Mullan, N.F. Ness, R.M. Skoug, J. Steinberg, Day the solar wind almost disappeared: magnetic field fluctuations, wave refraction and dissipation. J. Geophys. Res. **106**, 18625–18634 (2001a). doi:10.1029/2001JA000022

C.W. Smith, W.H. Matthaeus, G.P. Zank, N.F. Ness, S. Oughton, J.D. Richardson, Heating of the low-latitude solar wind by dissipation of turbulent magnetic fluctuations. J. Geophys. Res. **106**, 8253–8272 (2001b). doi:10.1029/2000JA000366

C.W. Smith, K. Hamilton, B.J. Vasquez, R.J. Leamon, Dependence of the dissipation range spectrum of interplanetary magnetic fluctuations on the rate of energy cascade. Astrophys. J. Lett. **645**, 85–88 (2006). doi:10.1086/506151

O. Stawicki, S.P. Gary, H. Li, Solar wind magnetic fluctuation spectra: dispersion versus damping. J. Geophys. Res. **106**, 8273–8282 (2001). doi:10.1029/2000JA000446

D. Telloni, R. Bruno, L. Trenchi, Radial evolution of spectral characteristics of magnetic field fluctuations at proton scales. Astrophys. J. **805**, 46 (2015). doi:10.1088/0004-637X/805/1/46

J.M. TenBarge, G.G. Howes, Evidence of critical balance in kinetic Alfvén wave turbulence simulations a). Phys. Plasmas **19**(5), 055901 (2012). doi:10.1063/1.3693974

C.-Y. Tu, E. Marsch, MHD structures, waves and turbulence in the solar wind: observations and theories. Space Sci. Rev. **73**(1/2), 1–210 (1995a). doi:10.1007/BF00748891

C.-Y. Tu, E. Marsch, MHD structures, waves and turbulence in the solar wind: observations and theories. Space Sci. Rev. **73**(1/2), 1–210 (1995b). doi:10.1007/BF00748891

A.J. Turner, G. Gogoberidze, S.C. Chapman, B. Hnat, W.-C. Müller, Nonaxisymmetric anisotropy of solar wind turbulence. Phys. Rev. Lett. **107** (2011). doi:10.1103/PhysRevLett.107.095002

F. Valentini, P. Veltri, Electrostatic short-scale termination of solar-wind turbulence. Phys. Rev. Lett. **102**(22) (2009). doi:10.1103/PhysRevLett.102.225001

F. Valentini, P. Veltri, F. Califano, A. Mangeney, Cross-scale effects in solar-wind turbulence. Phys. Rev. Lett. **101**(2) (2008). doi:10.1103/PhysRevLett.101.025006

B.J. Vasquez, C.W. Smith, K. Hamilton, B.T. MacBride, R.J. Leamon, Evaluation of the turbulent energy cascade rates from the upper inertial range in the solar wind at 1 AU. J. Geophys. Res. **112**(A11), 7101 (2007). doi:10.1029/2007JA012305

M.K. Verma, D.A. Roberts, M.L. Goldstein, Turbulent heating and temperature evolution in the solar wind plasma. J. Geophys. Res. **100**, 19839–19850 (1995). doi:10.1029/95JA01216

C.F. von Weizsäcker, The evolution of galaxies and stars. Astrophys. J. **114**, 165 (1951). doi:10.1086/145462

M. Wan, W.H. Matthaeus, H. Karimabadi, V. Roytershteyn, M. Shay, P. Wu, W. Daughton, B. Loring, S.C. Chapman, Intermittent dissipation at kinetic scales in collisionless plasma turbulence. Phys. Rev. Lett. **109**(19), 195001 (2012). doi:10.1103/PhysRevLett.109.195001

C.J. Wareing, R. Hollerbach, Forward and inverse cascades in decaying two-dimensional electron magnetohydrodynamic turbulence. Phys. Plasmas **16**(4) (2009). doi:10.1063/1.3111033

P. Wu, S. Perri, K. Osman, M. Wan, W.H. Matthaeus, M.A. Shay, M.L. Goldstein, H. Karimabadi, S. Chapman, Intermittent heating in solar wind and kinetic simulations. Astrophys. J. **763**, 30 (2013). doi:10.1088/2041-8205/763/2/L30

E. Yordanova, A. Vaivads, M. André, S.C. Buchert, Z. Vörös, Magnetosheath plasma turbulence and its spatiotemporal evolution as observed by the cluster spacecraft. Phys. Rev. Lett. **100**(20) (2008). doi:10.1103/PhysRevLett.100.205003

E. Yordanova, A. Balogh, A. Noullez, R. von Steiger, Turbulence and intermittency in the heliospheric magnetic field in fast and slow solar wind. J. Geophys. Res. **114** (2009). doi:10.1029/2009JA014067

G.P. Zank, W.H. Matthaeus, C.W. Smith, Evolution of turbulent magnetic fluctuation power with heliospheric distance. J. Geophys. Res. **101**, 17093–17108 (1996). doi:10.1029/96JA01275

Y. Zhou, W.H. Matthaeus, Non-WKB evolution of solar wind fluctuations: a turbulence modeling approach. Geophys. Res. Lett. **16**, 755–758 (1989). doi:10.1029/GL016i007p00755

Y. Zhou, W.H. Matthaeus, Transport and turbulence modeling of solar wind fluctuations. J. Geophys. Res. **95**(14), 10291–10311 (1990). doi:10.1029/JA095iA07p10291

Chapter 9
Conclusions and Remarks

There are several famous quotes on turbulence which describe the difficulty to treat mathematically this problem but, the following two are particularly effective. While, on one hand, Richard Feynman used to say "Turbulence is the most important unsolved problem of classical physics." Horace Lamb, on the other hand, asserted "I am an old man now, and when I die and go to heaven there are two matters on which I hope for enlightenment. One is quantum electrodynamics, and the other is the turbulent motion of fluids. And about the former I am rather optimistic.".

We believe that also our readers, looking at the various problems that we briefly touched in this review, will realize how complex is the phenomenon of turbulence in general and, in particular, in the solar wind. More than four decades of observations and theoretical efforts have not yet been sufficient to fully understand how this natural and fascinating phenomenon really works in the solar wind.

We certainly are convinced that we cannot think of a single mechanism able to reproduce all the details we have directly observed since physical boundary conditions favor or inhibit different generation mechanisms, like for instance, velocity-shear or parametric decay, depending on where we are in the heliosphere. On the other hand, there are some aspects which we believe are at the basis of turbulence generation and evolution like: (a) we do need non-linear interactions to develop the observed Kolmogorov-like spectrum; (b) in order to have non-linear interactions we need to have inward modes and/or convected structures which the majority of the modes can interact with; (c) outward and inward modes can be generated by different mechanisms like velocity shear or parametric decay; (d) convected structures actively contribute to turbulent development of fluctuations and can be of solar origin or locally generated.

In particular, ecliptic observations have shown that what we call Alfvénic turbulence, mainly observed within high velocity streams, tends to evolve towards the more "standard" turbulence that we mainly observe within slow wind regions, i.e., a turbulence characterized by $e^+ \sim e^-$, an excess of magnetic energy, and a

R. Bruno, V. Carbone, *Turbulence in the Solar Wind*, Lecture Notes in Physics 928, DOI 10.1007/978-3-319-43440-7_9

Kolmogorov-like spectral slope. Moreover, the presence of a well established "background" spectrum already at short heliocentric distances and the low Alfvénicity of the fluctuations suggest that within slow wind turbulence is mainly due to convected structures frozen in the wind which may well be the remnants of turbulent processes already acting within the first layers of the solar corona. In addition, velocity shear, whenever present, seems to have a relevant role in driving turbulence evolution in low-latitude solar wind.

Polar observations performed by Ulysses, combined with previous results in the ecliptic, finally allowed to get a comprehensive view of the Alfvénic turbulence evolution in the 3D heliosphere, inside 5 AU. However, polar observations, when compared with results obtained in the ecliptic, do not appear as a dramatic break. In other words, the polar evolution is similar to that in the ecliptic, although slower. This is a middle course between the two opposite views (a non-relaxing turbulence, due to the lack of velocity shear, or a quick evolving turbulence, due to the large relative amplitude of fluctuations) which were popular before the Ulysses mission. The process driving the evolution of polar turbulence still is an open question although parametric decay might play some role. As a matter of fact, simulations of non-linear development of the parametric instability for large-amplitude, broadband Alfvénic fluctuations have shown that the final state resembles values of σ_c not far from solar wind observations, in a state in which the initial Alfvénic correlation is partially preserved. As already observed in the ecliptic, polar Alfvénic turbulence appears characterized by a predominance of outward fluctuations and magnetic fluctuations. As regards the outward fluctuations, their dominant character extends to large distances from the Sun. At low solar activity, with the polar wind filling a large fraction of the heliosphere, the outward fluctuations should play a relevant role in the heliospheric physics. Relatively to the imbalance in favor of the magnetic energy, it does not appear to go beyond an asymptotic value. Several ways to alter the balance between kinetic and magnetic energy have been proposed (e.g., 2D processes, propagation in a non-uniform medium, and effect of magnetic structures, among others). However, convincing arguments to account for the existence of such a limit have not yet been given, although promising results from numerical simulations seem to be able to qualitatively reproduce the final imbalance in favor of the magnetic energy.

Definitely, the relatively recent adoption of numerical methods able to highlight scaling laws features hidden to the usual spectral methods, allowed to disclose a new and promising way to analyze turbulent interplanetary fluctuations. Interplanetary space is now looked at as a natural wind tunnel where scaling properties of the solar wind can be studied on scales of the order of (or larger than) 10^9 times laboratory scales.

Within this framework, intermittency represents an important topic in both theoretical and observational studies. Intermittency properties have been recovered via very promising models like the MHD shell models, and the nature of intermittent events has finally been disclosed thanks to new numerical techniques based on wavelet transforms. Moreover, similar techniques have allowed to tackle the problem of identify the spectral anisotropic scaling although no conclusive and final

analyses have been reported so far. In addition, recent studies on intermittency of magnetic field and velocity vector fluctuations, together with analogous analyses on magnitude fluctuations, contributed to sketch a scenario in which propagating stochastic Alfvénic fluctuations and advected structures, possibly flux tubes embedded in the wind, represent the main ingredients of interplanetary turbulence. The varying predominance of one of the two species, waves or structures would make the observed turbulence more or less intermittent. However, the fact that we can make measurements just at one point of this natural wind tunnel represented by the solar wind does not allow us to discriminate temporal from spatial phenomena. As a consequence, we do not know whether these advected structures are somehow connected to the complicated topology observed at the Sun surface or can be considered as by-product of chaotic developing phenomena. Comparative studies based on the intermittency phenomenon within fast and slow wind during the wind expansion would suggest a solar origin for these structures which would form a sort of turbulent background frozen in the wind. As a matter of fact, intermittency in the solar wind is not limited to the dissipation range of the spectrum but abundantly extends orders of magnitude away from dissipative scales, possibly into the inertial range which can be identified taking into account all the possible caveats related to this problem and briefly reported in this review. This fact introduces serious differences between hydrodynamic turbulence and solar wind MHD turbulence, and the same "intermittency" assumes a different intrinsic meaning when observed in interplanetary turbulence. In practice, coherent structures observed in the wind are at odds with filaments or vortices observed in ordinary fluid turbulence since these last ones are dissipative structures continuously created and destroyed by turbulent motion.

Small-scale turbulence, namely observations of turbulent fluctuations at frequencies greater than say 0.1 Hz. revealed a rich and yet poorly understood physics, mainly related to the big problem of dissipation in a dissipationless plasma. Data analysis received a strong impulse from the Cluster spacecrafts, thus revealing a few number of well established and not contradictory observations, as the presence of a double spectral breaks. However, the interpretation of the presence of a power spectrum at small scales is not completely clear and a number of contradictory interpretations can be found in literature. Numerical simulations, based on Vlasov–Maxwell, gyrokinetic and PIC codes, have been made possible due to the increasingly power of computers. They indicated some possible interpretation of the high-frequency part of the turbulent spectrum, but unfortunately the interpretation is not unequivocal. The study of the high-frequency part of the turbulent spectrum is a rapidly growing field of research and, in this review mainly dedicated to MHD scales, the kinetic range of fluctuations has been only marginally treated.

As a final remark, we would like to point out that we tried to describe the turbulence in the solar wind from a particular point of view. We are aware that there are still several topics which we did not discuss in this review and we apologize for the lack of some aspects of the phenomenon at hand which can be of particular interest for some of the readers.

Appendix A
On-Board Plasma and Magnetic Field Instrumentation

In this Appendix, we briefly describe the working principle of two popular instruments commonly used on board spacecraft to measure magnetic field and plasma parameters. For sake of brevity, we will only concentrate on one kind of plasma and field instruments, i.e., the top-hat ion analyzer and the flux-gate magnetometer. Ample review on space instrumentation of this kind can be found, for example, in Pfaff et al. (1998a,b).

A.1 Plasma Instrument: The Top-Hat

The top-hat electrostatic analyzer is a well known type of ion deflector and has been introduced by Carlson et al. (1982). It can be schematically represented by two concentric hemispheres, set to opposite voltages, with the outer one having a circular aperture centered around the symmetry axis (see Fig. A.1). This entrance allows charged particles to penetrate the analyzer for being detected at the base of the electrostatic plates by the anodes, which are connected to an electronic chain. To amplify the signal, between the base of the plates and the anodes are located the Micro-Channel Plates (not shown in this picture). The MCP is made of a huge amount of tiny tubes, one close to the next one, able to amplify by a factor up to 10^6 the electric charge of the incoming particle. The electron avalanche that follows hits the underlying anode connected to the electronic chain. The anode is divided in a certain number of angular sectors depending on the desired angular resolution.

R. Bruno, V. Carbone, *Turbulence in the Solar Wind*, Lecture Notes in Physics 928, DOI 10.1007/978-3-319-43440-7

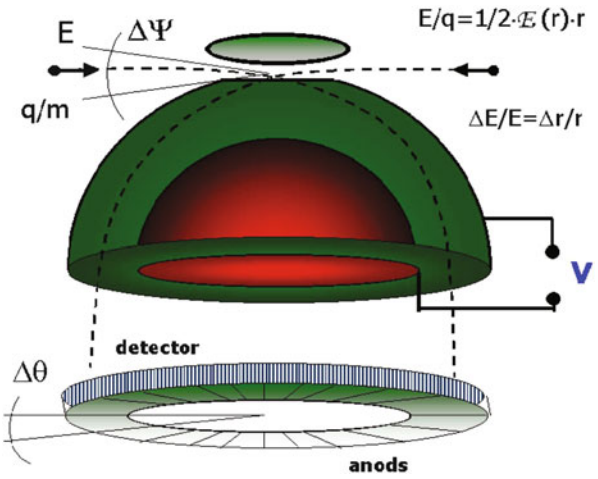

Fig. A.1 Outline of a top-hat plasma analyzer

The electric field $E(r)$ generated between the two plates when an electric potential difference δV is applied to them, is simply obtained applying the Gauss theorem and integrating between the internal (R_1) and external (R_2) radii of the analyzer

$$E(r) = \delta V \frac{R_1 R_2}{R_1 - R_2} \frac{1}{r^2}. \tag{A.1}$$

In order to have the particle q to complete the whole trajectory between the two plates and hit the detector located at the bottom of the analyzer, its centripetal force must be equal to the electric force acting on the charge. From this simple consideration we easily obtain the following relation between the kinetic energy of the particle E_k and the electric field $E(r)$:

$$\frac{E_k}{q} = \frac{1}{2} E(r) r. \tag{A.2}$$

Replacing $E(r)$ with its expression from Eq. (A.1) and differentiating, we get the energy resolution of the analyzer

$$\frac{\delta E_k}{E_k} = \frac{\delta r}{r} = \text{const.}, \tag{A.3}$$

where δr is the distance between the two plates. Thus, $\delta E_k/E_k$ depends only on the geometry of the analyzer. However, the field of view of this type of instrument is limited essentially to two dimensions since $\delta\Psi$ is usually rather small ($\sim 5°$). However, on a spinning s/c, a full coverage of the entire solid angle 4π is obtained by mounting the deflector on the s/c, keeping its symmetry axis perpendicular to the s/c spin axis. In such a way the entire solid angle is covered during half period of spin.

Such an energy filter would be able to discriminate particles within a narrow energy interval $(E_k, E_k + \delta E_k)$ and coming from a small element $d\Omega$ of the solid angle. Given a certain energy resolution, the 3D particle velocity distribution function would be built sampling the whole solid angle 4π, within the energy interval to be studied.

A.1.1 Measuring the Velocity Distribution Function

In this section, we will show how to reconstruct the average density of the distribution function starting from the particles detected by the analyzer. Let us consider the flux through a unitary surface of particles coming from a given direction. If $f(v_x, v_y, v_z)$ is the particle distribution function in phase space, $f(v_x, v_y, v_z)\, dv_x\, dv_y\, dv_z$ is the number of particles per unit volume (pp/cm^3) with velocity between v_x and $v_x + dv_x$, v_y and $v_y + dv_y$, v_z and $v_z + dv_z$, the consequent incident flux Φ_i through the unit surface is

$$\Phi_i = \int\int\int v f d^3\omega, \tag{A.4}$$

where $d^3\omega = v^2 dv \sin\theta\, d\theta\, d\phi$ is the unit volume in phase space (see Fig. A.2).

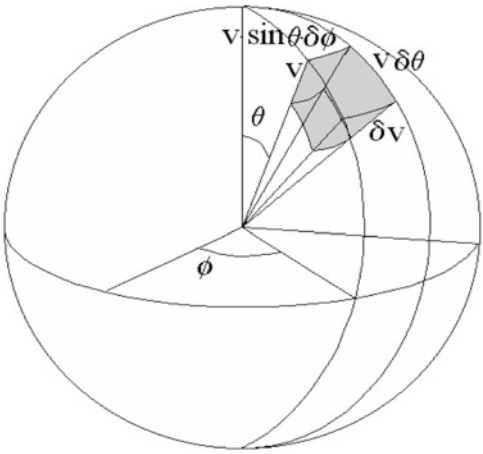

Fig. A.2 Unit volume in phase space

The transmitted flux C^t will be less than the incident flux Φ_i because not all the incident particles will be transmitted and Φ_i will be multiplied by the effective surface $S(< 1)$, i.e.,

$$C^t = \int\int\int Svfd^3\omega = \int\int\int Svfv^2\, dv \sin\theta\, d\theta\, d\phi \tag{A.5}$$

Since for a top-hat Equation A.3 is valid, then

$$v^2\, dv = v^3 \frac{dv}{v} \sim v^3.$$

We have that the counts recorded within the unit phase space volume would be given by

$$C^t{}_{\phi,\theta,v} = f_{\phi,\theta,v} S v^4 \delta\theta\delta\phi \frac{dv}{v} \sin\theta = f_{\phi,\theta,v} v^4 G, \tag{A.6}$$

where G is called *Geometrical Factor* and is a characteristic of the instrument. Then, from the previous expression it follows that the phase space density function $f_{\phi,\theta,v}$ can be directly reconstructed from the counts

$$f_{\phi,\theta,v} = \frac{C^t{}_{\phi,\theta,v}}{v^4 G}. \tag{A.7}$$

A.1.1.1 Computing the Moments of the Velocity Distribution Function

Once we are able to measure the density particle distribution function $f_{\phi,\theta,v}$, we can compute the most used moments of the distribution in order to obtain the particle number density, velocity, pressure, temperature, and heat-flux Paschmann et al. (1998).

If we simply indicate with $f(v)$ the density particle distribution function, we define as moment of order n of the distribution the quantity M_n, i.e.,

$$M_n = \int v_n f(v) d^3\omega. \tag{A.8}$$

It follows that the first 4 moments of the distribution are the following:

- the number density

$$n = \int f(v) d^3\omega, \tag{A.9}$$

- the number flux density vector

$$n\mathbf{V} = \int f(v)\mathbf{v}d^3\omega, \tag{A.10}$$

- the momentum flux density tensor

$$\Pi = m\int f(v)\mathbf{v}\mathbf{v}d^3\omega, \tag{A.11}$$

- the energy flux density vector

$$\mathbf{Q} = \frac{m}{2}\int f(\mathbf{v})v^2\mathbf{v}d^3\omega. \tag{A.12}$$

Once we have computed the zero-order moment, we can obtain the velocity vector from Eq. (A.10). Moreover, we can compute Π and $\mathbf{Q}$ in terms of velocity differences with respect to the bulk velocity, and Eqs. (A.11) and (A.12) become

$$\mathbf{P} = m\int f(\mathbf{v})(\mathbf{v}-\mathbf{V})(\mathbf{v}-\mathbf{V})\,d^3\omega, \tag{A.13}$$

and

$$\mathbf{H} = \frac{m}{2}\int f(\mathbf{v})|\mathbf{v}-\mathbf{V}|^2(\mathbf{v}-\mathbf{V})\,d^3\omega. \tag{A.14}$$

The new Eqs. (A.13) and (A.14) represent the pressure tensor and the heat flux vector, respectively. Moreover, using the relation $\mathbf{P} = nK\mathbf{T}$ we extract the temperature tensor from Eqs. (A.13) and (A.9). Finally, the scalar pressure P and temperature T can be obtained from the trace of the relative tensors

$$P = \frac{Tr(\mathbf{P}_{ij})}{3}$$

and

$$T = \frac{Tr(\mathbf{T}_{ij})}{3}.$$

A.2 Field Instrument: The Flux-Gate Magnetometer

There are two classes of instruments to measure the ambient magnetic field: scalar and vector magnetometers. While nuclear precession and optical pumping magnetometers are the most common scalar magnetometers used on board s/c

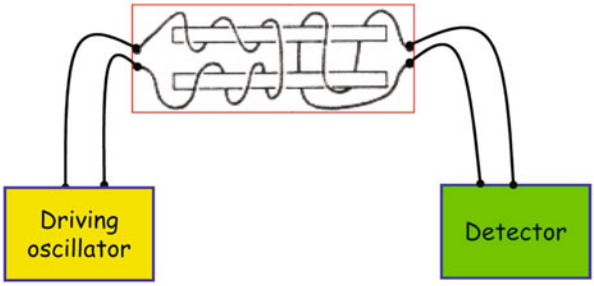

Fig. A.3 Outline of a flux-gate magnetometer. The driving oscillator makes an electric current, at frequency f, circulate along the coil. This coil is such to induce along the two bars a magnetic field with the same intensity but opposite direction so that the resulting magnetic field is zero. The presence of an external magnetic field breaks this symmetry and the resulting field $\neq 0$ will induce an electric potential in the secondary coil, proportional to the intensity of the component of the ambient field along the two bars

(see Pfaff et al. 1998b, for related material), the flux-gate magnetometer is, with no doubt, the mostly used one to perform vector measurements of the ambient magnetic field. In this section, we will briefly describe only this last instrument just for those who are not familiar at all with this kind of measurements in space.

The working principle of this magnetometer is based on the phenomenon of magnetic hysteresis. The primary element (see Fig. A.3) is made of two bars of high magnetic permeability material. A magnetizing coil is spooled around the two bars in an opposite sense so that the magnetic field created along the two bars will have opposite polarities but the same intensity. A secondary coil wound around both bars will detect an induced electric potential only in the presence of an external magnetic field.

The field amplitude BB produced by the magnetizing field H is such that the material periodically saturates during its hysteresis cycle as shown in Fig. A.4.

In absence of an external magnetic field, the magnetic field B_1 and B_2 produced in the two bars will be exactly the same but out of phase by 180° since the two coils are spooled in an opposite sense. As a consequence, the resulting total magnetic field would be 0 as shown in Fig. A.4. In these conditions no electric potential would be induced on the secondary coil because the magnetic flux Φ through the secondary is zero.

On the contrary, in case of an ambient field $H_A \neq 0$, its component parallel to the axis of the bar is such to break the symmetry of the resulting B (see Fig. A.5). H_A represents an offset that would add up to the magnetizing field H, so that the

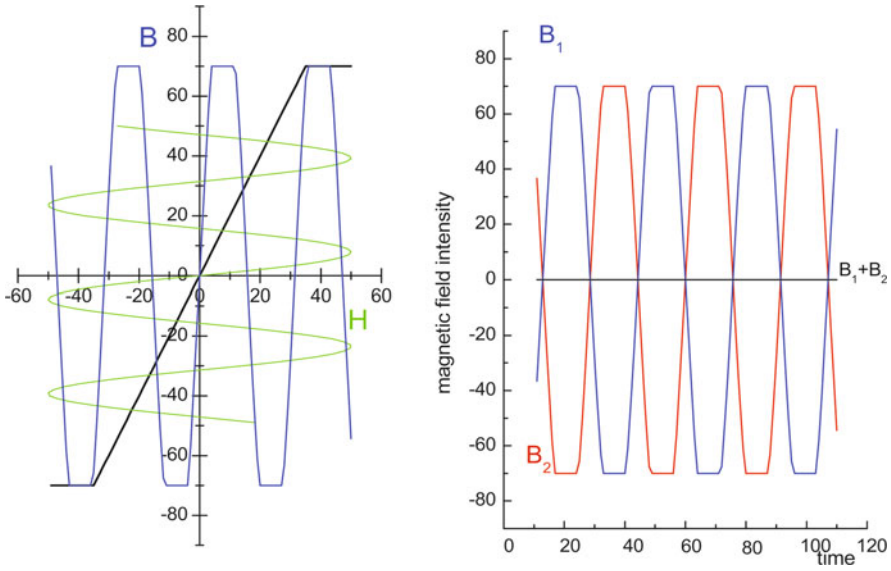

Fig. A.4 *Left panel:* This figure refers to any of the two sensitive elements of the magnetometer. The *thick black line* indicates the magnetic hysteresis curve, the *dotted green line* indicates the magnetizing field H, and the *thin blue line* represents the magnetic field B produced by H in each bar. The *thin blue line* periodically reaches saturation producing a saturated magnetic field B. The trace of B results to be symmetric around the zero line. *Right panel:* magnetic fields B_1 and B_2 produced in the two bars, as a function of time. Since B_1 and B_2 have the same amplitude but out of phase by 180°, they cancel each other

resulting field B would not saturate in a symmetric way with respect to the zero line. Obviously, the other sensitive element would experience a specular effect and the resulting field $B = B_1 + B_2$ would not be zero, as shown in Fig. A.5.

In these conditions the resulting field B, fluctuating at frequency f, would induce an electric potential $V = -d\Phi/dt$, where Φ is the magnetic flux of B through the secondary coil (Fig. A.6).

At this point, the detector would measure this voltage which would result proportional to the component of the ambient field H_A along the axis of the two bars. To have a complete measurement of the vector magnetic field **B** it will be sufficient to mount three elements on board the spacecraft, like the one shown in Fig. A.3, mutually orthogonal, in order to measure all the three Cartesian components.

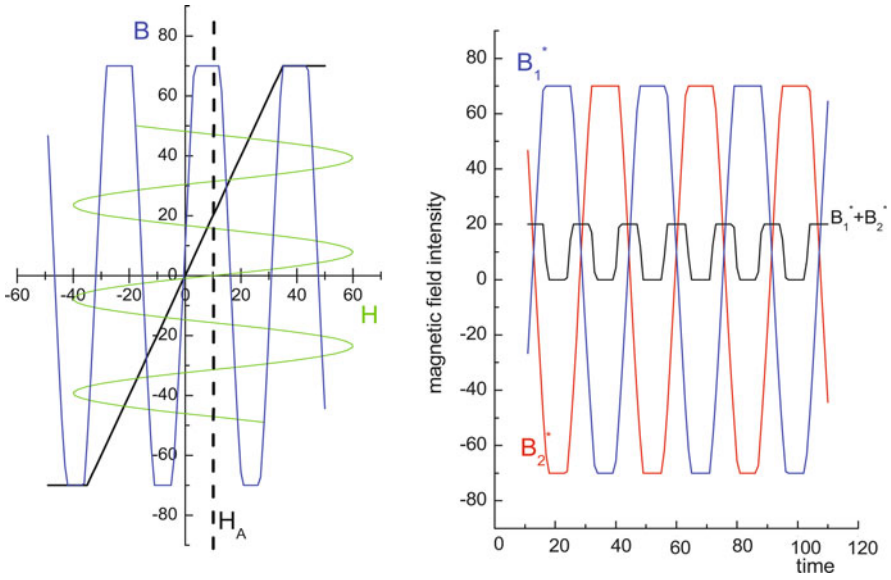

Fig. A.5 *Left panel:* the net effect of an ambient field H_A is that of introducing an offset which will break the symmetry of B with respect to the zero line. This figure has to be compared with Fig. A.4 when no ambient field is present. The upper side of the B curve saturates more than the lower side. An opposite situation would be shown by the second element. *Right panel:* trace of the resulting magnetic field $B = B_1 + B_2$. The asymmetry introduced by H_A is such that the resulting field B is different from zero

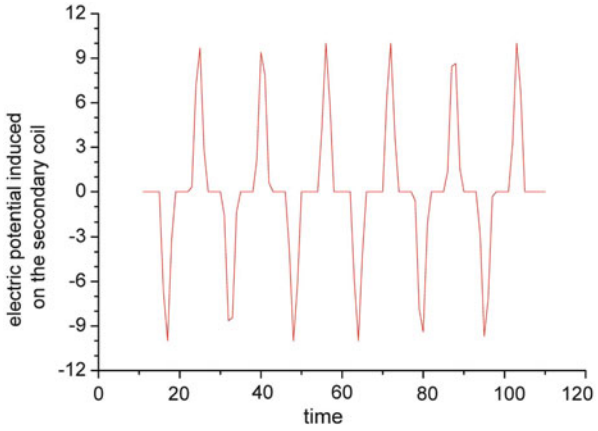

Fig. A.6 Time derivative of the curve $B = B_1 + B_2$ shown in Fig. A.5 assuming the magnetic flux is referred to a unitary surface

References

C.W. Carlson, D.W. Curtis, G. Paschmann, W. Michael, An instrument for rapidly measuring plasma distribution functions with high resolution. Adv. Space Res. **2**, 67–70 (1982). doi:10.1016/0273-1177(82)90151-X

G. Paschmann, A.N. Fazakerley, S. Schwartz, Moments of Plasma Velocity Distributions, in *Analysis Methods for Multi-Spacecraft Data*, ed. by G. Paschmann, P.W. Daly. ISSI Scientific Report, vol. SR-001 (ESA Publication Divisions for ISSI, Noordwijk, 1998), pp. 125–158

R.F. Pfaff, J.E. Borovsky, D.T. Young (eds.), *Measurement Techniques in Space Plasmas, Vol. 1: Particles*. Geophysical Monograph, vol. 102 (American Geophysical Union, Washington, DC, 1998a)

R.F. Pfaff, J.E. Borovsky, D.T. Young (eds.), *Measurement Techniques in Space Plasmas, Vol. 2: Fields*. Geophysical Monograph, vol. 102 (American Geophysical Union, Washington, DC, 1998b)